Universitat Autònoma de Barcelona

Development of tools for monitoring and controlling cell cultures through the metabolic analysis

Iván Martínez Monge

Development of tools for monitoring and controlling cell cultures through the metabolic analysis

Iván Martínez Monge

Supervisors:
Jordi Joan Cairó Badillo
Martí Lecina Veciana
Antoni Casablancas Mira

Universitat Autònoma de Barcelona

Department of Chemical, Biological and Environmental Engineering

July 2018

JORDI JOAN CAIRÓ BADILLO, professor titular del Departament d'Enginyeria Química de la Universitat Autònoma de Barcelona, ANTONI CASABLANCAS MIRA, Tècnic superior de suport a la recerca de la Universitat Autònoma de Barcelona i MARTI LECINA VECIANA, Professor ajudant doctor en el Institut Químic de Sarrià de la Universitat Ramon Llull.

CERTIFIQUEM:

Que el llicenciat Iván Martínez Monge ha dut a terme sota la nostra direcció, en els laboratoris del Departament d'Enginyeria Química, Biològica i Ambiental de la Universitat Autònoma de Barcelona, el treball que, amb el títol de "Development of tools for monitoring and controlling cell cultures through the metabolic analysis", es presenta en aquesta memòria, la qual constitueix la seva Tesi per optar al grau de Doctor en Biotecnologia.

I perquè en prengueu coneixement i tingui els efectes que corresponguin, presentem davant de l'Escola de Doctorat de la Universitat Autònoma de Barcelona l'esmentada Tesi signant aquesta certificació a

Bellaterra, Juliol de 2018

Jordi Joan Cairó Badillo Martí Lecina Veciana Antoni Casablancas Mira

AGRADECIMIENTOS

A mis directores Jordi Cairó, Martí Lecina, Antoni Casablancas y Jordi Prat, por su apoyo y soporte desde el primer día. A mis compañeros Pere Comas, Joan Miret, Ramón Roman, Marc Camps y Mercè Farràs, por su ayuda en todo momento. A mis estudiantes Blanca Camps, Joan Triquell, Alba Suárez, Javi Fuentes, Mariona Martínez y Marcos Fernández por su gran esfuerzo y dedicación. A Lars Nielsen y Igor Marín por su gran acogida durante mi estancia y por darme la oportunidad de seguir trabajando para formarme como investigador.

A mi familia, pilar fundamental y apoyo incondicional en todo momento. A mis amigos y todos los que me apoyaron en mayor o menor medida.

A todos, un millón de gracias.

SUMMARY

Mammalian cells are well established systems for the production of a wide range of high added value proteins with both diagnostic and therapeutic applications. About 60-70% of all biopharmaceuticals, including monoclonal antibodies, viral vaccines and gene therapy vectors are produced in mammalian cells. This is mainly due to the capacity of these cells to perform complex post-translational modifications to yield biologically active proteins.

The thesis presented is focused in the study and improvement of biopharmaceuticals production processes in mammalian cells. In this context, the thesis is divided into two main sections, with the aim of approach two fields in which the industry is directing much of the current efforts to increase productivity of the bioprocesses: the systems biology and the engineering bioprocess in Bioreactor. In other words, begin understanding cell metabolism and then developing new monitoring control systems to increase the performance of the process.

Focusing more on the work developped, one of the most important limitations of mammalian cells is their inefficient metabolism, characterized by the consumption of large quantities of glucose and concomitant production of similar amounts of by-products, like ammonia and lactate, which can detrimentally affect the cell growth. The minimization of lactate accumulation is an issue of high interest and it has been tackled from a myriad of different approaches. Significant reduction of lactate accumulation has been achieved, but it has never been completely suppressed in exponentially growing cells. Interestingly, we have observed that under certain culture conditions mammalian cells are able to co-consume both glucose and lactate during the exponential growth phase.

Chapters 3 and 4 are focused on presenting the different glucose and lactate metabolisms in cultures of HEK293 and CHO, two widely used cell lines in the industry. Three different glucose and lactate metabolisms have been obtained, captured in the three phases: Phase 1: glucose consumption and lactate production (exponentially growth), Phase 2: glucose and lactate simultaneous consumption (exponentially growth), and Phase 3: lactate consumption as a sole carbon source (no cell growth). These different metabolic phases were observed mainly depending on two cell culture conditions: the pH and the lactate concentration. In order to perform a deeper study of the different phases presented, an analysis of the intracellular flux distribution for the different phases have been performed for both cell lines by means of Flux Balance Analysis (FBA). To this end, a genome-scale metabolic model reconstruction has been performed for each cell line.

FBA showed that, in Phase 1, lactate is produced because pyruvate is converted to lactate to fulfill the NADH regeneration requirements in the cytoplasm and only a small amount of pyruvate is introduced into TCA through Acetyl-CoA. In glucose-lactate concomitant consumption (Phase 2), glucose uptake was significantly reduced and a balance between glycolysis and TCA cycle fluxes was reached, yielding a more efficient substrate consumption. We strongly believe that this phenomenon could open a door to obtain more efficient cell lines or to engineer new culture strategies to define more productive bioprocesses.

SUMMARY

Once understood the metabolism of mammalian cells in culture, the next step is to apply this knowledge in the engineering bioprocess area. In this connection, fed-batch and perfusion cultures are considered the most attractive choices for the industry. However, the efficient application of these processes requires the availability of reliable on-line measuring systems for cell density and cell metabolic activity estimation. To this end, a new robust on-line monitoring tool based on the alkali buffer addition used to maintain the pH set-point is presented in Chapter 5. This new tool is compared with a widely used monitoring tool based on the Oxygen Uptake Rate (O.U.R.) determination, by means of application of the dynamic method. The results demonstrated that both strategies are reliable tools for feed control in fed-batch processes of HEK293, maintaining the glucose concentration in a narrowed range during the culture.

The two alternatives presented have shown clear advantages in respect to final product titer and, especially, volumetric productivities. But better results have been obtained with the alkali addition strategy, increasing the total viable cell concentration and product titer by 178% and 257% respectively, and obtaining a 109% increment of the process volumetric productivity in respect to the batch culture. This is due to the culture constant distortions of the pO_2 and pH performed in every O.U.R. dynamic measurement.

To close the work performed in the thesis, a different non-invasive method for O.U.R. determination based on the stationary liquid mass balance was presented and tested in batch culture. The need for sophisticated instrumentation, like mass flow controllers and gas analyzers, has historically limited a wider implementation of such method. In the Chapter 6, a new simplified method based on inexpensive valves for the continuous estimation of O.U.R. in mammalian cell cultures is evaluated. The results demonstrated to be not only a cheap method, but also a reliable alternative to monitor the metabolic activity in bioreactors in many biotechnological processes, being a useful tool for high cell density culture strategies implementation based on O.U.R. monitoring.

RESUM

Les cèl·lules de mamífer esdevenen en l'actualitat un dels principals sistemes per a la producció d'una àmplia gamma de proteïnes de gran valor afegit amb aplicacions tant diagnòstiques com terapèutiques. Al voltant del 60-70% de tots els productes biofarmacèutics, inclosos els anticossos monoclonals, les vacunes virals i els vectors de teràpia gènica, es produeixen en cèl·lules de mamífer. Això es deu principalment a la capacitat d'aquestes cèl·lules de realitzar complexes modificacions post-translacionals amb l'objectiu de produir proteïnes biològicament actives.

La tesi presentada es centra en l'estudi i millora dels processos de producció de biofarmacèutics en cèl·lules de mamífer. En aquest context, la tesi es divideix en dues seccions principals, amb l'objectiu d'apropar-se als dos camps en què actualment la indústria està dirigint gran part dels seus esforços: la biologia de sistemes i l'enginyeria de bioprocès. En altres paraules, la idea és primer comprendre el metabolisme de les cèl·lules en cultiu en Bioreactor, per després desenvolupar nous sistemes de monitoratge i control amb l'objectiu d'augmentar el rendiment del bioprocessos.

Centrant-se en el treball desenvolupat i començant pel metabolisme, una de les principals limitacions de les cèl·lules de mamífer és el seu ineficient metabolisme en cultiu, caracteritzat pel consum de grans quantitats de glucosa i la alta producció de subproductes no desitjats, com l'amoníac i el lactat, que afecten negativament el creixement cel·lular. En aquest àmbit, la minimització de l'acumulació de lactat ha estat durant anys un tema de gran interès i s'ha arribat ha abordar des de diverses perspectives. Encara que s'ha aconseguit una reducció significativa de l'acumulació de lactat en cultiu, encara no s'ha arribat a suprimir completament aquesta generació. Curiosament, en el treball presentat en aquesta tesi, s'observa que sota certes condicions de cultiu, les cèl·lules de mamífer son també capaces de consumir el lactat, mantenint-se en la fase de creixement exponencial.

Els capítols 3 i 4 es centren en presentar les diferents fases del metabolisme de la glucosa i lactat en cultius de HEK293 i CHO, dues línies cel·lulars àmpliament utilitzades en la indústria. Depenent de les condicions de cultiu, s'han obtingut tres metabolismes diferents, capturats en tres fases: Fase 1: consum de glucosa i producció de lactat (creixement exponencial), Fase 2: consum simultani de glucosa i lactat (creixement exponencial) i Fase 3: consum de lactat com a única font de carboni (sense creixement cel·lular). L'obtenció d'aquestes diferents fases metabòliques depèn principalment de dues condicions de cultiu: el pH i la concentració extracel·lular de lactat. Per realitzar un estudi més profund de les diferents fases presentades, s'ha realitzat un anàlisi de la distribució de flux intracel·lular mitjançant un *Flux Balance Analysis* (FBA). Amb aquesta finalitat, s'ha realitzat una reconstrucció i adaptació dels models metabòlics a escala genòmica per cadascuna de les línies cel·lulars.

Aquest anàlisi demostra que, a la Fase 1, la generació de lactat es deguda a que el piruvat es converteix en lactat per complir els requisits de regeneració de NADH en el citoplasma i només una petita quantitat de piruvat s'introdueix en el TCA a través del Acetyl-CoA. En el consum concomitant de glucosa i lactat (Fase 2), el consum de glucosa es redueix significativament i es s'aconsegueix un equilibri entre la glicòlisi i els fluxos del TCA, produint un consum de substrats

molt més eficient. Amb els resultats presentats, creiem fermament que aquest fenomen podria obrir la porta per obtenir línies cel·lulars més eficients o per dissenyar noves estratègies de cultiu per definir bioprocessos més productius.

Un cop entès el metabolisme de les cèl·lules de mamífer en cultiu, el següent pas és aplicar aquest coneixement en l'àrea de l'enginyeria de bioprocessos. En aquest sentit, les estratègies de cultiu *Fed-batch* i perfusió són considerades les opcions més atractives per a la indústria. Tanmateix, l'aplicació eficient d'aquestes estratègies requereix la disponibilitat de sistemes de mesura en línia fiables que permetin l'estimació de la densitat cel·lular i l'activitat metabòlica. Amb aquesta finalitat, en el capítol 5 es presenta una nova eina de monitoratge en línia en Bioreactor basada en la mesura de l'addició de base per mantenir el pH constant. Aquesta nova eina és comparada amb una eina de monitoratge àmpliament utilitzada basada en la mesura de la velocitat de consum d'oxigen (O.U.R.), mitjançant l'aplicació del mètode dinàmic. Els resultats demostren que ambdues estratègies esdevenen eines fiables per al control de l'alimentació en processos *Fed-batch* amb HEK293, mantenint la concentració de glucosa constant durant el cultiu.

Les dues alternatives presentades han demostrat avantatges clars pel que fa a la concentració de producte final i, especialment, a les productivitats volumètriques. No obstant això, s'han obtingut millors resultats amb l'estratègia basada en l'addició de base, augmentant la concentració total de cèl·lules viables i la concentració final de producte en un 178% i un 257%, respectivament, i obtenint un increment del 109% de la productivitat volumètrica del procés respecte al cultiu de referència en *Batch*. Aquesta diferència entre les dues estratègies aplicades es deu a les distorsions constants que pateix el cultiu en quant al pO_2 i pH realitzades a cada mesura de la velocitat de consum d'oxigen amb el mètode dinàmic, suprimides amb l'aplicació de la mesura de l'addició de base.

Per tancar el treball realitzat a la tesi, s'ha desenvolupat un mètode no invasiu per a la determinació de la O.U.R. com alternativa al mètode dinàmic. Aquest mètode es basa en fer un balanç d'oxigen en la fase líquida mantenint la concentració d'oxigen constant en el líquid durant el cultiu. La necessitat d'una instrumentació sofisticada, així com la necessitat de controladors màssics i analitzadors de gasos, ha limitat històricament la implementació d'aquest mètode. En el Capítol 6, es presenta un nou mètode simplificat basat en vàlvules que tenen un baix cost per a l'estimació contínua de la O.U.R. en cultius de cèl·lules de mamífer. Els resultats demostren no només que el mètode desenvolupat és senzill i econòmic, sinó que també una alternativa fiable per monitoritzar l'activitat metabòlica en molts processos biotecnològics, sent una eina útil per a la implementació d'estratègies de cultiu on la finalitat és l'obtenció d'altes densitats cel·lulars basades en el seguiment de la O.U.R..

RESUMEN

Las células de mamífero son en la actualidad uno de los principales sistemas para la producción de una amplia gama de proteínas de gran valor añadido con aplicaciones tanto diagnósticas como terapéuticas. Alrededor del 60-70% de todos los productos biofarmacéuticos, incluidos los anticuerpos monoclonales, las vacunas virales y los vectores de terapia génica, se producen en células de mamífero. Esto se debe principalmente a la capacidad de estas células de realizar complejas modificaciones post-traslacionales con el objetivo de producir proteínas biológicamente activas.

La tesis presentada se centra en el estudio y mejora de los procesos de producción de biofarmacéuticos en células de mamífero. En este contexto, la tesis se divide en dos secciones, con el objetivo de abordar los dos campos en los que actualmente la industria está dirigiendo gran parte de sus esfuerzos: la biología de sistemas y la ingeniería de bioprocesos. En otras palabras, la idea es primero comprender el metabolismo de las células en cultivo en biorreactor, para después desarrollar nuevos sistemas de monitorización y control con el objetivo de aumentar el rendimiento de los bioprocesos.

Centrándose en el trabajo desarrollado y empezando por el metabolismo, una de las principales limitaciones de las células de mamífero es su ineficiente metabolismo en cultivo, caracterizado por el consumo de grandes cantidades de glucosa y la alta producción de subproductos no deseados, como el amoníaco y el lactato, que afectan negativamente el crecimiento celular. En este ámbito, la minimización de la acumulación de lactato ha sido durante años un tema de gran interés que se ha llegado a abordar desde diversas perspectivas. Aunque se ha logrado una reducción significativa de la acumulación de lactato en cultivo, aún no se ha llegado a suprimir completamente su generación. Curiosamente, en el trabajo presentado en esta tesis, se observa que, bajo ciertas condiciones de cultivo, las células de mamífero son también capaces de consumir el lactato, manteniéndose en la fase de crecimiento exponencial.

Los capítulos 3 y 4 se centran en presentar las diferentes fases del metabolismo de la glucosa y lactato en cultivos de HEK293 y CHO, dos líneas celulares ampliamente utilizadas en la industria. Dependiendo de las condiciones de cultivo, se han obtenido tres metabolismos diferentes, capturados en tres fases: Fase 1: consumo de glucosa y producción de lactato (crecimiento exponencial), Fase 2: consumo simultáneo de glucosa y lactato (crecimiento exponencial) y Fase 3: consumo de lactato como única fuente de carbono (sin crecimiento celular). La obtención de estas diferentes fases metabólicas depende principalmente de dos condiciones de cultivo: el pH y la concentración extracelular de lactato. Para realizar un estudio más profundo de las diferentes fases presentadas, se ha realizado un análisis de la distribución de flujo intracelular mediante un *Flux Balance Analysis* (FBA). Con esta finalidad, se ha realizado la reconstrucción y adaptación de los modelos metabólicos a escala genómica para cada una de las líneas celulares.

Este análisis demuestra que, en la Fase 1, la generación de lactato se debe a que el piruvato se convierte en lactato para cumplir los requisitos de regeneración de NADH en el citoplasma y sólo una pequeña cantidad de piruvato se introduce en el TCA a través del acetil-CoA. En el consumo concomitante de glucosa y lactato (Fase 2), el consumo de glucosa se reduce significativamente y se consigue un equilibrio entre glicólisis y los flujos del TCA, llevando a un consumo de

sustratos mucho más eficiente. Con los resultados presentados, creemos firmemente que este fenómeno podría abrir la puerta para obtener líneas celulares más eficientes o para diseñar nuevas estrategias de cultivo para definir bioprocesos más productivos.

Una vez entendido el metabolismo de las células de mamífero en cultivo, el siguiente paso es aplicar este conocimiento en el área de la ingeniería de bioprocesos. En este sentido, las estrategias de cultivo *Fed-batch* y perfusión son consideradas las opciones más atractivas para la industria. Sin embargo, la aplicación eficiente de estas estrategias requiere la disponibilidad de sistemas de medida en línea fiables que permitan la estimación de la densidad celular y la actividad metabólica. Con este fin, en el capítulo 5 se presenta una nueva herramienta de monitorización en línea en Biorreactor basada en la medida de la adición de base para mantener el pH constante. Esta nueva herramienta es comparada con una herramienta de monitorización ampliamente utilizada basada en la medida de la velocidad de consumo de oxígeno (O.U.R.), mediante la aplicación del método dinámico. Los resultados demuestran que ambas estrategias son herramientas fiables para el control de la alimentación en procesos *Fed-batch* con HEK293, manteniendo la concentración de glucosa constante durante el cultivo.

Las dos alternativas presentadas han demostrado ventajas claras en cuanto a la concentración de producto final y, especialmente, a las productividades volumétricas. Sin embargo, se han obtenido mejores resultados con la estrategia basada en la adición de base, aumentando la concentración total de células viables y la concentración final de producto en un 178% y un 257%, respectivamente, y obteniendo un incremento del 109% de la productividad volumétrica del proceso respecto al cultivo de referencia en *Batch*. Esta diferencia entre las dos estrategias aplicadas se debe a las distorsiones constantes que sufre el cultivo en cuanto al pO_2 y pH realizadas en cada medida de la velocidad de consumo de oxígeno con el método dinámico, suprimidas con la aplicación de la medida de la adición de base.

Para cerrar el trabajo realizado en la tesis, se ha desarrollado un método no invasivo para la determinación de la O.U.R. como alternativa al método dinámico. Este método se basa en realizar un balance de oxígeno en la fase líquida manteniendo la concentración de oxígeno constante en el líquido durante el cultivo. La necesidad de una instrumentación sofisticada, así como la necesidad de controladores másicos y analizadores de gases, ha limitado históricamente la implementación de este método. En el Capítulo 6, se presenta un nuevo método simplificado basado en válvulas que tienen un bajo coste para la estimación continua de la O.U.R. en cultivos de células de mamífero. Los resultados demuestran no sólo que el método desarrollado es sencillo y económico, sino que también una alternativa fiable para monitorizar la actividad metabólica en muchos procesos biotecnológicos, siendo una herramienta útil para la implementación de estrategias de cultivo donde la finalidad es la obtención de altas densidades celulares basadas en el seguimiento de la O.U.R..

LIST OF PUBLICATIONS

I. Fontova, A., Lecina, M., López-Repullo, J., Martínez-Monge, I., Comas, P., Bragós, R., & Cairó, J. J. (2018). A simplified implementation of the stationary liquid mass balance method for on-line O.U.R. monitoring in animal cell cultures. *Journal of Chemical Technology & Biotechnology*, *93*(6), 1757-1766. (Published)

II. Martínez-Monge, I., Albiol, J., Lecina, M., Liste-Calleja, L., Miret, J., Solà, C., & Cairó, J.J. (2018). Metabolic Flux Balance Analysis during lactate and glucose concomitant consumption in HEK293 cell cultures. (Submitted)

III. Martínez-Monge, I., Comas, P., Triquell, J., Lecina, M., Casablancas, A. & Cairó, J.J. (2018). A new strategy for fed-batch process control of HEK293 cell cultures based on alkali buffer addition monitoring: comparison with O.U.R. dynamic method. (Submitted)

IV. Martínez-Monge, I., Comas, P., Triquell, J., Lecina, M. & Cairó, J.J. (2018). Study of glucose and lactate concomitant consumption in CHO cells by means of Flux Balance Analysis. (Manuscript in preparation)

V. Román, R., Farràs, M., Camps, M., Martínez-Monge, I., Lecina, M., Casablancas, A. & Cairó, J.J. (2018) Metabolic shift triggering to concomitant consumption of glucose and lactate by means of continuous CO_2 inlet and free pH evolution. Effect on HEK293 cell density and hIL-11 titer in 50L-Single-Use Bioreactor. (Accepted)

VI. Hefzi, H., Min, S., Martínez-Monge, I., Decker, M., Arnsdorg, J., Kol, S., Pristovsek, N., Holmgaard, A, Petersen, S., Kathrine, K., Maria, E., Lund, K., Kallehauge, T., Ley, D., Ménard, P., Munk, H., Sukhova, Z., Voldborg, B.G., Nielsen, L.K., Lee, G., Faustrup, H., Lewis, N. (2017) Multiplex genome editing eliminates the Warburg Effect without affecting oxidative metabolism or growth rate. (Submitted)

TABLE OF CONTENTS

CHAPTER 1. GENERAL INTRODUCTION

1.1 Biotechnology and Biopharmaceutical Industry

1.1.1 Biotechnology as a modern concept

Although the definition of Biotechnology covers a large field of study, in a simplest way it can be considered as the use of biological processes together with technology to make or modify useful products and to develop processes for a specific use. This use of living organism for benefiting human beings includes diverse fields of study as biology, chemistry and engineering. The first definition of Biotechnology comes from the Hungarian engineer *Karoly Ereky* in 1919, to describe a technology based on converting raw materials into a useful product (Fári and Kralovánszky, 2006). Even though Biotechnology can be considered as a modern science, the humanity has been using biological processes of microorganisms for more than 6000 years, to make different products, as bread or cheese. Undoubtedly, chemistry and physics has dominated the twentieth century, with the emergence of the petrochemicals and pharmaceuticals industries, as well as others humanity discoveries, as the microchips or the atomic energy. Even so, there still exists a huge understanding about fundamentals of life, that leads the twenty-first century to be dominated by biology and its associated technologies (Smith, 2009).

The concept of Modern Biotechnology began with the introduction of the genetic engineering into the natural biological processes. Stanford medical professor Stanley Cohen and biochemist Herbert Boyer from the University of California are considered the founders of the Modern Biotechnology, for being the first to use genetic engineering to generate the first genetically-modified bacterium in the mid-1970s (Russo, 2003). But the history began long before with the scientist J.D. Watson and F.H.C. Crick in 1953, giving the first structural double-helix model of DNA (Watson and Crick, 1953). The discovery of the structure of DNA together with the progress in genetic engineering resulted in an explosion of research in molecular biology and genetics, leading the way for the biotechnology revolution. In 1982, the first genetically engineered drug was approved for its commercialization; it was insulin produced by genetically-modified bacteria, sold under the brand name Humulin® by the company Eli Lilly. 36 years later, about 300 products have been approved and the sales in 2014 were about 195 billion USD, that represents the 18% of drug sales worldwide (Evens, 2015).

1.1.2 Biotechnology classification

There exist many ways to classify the Biotechnology and its different applications, but the most common used is classification in a spectrum of colors. Mostly, five major colors are considered (Kafarski, 2012; DaSilva, 2004):

- Red biotechnology: focused on health preservation (human and veterinarian), includes the production of vaccines and antibiotics, discovery of new drugs, regenerative therapies, construction of artificial organs and new diagnostics.

- Green biotechnology: devoted on the development of agriculture, including the generation of new species of interests and the production of biofertilizers and biopesticides.
- White biotechnology: commonly known as industrial biotechnology, relays on application of biocatalysts in industrial processes, and focused on the generation of chemicals and new materials.
- Grey biotechnology: devoted to the problems of environmental protection.
- Blue biotechnology: based on exploiting marine resources for the generation of products and applications of industrial interests.

1.1.3 Biopharmaceuticals and synthetic drugs

The differences between Biopharmaceuticals and synthetic drugs come from the nature of the product. Most of synthetic drugs are small molecules that can be generated by chemical synthesis obtaining high pure products with a very well-defined structures (Kesik-Brodacka, 2017). Biopharmaceuticals are formed by large and complicated molecules or even mixtures of molecules very difficult to characterize by testing methods available in the laboratory (Covic and Kuhlmann, 2007). Biopharmaceuticals also exhibit much more complex mechanisms of actions, leading a hold great promise for treating some of the most intractable medical conditions such as cancer and autoimmune disease (Kesik-Brodacka, 2017). To reflect the complexity of the Biopharmaceuticals compared with synthetic drugs a visual molecular weight comparison for five different commercially available drugs is presented in **Figure 1.1**. The complexity of Biopharmaceuticals makes unfeasible to produce using chemical processes.

This ability for living cells to produce complex compounds is also reflected in how the use of Biotechnology in industry is replacing in some cases traditional chemical processes. This change reduces the impact factors as energy or raw materials as well as cost production for the process. Two examples must be pointed out: the production of Vitamin B2, usually done using a complex eight-step chemical processes, that is being replaced to one-step process made by a microorganism; and the production of Cephalexin, made by 10-step (bio)chemical synthesis that is starting to change to a combination of fermentation and enzymatic reaction (Sijbesma and Schepens, 2003).

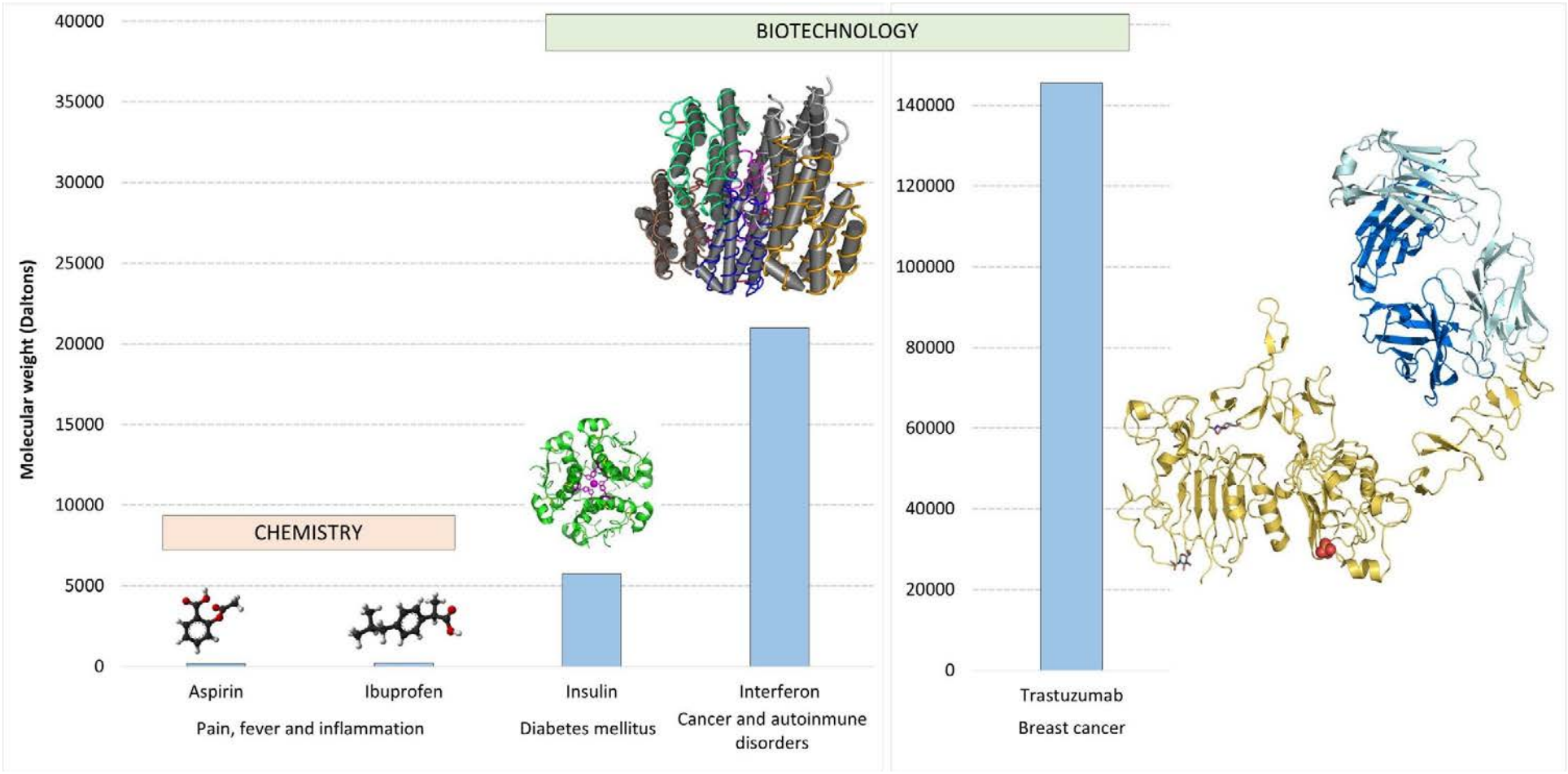

Figure 1.1 Molecular weight comparison of five different commercial drugs made by chemical synthesis and biotechnology processes (self-made graph).

1.1.4 Biopharmaceutical benchmarks

Focusing on the red biotechnology and the current market, Biopharmaceuticals are increasingly being used in practically all branches of medicine and its use has become the most effective treatment a wide range of diseases. Furthermore, biotech products comprise seven of the top ten drugs based worldwide sales at present (**Figure 1.2**). In addition, 52 biotechnological products were blockbusters, defined as a product with $1 billion sales per year; and considering that at present there are only 67 blockbusters drugs in total, the strength of biotechnology industry is absolutely proved (Evens, 2015; Walsh, 2014).

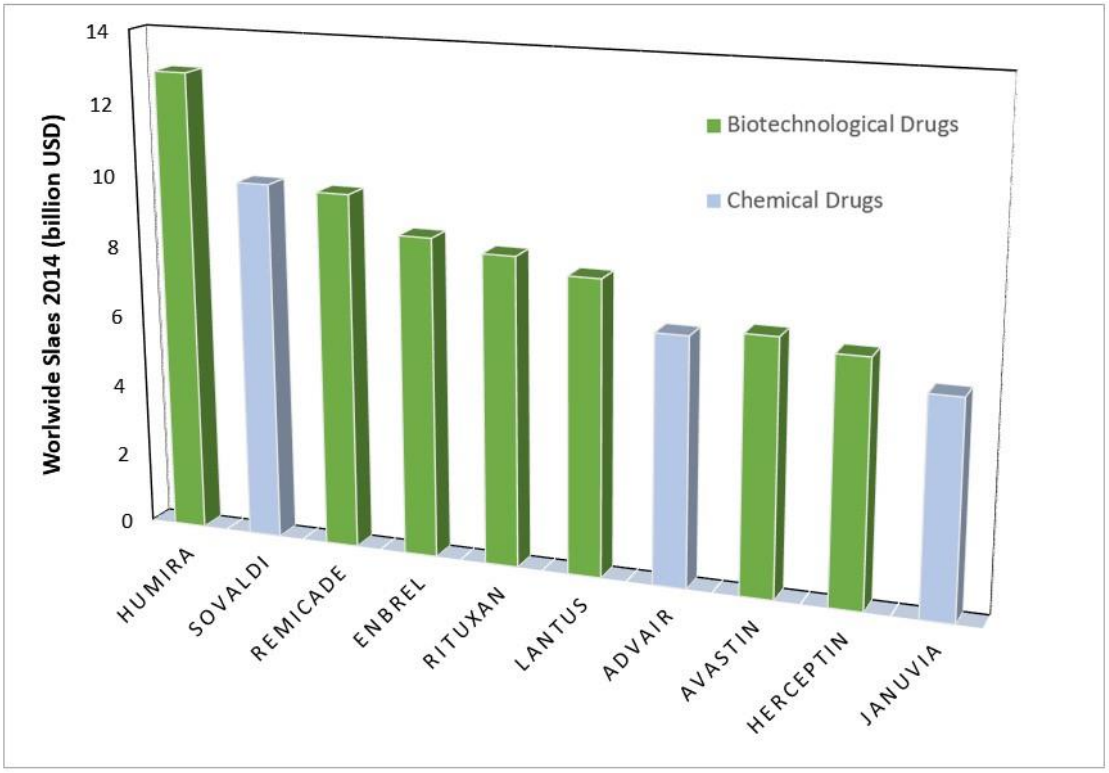

Figure 1.2 Top ten drugs based on the 2014 worldwide sales (self-made graph with the data from Evens, 2015).

The growth of FDA approved Biopharmaceutical has grown to be about 12 products per year over the last 15 years. In the **Figure 1.3**, all the products approved are classified according its class (Evens, 2015). What becomes clear is the huge impact of Biopharmaceuticals in the health care for the last years, that explains the commercial success of biotech products.

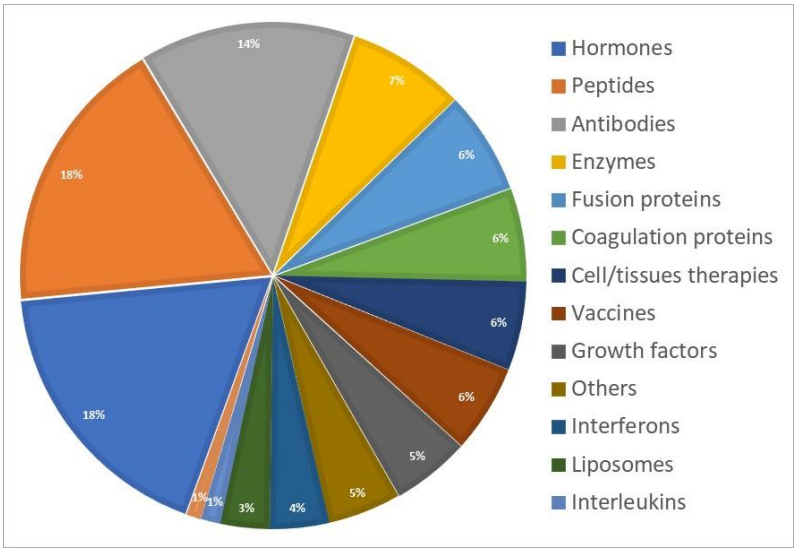

Figure 1.3 Biotechnological products approved for its commercialization by FDA to date (self-made graph constructed with the data from Evens, 2015).

1.1.5 Systems for the production of Biopharmaceuticals

Different living systems are being used to produce Biopharmaceuticals, going from prokaryotic to eukaryotic systems. The different systems have advantatges and drawbakcs and, at the end, their use depends on the type of product desired, the final application and the yield required.

Before presenting the systems used for the industry to produce recombinant proteins, it is must point out that not only is important the quantity of protein produced, but also the quality. This included the capability of the production system to perform complex post-translational modifications that are often required for efficient secretion, drug efficacy, and stability. Such modifications may have consequences for the patient if the final application is therapeutic utilitzation, as incorrect modifications and aggregation can lead to an indesired immune response (Jenkins et al., 2008). Post-translational modifications performed by mammalian cells include proteolytic processing, disulphide bond formation, glycosylation, γ-carboxylation, β-hydroxylation, O-sulphation and amidation (Walsh and Jefferis, 2006).

This said, the most widely used organisms for protein expression are bacteria, yeast, insect an mammalian cells; and the correct choose of the right system is important for posterior succesful production:

- Bacteria: in this group the bacteria *Escherichia coli* are the most commonly used. They grow fast and they are easy and inexpensive to culture. In addition, high yields of recombinant protein are normally obtained. The main drawback of this system becomes when the production of complex recombinant biopharmaceuticals in which mammalian-like posttranslational modifications, such as glycosylation, phosphorylation, and proteolytic processing are required. Another limitations are the insolubility of some proteins as inclusion bodies that are difficult to recover and refold, the impossibility to perform disulfide bonds, and the presence of endotoxines in the final product (Baeshen et al., 2015). It must also be added that bacteria systems are not

able to secrete the protein to the extracelular media, making the purification much more difficult to perform.

- Yeast: the lest expensibe and quickest eukariotic system. Two major systems cell lines are used in this group: *Sacharomyces cerevisiae* and *Pichia pastoris*. Although both are able to perform diverse folding and posstranslational modifications, they usually perform some improper or excessive glycosilation patterns that potentially yield an altered immunogenic response in therapeutic applications. Their rapid growth as well as the ability to secrete the protein extracellularly are the main advatatges of yeasts systems (Kesik-Brodacka, 2017).
- Insect cells: this system allows to perform high quality and more complex posttranslational modifications than bacteria and yeast, but for some proteins it does not preserve the original glycosylation pattern (Gowder, 2017). They have the ability to growth to higher cell densities in culture and the virus production is one of the main applications, although their production can be time consuming with challenging culture conditions (Kesik-Brodacka, 2017).
- Mammalian cells: the preferred system for manufacturing Biopharmaceuticals in the last years. Their ability to produce large and complex molecules with specific posttranslational modifications that can only be done in mammalain systems are the most important advantatge of these systems. The main drawbacks are the complex nutritional requiriments, slow growth and high production time and cost (Sanchez-Garcia et al., 2016). The most common mammalian systems for protein production are Chinese Hamster Ovary (CHO) and Human Embrionik Kidney (HEK293) cell lines (Estes and Melville, 2013).

1.2 Mammalian cells for Biopharmaceutical production

1.2.1 Mammalian cells as the preferred expression system

The increasing demand in the last years for Biopharmaceuticals production with convenient posttranslational modifications has lead mammalian cell lines to be the prevailing system for proteins with clinical and therapeutic applications. As explained in the last section, the major advantage of mammalian cells is this capacity to perform post-translational modifications and human protein-like molecular structure assembly. This explains why bacteria has lost its leading role in the field of drug production, although about 30% of marketed Biopharmaceuticals are still produced in this system (Baeshen et al., 2015; Overton, 2014). In any case, it is not surprising that development of new protein production platforms has ben focused in enhancing the drug functionality through obtaining appropriate protein folding and post-translational modifications (Sanchez-Garcia et al., 2016).

This, together with the fact that among the top ten selling protein Biopharmaceuticals in 2014 six are antibodies or antibody-derived proteins, in which post-translational modifications are required, have driven mammalian cells to be the preferred protein production system. Furthermore, monoclonal antibodies-based drugs production using mammalian cell-based system in the 2016 reached almost the double of the 2010 value (Walsh, 2014). To reflect this, in the **Figure 1.4** the percentage of biotech drugs approvals using mammalian versus

nonmammalian expression systems among the last years is presented, reflecting the prevalence of mammalian-based systems over nonmammalian for the production of approved Biopharmaceuticals.

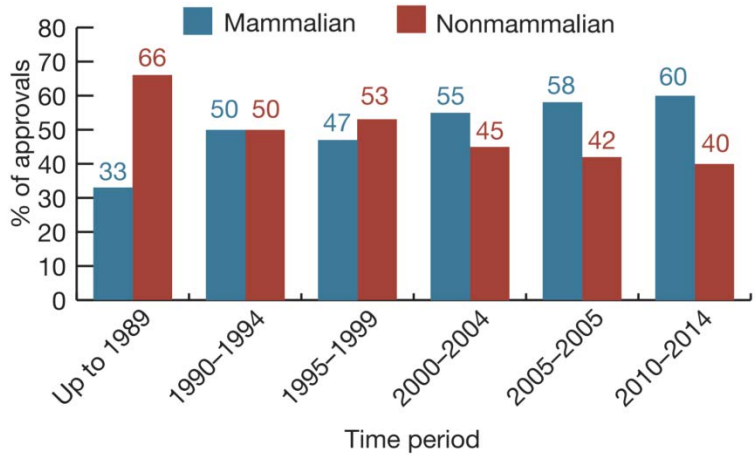

Figure 1.4: Relative application of mammalian versus nonmammalian-based expression systems in the production of biopharmaceuticals approved over the indicated periods (Walsh, 2014).

1.2.2 Mammalian cell line selection

Focusing on the different mammalian expression platforms, Chinese hamster ovary (CHO) cell lines remain the most commonly used system (**Figure 1.5**), although the mouse myeloma (NS0), baby hamster kidney (BHK), human embryonic kidney (HEK293) or human-retina-derived (PERC6) cells are also used (Butler, 2005). The characterization of the CHO cell line and continued usage over several decades without any clear adverse effects have allowed regulatory approval of over 100 biopharmaceuticals (Butler and Meneses-Acosta, 2012). The advantage of CHO cells is that there are well-characterized platform technologies that allow for transfection, amplification and selection of high-producer clones. Transfection of cells with the target gene along with an amplifiable gene such as dihydrofolate reductase (DHFR) or glutamine synthetase (GS) has offered effective platforms for expression of the required proteins (Butler, 2005).

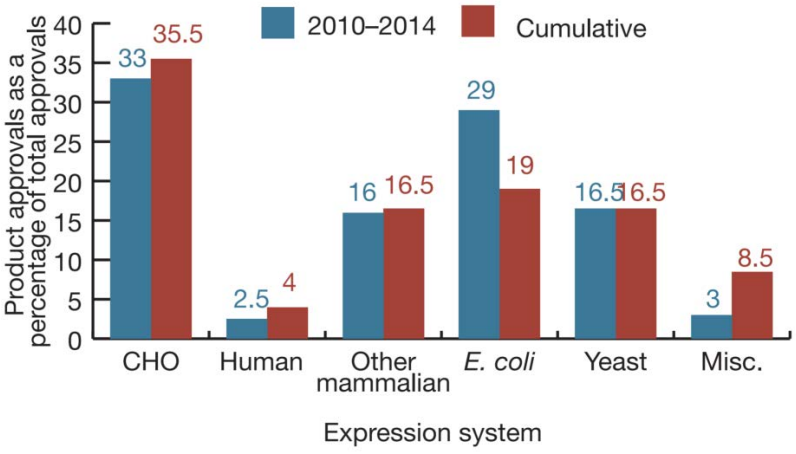

Figure 1.5: Product approvals, cumulative (1982–2014) and for the last period (2010–2014) in the context of expression systems employed. Each data set is expressed as a percentage of total biopharmaceutical product approvals for the period in question (Walsh, 2014).

The weak point of CHO relays in that they cannot perform all types of human glycosylation. CHO cells lack certain sugar transferring enzymes such as α(2–6) sialyltransferase and α(1–3/4) fucosyltransferases (Grabenhorst et al., 1999). In addition, CHO cells are known to add potentially immunogenic glycan structures, which can result in increased clearance of the drug and reduced efficacy (Durocher and Butler, 2009). Is for these reasons that, in some cases, is necessary to produce certain recombinant proteins in human cells, such as HEK293.

One example is Xigris (activated protein C), which is produced in HEK293 cells as the post-transitional modifications performed by CHO cells were found to be inadequate (Durocher and Butler, 2009). In addition, to being a stable host for production of several protein therapeutics, HEK293 is the predominant cell line for transient expression of recombinant proteins (Baldi et al., 2007; Geisse and Fux, 2009). Therefore, many research studies are focusing on improving the protein capacity of HEK293 in a transient and stable setting, as well as to gain a better understanding of the cellular mechanics underlying high productivity in HEK293 cells (Dietmair et al., 2012).

1.3 Bioprocess optimization

The process development can take several months as it requires many steps involving many participants. The cost of the development really depends on the final product and the complexity of the process, with an average cost of $300-800 million taking 10-15 years for a new Biopharmaceutical. The goal is to create an overall optimal process that maybe have some steps that are deviating from the optimal operation but optimize the full process.

1.3.1 Elements of bioprocess

Bioprocess can be divided in three parts each containing a set of unit operations that take place sequentially (Heinzle et al., 2006):

- Upstream processing: includes all operations that are performed before the bioreactor step, as preparation of the medium, sterilization of raw materials and the inoculum preparation.
- Bioreactor: the part of the process in which the desired product is produced by the cells. It can be done in different mode of operation depending on the needs (batch, fed-batch, continuous or perfusion).
- Downstream processing: includes all operations for separation (as centrifugation or filtration), purification (as chromatography or dialysis) and the assembling of the final product.

The development of bioprocess is not a trivial task and designing an appropriate flowsheet, including every step of the process, is essential to detect the possible bottlenecks. Understanding the interactions between operations and how the process can change as function of key operating variables should lead to design an optimal process for the desired product.

1.3.2 The concept of productivity

The volumetric productivity in the bioreactor is an essential parameter for obtaining an economically viable process. This concept must be understood as the amount of product that can be generated per bioreactor volume and per time. Consequently, the bioreactor volume, as well of all the other unit operations of the process, highly depends on this parameter. In other words, to achieve the desired total production rate using a small vessel, the volumetric productivity of the bioreactor must be sufficiently high (Doran, 2013).

The volumetric productivity (V_p) depends, in turn, on two very important terms, as shown in **Equation 1.1**: the specific productivity (q_p) and the biomass generated in the bioreactor (X).

$$V_p\left(\frac{Product\ quantity}{Volume \cdot Time}\right) = q_p\left(\frac{Product\ quantity}{Biomass \cdot Time}\right) \cdot X\left(\frac{Biomass}{Volume}\right) \qquad Equation\ 1.1$$

That means that getting an optimal productivity highly depends on the specific production capability of the organism selected, as well as the maximum biomass concentration that can be obtained in the bioreactor. The interesting fact is how two inter-connected biotechnology disciplines play their own important role in the final bioprocess design: synthetic biology and bioprocess engineering.

Synthetic biology, including molecular biology as well as genetic engineering, combines different disciplines to generate biological systems with high specific productivities for bioprocess applications. By contrast, bioprocess engineering is focused on the process and equipment for manufacturing the products. An example of both parts can be CRISPR/Cas9 for targeted genome editing for the systems biology (Haurwitz et al., 2010); and the designing of a new control strategies to achieve optimal cell culture conditions in the bioreactor for bioprocess engineering (Casablancas et al., 2013).

1.3.3 Culture strategies in bioreactor

Current industrial mammalian cell-based processes for large-scale production are mostly produced using suspension cultures in stirred-tank bioreactors. More specifically, at least 70% of licensed process for therapeutic recombinant proteins productions are produced using stirred-tank bioreactors (Chu and Robinson, 2001). The ability to adapt many cell types to suspension culture and the use of polymeric additives to reduce shear damage have enabled the widespread application of suspension cell culture (van der Pol and Tramper, 1998). Furthermore, stirred-tank bioreactors offer an easy monitoring and control of the process (pH, pO2, temperature and others), homogeneous cell cultures due to the stirring and feasible scale-up.

Different operation strategies can be used in stirred-tank mammalian cell-based cultures depending on the application. The choice must be done according a compromise between the final productivity desired, the scale of the process and the investment in both cost and time (Kadic and Heindel, 2014). The most common culture strategies used by the biotechnological industry are shown in the **Figure 1.6** and the main characteristics are detailed below (Hu and Zhou, 2012):

- Batch: the simplest strategy in which cells are cultured in a finite media until they stop growing. Disadvantages are the nutrient limitation, the low cell densities achieved, the low productivity and high toxic accumulation by-products from the cell metabolism.
- Fed-batch: in which a gradual addition of a fresh concentrated medium is done. This operation mode avoids the nutrient limitation in culture, obtaining higher cell densities and final product concentration compared with batch. As in the batch mode, the accumulation of toxic metabolites in the culture broth leads cells to stop growing at some point.
- Continuous: the feed is continuously being introduced into the bioreactor, and product stream is continuously being obtained. Although is very used to perform metabolic studies, due to the possibility to obtain steady-state cell cultures, it is not widely used by the industry due to the low productivities achieved, in part due to the lost of the cells in the output medium.
- Perfusion: a continuous supply of fresh media is fed into the bioreactor while growth-inhibitory by-products are constantly removed, maintaining the cells in the bioreactor by using a cell retention device. There exists an increasing interest in the use of perfusion culture attributed to the higher product output from a reduced reactor size.

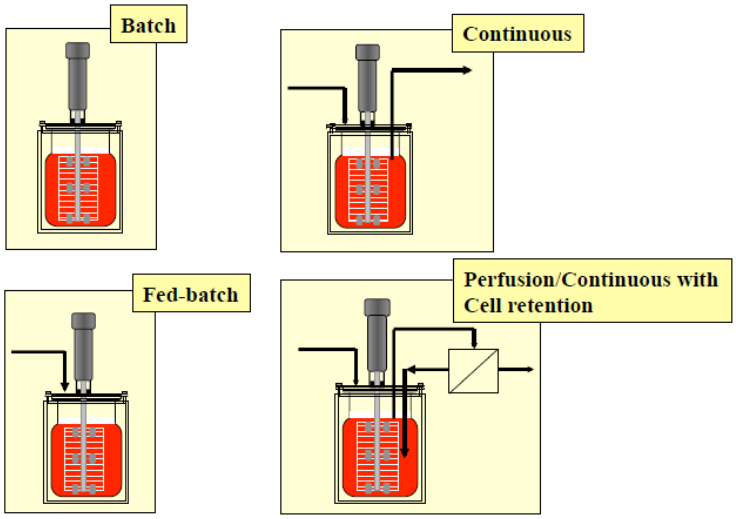

Figure 1.6: Scheme of the main cell culture operation strategies used in mammalian cell-based production processes.

In many cases, the cell density in batch is not sufficiently high and fed-batch and perfusion cultures are considered the more attractive choices. However, the efficient application of these processes requires the availability of reliable monitoring systems for cell density and cell metabolic activity estimation. As in general the product concentration is proportional to the cell density achieved, the **Figure 1.7** illustrates very well the different operations presented according to the cell density that can be achieved in the Bioreactor.

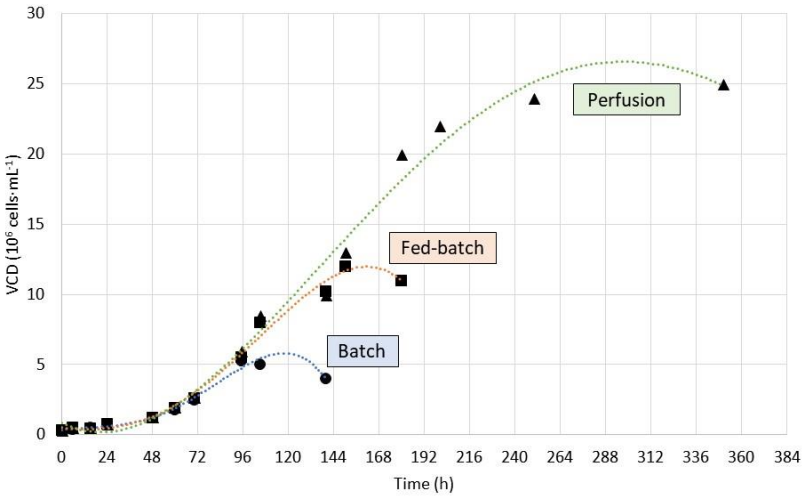

Figure 1.7: Viable cell density (VCD) achieve in different operation strategies in mammalian cell-based cell cultures (visual example).

1.4 The era of Systems Biology

1.4.1 The State of the Art of Biotechnology

Although there isn't yet a consensus as to what is meant by "Systems Biology", the clear goal of this field is to understand biological systems studying the structure and dynamics of cellular function, rather the characteristic of isolated parts of a cell; leading to the idea that the whole is greater than the sum of parts (Kitano, 2002).

This means that a cell system is not just an assembly of genes and proteins that can be listed as individual components. The idea is to know how these parts are assembled to form the structure of a cell, how changes to one part may affect the others, how individual components interact dynamically during operation (Kitano, 2002; Nurse and Hayles, 2011). With that in mind, Systems Biology are mainly focused in answering two key questions: What is the nature of the links between the components in a biological network and what are the functional states and properties of biological network.

PubMed (NCBI) listed more than 3000 articles in which Systems Biology is in one way or other used in the publications, compared with only 3 articles in the last century (Hübner et al., 2011). A very wide application that goes from bioprocess to medicine and life sciences have made many companies to integrate systems biology approaches in innovation pipelines. As a result, a steadily increasing number of universities start to offer MSc and doctoral programs in systems biology (Goble et al., 2016).

1.4.2 A Cross-disciplinary field

Systems biology involves many disciplines such as biology, mathematics, physics, chemistry, engineering and computer science. In turn, the contributions made by those disciplines have made biology more understandable from a quantitative point of view (Gerloff and Kang, 2016). The studies normally include the collection of large sets of experimental data, proposal of

mathematical models, find an accurate computer solution of the mathematical equations to obtain numerical predictions and assessment of the quality of the model by comparing numerical simulations with the experimental data (Kriete and Eils, 2006).

The cycle of research in Systems Biology (**Figure 1.8**) begins with the selection of the biological subject of study and the creation of a model representing the phenomenon. The model represents a computable set of assumptions and hypotheses that need to be tested or supported experimentally. Computational "in silico" experiments, such as simulation, on models reveal computational adequacy of the assumptions and hypotheses embedded in each model. Inadequate models would expose inconsistencies with established experimental facts, and thus need to be rejected or modified. Models that pass this test become subjects of a system analysis where a number of predictions may be made. Then, a set of predictions is selected for "laboratory" experiments. Successful experiments are those that eliminate inadequate models. Models that survive this cycle are deemed to be consistent with existing experimental evidence (Kitano, 2002).

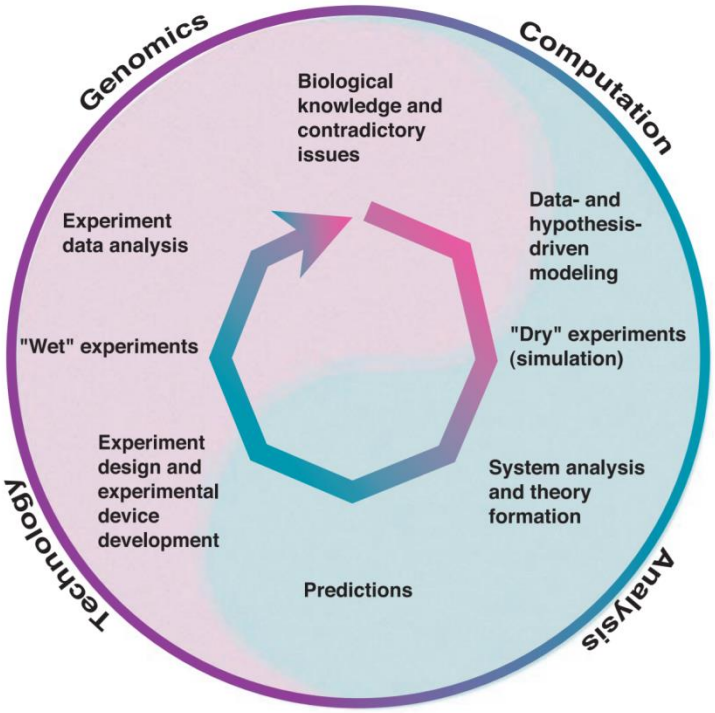

Figure 1.8: Hypothesis-driven research in systems biology, research cycle (Kitano, 2002).

1.4.3 Omics data in Systems Biology

The advent of high-throughput experimental technologies is forcing biologists to view cells as systems, rather than focusing their attention on individual cellular components. Not only are high-throughput technologies forcing the systems point of view, but they also enable us to study cells as systems. Over the past decade, this process has been greatly accelerated with the emergence of Omics, immense data sets that allow the characterization and quantification of biological molecules that translate into the structure, function and dynamics of an organism (Palsson, 2006). These new technologies allow to analyze and quantify massively the different biochemical constituents existing within the cell increasing the amount, quality and variety of molecular data (Ram et al., 2012). On this basis, investigators are making progress in identifying, extracting and interpreting biological insights from Omics data sets (Joyce and Palsson, 2006). Current Omics permit to identify and quantify molecules at different layers connecting the genotype with the phenotype, as shown in **Figure 1.9** (Marín de Mas, 2015).

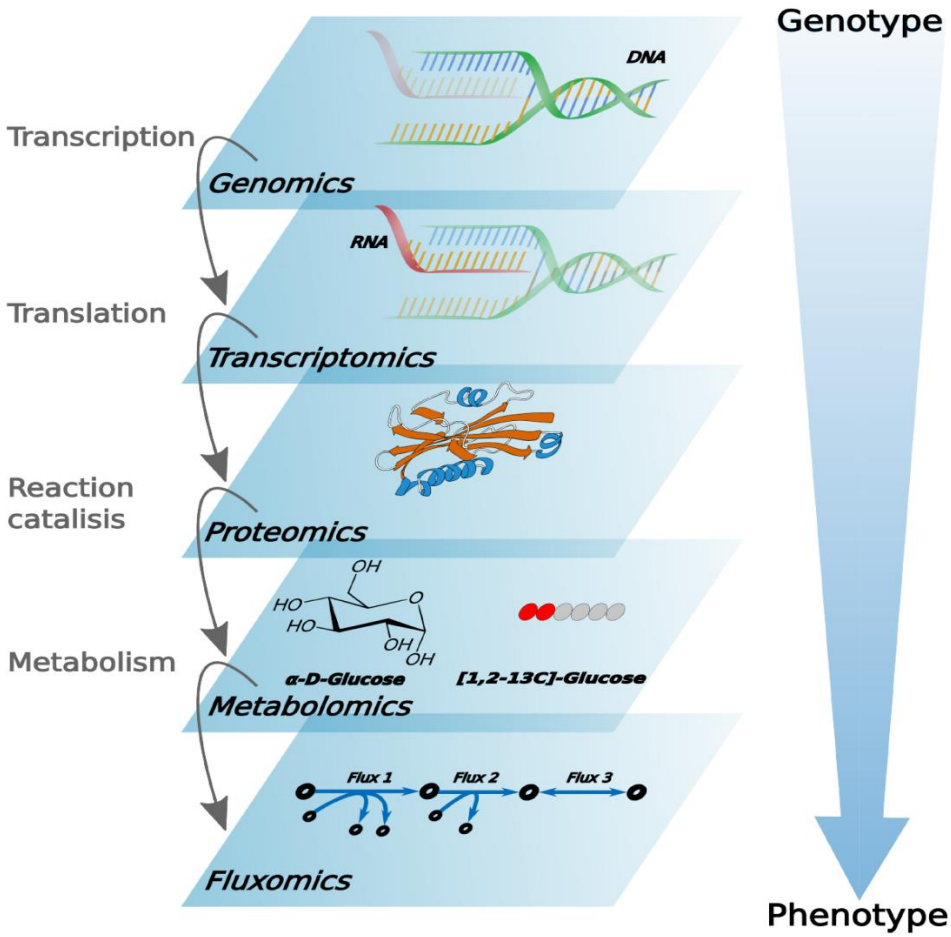

Figure 1.9: The most relevant Omic data in integrated Omic studies, represented as the different layers of biological information (Marín de Mas, 2015).

The following list briefly introduces the most common used Omics technologies that are used by to generate these data sets:

- Genomics: the study of the genome sequence and the information contained therein. More than 300 genome-sequencing corresponding to a different organisms have been published and hundreds are underway (Liolios et al., 2007). In this field, genome annotation defines the complement proteins and RNAs corresponding to the genome that are available for the cell (Joyce and Palsson, 2006).
- Transcriptomics: provides information about the identification and quantification of RNA transcripts, indicating the active compounds within the cell and giving crucial information regarding the expression state (Joyce and Palsson, 2006). Two key techniques are used: microarrays (hybridation of mRNA in a matrix enclosing the corresponding complementary sequence) and RNA-Seq (high-throughput sequencing to record all transcripts) (Wang et al., 2009).
- Proteomics: identification and quantification of proteins levels encoded by the genome (Cox and Mann, 2011). The methods based on two-dimensional gel electrophoresis and mass spectrometry are the most used strategies. Proteomics is a particularly rich source of biological information because proteins are involved in almost all biological activities and they also have diverse properties, which collectively contribute greatly to our understanding of biological systems (Patterson and Aebersold, 2003).
- Metabolomics: identification and quantification of the complete set of metabolites of the cell (metabolome). The metabolome represents the output that results from the cellular integration of the transcriptome, proteome and the result of protein-DNA and protein-protein interactions. Therefore, provides not only a list of metabolite components but also a functional readout of the cellular state (Joyce and Palsson, 2006).
- Fluxomics: the total set of fluxes in the cell metabolic network. Represents the integrative information on several cellular processes, and hence there is a unique phenotypic characteristic of cells. Flux analysis provides a true dynamic picture of the phenotype capturing the metabolome in its functional interactions with the environment and the genome (Cascante and Marin, 2008).

1.4.4 Genome-scale metabolic models and constraint-based methods

Genome-scale metabolic reconstruction and their posterior analysis using constraint-based modeling have been gained enormous importance in cell metabolism study and Systems Biology (Zhang and Hua, 2016). Since the first genome scale metabolic model (GEM) for *Escherichia coli* was published in 2000 (Edwards and Palsson, 2000), GEMs have covered considerable research attention. To standardize GEMs, in 2005 it was created the first BioModels Database, providing free access to published, peer-reviewed, quantitative models of biochemical and cellular systems (Le Novere et al., 2006). The best evidence of the growing interest in GEMs is the large collection of models from today's date. BioModels currently hosts over 1200 models derived directly from the literature, as well as more than 140.000 models automatically generated from pathway resources (Path2Models) (Chelliah et al., 2015). In **Figure 1.10**, the growth of BioModels content since 2005 it is presented.

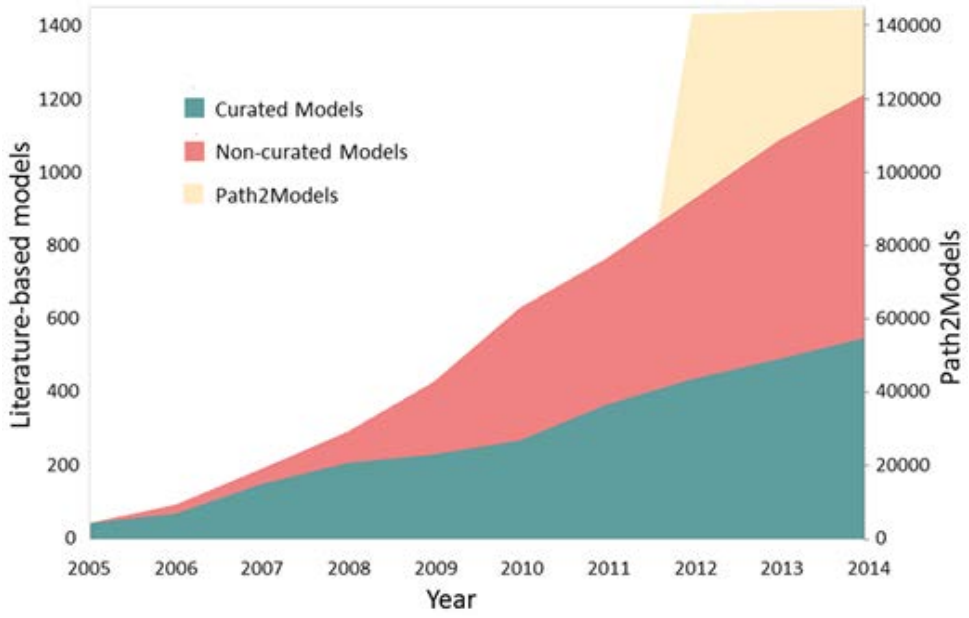

Figure 1.10: Number of models submitted to BioModels database since 2005 (Chelliah et al., 2015).

GEM are networks in which the metabolites are linked with each other by reactions, associated with enzymes encoded by genes. From the first draft of the metabolic model produced by the different tools to sequence the genome, a reconstruction must be done in order to obtain the final curated GEM. Different protocols have been published, explaining step-by-step the instructions for the model reconstruction, with special detail in these steps that are critical or difficult to be done (Santos et al., 2011). Often, the reconstruction consist in iterative and several rounds of analysis and comprehensive revalidations are required to achieve a high-quality network reconstruction (**Figure 1.11**) (Shoaie and Nielsen, 2014). This metabolic reconstruction process is usually very labor and time intensive, spanning from 6 months for well-studied, medium-sized bacterial genomes, to 2 years (and six people) for the metabolic reconstruction of human metabolism (Duarte et al., 2007; Thiele and Palsson, 2010).

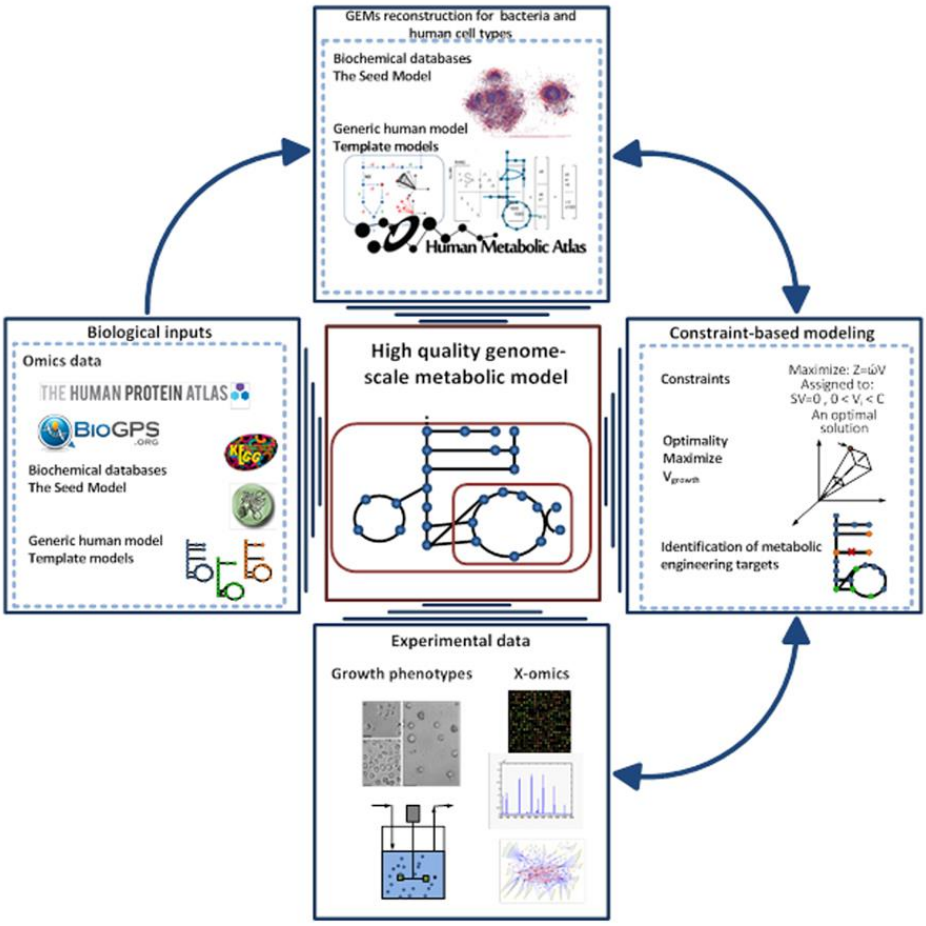

Figure 1.11: Pipeline for high-quality GEM reconstruction (Shoaie and Nielsen, 2014).

The analysis of genome-scale metabolic models, applying mass-balance and capacity constraints, is collectively named as constraint-based reconstruction and analysis (COBRA) modeling. A wide variety of COBRA methods have been developed (Price et al., 2004) and used in hundreds of research articles over the past decade (Durot et al., 2009).

The COBRA approach focuses on using physicochemical data-driven and biological constraints to enumerate the set of feasible phenotypic states of a reconstructed biological network in a given condition (**Figure 1.12**) (Schellenberger et al., 2011). Of the different COBRA methods, Flux Balance Analysis (FBA) is by far the most used for analyzing the reaction's flux in a specific network. Briefly, FBA uses linear optimization to determine the steady-state flux distribution by maximizing an objective function (Raman and Chandra, 2009). The variables used for FBA includes the fluxes through transport and metabolic reactions; as well as other model parameters as reaction stoichiometry, biomass composition, ATP requirements, and the upper and lower bounds for individual fluxes, which define the maximum and minimum allowable fluxes of the reactions in the model (Marín de Mas, 2015). Different computational packages have been developed for using COBRA methods in a simple way, in different programming languages as Matlab (COBRA Toolbox) or Python (COBRApy) (Becker et al., 2007; Ebrahim et al., 2013).

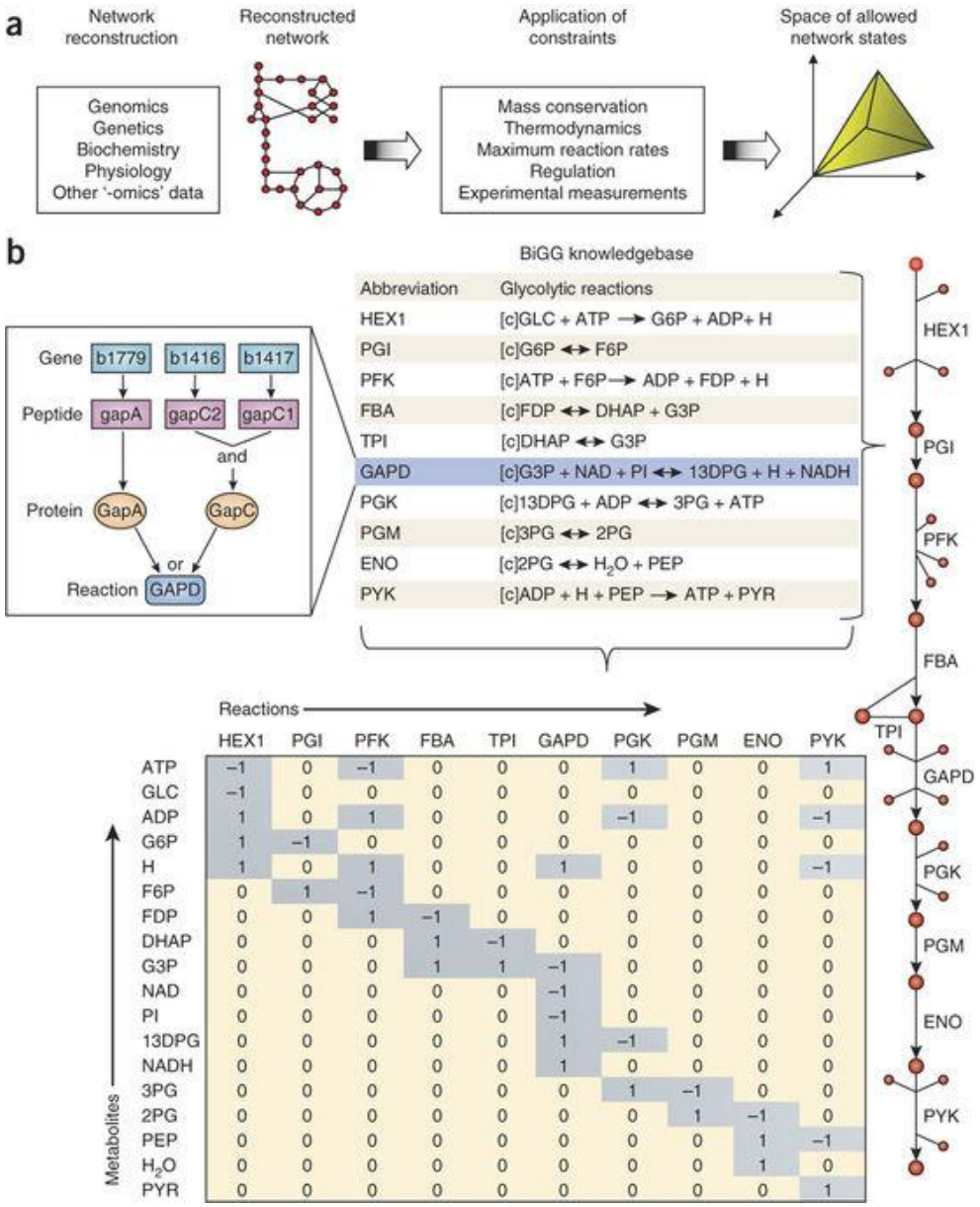

Figure 1.12: Constrained-based reconstruction and analysis of biological networks overview (Schellenberger et al., 2011).

For the work presented in the thesis, two reconstructed models have been obtained, one for each cell line, based on the corresponding genome-scale metabolic model. A constrained-based method (Flux Balance Analysis) have been perfomed for studying the core metabolism of mammalian cells in culture using the exometabolomic data obtained.

1.5 References

1. Baeshen MN, Al-Hejin AM, Bora RS, Ahmed MMM, Ramadan HAI, Saini KS, Baeshen NA, Redwan EM. 2015. Production of Biopharmaceuticals in E. coli: Current Scenario and Future Perspectives. *J. Microbiol. Biotechnol.* **25**:953–962. http://www.jmb.or.kr/journal/view.html?doi=10.4014/jmb.1412.12079.
2. Baldi L, Hacker DL, Adam M, Wurm FM. 2007. Recombinant protein production by

large-scale transient gene expression in mammalian cells: state of the art and future perspectives. *Biotechnol. Lett.* **29**:677–684. http://www.ncbi.nlm.nih.gov/pubmed/17235486.

3. Becker SA, Feist AM, Mo ML, Hannum G, Palsson BØ, Herrgard MJ. 2007. Quantitative prediction of cellular metabolism with constraint-based models: the COBRA Toolbox. *Nat. Protoc.* **2**:727–738. http://www.nature.com/articles/nprot.2007.99.
4. Butler M, Meneses-Acosta A. 2012. Recent advances in technology supporting biopharmaceutical production from mammalian cells. *Appl. Microbiol. Biotechnol.* **96**:885–894. http://link.springer.com/10.1007/s00253-012-4451-z.
5. Butler M. 2005. Animal cell cultures: recent achievements and perspectives in the production of biopharmaceuticals. *Appl. Microbiol. Biotechnol.* **68**:283–291. http://www.ncbi.nlm.nih.gov/pubmed/15834715.
6. Casablancas A, Gámez X, Lecina M, Solà C, Cairó JJ, Gòdia F. 2013. Comparison of control strategies for fed-batch culture of hybridoma cells based on on-line monitoring of oxygen uptake rate, optical cell density and glucose concentration. *J. Chem. Technol. Biotechnol.* **88**:1680–1689. http://doi.wiley.com/10.1002/jctb.4019.
7. Cascante M, Marin S. 2008. Metabolomics and fluxomics approaches. *Essays Biochem.* **45**:67–81. http://www.ncbi.nlm.nih.gov/pubmed/18793124.
8. Chelliah V, Juty N, Ajmera I, Ali R, Dumousseau M, Glont M, Hucka M, Jalowicki G, Keating S, Knight-Schrijver V, Lloret-Villas A, Natarajan KN, Pettit J-B, Rodriguez N, Schubert M, Wimalaratne SM, Zhao Y, Hermjakob H, Le Novère N, Laibe C. 2015. BioModels: ten-year anniversary. *Nucleic Acids Res.* **43**:D542–D548. http://www.ncbi.nlm.nih.gov/pubmed/25414348.
9. Chu L, Robinson DK. 2001. Industrial choices for protein production by large-scale cell culture. *Curr. Opin. Biotechnol.* **12**:180–187. https://www.sciencedirect.com/science/article/pii/S095816690000197X.
10. Covic A, Kuhlmann MK. 2007. Biosimilars: recent developments. *Int. Urol. Nephrol.* **39**:261–266. http://link.springer.com/10.1007/s11255-006-9167-5.
11. Cox J, Mann M. 2011. Quantitative, High-Resolution Proteomics for Data-Driven Systems Biology. *Annu. Rev. Biochem.* **80**:273–299. http://www.annualreviews.org/doi/10.1146/annurev-biochem-061308-093216.
12. DaSilva EJ. 2004. The colours of biotechnology: science, development and humankind. *Electron. J. Biotechnol.* **7**:1–2.
13. Dietmair S, Hodson MP, Quek L-E, Timmins NE, Gray P, Nielsen LK. 2012. A Multi-Omics Analysis of Recombinant Protein Production in Hek293 Cells. Ed. Mikael Rørdam Andersen. *PLoS One* **7**:e43394. http://dx.plos.org/10.1371/journal.pone.0043394.
14. Doran PM. 2013. Bioprocess engineering principles. Elsevier/Academic Press 919 p. https://www.sciencedirect.com/science/book/9780122208515.
15. Duarte NC, Becker SA, Jamshidi N, Thiele I, Mo ML, Vo TD, Srivas R, Palsson BØ. 2007. Global reconstruction of the human metabolic network based on genomic and bibliomic data. *Proc. Natl. Acad. Sci. U. S. A.* **104**:1777–82. http://www.ncbi.nlm.nih.gov/pubmed/17267599.
16. Durocher Y, Butler M. 2009. Expression systems for therapeutic glycoprotein production. *Curr. Opin. Biotechnol.* https://www.sciencedirect.com/science/article/pii/S0958166909001360.

17. Durot M, Bourguignon P-Y, Schachter V. 2009. Genome-scale models of bacterial metabolism: reconstruction and applications. *FEMS Microbiol. Rev.* **33**:164–190. http://www.ncbi.nlm.nih.gov/pubmed/19067749.

18. Ebrahim A, Lerman JA, Palsson BO, Hyduke DR. 2013. COBRApy: COnstraints-Based Reconstruction and Analysis for Python. *BMC Syst. Biol.* **7**:74. http://bmcsystbiol.biomedcentral.com/articles/10.1186/1752-0509-7-74.

19. Edwards JS, Palsson BO. 2000. The Escherichia coli MG1655 in silico metabolic genotype: its definition, characteristics, and capabilities. *Proc. Natl. Acad. Sci. U. S. A.* **97**:5528–33. http://www.ncbi.nlm.nih.gov/pubmed/10805808.

20. Estes S, Melville M. 2013. Mammalian Cell Line Developments in Speed and Efficiency. In: . Springer, Berlin, Heidelberg, pp. 11–33. http://link.springer.com/10.1007/10_2013_260.

21. Evens R. 2015. Product and sales data-on-file from 2014/2015 company annual reports at Tufts Center for the Study of Drug Development.

22. Fári MG, Kralovánszky UP. 2006. The founding father of biotechnology: Károly (Karl) Ereky. *Int. J. Hortic. Sci.* **12**:9–12.

23. Geisse S, Fux C. 2009. Chapter 15 Recombinant Protein Production by Transient Gene Transfer into Mammalian Cells. In: . *Methods Enzymol.*, Vol. 463, pp. 223–238. http://www.ncbi.nlm.nih.gov/pubmed/19892175.

24. Gerloff DL, Kang J. 2016. Systems Biology for 21st-Century Quantitative Scientists. *CBE—Life Sci. Educ.* **15**:fe11. https://www.lifescied.org/doi/10.1187/cbe.16-09-0275.

25. Goble C, Katalin C, Nagy Z. 2016. SYSTEMS BIOLOGY IN EUROPE 2016. https://fair-dom.org/wp-content/uploads/2016/08/Strategic-Research-Agenda-Systems-Biology-in-Europe-2016.pdf.

26. Gowder SJT ed. 2017. New Insights into Cell Culture Technology. InTech. http://www.intechopen.com/books/new-insights-into-cell-culture-technology.

27. Grabenhorst E, Schlenke P, Pohl S, Nimtz M, Conradt HS. 1999. Genetic engineering of recombinant glycoproteins and the glycosylation pathway in mammalian host cells. *Glycoconj. J.* **16**:81–97. http://www.ncbi.nlm.nih.gov/pubmed/10612409.

28. Haurwitz RE, Jinek M, Wiedenheft B, Zhou K, Doudna JA, Snijders AP, Dickman MJ, Makarova KS, Koonin E V., Oost J van der. 2010. Sequence- and Structure-Specific RNA Processing by a CRISPR Endonuclease. *Science (80-.).* **329**:1355–1358. http://www.ncbi.nlm.nih.gov/pubmed/20829488.

29. Heinzle E, Biwer AP, Cooney CL, Wiley InterScience (Online service). 2006. Development of sustainable bioprocesses : modeling and assessment. John Wiley & Sons 294 p.

30. Hu W-S, Zhou W. 2012. Cell culture bioprocess engineering 327 p. https://books.google.dk/books/about/Cell_Culture_Bioprocess_Engineering.html?id=opBfngEACAAJ&redir_esc=y.

31. Hübner K, Sahle S, Kummer U. 2011. Applications and trends in systems biology in biochemistry. *FEBS J.* **278**:2767–2857. http://doi.wiley.com/10.1111/j.1742-4658.2011.08217.x.

32. Jenkins N, Murphy L, Tyther R. 2008. Post-translational Modifications of Recombinant Proteins: Significance for Biopharmaceuticals. *Mol. Biotechnol.* **39**:113–118. http://link.springer.com/10.1007/s12033-008-9049-4.

33. Joyce AR, Palsson BØ. 2006. The model organism as a system: integrating “omics” data sets. *Nat. Rev. Mol. Cell Biol.* **7**:198–210. http://www.nature.com/articles/nrm1857.
34. Kadic E, Heindel TJ. 2014. An introduction to bioreactor hydrodynamics and gas-liquid mass transfer. https://www.wiley.com/en-us/An+Introduction+to+Bioreactor+Hydrodynamics+and+Gas+Liquid+Mass+Transfer-p-9781118104019.
35. Kafarski P. 2012. Rainbow code of biotechnology. *Chemik* **66**:811–816.
36. Kesik-Brodacka M. 2017. Progress in biopharmaceutical development. *Biotechnol. Appl. Biochem.* http://doi.wiley.com/10.1002/bab.1617.
37. Kitano H. 2002. Systems Biology: A Brief Overview. *Science (80-.).* **295**:1662–1664. http://www.sciencemag.org/cgi/doi/10.1126/science.1069492.
38. Kriete A, Eils R. 2006. Computational systems biology. Elsevier 409 p.
39. Liolios K, Mavromatis K, Tavernarakis N, Kyrpides NC. 2007. The Genomes On Line Database (GOLD) in 2007: status of genomic and metagenomic projects and their associated metadata. *Nucleic Acids Res.* **36**:D475–D479. https://academic.oup.com/nar/article-lookup/doi/10.1093/nar/gkm884.
40. Marín de Mas IB. 2015. Development and application of novel model-driven and data-driven approaches to study metabolism in the framework of systems medicine. http://diposit.ub.edu/dspace/handle/2445/65987.
41. Le Novere N, Bornstein B, Broicher A, Courtot M, Donizelli M, Dharuri H, Li L, Sauro H, Schilstra M, Shapiro B, Snoep JL, Hucka M. 2006. BioModels Database: a free, centralized database of curated, published, quantitative kinetic models of biochemical and cellular systems. *Nucleic Acids Res.* **34**:D689–D691. https://academic.oup.com/nar/article-lookup/doi/10.1093/nar/gkj092.
42. Nurse P, Hayles J. 2011. The Cell in an Era of Systems Biology. *Cell* **144**:850–854. https://www.cell.com/cell/pdf/S0092-8674(11)00235-2.pdf.
43. Overton TW. 2014. Recombinant protein production in bacterial hosts. *Drug Discov. Today* **19**:590–601. http://linkinghub.elsevier.com/retrieve/pii/S1359644613004029.
44. Palsson B. 2006. Systems biology : properties of reconstructed networks. Cambridge University Press 322 p. http://www.cambridge.org/gb/academic/subjects/life-sciences/genomics-bioinformatics-and-systems-biology/systems-biology-properties-reconstructed-networks?format=HB&isbn=9780521859035#QRQkVcEsYolAmQQh.97.
45. Patterson SD, Aebersold RH. 2003. Proteomics: the first decade and beyond. *Nat. Genet.* **33**:311–323. http://www.nature.com/doifinder/10.1038/ng1106.
46. van der Pol L, Tramper J. 1998. Shear sensitivity of animal cells from a culture-medium perspective. *Trends Biotechnol.* **16**:323–8. http://www.ncbi.nlm.nih.gov/pubmed/9720320.
47. Price ND, Reed JL, Palsson BØ. 2004. Genome-scale models of microbial cells: evaluating the consequences of constraints. *Nat. Rev. Microbiol.* **2**:886–897. http://www.ncbi.nlm.nih.gov/pubmed/15494745.
48. Ram PT, Mendelsohn J, Mills GB. 2012. Bioinformatics and systems biology. *Mol. Oncol.* **6**:147–154. http://doi.wiley.com/10.1016/j.molonc.2012.01.008.
49. Raman K, Chandra N. 2009. Flux balance analysis of biological systems: applications and challenges. *Brief. Bioinform.* **10**:435–449. https://academic.oup.com/bib/article-

lookup/doi/10.1093/bib/bbp011.

50. Russo E. 2003. Special Report: The birth of biotechnology. *Nature* **421**:456–457. http://www.nature.com/doifinder/10.1038/nj6921-456a.
51. Sanchez-Garcia L, Martín L, Mangues R, Ferrer-Miralles N, Vázquez E, Villaverde A. 2016. Recombinant pharmaceuticals from microbial cells: a 2015 update. *Microb. Cell Fact.* **15**:33. http://www.ncbi.nlm.nih.gov/pubmed/26861699.
52. Santos F, Boele J, Teusink B. 2011. A Practical Guide to Genome-Scale Metabolic Models and Their Analysis. *Methods Enzymol.* **500**:509–532. https://www.sciencedirect.com/science/article/pii/B9780123851185000244?via%3Dihub.
53. Schellenberger J, Que R, Fleming RMT, Thiele I, Orth JD, Feist AM, Zielinski DC, Bordbar A, Lewis NE, Rahmanian S, Kang J, Hyduke DR, Palsson BØ. 2011. Quantitative prediction of cellular metabolism with constraint-based models: the COBRA Toolbox v2.0. *Nat. Protoc.* **6**:1290–1307. http://www.nature.com/doifinder/10.1038/nprot.2011.308.
54. Shoaie S, Nielsen J. 2014. Elucidating the interactions between the human gut microbiota and its host through metabolic modeling. *Front. Genet.* **5**:86. http://journal.frontiersin.org/article/10.3389/fgene.2014.00086/abstract.
55. Sijbesma F, Schepens H. 2003. White biotechnology: gateway to a more sustainable future. *en línia]. Eur. www. Eur. org*.
56. Smith JE. 2009. Biotechnology. Cambridge: Cambridge University Press. http://ebooks.cambridge.org/ref/id/CBO9780511802751.
57. Thiele I, Palsson BØ. 2010. A protocol for generating a high-quality genome-scale metabolic reconstruction. *Nat. Protoc.* **5**:93–121. http://www.nature.com/articles/nprot.2009.203.
58. Walsh G. 2014. Biopharmaceutical benchmarks 2014. *Nat. Biotechnol.* **32**:992–1000. http://www.nature.com/articles/nbt.3040.
59. Walsh G, Jefferis R. 2006. Post-translational modifications in the context of therapeutic proteins. *Nat. Biotechnol.* **24**:1241–1252. http://www.ncbi.nlm.nih.gov/pubmed/17033665.
60. Wang Z, Gerstein M, Snyder M. 2009. RNA-Seq: a revolutionary tool for transcriptomics. *Nat. Rev. Genet.* **10**:57–63. http://www.nature.com/articles/nrg2484.
61. Watson JD, Crick FHC. 1953. Molecular Structure of Nucleic Acids: A Structure for Deoxyribose Nucleic Acid. *Nature* **171**:737–738. http://www.nature.com/doifinder/10.1038/171737a0.
62. Zhang C, Hua Q. 2016. Applications of Genome-Scale Metabolic Models in Biotechnology and Systems Medicine. *Front. Physiol.* **6**:413. http://journal.frontiersin.org/Article/10.3389/fphys.2015.00413/abstract.

CHAPTER 2. OBJECTIVES

The work presented in the thesis have been developed into the Cellular and Bioprocess Engineering Group, which the main objective is the development, optimization and scaling up bioprocess based on different organisms, but specially on mammalian cell lines. In particular, this work is focused on the study and improvement of biopharmaceuticals production in two mammalian cell lines: one widely used by the industry (CHO) and other that are becoming increasingly used for its promising capabilities (HEK293). The aim of the thesis is first to study the metabolism of both cell lines in culture and then apply this knowledge to design new control systems for obtaining higher cell densities in culture.

This main objective can be divided in the following sub-sections:

- Present the physiology of the different glucose and lactate metabolisms in CHO/HEK293 cell cultures.
- Study the metabolism by Metabolic Flux Analysis of the different glucose and lactate metabolisms presented in CHO/HEK293.
- Implement a new monitoring system based on the alkali buffer addition to estimate the biomass concentration in HEK293 cell cultures. Comparison with a widely used method as dynamic Oxygen Uptake Rate measurement.
- Develop a new control system to optimize the feeding in HEK293 fed-batch cell cultures based on the monitoring tool previously implemented.
- Develop a new control system to optimize the feeding based the pH variations in HEK293 perfusion cell cultures.
- Develop a new simple and non-invasive Oxygen Uptake Rate measurement to overcome the limitations of the dynamic method.

CHAPTER 3. RESULTS (I) PHISIOLOGY OF DIFFERENT GLUCOSE/LACTATE METABOLISMS IN HEK293/CHO CELL CULTURES

Abstract

The purpose of this chapter is to present the different glucose-lactate metabolism of HEK293 and CHO cell lines cultured in both Shake-Flasks and Bioreactor, depending on the pH-control and extracellular lactate concentration.

Mammalian cells show an inefficient metabolism characterized by high rates of glucose consumption and lactate secretion, a well-known growth inhibitor by-product. Recently, we have observed that under certain culture conditions, both HEK293 and CHO cells are able to co-metabolize glucose and lactate, even during the exponential growth phase. Extracellular pH and lactate concentration appears to be the key factor to trigger the metabolic shift from glucose consumption and lactate production to lactate and glucose concomitant consumption.

HEK293 and CHO cell lines showed different metabolic behavior when cultured in Shake-Flasks compared to pH-controlled Bioreactors. In pH-controlled cultures in Bioreactor, an initial phase where glucose uptake and lactate production was observed (Phase 1). Once glucose was depleted from the media, a second phase in which only lactate was consumed with a significant growth rate decrease was obtained (Phase 3). In non pH-controlled cultures in Shake-Flasks, Phase 1 was also reproduced at the beginning of the culture, but then a second phase in which glucose and lactate are simultaneously consumed was triggered (Phase 2), maintaining the same growth rate in CHO and a slightly lower growth rate in HEK293. In other words, a metabolic shift from glucose consumption/lactate production to glucose and lactate co-consumption was observed when pH was non-controlled in the cultures. In this context, identically metabolic behavior was obtained in non pH-controlled Bioreactor cell cultures compared as the ones in Shake-Flasks, showing that the metabolic switch was triggered when pH dropped to 6.8, due to the lactate generation.

The hypothesis proposed for triggering this metabolic shift to lactate and glucose concomitant consumption is that HEK293/CHO cells metabolize extracellular lactate as a response to extracellular protons and lactate accumulation, by means of co-transporting extracellular protons together with lactate into the cytosol. To demonstrate this, glucose and lactate co-consumption was reproduced in Bioreactor from the onset of the culture in CHO cell cultures when adding lactate to the initial media and setting the pH at 6.8. As far as we know, such metabolism observed at early stages of culture and in exponentially growing cells has never been reported before for CHO cells.

Nomenclature

q_m: specific consumption/production rate of the metabolite m (nmols·10^6cells $^{-1}$·h^{-1}) or (nmols·mg_{DW}^{-1}·h^{-1})
C_{O_2}: oxygen concentration in the liquid phase (mmols·L^{-1})
$C_{m,0}$: concentration of the metabolite m at time t_0 (mmols·L^{-1})
C_m: concentration of the metabolite m (mmols·L^{-1})
D.O.: relative oxygen concentration in the liquid phase in respect to the air saturation in equilibrium (%)
K_{des}: O_2 desorption constant in N_2 (headspace) (h^{-1})
$X_{v,0}$: viable cell concentration at time t_0 (10^6cells·mL^{-1})
X_v: viable cell concentration (10^6cells·mL^{-1})
k_d: glutamine descomposition rate (h^{-1})
r_X: growth rate (10^6cells·mL^{-1}·h^{-1})
r_m: consumption/production rate of the metabolite m (mmols·L^{-1}·h^{-1})
μ_{max}: maximum specific growth rate (h^{-1})
D_{time}: duplication time of the cells in culture (h)
O.U.R.: oxygen uptake rate (mmols·L^{-1}·h^{-1})
t: time (h)
Xv_{max}: maximum viable cell density reached in the culture (10^6cells·mL^{-1})

3.1 Introduction

A large fraction of proteins for both diagnostic and therapeutic applications are produced with Chinese hamster ovary (CHO) cells (Walsh, 2010; Wurm, 2004). Some of the advantages of CHO cells are 1) their capability to fold and make human-compatible post-translational modifications on recombinant proteins, 2) they can be grown in suspension cultures using chemically defined media maintaining a stable metabolism for long periods in cultivation (Huang et al., 2010; Xu et al., 2011), and 3) high titers of protein of interest can be reached (about 3-10 g/L) (Editors, 2007). Nevertheless, HEK293 cells has been gaining importance during the last decade, due to its capacity to perform some post-transitional modifications that other widely used cell lines, as CHO cells, perform inadequately (Durocher and Butler, 2009). The increasing interest of industries for HEK293-based bioprocesses has moved their applications from viral vector expression for gene therapy (Delenda et al., 2007; Liste-Calleja et al., 2014; Somia and Verma, 2000) to protein expression (Dumont et al., 2016; Román et al., 2016), in which human glycosylation patterns are needed (Durocher and Butler, 2009).

One of the most important limitation of both HEK293 and CHO, as other mammalian cell lines, cell-based processes is their inefficient metabolism, characterized by the consumption of large quantities of glucose and the concomitant production of large quantities of lactate (widely known as the Warburg effect), a by-product widely reported to inhibit cell growth (Hassell et al., 1991; Ozturk et al., 1992).

Due to the adverse effects of lactate accumulation on cell growth, big efforts have been performed to reduce its accumulation in mammalian cell cultures. The use of alternative carbon

sources to glucose, like fructose or galactose (Altamirano et al., 2000; Altamirano et al., 2001) and media optimization in terms of amino acids composition (Xing et al., 2011) has been reported to reduce lactate formation, but resulting in a significant lowering of growth rate. An alternative for reducing lactate production consisting in keeping low glucose concentration in culture has been demonstrated in continuous cultures (Cruz et al., 1999; Europa et al., 2000). Moreover, different fed-batch strategies limiting glucose concentration have been performed to this end obtaining significantly reduction of lactate formation in culture (Casablancas et al., 2013; Zhang et al., 2004).

Alternatively, several efforts in the field of cell engineering have been done to in order to reduce significantly lactate production. Suppressing of main carbon sugar membrane transporters (Wlaschin and Hu, 2007), expression of pyruvate carboxylase in the cytoplasm for restoring the link between glycolysis and TCA (Henry and Durocher, 2011; Irani et al., 1999) and down-regulating lactate dehydrogenase (Chen et al., 2001; Kim and Lee, 2007) have been reported in order to reduce lactate formation. However, while in some specific cases lactate formation was somehow reduced, it has never been completely suppressed.

Interestingly, it has also been reported that on certain conditions mammalian cells are able to switch to a different carbon metabolism in which lactate is consumed instead of being produced. Nonetheless, in such cases lactate consumption appears in non-growing phases of cell cultures. (Martínez et al., 2013), observed lactate consumption in CHO cells when glucose was completely depleted during the plateau phase of cultures.

Even more interesting is a different lactate metabolism that consists in simultaneous consumption of glucose and lactate. Zagari et al., 2013 and Wahrheit et al., 2014 glucose and lactate concomitant consumption in CHO cells at the end of the exponential growth phase when glutamine was depleted from medium. Additionally, glucose and lactate concomitant consumption has also been reported in late stages of fed-batch cultures, but again cell growth followed a linear profile, what indicates a cell growth limitation (Ahn and Antoniewicz, 2011; Mulukutla et al., 2012; Pascoe et al., 2007).

Li et al., 2012 observed that after feeding exogenous lactate in CHO cell cultures and replacing CO_2 by lactic acid for pH control, led to a reduction of ammonia and pCO_2 accumulation. To go beyond, Gagnon et al., 2011 applied a feed strategy based on pH control in CHO fed-batch cultures in order to suppress the lactate accumulation. A metabolic analysis to study the correlation between copper and the lactate metabolic shift in chemically defined medium was carried out by Luo et al., 2012 with two CHO different cell lines, indicating that the lactate metabolic shift is related to the cells oxidative metabolic capacity.

Up recently, we have observed a different glucose and lactate concomitant consumption metabolic behavior in HEK293 and CHO cultures (Liste-Calleja et al., 2015). Under certain culture conditions both cell lines are able to co-metabolize glucose and lactate simultaneously, remaining in the exponential growth phase, resulting in more efficient substrate consumption (more efficient carbon usage). Lactate consumption could also be triggered at will by modifying culture conditions, based on keeping pH below 6.8 and adding exogenous lactate to the medium

(Liste-Calleja et al., 2015). Ivarsson et al., 2015 found that NS0 cells were also able to consume lactate in presence of glucose, keeping pH below 6.8, but in this case it resulted in a significantly reduction of the growth rate.

3.2 Materials and Methods

3.2.1 Cell lines and cell maintenance

The cell lines used in this work were HEK293SF-3F6 cell line kindly provided by Dr. A. Kamen (National Research Council of Canada) which was obtained as reported before (Côté et al., 1998); and FreeStyle™ CHO-S Cells (Invitrogen, Thermo Scientific). Both cell lines were cultured in 125 mL polycarbonate shake flask (Corning Inc.) with a working volume of 12 mL incubated in a 5% CO_2 air mixture and in a humidified atmosphere at 37ºC (Steri-cult 2000 Incubator, Forma Scientific). Flasks were continuously agitated at 110 rpm on an orbital shaking platform (Stuart SSL110 Incubator, Forma Scientific). Cultures were passaged every 2 or 3 days using a seeding density of $3.0 \cdot 10^5$ cells·mL^{-1}.

3.2.2 Cell media

Cell media used for the experiments and for cell maintenance of HEK293 cells were SFMTransFx-293 (HyClone, Thermo Scientific), supplemented with 4 mM GlutaMAX (Gibco, Life Technologies, NY, USA), 5 % (v/v) FBS (Sigma Aldrich, MO, USA), and 10 % (v/v) of Cell Boost 5 solution (80 g·L^{-1}) (HyClone, Thermo Scientific, UT, USA).

The basal medium used for all experiments and cell maintenance of CHO cells was CD OptiCHO™ (Gibco, Life Technologies), supplemented with 8 mM of GlutaMAX (Gibco, Life Technologies), 50 ppm Antifoam C Emulsion (Sigma Aldrich) and 2 g·L^{-1} Kolliphor® P 188 (Sigma Aldrich).

For the experiment in which concomitant glucose and lactate consumption was triggered from the beginning of the culture with CHO, exogenous lactate was added to the initial medium using a stock solution of Sodium Lactate, $NaC_3H_5O_3$ 1.6M (Panreac), in MilliQ water and sterile filtered, to obtain an initial concentration of 15mM in the Bioreactor. Medium pH was adjusted into the Bioreactor using a sterile stock solution of HCl 0.5M (Panreac) in MilliQ water.

3.2.3 Shake flasks culturing platform

For Shake flasks experiments, HEK293 and CHO cell line was inoculated at the desired cell density in 250-mL polycarbonate shake flask (Corning Inc.) with 50-mL of working volume following the same conditions that those described in cell maintenance. Sampling volume was about 1000 µL.

3.2.4 Bioreactor and operational conditions

Bioreactor cell cultures were performed in a Biostat Bplus (Sartorius Stedim Biotech), equipped with a 2L cylindrical vessel. Dissolved oxygen concentration was measured with an optical probe (VisiFerm DO, Hamilton) and maintained at 30% of saturation by a gas mix air/oxygen unit and an aeration flow fixed at 0.175 vvm. pH was measured with a standard electrode (EasyFerm Plus,

Hamilton). For all the experiments, a 5% CO_2 set-point in the gas-mixing was fixed and maintained during the culture. For the experiment in which pH was set at 6.8 from the beginning of the culture, the pH was controlled by using a stock solution of HCl 0.5M (Panreac).

Temperature was maintained at 37ºC, the stirrer was equipped with two marine impellers and the stirrer speed was set at 80 rpm (HEK293) and 100 rpm (CHO). In pH controlled experiments, the pH was set at 7.1 (HEK293) and 7.2 (CHO). Sampling volume was about 5 mL.

3.2.5 Analytical methods

Cell number

Cell number was determined by manual counting using a Neubauer hemocytometer and a phase contrast microscope (Nikon eclypse, TS100). Cell viability was determined by the Trypan blue dye exclusion method (1:1 mixture of a 0.2% Trypan blue (Gibco, Life Technologies)).

Metabolites concentration

Sample was previously centrifuged at 3000 g for 3 min (Spectrafuge) and the supernatant was filtered using a 0.22 µm filter (Merck Millipore) to remove the cells and cell debris. Glucose and lactate concentration were determined using an automatic glucose and lactate analyzer (YSI, Yellow Springs Instruments, 2700 Select). Amino acids and ammonia analysis were necessary to perform further flux analysis. Ammonium was measured with an automatic enzymatic test analyzer (Biosystems Y15).

Amino acids and GlutaMAX concentrations were determined by HPLC using post-column derivation method in a PEEK manufactured column with cation-exchange resin (Ultropac, polystyrene/divinylbenzene sulfonate) 5 µm, 200x4 mm (Biochrm LTd.). Derivatized amino acids were detected colorimetrically at 570 and 440 nm wavelengths.

3.2.6 Oxygen uptake rate (O.U.R.)

Determination of the oxygen uptake rate (O.U.R) was necessary to determine the specific oxygen consumption (qO_2) for further flux analysis presented in Chapter 4. O.U.R. was performed applying the dynamic method. In short, D.O. (dissolved oxygen, relative oxygen concentration in the liquid phase in respect to the air saturation in equilibrium (%)) is initially increased over 60% of air saturation. Afterwards, air supply is stopped and a N_2 flow (0.075 vvm) is introduced into the Bioreactor headspace in order to obtain an oxygen-free gas phase and to avoid any oxygen transport back to the culture medium. O.U.R. calculation was performed from the decreasing profile between 60 and 30% of air saturation. The N_2 inlet into the headspace drives oxygen desorption from the liquid that has been previously determined and considered in the mass balance equation through the desorption constant, K_{des}. To convert D.O. into absolute oxygen concentration (C_{O2}), the oxygen solubility was considered constant during the culture and equal to 0.194 mmol/L (Higareda et al., 1997; Miller et al., 1988; Ramirez and Mutharasan, 1990). As shown in **Equation 3.1**, the dissolved oxygen concentration decreases due to both the respiratory activity of cells (first factor) and to the oxygen desorption from the

liquid phase to the gas phase of the Bioreactor (second factor). When D.O. drops below 30%, N_2 gas inflow is stopped and dissolved oxygen control resumed again. The specific methodology used in this work is detailed somewhere else (Lecina et al., 2006) and the O.U.R. measurements were conducted with a lapse time of 6 hours.

$$O.U.R. = \frac{C_{O_2}(t_0) - C_{O_2}(t_f)}{t_f - t_0} + \frac{\int_{t_0}^{t_f}(-K_{des} \cdot C_{O_2}(t)) \cdot dt}{t_f - t_0} \qquad [3.1]$$

3.2.7 Specific rates calculations

Cell growth rate can be expressed by **Equation 3.2**. The maximum specific growth rate (μ_{max}) was calculated in the exponential growth phase from the **Equation 3.3**.

$$\frac{dX_v}{dt} = r_X = \mu_{max} \cdot X_v \qquad [3.2]$$

$$\ln(X_v) = \ln(X_{v,0}) + \mu_{max} \cdot (t - t_0) \qquad [3.3]$$

The consumption/production rate for glucose and lactate is expressed in **Equation 3.4** for each metabolite. The specific consumption/production rate (q_m) was calculated from the **Equation 3.5** (by integration and rearrangement of **Equations 3.2** and **3.4**).

$$\frac{dC_m}{dt} = r_m = q_m \cdot 10^{-3} \cdot X_v \qquad [3.4]$$

$$C_m = C_{m,0} + \frac{q_m \cdot 10^{-3} \cdot X_{v,0}}{\mu_{max} \cdot e^{\mu_{max} \cdot t_0}} \cdot [e^{\mu_{max} \cdot t} - e^{\mu_{max} \cdot t_0}] \qquad [3.5]$$

As previously described by Lin and Agrawal, 1988, glutamine spontaneously decomposes to form ammonia following first-order kinetics. The consumption rate for glutamine and the production rate for ammonia are expressed by **Equations 3.6** and **3.7**, where the decomposition rate (k_d) has been evaluated in identical experimental conditions of this work, obtaining a value of $3.45 \cdot 10^{-3}$ h^{-1}.

$$\frac{dC_{Glutm}}{dt} = r_{Glutm} = q_{Glutm} \cdot 10^{-3} \cdot X_v - k_d \cdot C_{Glutm} \qquad [3.6]$$

$$\frac{dCNH_4^+}{dt} = r_{NH_4^+} = q_{NH_4^+} \cdot 10^{-3} \cdot X_v + k_d \cdot C_{Glutm} \qquad [3.7]$$

The specific consumption rate for glutamine (q_{Glutm}) and specific production rate for ammonia (q_{NH4+}) were calculated integrating and rearranging **Equations 3.6** and **3.7**, using Laplace transform, obtaining the **Equations 3.8** and **3.9**.

$$C_{Glutm} = C_{Glutm,0} \cdot e^{-k_d \cdot t} + \frac{q_{Glutm} \cdot 10^{-3} \cdot X_{v,0}}{k_d + \mu_{max}} \cdot [e^{\mu_{max} \cdot t} - e^{-k_d \cdot t}] \qquad [3.8]$$

$$CNH_4{}^+ = CNH_4{}^+{}_0 + \left[\frac{q_{Glutm} \cdot 10^{-3} \cdot X_{v,0}}{k_d + \mu_{max}} - C_{Glutm,0}\right] \cdot [e^{-k_d \cdot t} - 1] + \frac{X_{v,0}}{\mu_{max}} \cdot \left[q_{NH_4{}^+{}_0} \cdot 10^{-3} + \frac{q_{Glutm} \cdot 10^{-3} \cdot k_d}{k_d + \mu_{max}}\right] \cdot [e^{\mu_{max} \cdot t} - 1] \quad [3.9]$$

3.3 Results

3.3.1 Comparison of experiments in Shake-Flasks and in pH-controlled Bioreactor with HEK293 and CHO cells

Two different experiments were performed in non pH-controlled Shake-Flasks (working volume of 50 mL) and in 2L Bioreactor under pH-controlled conditions with HEK293 and CHO cells. The evolution of macroscopic variables (Viable cell concentration, Viability, pH (Bioreactor), Glucose and Lactate concentration) are depicted in **Figure 3.1** and **3.2** for HEK293 and CHO cell lines respectively.

As observed in Shake-Flasks experiments (**Figure 3.1-A and 3.2-A**), clearly, two different glucose-lactate metabolisms can be distinguished. Glucose and lactate concentration evolution showed an initial phase of glucose consumption and lactate generation, onwards known as Phase 1 (P1_SF), followed by a metabolic shift to co-consumption of glucose and lactate remaining in a similar growth rate, onwards known as Phase 2 (P2_SF). It is worth to point out that all growth phases analyzed have a high cell viability (>90%). Therefore, cells showed an active metabolic state.

Nevertheless, cells cultured in a pH-controlled Bioreactor (**Figure 3.1-B and 3.2-B**) did not show comparable behavior since no metabolic shift was observed, as pH was kept constant throughout the culture. This situation led to a constant glucose uptake and lactate accumulation. Consequently, two different metabolic phases were observed for HEK293 and CHO cells. Phase 1 was also observed (P1_B1), where glucose was consumed, and large amounts of lactate was produced. Once glucose was depleted from the media, another metabolic phase in which only lactate was consumed with a significant growth rate decrease was obtained (P3_B1), onwards known as the Phase 3.

The results presented above show that as a consequence of leaving pH free in the Shake-Flasks cell cultures, a second phase in which glucose and lactate were simultaneously consumed remaining in exponential growth was triggered. This metabolism is very interesting from a production point of view as lactate is widely known to be a growth inhibitor in cell culture (lactate was being consumed instead of being produced).

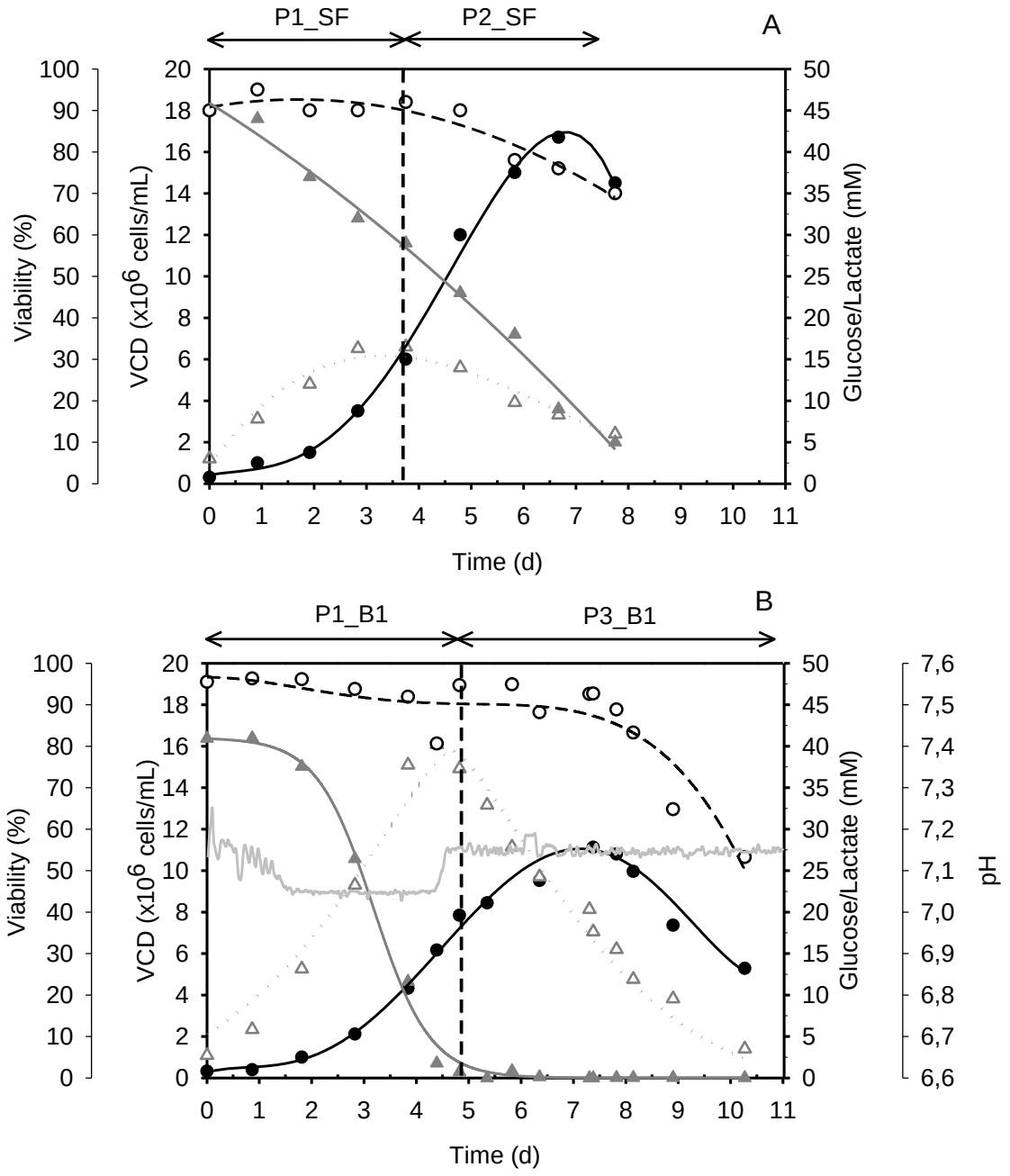

Figure 3.1: Batch cultures of HEK293 cells in a Shake-Flasks (A) and 2-L Bioreactor (B) under pH-controlled conditions at 7.1 by means of CO_2 sparing, alkali or acid buffer addition depending on the needs. Evolution profiles for cell density (●), viability (○), glucose concentration (▲), lactate concentration (△) and pH (—).

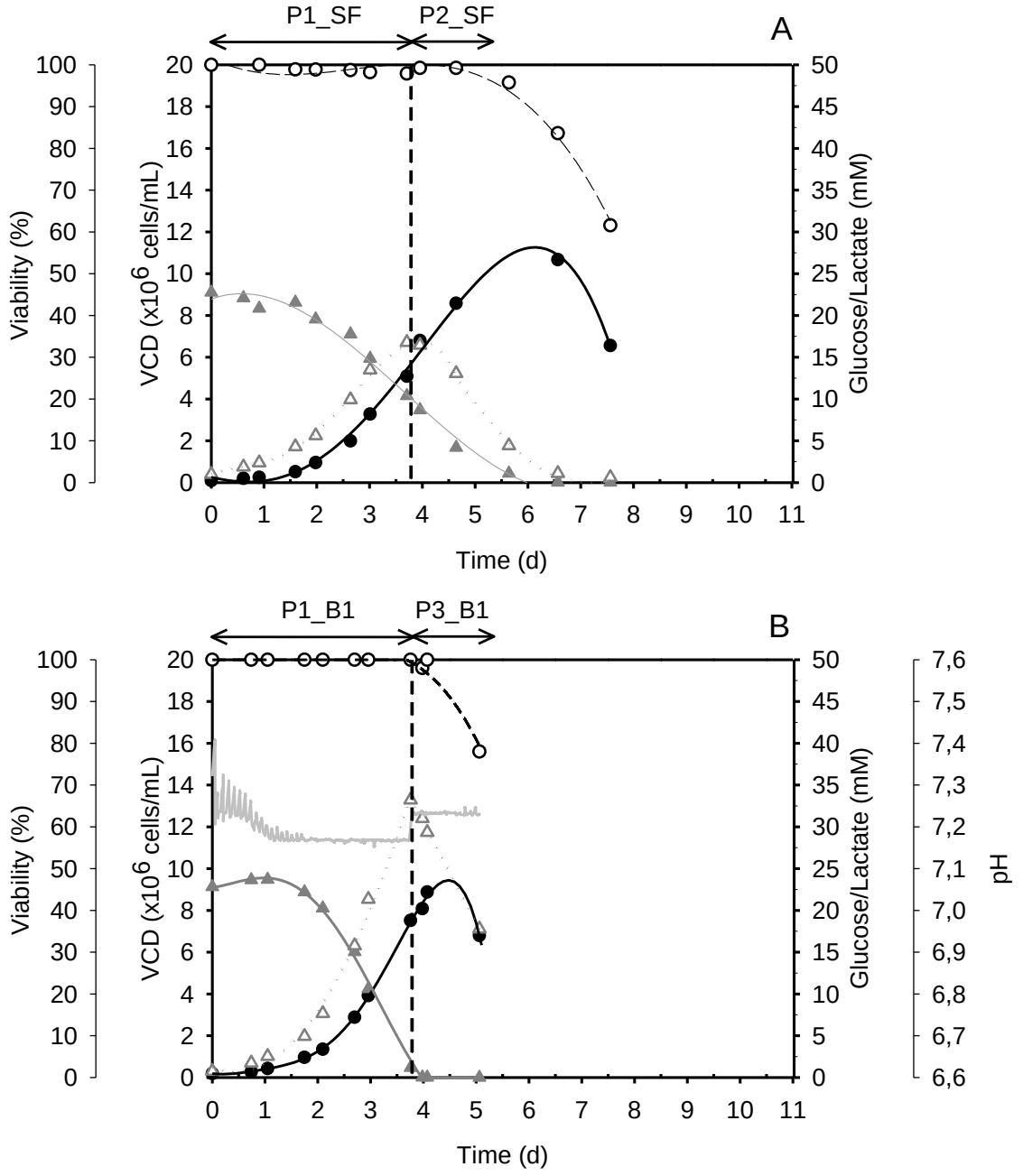

Figure 3.2: Batch cultures of CHO cells in a Shake-Flasks (A) and 2-L Bioreactor (B) under pH-controlled conditions at 7.2 by means of CO_2 sparing, alkali or acid buffer addition depending on the needs. Evolution profiles for cell density (●), viability (○), glucose concentration (▲), lactate concentration (△) and pH (—).

3.3.2 Experiments in non pH-controlled Bioreactor with HEK293 and CHO cells

In order to confirm the effect of pH in triggering the metabolic shift in HEK293 and CHO cell lines observed in Shake-Flasks, analog 2-L Bioreactor experiments were performed, switching off the pH control as detailed in Materials and Methods section. The evolution of macroscopic variables (Viable cell concentration, Viability, pH (Bioreactor), Glucose and Lactate concentration) are depicted in **Figure 3.3** and **3.4** for HEK293 and CHO cell lines respectively.

In this case, Bioreactor cultured cells behaved identically as the ones cultured in Shake-Flasks, by obtaining both metabolic phases 1 and 2. Phase 1 was reproduced until pH dropped to 6.8 due to lactate accumulation. When pH dropped below 6.8, due to acid lactic secretion and accumulation, Phase 2 was identified, in which concomitant consumption of glucose and lactate was observed even during the exponential growth phase.

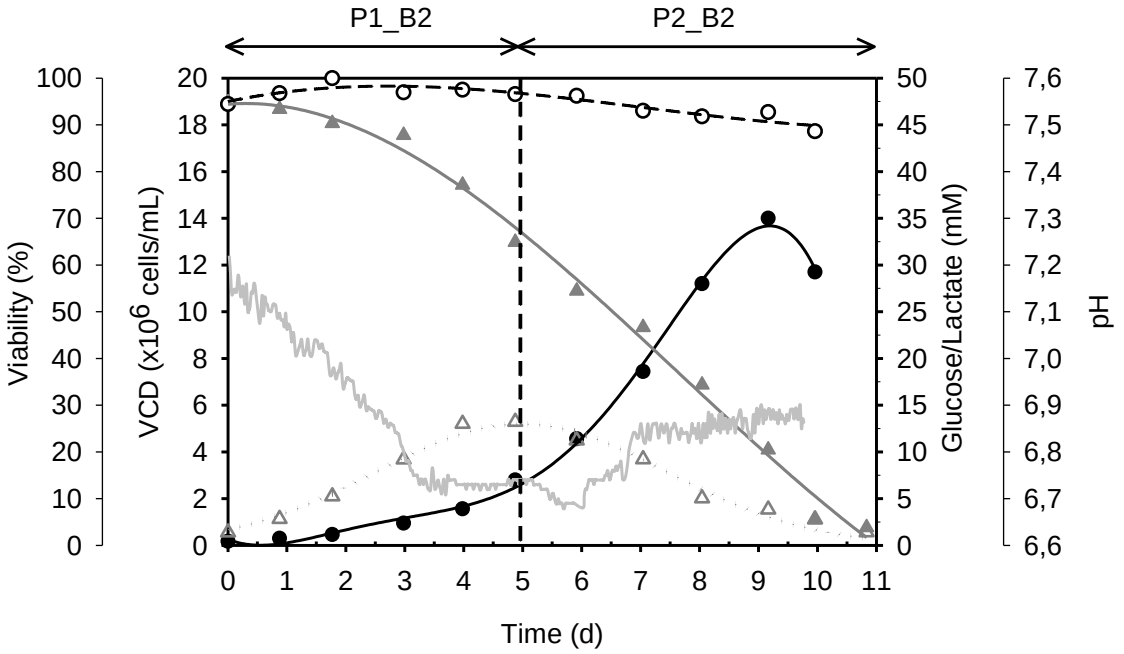

Figure 3.3: Batch culture of HEK293 cells in a 2-L Bioreactor with free evolution of pH (only a constant flow of CO_2 was constantly injected into the Bioreactor, as detailed in materials and methods section). Evolution profiles for cell density (●), viability (○), glucose concentration (▲), lactate concentration (△) and pH (⎯).

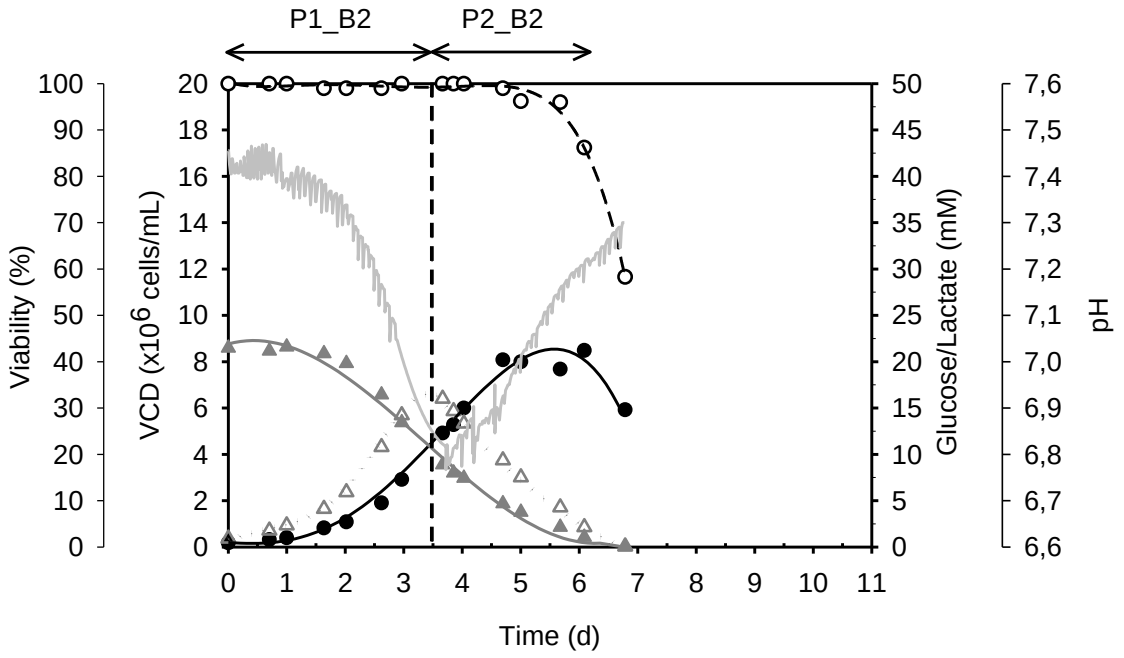

Figure 3.4: Batch culture of CHO cells in a 2-L Bioreactor with free evolution of pH (only a constant flow of CO_2 was constantly injected into the Bioreactor, as detailed in materials and methods section). Evolution profiles for cell density (●), viability (○), glucose concentration (▲), lactate concentration (△) and pH (—).

What becomes clear from the results obtained in controlled and non pH-controlled experiments is the ability of the HEK293 and CHO cell lines to both secrete and utilize lactate depending of the external conditions of the cell culture. Moreover, lactate can be consumed both simultaneously with glucose and as a solely carbon source, but only when lactate was being consumed together with glucose (Phase 2) cells could growth exponentially, and none growth was observed when lactate was consumed as a sole carbon source (Phase 3 in both cell lines). In respect of simultaneous glucose and lactate consumption phase, both the pH culture as well as the external lactate concentration in the media seem to be the key factors for triggering the metabolic switch from lactate secretion to lactate consumption together with glucose.

3.3.3 Concomitant glucose and lactate consumption from the beginning of CHO culture in Bioreactor

An experiment to trigger simultaneous glucose and lactate consumption at will was performed in Bioreactor with CHO cell line (**Figure 3.5**), with the aim to get the Phase 2 from the beginning of the culture. To that purpose, considering the results obtained in experiments in which pH were not controlled in the Bioreactor (**Figure 3.4**), lactate must be present in the media and the pH must keep below 6.80. Wherefore, exogenous sodium lactate was added to the initial media to obtain an initial concentration of 15 mM (the same concentration when the second phase starts in non-controlled pH Bioreactor) and the pH was dropped and maintained to 6.80 through the addition of an acid buffer solution. In this case, the second phase in which glucose and

lactate were simultaneous consumed (P2_B3) was obtained from the beginning of the culture in exponentially growth phase.

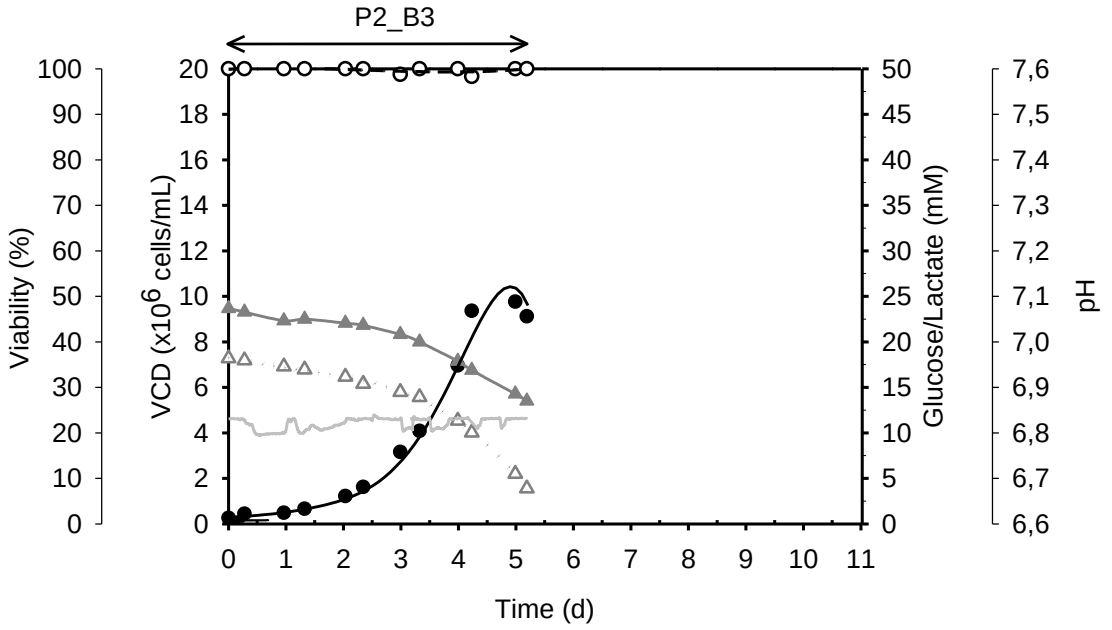

Figure 3.5: Batch culture of CHO cells in a 2-L Bioreactor in pH-controlled at 6.8 by means of CO_2 sparing and acid buffer addition depending on the needs and adding 15 mM of sodium lactate in the initial media. Evolution profiles for cell density (●), viability (○), glucose concentration (▲), lactate concentration (△) and pH (grey line without markers).

3.3.4 Growth parameters and discussion for the different glucose/lactate metabolic phases in HEK293/CHO

For a deeper discussion, a summary of the main cell growth and metabolic parameters obtained from the different experiments performed with HEK293 and CHO is presented in **Table 3.1**. A similar behavior in respect to the different metabolic phases were obtained for both cell lines, but different values were achieved in respect of growth rate depending on the phase considered.

The values obtained for maximum specific growth rate in Phase 1 (P1_SF/P1_B1/P1_B2) and in Phase 2 for the CHO cell line when glucose and lactate at triggered from the beginning (P2_B3) were very similar. That means that can be obtained exponentially growth also in Phase 2 when glucose and lactate are simultaneously consumed. Thus, the decrease in the growth rate observed in Phase 2 in non pH-controlled experiments both in Shake-Flasks and Bioreactor (P2_SF/P2_B2) was not due to the metabolic switch and it could be related to some metabolite depletion in the media.

By contrast, for HEK293 significant differences in maximum specific growth rates were obtained comparing Phase 1 of pH and non pH-controlled experiments. The growth rate was reduced of 39.5% in Phase 1 of non-pH controlled (P1_B2) in respect of Phase 1 pH-controlled experiments in Bioreactor (P1_B1). More notable was the reduction obtained in Phase 2 when pH was not controlled (P2_B2). It is also worth noting that in CHO similar maximum viable cells has been reached in both experiments, but in HEK293 an increment of 25.9% has been obtained in non pH-controlled experiment in Bioreactor. In Phase 3 in pH-controlled Bioreactor (P3-B1) non-growth or very low growth was observed for both cell lines.

A significant difference in terms of glucose and lactate specific consumption/production rate was observed in the different experiments performed. In agreement with the exposed above, glucose uptake rates were reduced of 22.9% in HEK293/39.0% in CHO and 64.4% in HEK293/31.2% in CHO for lactate production rates in Phase 1 in non-controlled pH experiments in Bioreactor (P1_B2) compared with the experiments in which pH was controlled (P1_B1). In other words, as pH is lower the lactate secretion rate was reduced, provoking a drop in glucose consumption.

More interesting is the fact that when lactate was consumed together with glucose in Phase 2, the glucose uptake rate was reduced of 92.2% in HEK293/87.2% in CHO compared with Phase 1 in controlled pH culture and 90.2% in HEK293/79.0% in CHO compared with Phase 1 in non-controlled pH, and lactate was consumed instead of being produced. From a global point of view these results indicate that a redistribution of cell metabolic fluxes has occurred in the second phase in both cell lines, and that is very interesting from the production point of view, because cells are still growing exponentially.

In terms of the cause of the pH dropping and rising in the experiments performed, it is widely known that proton-linked monocarboxylate transporters (MCTs) are largely the responsible for the lactate secretion/utilization trough the cell membrane, and the capacity of these carriers are very high (Halestrap and PRICE, 1999; Poole and Halestrap, 1993). These transporters enable the facilitated diffusion of lactate together with a proton. This leads to a protons released when lactate is being excreted and a proton income when lactate is being consumed, causing the culture pH changes depending on the metabolic phase of the cells.

In the first phase of both cell lines, where pH was not controlled, lactate was being secreted to external media together with protons due to the lactate proton symport transport, causing the pH drop observed in cell culture. In respect of the second phase, when pH was non-controlled, the pH raises due to the protons consumption together with lactate. In the first phase obtained in pH-controlled Bioreactor, to maintain the pH at the fixed set-point, the protons secretion was neutralized with the addition of an alkali buffer solution by means of the Bioreactor pH controller (data not shown).

		Shake-Flasks		pH-controlled		Non pH-controlled		pH-controlled + 15mM $NaC_3H_5O_3$
		P1_SF	P2_SF	P1_B1	P3_B1	P1_B2	P2_B2	P2_B3
		Phase 1	Phase 2	Phase 1	Phase 3	Phase 1	Phase 2	Phase 2
HEK293	Xv_{max} (10^6 cells·mL^{-1})	16.640		11.120		14.000		-
	μ_{max} (h^{-1})	0.032	0.014	0.038	0.005	0.023	0.015	-
	D_{time} (h)	21.648	48.772	18.241	138.629	30.137	46.210	-
	$q_{glucose}$ (nmols·mg_{DW}^{-1}·h^{-1})	-510.422	-74.654	-760.000	-53.000	-600.000	-59.000	-
	$q_{lactate}$ (nmols·mg_{DW}^{-1}·h^{-1})	461.651	-32.675	995.000	-1.700	354.000	-79.000	-
CHO	Xv_{max} (10^6 cells·mL^{-1})	10.667		8.880		8.080		9.760
	μ_{max} (h^{-1})	0.047	0.021	0.044	-	0.039	0.020	0.038
	D_{time} (h)	14.877	32.484	15.816	-	17.959	34.187	18.403
	$q_{glucose}$ (nmols·mg_{DW}^{-1}·h^{-1})	-360.279	-60.867	-562.288	-	-343.120	-71.808	-77.573
	$q_{lactate}$ (nmols·mg_{DW}^{-1}·h^{-1})	547.510	-87.068	807.303	-156.366	555.290	-80.395	-87.608

Table 3.1 Summary of the growth parameters related to cell physiology calculated from experiments performed with HEK293 and CHO cell lines.

3.4 Conclusions

Three different glucose and lactate metabolisms have been obtained in the different experiments performed with for HEK293 and CHO cells in Shake-Flasks and Bioreactor, captured in the three phases mentioned above (Phase 1: glucose consumption and lactate production (exponentially growth), Phase 2: glucose and lactate simultaneous consumption (exponentially growth), and Phase 3: lactate consumption as a sole carbon source (no cell growth)).

These different metabolic phases were observed mainly depending on two cell culture conditions: the pH and the lactate concentration in the culture media. When pH was controlled in the Bioreactor, Phase 1 appeared at the beginning of the culture, but when glucose was depleted Phase 3 was obtained. In contrast, when pH was leaved free both in Shake-Flasks and Bioreactor, Phase 1 was obtained but when pH dropped below 6.80, due to lactic acid secretion, the Phase 2 appeared, both in exponentially growth phase.

More interesting is the fact that Phase 2 can be triggered at will by adding lactate to the initial media and keeping pH below 6.80 (experiment done with CHO cell line). As far as we know, any experiment in which glucose and lactate simultaneous consumption is obtained from the beginning of the culture has been reported for mammalian cells in the literature. It is worth to point that for CHO Phase 2, in which glucose and lactate were simultaneously consumed, was obtained maintaining the maximum growth rate observed in Phase 1. On the contrary,t in HEK293 a significant growth decrease was obtained. In contrast, an increment of 25.9% of final viable cell concentration was obtained for HEK293 in non pH-controlled experiment compared with the one in which pH was controlled. For CHO similar cell density was reached for both experiments.

The lactate shift from production phase to net lactate consumption and its use as carbon source has clearly been linked to the depletion of glucose in the case of pH-controlled Bioreactor. This fact has extensively been described in the literature (Gagnon et al., 2011; Kuwae et al., 2005; Zagari et al., 2013). In the present work, in non pH-controlled experiments, a net lactate consumption was observed in spite of significant glucose concentration. The lactate metabolism shift from Phase 1 to Phase 2 was observed when lactate concentration was around 15mM and pH lower than 6.8. In other words, a concomitant consumption of glucose and lactate was detected in a second phase of non pH-controlled cultures, while a sequential consumption of glucose and afterwards lactate was observed in pH-controlled cultures.

This new behavior observed in which glucose and lactate are simultaneous consumed in HEK293/CHO cells could open a door to re-direct genetic engineering strategies in order to obtain more efficient cell lines and also to further develop animal cell technology applications.

In order to gain a deeper insight in the cell metabolic redistribution due to the effects of environmental conditions, as a preliminary step before applying more advanced experimental techniques (13C-labeling experiments, multi-omics), in the following chapter we performed a metabolic flux balance analysis for HEK293 and CHO of the different phases presented above.

3.5 References

1. Ahn WS, Antoniewicz MR. 2011. Metabolic flux analysis of CHO cells at growth and non-growth phases using isotopic tracers and mass spectrometry. *Metab. Eng.* **13**:598–609. http://www.ncbi.nlm.nih.gov/pubmed/21821143.
2. Altamirano C, Illanes A, Casablancas A, Gamez X, Cairo JJ, Godia C. 2001. Analysis of CHO Cells Metabolic Redistribution in a Glutamate-Based Defined Medium in Continuous Culture. *Biotechnol. Prog.* **17**:1032–1041. http://doi.wiley.com/10.1021/bp0100981.
3. Altamirano C, Paredes C, Cairo JJ, Godia F. 2000. Improvement of CHO Cell Culture Medium Formulation: Simultaneous Substitution of Glucose and Glutamine. *Biotechnol. Prog.* **16**:69–75. http://doi.wiley.com/10.1021/bp990124j.
4. Casablancas A, Gámez X, Lecina M, Solà C, Cairó JJ, Gòdia F. 2013. Comparison of control strategies for fed-batch culture of hybridoma cells based on on-line monitoring of oxygen uptake rate, optical cell density and glucose concentration. *J. Chem. Technol. Biotechnol.* **88**:1680–1689. http://doi.wiley.com/10.1002/jctb.4019.
5. Chen K, Liu Q, Xie L, Sharp PA, Wang DIC. 2001. Engineering of a mammalian cell line for reduction of lactate formation and high monoclonal antibody production. *Biotechnol. Bioeng.* **72**:55–61. http://doi.wiley.com/10.1002/1097-0290%2820010105%2972%3A1%3C55%3A%3AAID-BIT8%3E3.0.CO%3B2-4.
6. Côté J, Garnier A, Massie B, Kamen A. 1998. Serum-free production of recombinant proteins and adenoviral vectors by 293SF-3F6 cells. *Biotechnol. Bioeng.* **59**:567–575. http://doi.wiley.com/10.1002/%28SICI%291097-0290%2819980905%2959%3A5%3C567%3A%3AAID-BIT6%3E3.0.CO%3B2-8.
7. Cruz HJ, Moreira JL, Carrondo MJ. 1999. Metabolic shifts by nutrient manipulation in continuous cultures of BHK cells. *Biotechnol. Bioeng.* **66**:104–13. http://www.ncbi.nlm.nih.gov/pubmed/10567068.
8. Delenda C, Chillon M, Douar A-M, Merten O-W. 2007. Cells for Gene Therapy and Vector Production. In: . Humana Press, pp. 23–91. http://link.springer.com/10.1007/978-1-59745-399-8_2.
9. Dumont J, Euwart D, Mei B, Estes S, Kshirsagar R. 2016. Human cell lines for biopharmaceutical manufacturing: history, status, and future perspectives. *Crit. Rev. Biotechnol.* **36**:1110–1122. https://www.tandfonline.com/doi/full/10.3109/07388551.2015.1084266.
10. Durocher Y, Butler M. 2009. Expression systems for therapeutic glycoprotein production. *Curr. Opin. Biotechnol.* https://www.sciencedirect.com/science/article/pii/S0958166909001360.
11. Editors BI. 2007. The Evolution of Protein Expression and Cell Culture. http://www.biopharminternational.com/evolution-protein-expression-and-cell-culture.
12. Europa AF, Gambhir A, Fu PC, Hu WS. 2000. Multiple steady states with distinct cellular metabolism in continuous culture of mammalian cells. *Biotechnol. Bioeng.* **67**:25–34. http://www.ncbi.nlm.nih.gov/pubmed/10581433.
13. Gagnon M, Hiller G, Luan Y-T, Kittredge A, DeFelice J, Drapeau D. 2011. High-End pH-controlled delivery of glucose effectively suppresses lactate accumulation in CHO Fed-

batch cultures. *Biotechnol. Bioeng.* **108**:1328–1337. http://doi.wiley.com/10.1002/bit.23072.

14. Halestrap AP, PRICE NT. 1999. The proton-linked monocarboxylate transporter (MCT) family: structure, function and regulation. *Biochem. J.* **343**:281–299.
15. Hassell T, Gleave S, Butler M. 1991. Growth inhibition in animal cell culture. *Appl. Biochem. Biotechnol.* **30**:29–41. http://link.springer.com/10.1007/BF02922022.
16. Henry O, Durocher Y. 2011. Enhanced glycoprotein production in HEK-293 cells expressing pyruvate carboxylase. *Metab. Eng.* **13**:499–507. https://www.sciencedirect.com/science/article/pii/S109671761100053X.
17. Higareda AE, Possani LD, Ramírez OT. 1997. The use of culture redox potential and oxygen uptake rate for assessing glucose and glutamine depletion in hybridoma cultures. *Biotechnol. Bioeng.* **56**:555–563. http://doi.wiley.com/10.1002/%28SICI%291097-0290%2819971205%2956%3A5%3C555%3A%3AAID-BIT9%3E3.0.CO%3B2-H.
18. Huang Y-M, Hu W, Rustandi E, Chang K, Yusuf-Makagiansar H, Ryll T. 2010. Maximizing productivity of CHO cell-based fed-batch culture using chemically defined media conditions and typical manufacturing equipment. *Biotechnol. Prog.* **26**:1400–1410. http://doi.wiley.com/10.1002/btpr.436.
19. Irani N, Wirth M, van den Heuvel J, Wagner R. 1999. Improvement of the primary metabolism of cell cultures by introducing a new cytoplasmic pyruvate carboxylase reaction. *Biotechnol. Bioeng.* **66**:238–246. http://doi.wiley.com/10.1002/%28SICI%291097-0290%281999%2966%3A4%3C238%3A%3AAID-BIT5%3E3.0.CO%3B2-6.
20. Ivarsson M, Noh H, Morbidelli M, Soos M. 2015. Insights into pH-induced metabolic switch by flux balance analysis. *Biotechnol. Prog.* **31**:347–357. http://doi.wiley.com/10.1002/btpr.2043.
21. Kim SH, Lee GM. 2007. Down-regulation of lactate dehydrogenase-A by siRNAs for reduced lactic acid formation of Chinese hamster ovary cells producing thrombopoietin. *Appl. Microbiol. Biotechnol.* **74**:152–159. http://link.springer.com/10.1007/s00253-006-0654-5.
22. Kuwae S, Ohda T, Tamashima H, Miki H, Kobayashi K. 2005. Development of a fed-batch culture process for enhanced production of recombinant human antithrombin by Chinese hamster ovary cells. *J. Biosci. Bioeng.* **100**:502–510. https://www.sciencedirect.com/science/article/pii/S1389172305705016.
23. Lecina M, Soley A, Gràcia J, Espunya E, Lázaro B, Cairó JJ, Gòdia F. 2006. Application of on-line OUR measurements to detect actions points to improve baculovirus-insect cell cultures in bioreactors. *J. Biotechnol.* **125**:385–394. https://www.sciencedirect.com/science/article/pii/S0168165606002112.
24. Li J, Wong CL, Vijayasankaran N, Hudson T, Amanullah A. 2012. Feeding lactate for CHO cell culture processes: Impact on culture metabolism and performance. *Biotechnol. Bioeng.* **109**:1173–1186. http://doi.wiley.com/10.1002/bit.24389.
25. Lin A, Agrawal P. 1988. Glutamine decomposition in DMEM: Effect of pH and serum concentration. *Biotechnol. Lett.* **10**:695–698. http://link.springer.com/10.1007/BF01025284.

26. Liste-Calleja L, Lecina M, Cairó JJ. 2014. HEK293 cell culture media study towards bioprocess optimization: Animal derived component free and animal derived component containing platforms. *J. Biosci. Bioeng.* **117**:471–477. https://www.sciencedirect.com/science/article/pii/S1389172313003551.
27. Liste-Calleja L, Lecina M, Lopez-Repullo J, Albiol J, Solà C, Cairó JJ. 2015. Lactate and glucose concomitant consumption as a self-regulated pH detoxification mechanism in HEK293 cell cultures. *Appl. Microbiol. Biotechnol.* **99**:9951–9960. http://link.springer.com/10.1007/s00253-015-6855-z.
28. Luo J, Vijayasankaran N, Autsen J, Santuray R, Hudson T, Amanullah A, Li F. 2012. Comparative metabolite analysis to understand lactate metabolism shift in Chinese hamster ovary cell culture process. *Biotechnol. Bioeng.* **109**:146–156. http://doi.wiley.com/10.1002/bit.23291.
29. Martínez VS, Dietmair S, Quek L-E, Hodson MP, Gray P, Nielsen LK. 2013. Flux balance analysis of CHO cells before and after a metabolic switch from lactate production to consumption. *Biotechnol. Bioeng.* **110**:660–666. http://doi.wiley.com/10.1002/bit.24728.
30. Miller WM, Blanch HW, Wilke CR. 1988. A kinetic analysis of hybridoma growth and metabolism in batch and continuous suspension culture: Effect of nutrient concentration, dilution rate, and pH. *Biotechnol. Bioeng.* **32**:947–965. http://doi.wiley.com/10.1002/bit.260320803.
31. Mulukutla BC, Gramer M, Hu W-S. 2012. On metabolic shift to lactate consumption in fed-batch culture of mammalian cells. *Metab. Eng.* **14**:138–149. https://www.sciencedirect.com/science/article/pii/S1096717611001285.
32. Ozturk SS, Riley MR, Palsson BO. 1992. Effects of ammonia and lactate on hybridoma growth, metabolism, and antibody production. *Biotechnol. Bioeng.* **39**:418–431. http://doi.wiley.com/10.1002/bit.260390408.
33. Pascoe DE, Arnott D, Papoutsakis ET, Miller WM, Andersen DC. 2007. Proteome analysis of antibody-producing CHO cell lines with different metabolic profiles. *Biotechnol. Bioeng.* **98**:391–410. http://doi.wiley.com/10.1002/bit.21460.
34. Poole RC, Halestrap AP. 1993. Transport of lactate and other monocarboxylates across mammalian plasma membranes. *Am. J. Physiol. Physiol.* **264**:C761–C782. http://www.physiology.org/doi/10.1152/ajpcell.1993.264.4.C761.
35. Ramirez OT, Mutharasan R. 1990. Cell cycle- and growth phase-dependent variations in size distribution, antibody productivity, and oxygen demand in hybridoma cultures. *Biotechnol. Bioeng.* **36**:839–848. http://doi.wiley.com/10.1002/bit.260360814.
36. Román R, Miret J, Scalia F, Casablancas A, Lecina M, Cairó JJ. 2016. Enhancing heterologous protein expression and secretion in HEK293 cells by means of combination of CMV promoter and IFNα2 signal peptide. *J. Biotechnol.* **239**:57–60. https://www.sciencedirect.com/science/article/pii/S0168165616315541.
37. Somia N, Verma IM. 2000. Gene therapy: trials and tribulations. *Nat. Rev. Genet.* **1**:91–99. http://www.nature.com/doifinder/10.1038/35038533.
38. Wahrheit J, Niklas J, Heinzle E. 2014. Metabolic control at the cytosol–mitochondria interface in different growth phases of CHO cells. *Metab. Eng.* **23**:9–21. https://www.sciencedirect.com/science/article/pii/S109671761400007X.

39. Walsh G. 2010. Biopharmaceutical benchmarks 2010. *Nat. Biotechnol.* **28**:917–924. http://www.nature.com/articles/nbt0910-917.

40. Wlaschin KF, Hu W-S. 2007. Engineering cell metabolism for high-density cell culture via manipulation of sugar transport. *J. Biotechnol.* **131**:168–176. https://www.sciencedirect.com/science/article/pii/S0168165607004233.

41. Wurm FM. 2004. Production of recombinant protein therapeutics in cultivated mammalian cells. *Nat. Biotechnol.* **22**:1393–1398. http://www.nature.com/articles/nbt1026.

42. Xing Z, Kenty B, Koyrakh I, Borys M, Pan S-H, Li ZJ. 2011. Optimizing amino acid composition of CHO cell culture media for a fusion protein production. *Process Biochem.* **46**:1423–1429. https://www.sciencedirect.com/science/article/pii/S1359511311001218.

43. Xu X, Nagarajan H, Lewis NE, Pan S, Cai Z, Liu X, Chen W, Xie M, Wang W, Hammond S, Andersen MR, Neff N, Passarelli B, Koh W, Fan HC, Wang J, Gui Y, Lee KH, Betenbaugh MJ, Quake SR, Famili I, Palsson BO, Wang J. 2011. The genomic sequence of the Chinese hamster ovary (CHO)-K1 cell line. *Nat. Biotechnol.* **29**:735–741. http://www.nature.com/articles/nbt.1932.

44. Zagari F, Jordan M, Stettler M, Broly H, Wurm FM. 2013. Lactate metabolism shift in CHO cell culture: the role of mitochondrial oxidative activity. *N. Biotechnol.* **30**:238–245. https://www.sciencedirect.com/science/article/pii/S1871678412001239.

45. Zhang L, Shen H, Zhang Y. 2004. Fed-batch culture of hybridoma cells in serum-free medium using an optimized feeding strategy. *J. Chem. Technol. Biotechnol.* **79**:171–181. http://doi.wiley.com/10.1002/jctb.940.

CHAPTER 4. RESULTS (II) METABOLIC FLUX BALANCE ANALYSIS FOR THE DIFFERENT GLUCOSE/LACTATE METABOLISMS IN KEK293 AND CHO CELL CULTURES

Abstract

The different glucose and lactate metabolisms observed for HEK293 and CHO cells has been presented in the previous chapter, showing that under certain culture conditions, both cell lines are able to co-metabolize glucose and lactate, even during the exponential growth phase.

In order to perform a deeper study of the different phases presented, as well as to understand the triggering to glucose and lactate concomitant consumption, an analysis of the intracellular flux distribution is presented for both cell lines. In this context, the different glucose/lactate metabolic phases have been characterized for the first time in HEK293 and CHO cells by means of Flux Balance Analysis (FBA), using a reconstruction of genome-scale metabolic model.

HEK293 and CHO cells metabolize extracellular lactate as a response to both extracellular protons and lactate accumulation, by means of co-transporting them (extracellular protons and lactate) into the cytosol. At this point, there exists a considerable controversy about how lactate reaches the mitochondrial matrix: the first hypothesis proposes that lactate is converted into pyruvate in the cytosol, and afterwards, pyruvate enters the mitochondria; the second alternative considers that lactate enters first into the mitochondria, and then, is converted into pyruvate. In this chapter, lactate transport and metabolization into mitochondria is shown to be feasible, as evidenced by means of respirometry tests with isolated active HEK293 mitochondria, and the evolution of lactate concentration of the respirometry suspension.

Although the capability of lactate metabolization by isolated mitochondria is demonstrated, the possibility of lactate being converted into pyruvate in the cytosol cannot be excluded from the discussion. For this reason, the calculation of the metabolic fluxes for both cell lines was performed for the different metabolic phases, considering both hypothesis.

One of the objectives of this work is to evaluate the redistribution of cell's metabolism and compare the differences or similarities between the phases before and after the metabolic shift of HEK293 and CHO cells (shift observed when pH is not controlled). That is from a glucose consumption/lactate production phase to a glucose-lactate co-consumption phase.

In this context, FBA confirmed that in phase 1, pyruvate generated through glycolysis is converted to lactate to fulfill the NADH regeneration requirements in the cytoplasm and only a small amount of pyruvate is introduced into TCA through Acetyl-CoA. Lactate is then secreted to the extracellular media. Differently, in glucose-lactate concomitant consumption (Phase 2), glucose uptake was significantly reduced up to 4-5 folds. Thus, a balance between glycolysis and TCA cycle fluxes was reached yielding to a more efficient substrate consumption, since all pyruvate generated is metabolized in the TCA.

A deeper knowledge on such metabolism in which glucose and lactate are simultaneous consumed in HEK293/CHO cells could help to design new engineered cell lines or cell culture strategies with the aim of obtaining more efficient bioprocesses for mammalian cell technology applications.

Nomenclature

q_m: specific consumption/production rate of the metabolite m (nmols·10^6cells^{-1}·h^{-1}) or (nmols·mg_{DW}^{-1}·h^{-1})
X_v: viable cell concentration (10^6cells·mL^{-1})
qO_2: specific oxygen consumption rate ($nmol_{O2}$·10^6cells^{-1}·h^{-1}) or (nmols·mg_{DW}^{-1}·h^{-1})
A: stoichiometric matrix with (*m*,*r*) dimensions (*m*: metabolites and *r*: reactions)
D.O.: relative oxygen concentration in the liquid phase in respect to the air saturation in equilibrium (%)
f: vector of reaction fluxes (r rows for reactions) (nmols·10^6cells^{-1}·h^{-1}) or (nmols·mg_{DW}^{-1}·h^{-1})
f_r: flux of reaction r (nmols·10^6cells^{-1}·h^{-1}) or (nmols·mg_{DW}^{-1}·h^{-1})
O.U.R.: oxygen uptake rate (mmols·L^{-1}·h^{-1})
q: vector of specific consumption/production rate for each metabolite (*m* rows for metabolites) (nmols·10^6cells^{-1}·h^{-1}) or (nmols·mg_{DW}^{-1}·h^{-1})
$\alpha_{(m,r)}$: stoichiometric coefficient of metabolite *m* in the reaction *r*

4.1 Introduction

Achievement of optimal productivity and yields in bioprocess using living cells generally requires redirection of cellular metabolic activity. The metabolism of the native organism is rarely optimized for its process application, because the bioreactor conditions are significantly different from the natural environment wher the cells used to be (i.e. levels of carbon, nitrogen and energy sources). Thus, metabolism has to be studied in order to find the bottlenecks susceptible of modification.

This optimization can be done by means of external operational strategies related to bioprocess engineering (nutrient feeding, co-substrate metabolism, two or more stages, operation modes…) and/or internal manipulations of the metabolic pathways by means of metabolic engineering strategies. Biological engineers have been practicing, for a long time, environmental (i.e. external) manipulation by choosing operating conditions to improve cell growth and productivity. Nowadays more rational internal manipulations than random mutagenesis and selection can be performed using recent developments in genetic technology (Lee et al. 2015).

In order to perform a rational management of external or internal variables, the patterns of metabolic regulation have to be known. It is well recognized that metabolic fluxes are key variables that must be determined in order to perform such a work. Thus, their quantitative analysis is a useful tool for the investigation of cell physiology.

In the last years the knowledge of the biochemical pathways and the complete genome sequence has been used to build stoichiometric models for several mammalian cell lines (Altamirano et al., 2006; Bonarius et al., 1996; Martínez et al., 2013; Paredes et al., 1998; Quek et al., 2010). Metabolic models allow to quantitatively describe the steady-state flux distributions of the cellular metabolic network. Since metabolic transients are typically rapid, cell growth can be considered as a succession of pseudo-steady states (Vallino and Stephanopoulos, 1993). This includes bioprocess situations in which the process variables rate

of change is much slower than those associated with metabolism (Henry et al., 2005; Martínez et al., 2013; Sellick et al., 2011; Zupke et al., 1995). Application of optimization strategies using constraint based metabolic models (Savinell and Palsson, 1992) allow to estimate the cellular metabolic flux distribution.

From a physiological point of view, along the exponential growth phase, both HEK293 and CHO cell cultures typically produce lactate, ammonia and some amino acids when metabolizing the carbon and energy sources, glucose and glutamine. In batch cell cultures, the secretion and accumulation of lactate as a by-product of glucose metabolism is an important limitation. Harmful effects of lactate and ammonia accumulation have extensively been documented. Among them cell growth inhibition, protein expression efficiency decrease (Cruz et al., 1999; Martinelle et al., 1996; Ozturk et al., 1992), and alteration of protein glycosylation patterns (Andersen and Goochee, 1995; Yang and Butler, 2000) are the most relevant. The reason for the secretion of lactate is that only a small amount of pyruvate generated through the glycolytic pathway enters to the Tricarboxylic acid cycle (TCA). Consequently, NADH regeneration has to be done in the cytoplasm, with the concomitant production of high amounts of lactate which is eventually secreted to the culture broth.

The fluxes obtained with this approach become the starting point of cell metabolism understanding. Three different phases were observed in both HEK293 and CHO cells batch cultures depending on the culture conditions, namely glucose consumption/lactate production, lactate consumption as a sole carbon and energy source and, the most interesting from the physiological point of view, glucose and lactate co-consumption phase.

The objective of this chapter is to evaluate the redistribution of cell's metabolism for the different phases in order to define both potential genetic modifications of the cell line and to define new bioprocess strategies. This will allow the control of cell metabolism in order to extend cell growth and product generation, two of the main parameters to be considered when optimizing bioprocesses.

4.2 Materials and Methods

4.2.1 Operational conditions of experiments performed and metabolite analysis

The cell lines, media and maintenance as well as operational conditions in the different experiments performed in the Bioreactor were detailed in the Materials and Methods section in chapter 3. The experiments performed in that chapter were used to performed flux analysis. The metabolite analysis necessary for performing such flux analysis were also presented in the previous chapter.

The oxygen specific consumption rate (qO_2) can be obtained through the slope resulting from the direct representation of O.U.R. values versus the concentration of viable cells, as presented in **Equation 4.1**.

$$\frac{dO_2}{dt} = O.U.R. = qO_2 \cdot X_v \cdot 10^{-3} \quad [4.1]$$

4.2.2 Mitochondria isolation and Respirometry assay

The Mitochondrial isolation kit for cultured cells (Thermo Scientific, UT, USA) based on reagent A method was used for HEK293 cells mitochondria isolation following the manufacturer's instructions. Mitochondria were isolated from a HEK293 cells cultured in the same media described before. Cells were harvested when cell concentration was about $4 \cdot 10^6$ cell·mL^{-1} and were centrifuged at 850g for 2 minutes, and then, the Thermo Fisher protocol was followed. Importantly, the whole procedure was performed at 4 ºC in pre-cooled centrifuge tubes and the incubation steps were carried out in ice. After the last step indicated by the manufacturer, the pellet was resuspended in 150 µL of incubation buffer (IB) and stored at 4ºC until performing the respirometry assay. The incubation buffer composition was (for 100 mLMilli-AQwater): Mannitol 4.10 g (225 mM), Sucrose 2.57 g (75 mM), EDTA 29.22 mg (1 mM), HEPES 119.15 mg (5 mM), BSA 100 mg (1 mg·ml^{-1}), KCl until pH is 7.4.

The respirometry assay was performed within the following 4 hours after mitochondria isolation was completed. Before respirometry, protein quantification was performed by means of Bradford method (Bradford, 1976). Mitochondrial protein concentration was within the range 40-80 mg·mL^{-1}.

Preparation of the mitochondrial pool (mitochondria suspended in isolation buffer) was done by diluting the sample to approximately 200-500 µg·mL^{-1} in respiration buffer. This buffer composition was as follows (for 100 mL MilliQwater): Mannitol 218.60 mg (12 mM), Sucrose 1.54 g (45 mM), EDTA 29.22 mg (7 mM), Tris-HCl 30.29 mg (25 mM), MgCl2 47.61 mg (5 mM), K2HPO4 261.30 mg (15 mM), KH2PO4 204.13 mg (15 mM), KCl 111.83 mg (15 mM), BSA 0.2 mg (0.2% p/v).

Lactate, pyruvate or α-cyano-4-hydroxycinnamicacid (CINN, Sigma-Aldrich, MO, USA), a MCT (monocarboxylate transporter) blocking agent, were added to the respiration buffer (previously tempered) containing the mitochondria pool. Oxygen was measured with an oxygen probe (Waveport DCU) hermetically fitted to the lid of the sample container. Lactate concentration evolution profile was determined in parallel in duplicate experiments using an enzymatic analyzer YSI (Yellow Springs Instrument, 2700 Select, US, OH).

4.2.3 HEK293 Metabolic Model

The HEK293 metabolic model was derived from the last reconstruction published for the *Homo sapiens* RECON2.2 (Swainston et al., 2016). The RECON2.2 consists in the most complete and best annotated consensus of human metabolic reconstruction available from Biomodels database.

The model contains 5324 metabolites and 7785 reactions, and this implies that cells have access to all functionality encoded by the genome, which is not realistic from the point of view of the cell culture. The metabolic model was reduced following the protocol performed by Quek (Quek et al., 2014) for adaptation of the RECON2.0 (Thiele et al., 2013) model for HEK293 cells. Thus, in a first step Quek revised RECON2 correcting minor bugs and the resulting model is available

from Biomodels database (MODEL1504080000; Li et al., 2010). In a second step Quek adapted the resulting model to the specific context of HEK293 cell culture.

A few additional adaptations and constraint modifications were performed to further adapt this model to our experimental conditions. Namely, to allow for Glutamax metabolization, gluconeogenesis when lactate alone was consumed and allowing for active mitochondrial lactate transport and metabolization. It must be stressed that the mitochondrial lactate metabolization capacities were already present in the initial model and only directional constraints were modified. The resulting model, that contains 354 reactions and 335 metabolites, used for the metabolic flux calculation is detailed in ***Appendix A***.

4.2.4 CHO Metabolic Model

The CHO metabolic model used in this study was derived from the reduced model obtained from a generic *Mus musculus* genome-scale metabolic model (Quek and Nielsen, 2008). The reduced model was first developed by Quek et al., 2010 and afterwards used by Martínez et al., 2013; and is free available in Systems Biology Markup Language (SBML) format in the supplementary files of the second publication (two models are available, one for each metabolic state studied).

Both models available do not contain the biomass equation because the authors maximized the ATP yield as objective function. Therefore, a biomass equation was developed based on the literature, as presented in detail in ***Appendix B***. For this purpose, the detailed method published by Oliveira et al., 2005 was followed due to it gives an extensive and useful account of the data and computation that is required. The chemical composition of cells in culture was obtained first for the biomass general composition and then for macromolecular compounds: proteins, DNA, RNA, lipids and carbohydrates (Altamirano et al., 2001; Bonarius et al., 1996; Lodish et al., 2008; Savinell and Palsson, 1992; Sheikh et al., 2005; Vriezen and van Dijken, 1998; Xie and Wang, 2000). The biomass equation also accounts for the energy requirements (ATP) for polymerization of macromolecules (proteins, DNA and RNA), which requires in total 29.18 mmol ATP per gram of biomass dry weight (Sheikh et al., 2005).

Therefore, a total of 14 reactions were added to the model, including biomass equation and formation reactions of all metabolites non-included in the base model and required for the biomass generation (DNA and RNA macromolecules). A list of all included reactions for the biomass formation is presented in **Table 4.1**. The dry weight for exponentially growing CHO-S cells was considered to be $0.36 mg \cdot 10^6 cells^{-1} \cdot mL^{-1}$, very similar to previously reported (Hefzi et al., 2016).

Table 4.1 List of reactions added to the CHO base model for including the biomass formation.

Reaction ID	Function	Stoichiometry
BIOM_AA	Protein formation	0.0909 LAlanine + 0.0505 LArginine +0.0505 LAspartate + 0.0404 LAsparagine + 0.0202 LCysteine + 0.0505 LGlutamine + 0.0606 LGlutamate + 0.0808 Glycine + 0.0202 LHistidine + 0.0505 LIsoleucine + 0.0808 LLeucine + 0.0808 LLysine + 0.0202 LMethionine + 0.0303 LPhenylalanine + 0.0505 LProline + 0.0606 LSerine + 0.0606 LThreonine + 0.0101 LTryptophan + 0.0303 LTyrosine + 0.0606 LValine + 4.306 ATP + 3.306 H2O -> PROT + 4.306 ADP + 4.306 Orthophosphate
BIOM_dAMP	DNA (dAMP) formation	dATP + 2 H2O -> dAMP + 2 Orthophosphate
BIOM_dCMP	DNA (dCMP) formation	dCTP + 2 H2O -> dCMP + 2 Orthophosphate
BIOM_dGMP	DNA (dGMP) formation	dGTP + 2 H2O -> dGMP + 2 Orthophosphate
BIOM_dTMP	DNA (dTMP) formation	dTTP + 2 H2O -> dTMP + 2 Orthophosphate
BIOM_AMP	RNA (AMP) formation	ATP + 2 H2O -> AMP + 2 Orthophosphate
BIOM_CMP	RNA (CMP) formation	CTP+ 2 H2O -> CMP + 2 Orthophosphate
BIOM_GMP	RNA (GMP) formation	GTP +2 H2O -> GMP + 2 Orthophosphate
BIOM_UMP	RNA (TMP) formation	UTP + 2 H2O -> UMP + 2 Orthophosphate
BIOM_DNA	DNA formation	0.3 dAMP + 0.2 dCMP + 0.2 dGMP + 0.3 dTMP + 1.372 ATP + 1.372 H2O -> DNA + 1.372 ADP + 1.372 Orthophosphate
BIOM_RNA	RNA formation	0.18 AMP + 0.30 CMP + 0.34 GMP + 0.18 UMP + 0.4 ATP + 0.4 H2O -> RNA + 0.4 ADP + 0.4 Orthophosphate
BIOM_LIP	Lipids formation	0.1315 Cholesterol + 0.5006 Phosphatidylcholine + 0.1898 Phosphatidylethanolamine + 0.0688 1PhosphatidylDmyoinositol + 0.0189 Phosphatidylserine + 0.0096 Phosphatidylglycerol + 0.0204 Cardiolipin + 0.0605 Sphingomyelin -> LIP
BIOM_CARBO	Carbohydrates formation	Amylose -> CAR
BIOM_T	**Biomass formation**	**6.990 PROT + 0.050 DNA + 0.1910 RNA + 0.144 LIP + 0.280 CAR -> BIOMASS**

For the adapted genome-scale metabolic model used in this study, a combination of the two CHO available models in Martínez et al., 2013 were used. Degradation of methionine, cysteine and arginine were added to the base model using the pathways included in the generic model published for *Mus musculus* (Quek and Nielsen, 2008; Sheikh et al., 2005). The biomass formation and GlutaMAX degradation were also added, as presented above.

For the phase in which lactate is consumed (Phase 2), two pathways of lactate metabolization were considered: cytoplasmatic and mitochondrial lactate degradation to pyruvate. Cytoplasmic lactate transport and metabolization were already included in the base model, but active mitochondrial lactate transport and metabolization had to be added. It was noted that in the generic model from *Mus musculus* (Quek and Nielsen, 2008; Sheikh et al., 2005) as well as a more recent generic model derived from *Cricetulus griseus* (Chinese Hamster) (Hefzi et al., 2016) lactate transport through mitochondrial membrane were already present in both models. For the mitochondrial lactate dehydrogenase, it was only present in *Cricetulus griseus* generic model, which derived from the Chinese Hamster genome.

The adapted model obtained contains 361 internal and 36 external reactions, and it includes 395 metabolites. A list of all included metabolites and reactions in the model, and the adaptation process; as well as the model in SBML format are detailed in ***Appendix C***, respectively. Reactions fluxes over the metabolic network are presented in nmols·mg_{DW}^{-1}·h^{-1}, except for the biomass reaction that is represented in mg·g_{DW}^{-1}·h^{-1}.

4.2.5 Flux calculation and model visualization

Flux Balance Analysis (FBA) is mathematically based on Linear Programming formulation to calculate the values of all the reactions fluxes over the network metabolism. For each metabolite included in the model, a mass balance has been carried out considering the specific consumption/production rate. Mass balance must include transport rate across the external and mitochondrial membrane (if necessary). The specific consumption/production rate (q_m) for each metabolite was obtained from **Equation 4.2**, where $\alpha_{(m,r)}$ is the stoichiometric coefficient of metabolite *m* in the reaction *r* and f_r is the flux of reaction r.

$$q_m = \sum \alpha_{(m,r)} \cdot f_r \qquad [4.2]$$

The set of equations are represented in matrix notation in **Equation 4.3**, where A is the stoichiometric matrix with (*m*,*r*) dimensions (*m*: metabolites and *r*: reactions); q is the vector of specific consumption/production rate for each metabolite (*m* rows for metabolites) and *f* is the vector of reaction fluxes (r rows for reactions).

$$q_{(m,1)} = A_{(m,r)} \cdot f_{(r,1)} \qquad [4.3]$$

The specific consumption/production rates (q_m) for each extracellular metabolite measured was calculated as presented above with the concentration data obtained during the cell culture; and it corresponds to the specific rate of the transport reaction in the external cell membrane. As

explained above, external reactions were included in the model, therefore in **Equation 4.3** these reactions are included into the stoichiometric matrix and into the fluxes vector.

Considering pseudo steady state, where the concentration of a metabolite doesn't change over time inside the cell, and considering the conservation of mass law, the q vector term becomes zero, obtaining **Equation 4.4**. For example, the glucose input flux through cell membrane must be transformed into other metabolites over the metabolism network, without possibility of accumulation inside the cell and without a concentration change over the time.

$$A_{(m\,x\,r)} \cdot f_{(r\,x\,1)} = 0 \qquad [4.4]$$

Parsimonia metabolic flux maximization approach (p-FBA) was performed using Optflux 3.2.7 Software (Rocha et al., 2010), a user-friendly computational tool for metabolic engineering applications. The graphical representation of the p-FBA was performed using Omix Visualization Software (GmbH&Co.KG) as described in Droste et al., 2011, where only the most significant fluxes for this study were represented. Specific consumption/production rates of experimental metabolites measured were added to the model with ±5% admitted deviation.

As usual in FBA with genomic models, the system was under-determined and there existed some degrees of freedom. For example, for the CHO case, the system had 397 variables (one flux for each reaction) and 395 equations (one for each metabolite), but some equations became linearly dependents, making the model to have 35 degrees of freedom. Once external measured fluxes were added as additional constraints, the degrees of freedom of the system were reduced to 10, therefore the system had a large space of possibility solutions in the metabolic network. To find the optimal state, pFBA uses the optimization of a certain objective function, in this case the maximum value of ATP generation. In addition, the Malate-Aspartate Shuttle was constrained to go in the direction of NADH regeneration into the cytoplasm for pFBA's performed (Barron et al., 1998).

4.3 Results

4.3.1 Lactate metabolism in isolated mitochondria of HEK293 cells

Several authors have reported the consumption of lactate by mammalian cells (Altamirano et al., 2006; Brunner et al., 2018; Martínez et al., 2013; Mulukutla et al., 2012). Among these studies, there is a considerable controversy about how lactate reaches the mitochondrial matrix. While some authors have reported the possibility of direct entrance of lactate through the mitochondrial transporters (Luo et al., 2012; Passarella et al., 2008; Passarella et al., 2014), many others have stated that lactate is converted to pyruvate at the cytosol and thereafter, pyruvate is transported inside the mitochondria (Martínez et al., 2013; Mulukutla et al., 2012).

The feasibility of lactate entrance to the mitochondria was evidenced by analysis of respirometry with isolated mitochondria from HEK293 cells. The main function of mitochondria is the generation of energy in the form of ATP, that is used to sustain cell growth and maintenance. Besides carbon sources, mitochondria also consume oxygen for the production of ATP (Brown, 1992) through the oxidative phosphorylation pathway. Therefore, respirometry is a technique that enables to measure respiratory activity of living cells by measuring changes on O_2 and/or CO_2 rates (Brooks et al., 1999; Iglesias-González et al., 2012; Jastroch et al., 2012). Hence, this methodology has been used for the assessment of mitochondrial activity, since the high O_2 consumption is related to the metabolic pathways that take place into the isolated mitochondria.

The protocol used for mitochondrial isolation and the methodology used for O_2 measurement is detailed in Material and Methods section. The analysis of respirometry revealed that when mitochondria were resuspended in the presence of lactate, the oxygen consumption was higher than when the organelles were resuspended in presence of pyruvate (**Figure 4.1**). If the conversion of lactate to pyruvate was mandatory previous to entering the mitochondria (in case that there was some residual lactate dehydrogenase in the resuspension buffer), then the activity of mitochondria would be the same, regardless the metabolite (pyruvate or lactate) present in media. On the other hand, if lactate dehydrogenase (LDH) was not present neither in the mitochondrial suspension or, at least, at the outer part of the mitochondrial external membrane, the activity with lactate would be equal to the control without substrate.

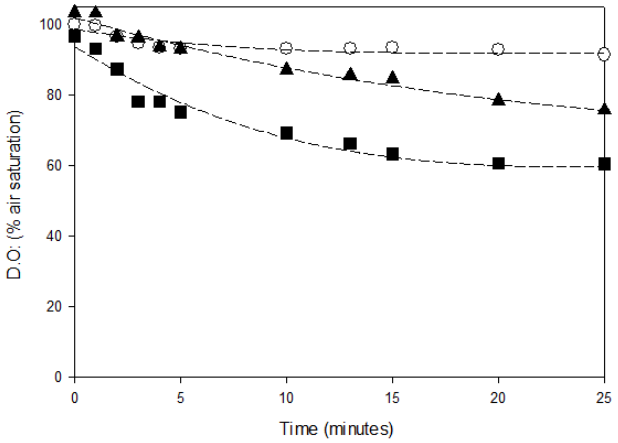

Figure 4.1: Oxygen consumption of mitochondria (185 µg·mL^{-1}) in respiration buffer (○), respiration buffer + pyruvate (10 mM) (▲) or respiration buffer + lactate (10 mM) (■).

The fact that mitochondria were more active when was resuspended in the respirometry buffer with lactate indicate that this metabolite could enter the mitochondria either through the same transporter than pyruvate or using an alternative route, not related to pyruvate conversion. Lactate is a more reduced compound than pyruvate and this fact can explain the higher level of oxygen consumption in presence of lactate than in pyruvate as sole carbon and redox sources. The feasible mechanism could be the direct entrance through mitochondrial Monocarboxilate transporters (MCT) and the presence of an LDH in the inner or outer part of mitochondria internal membrane. The presence of both MCT and LDH have been reported in mammalian mitochondria and, consequently, included in the genome-scale metabolic reconstructions (Hashimoto et al., 2006; Hashimoto et al., 2008; Passarella et al., 2014).

In order to further evaluate the hypothesis of the transport of lactate into mitochondria, mitochondria were resuspended under the presence of lactate and α-cyano-4-hydroxycinnamic acid (CINN), an inhibitor of various subtypes of MCTs (Fox et al., 2000; Kennedy and Dewhirst, 2010).

As shown in **Figure 4.2**, only when lactate was present in the respiratory buffer, an oxygen consumption profile similar to the one previously shown was obtained. The measurement of extracellular lactate confirmed that the respiratory activity detected was due to the consumption of this metabolite. When MCTs were blocked with the addition of CINN, the mitochondria respiratory activity was completely stopped, and the oxygen consumption profile was similar to the negative control (buffer without carbon source).

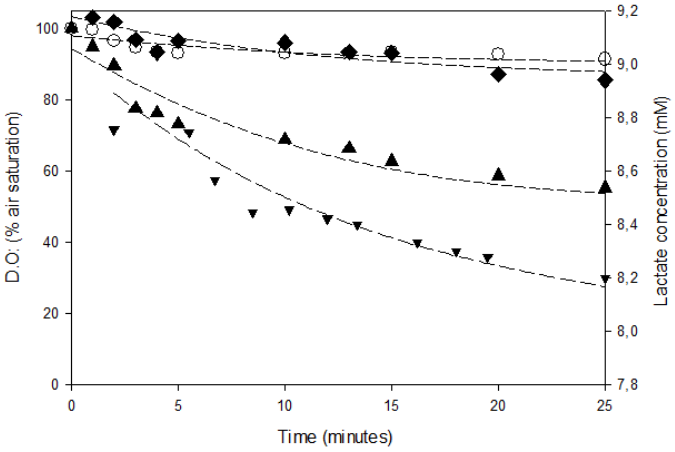

Figure 4.2: Oxygen consumption of mitochondria (205 µg·mL^{-1}) in respiration buffer (○), respiration buffer+lactate (10 mM) + CINN (5 mM) (♦), and respiration buffer+lactate (10 mM) (▲). Lactate concentration (▼) (right axis) measured with an YSI analyzer that belongs to the condition in which no CINN (blocking agent) was added.

The reduction of mitochondrial activity after blocking MCTs has been previously reported in other cell types (De Bari et al., 2004; Brooks et al., 1999), but never for HEK293 cells. Although this data is not sufficient to completely rule out the entrance of lactate in mitochondria via prior conversion to pyruvate, the thermodynamics of the LDH reaction might provide some additional data to this discussion. The thermodynamics of the conversion from pyruvate to lactate is energetically favorable, being the ΔGº of this reaction of -25.1 (KJ·mol^{-1}). Hence, the reverse reaction of conversion of L-lactate to pyruvate in the cytosol would not be thermodynamically favorable for the range of concentrations physiologically feasible when also glucose is consumed (unless pyruvate crosses the mitochondrial membrane at very high rates). Nevertheless, further research is currently being addressed in order to experimentally demonstrate the mechanism of lactate entrance to the mitochondria.

For the above considerations, the calculation of metabolic fluxes for HEK293/CHO presented in the next section, both mechanisms have been considered: The direct lactate entrance to the mitochondria and the lactate conversion to pyruvate at the cytosol and its transport inside the mitochondria.

4.3.2 Metabolic flux analysis in the different glucose/lactate metabolism in HEK293

In order to gain a deeper insight in the cell metabolic redistribution due to the effects of environmental conditions, as a preliminary step before applying more advanced experimental techniques (13C-labeling experiments), we performed a metabolic flux balance analysis first for HEK293 of the different phases obtained in Bioreactor. To this purpose we used the HEK293 context specific model described in Materials and Methods section. For metabolic flux calculation the model was constrained using the input-output data of the corresponding metabolites at each phase. As this data includes the biomass formation, the optimization was performed using the maintenance ATP as the objective function.

For the phases in which lactate was consumed (P3_B1 and P2_B2), the two alternatives for lactate metabolization are presented: the first in which lactate is converted into pyruvate in cytosol and then pyruvate enters the mitochondria (c-LDH, cytosolic LDH); and the second possibility, in which lactate enters first into the mitochondria and then is converted into pyruvate (m-LDH, mitochondrial LDH).

Six pFBA for the different glucose/lactate metabolisms presented in the chapter 3 are depicted in **Figures 4.3** to **4.8**:

1. **FBA1_HEK293**: Phase 1, pH-controlled (P1_B1): glucose consumption, lactate production (**Figure 4.3** for c-LDH).
2. **FBA2_HEK293**: Phase 3, pH-controlled (P3_B1): lactate consumption as a sole substrate (**Figure 4.4** for c-LDH and **Figure 4.5** for m-LDH).
3. **FBA3_HEK293**: Phase 1, non pH-controlled (P1_B2): glucose consumption, lactate production (**Figure 4.6** for c-LDH).
4. **FBA4_HEK293**: Phase 2, non pH-controlled (P2_B2): glucose and lactate concomitant consumption (**Figure 4.7** for c-LDH and **Figure 4.8** for m-LDH).

Experimental consumption/production rates for the different metabolic phases modelized for HEK293 are summarized in **Table 4.2**.

Table 4.2: Summary of input/output experimental fluxes of the different metabolic phases modelized for HEK293. All data in nmol·mg_{DW}^{-1}·h^{-1} except biomass mg·g_{DW}^{-1}·h^{-1}.

	Phase 1 (P1_B1)	Phase 3 (P3_B1)	Phase 1 (P1_B2)	Phase 2 (P2_B2)
	pH-controlled		Non pH-controlled	
Alanine	19 ± 12	1 ± 1	48 ± 13	-3 ± 1
Arginine	-17 ± 4	-2.1 ± 0.4	-26 ± 3	-10 ± 6
Asparagine	-9 ± 3	-2.2 ± 1.5	-27 ± 11	-8.1 ± 1.5
Aspartate	-19.8 ± 19.8	-1.9 ± 1	-41.3 ± 7.9	-8.2 ± 1
Biomass	35.8 ± 0.4	5 ± 0.23	23.2 ± 0.6	14.6 ± 0.9
Cysteine	-4.6 ± 0.5	-0.1 ± 0.1	-3 ± 1	-1.3 ± 1
Glucose	-760 ± 134	0 ± 0.001	-354 ± 66	-79 ± 6
Glutamine	-7 ± 2	-1 ± 0	59 ± 28	-0.5 ± 0.5
GlutaMax	-2.4 ± 1.8	-1.2 ± 1	-31 ± 3	-1.4 ± 0.6
Glutamate	-7.1 ± 7.1	-1.7 ± 0.4	-20.1 ± 6.5	-5.7 ± 1
Glycine	17.6 ± 3.8	3.2 ± 1.3	26.7 ± 10.3	1.2 ± 0.6
Histidine	-12 ± 6	-1.5 ± 0.3	-7.7 ± 2.8	-2.5 ± 2
Isoleucine	-23.6 ± 9	-3.6 ± 0.4	-23 ± 4	-10 ± 7
Lactate	995 ± 109	-53 ± 10	600 ± 54	-59 ± 5
Leucine	-34 ± 11	-3.7 ± 0.8	-22.7 ± 9.5	-12.3 ± 5.3
Lysine	-36 ± 15	-6 ± 6	-20 ± 7	-9 ± 1
Methionine	-9 ± 4	-1.3 ± 0.6	-11 ± 7	-4 ± 3
NH_4^+	27 ± 4	-7.6 ± 1	30 ± 3	11 ± 11
Oxygen	-700 ± 12	-142 ± 46	-801 ± 70	-526 ± 128
Ornithine	2.7 ± 2.7	-0.7 ± 0.3	10.3 ± 10.3	-2.9 ± 0.7
Phenylalanine	-9.4 ± 6.4	-1.7 ± 0.5	-11.2 ± 6.3	-4.1 ± 1.8
Proline	-8.1 ± 0.1	-1.8 ± 0.8	-33 ± 25	0.8 ± 0.8
Serine	-81 ± 55	-8 ± 8	-40 ± 1	-16 ± 2
Threonine	-16 ± 12	-2 ± 1	-18 ± 12	-5 ± 1
Tryptophan	-2.8 ± 1.6	-0.04 ± 0.03	-3.6 ± 3.4	-0.9 ± 0.9
Tyrosine	-6 ± 3	-1 ± 1	-10.2 ± 10	-3.1 ± 2
Urea	1 ± 0.3	3.1 ± 3.1	22 ± 4	6 ± 1
Valine	-23 ± 11	-3.8 ± 3.8	-28 ± 10	-10 ± 6

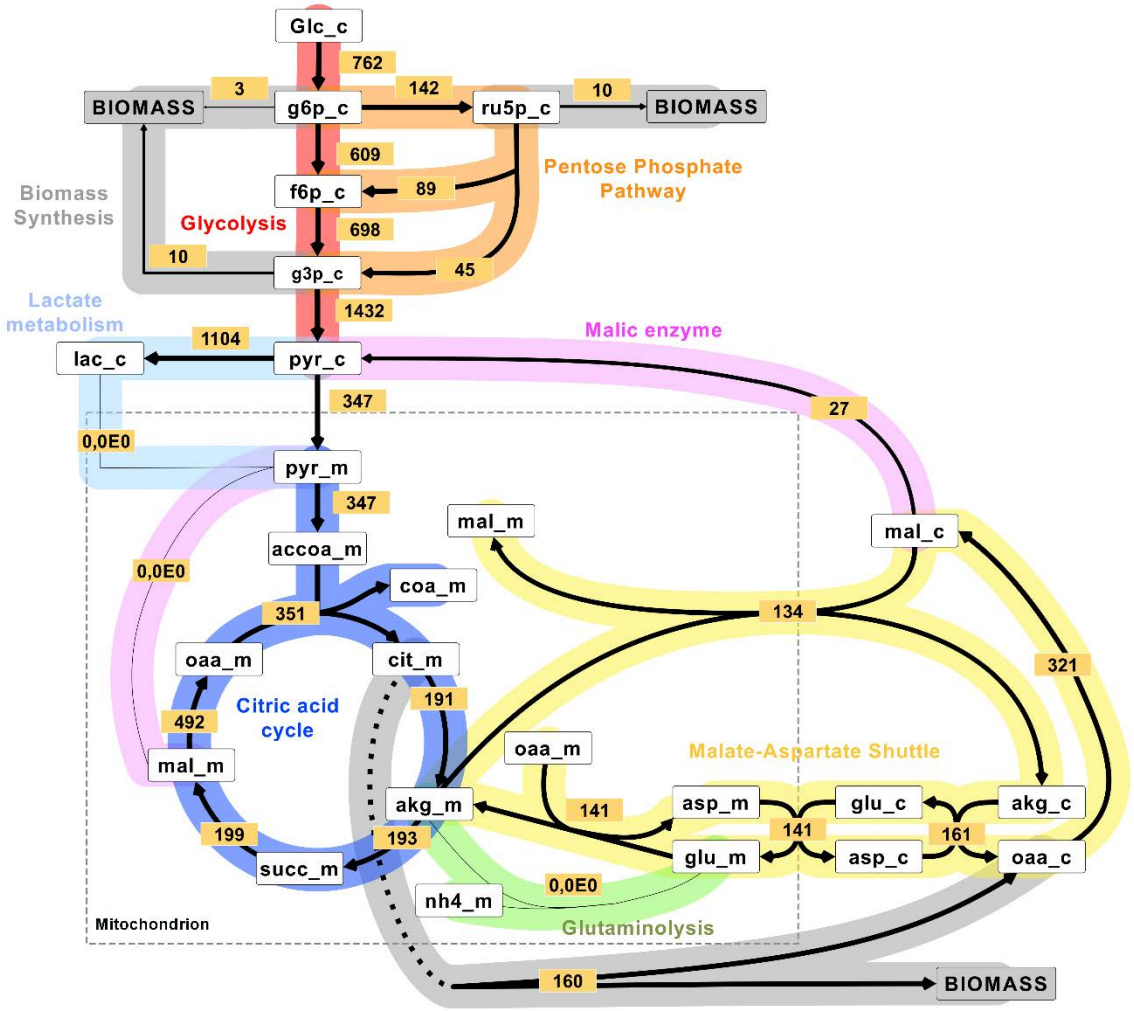

Figure 4.3: Scheme of the main metabolic fluxes calculated for HEK293 in Phase 1 when pH is controlled to 7.1 (glucose consumption and lactate production phase; Phase P1_B1). Arrows indicate the direction of the flux and their width the magnitude of fluxes (the exact value is detailed close to the arrows). The box represents the mitochondrion.

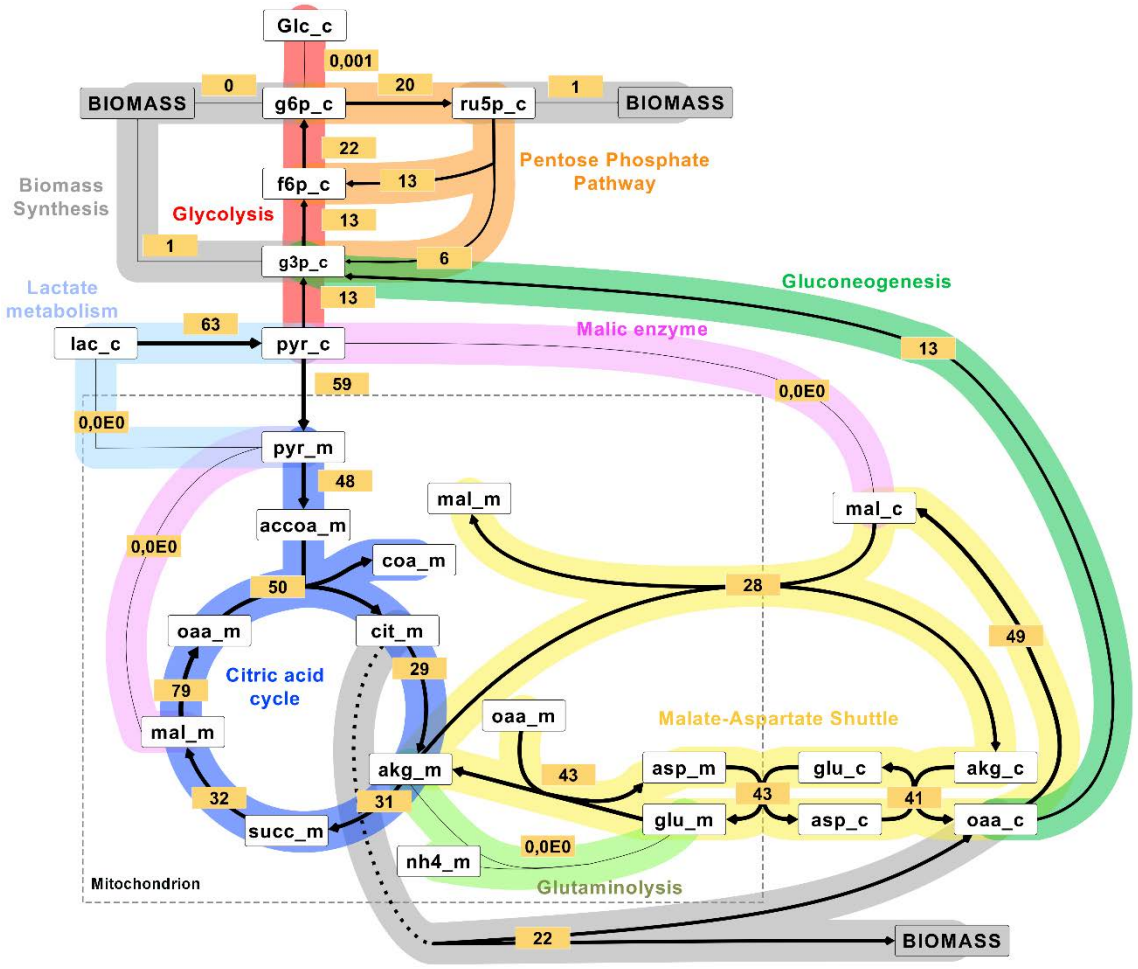

Figure 4.4: Scheme of the main metabolic fluxes calculated for HEK293 in Phase 3 when pH is controlled to 7.1 considering c-LDH (lactate consumption as a sole substrate phase; Phase P3_B1 c-LDH). Arrows indicate the direction of the flux and their width the magnitude of fluxes (the exact value is detailed close to the arrows). The box represents the mitochondrion.

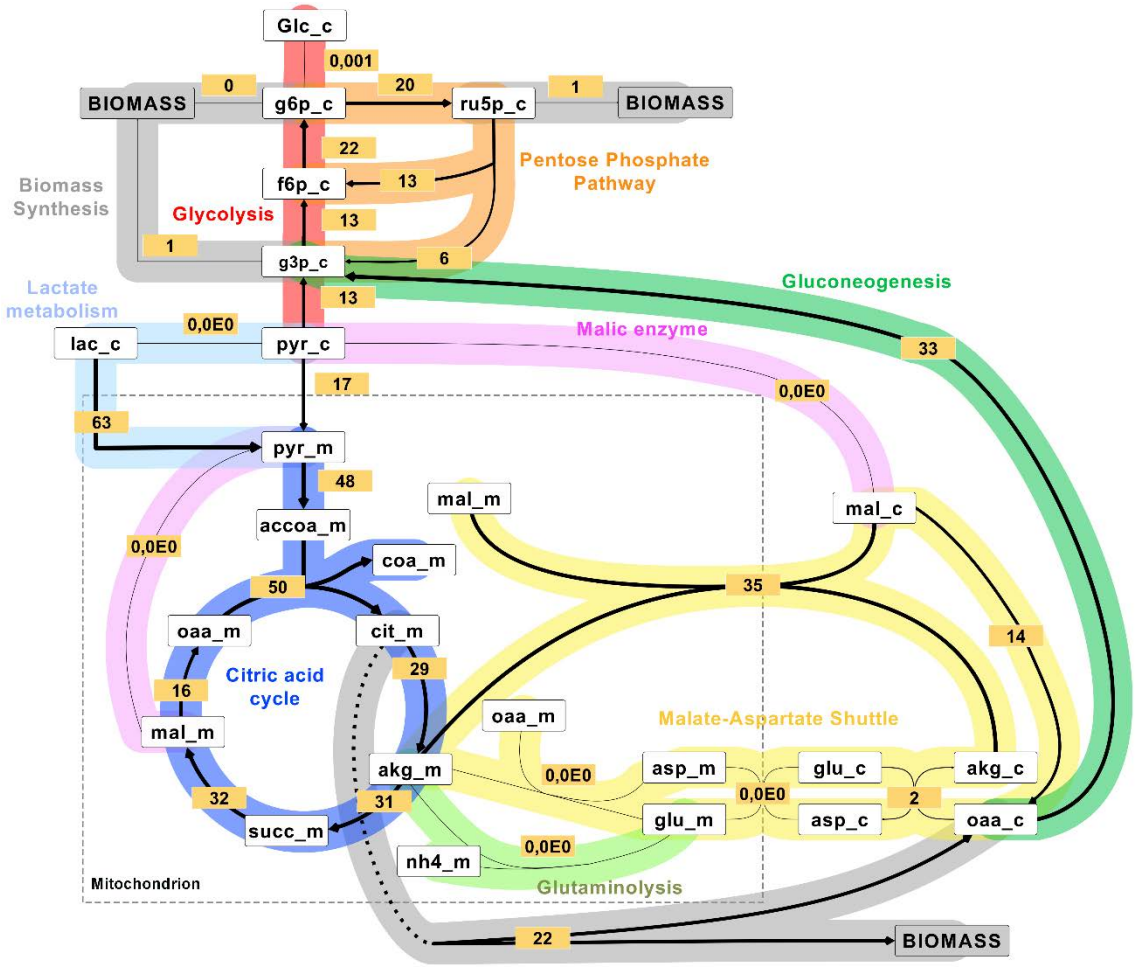

Figure 4.5: Scheme of the main metabolic fluxes calculated for HEK293 in Phase 3 when pH is controlled to 7.1 considering m-LDH (lactate consumption as a sole substrate phase; Phase P3_B1 m-LDH). Arrows indicate the direction of the flux and their width the magnitude of fluxes (the exact value is detailed close to the arrows). The box represents the mitochondrion.

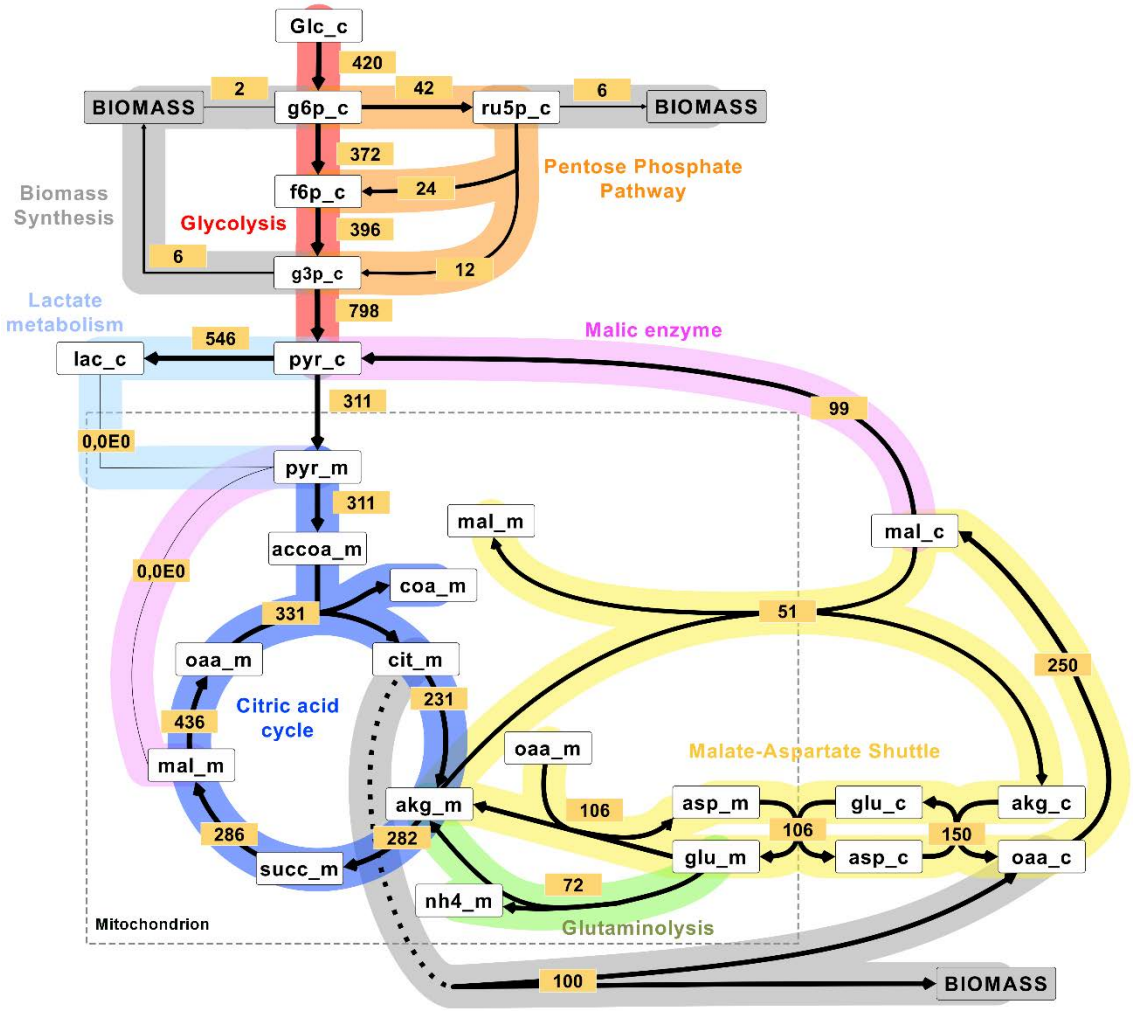

Figure 4.6: Scheme of the main metabolic fluxes calculated for HEK293 in Phase 1 when pH is non-controlled (glucose consumption and lactate production phase; Phase P1_B2). Arrows indicate the direction of the flux and their width the magnitude of fluxes (the exact value is detailed close to the arrows). The box represents the mitochondrion.

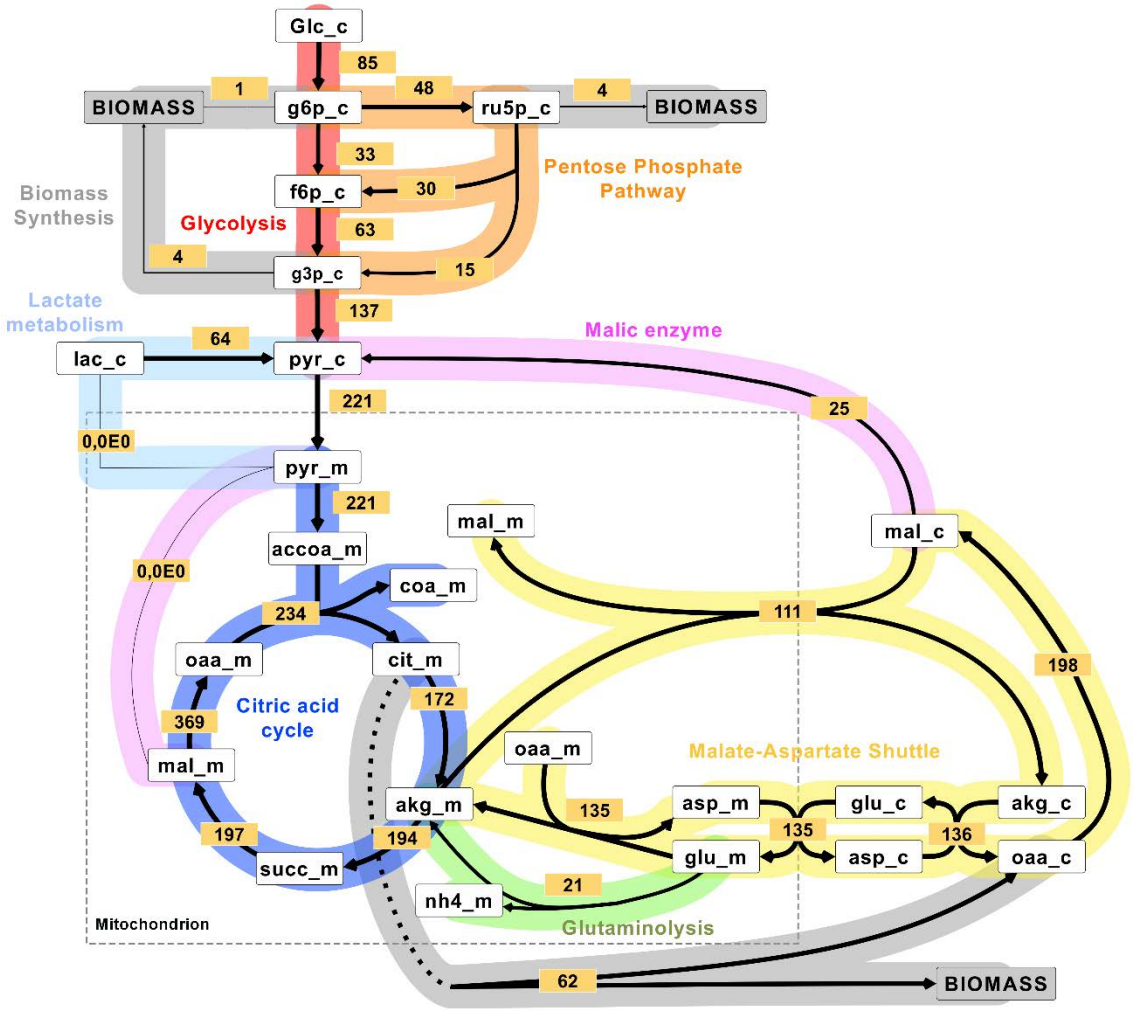

Figure 4.7: Scheme of the main metabolic fluxes calculated for HEK293 in Phase 2 when pH is non-controlled considering c-LDH (glucose and lactate concomitant consumption phase; Phase P2_B2 c-LDH). Arrows indicate the direction of the flux and their width the magnitude of fluxes (the exact value is detailed close to the arrows). The box represents the mitochondrion.

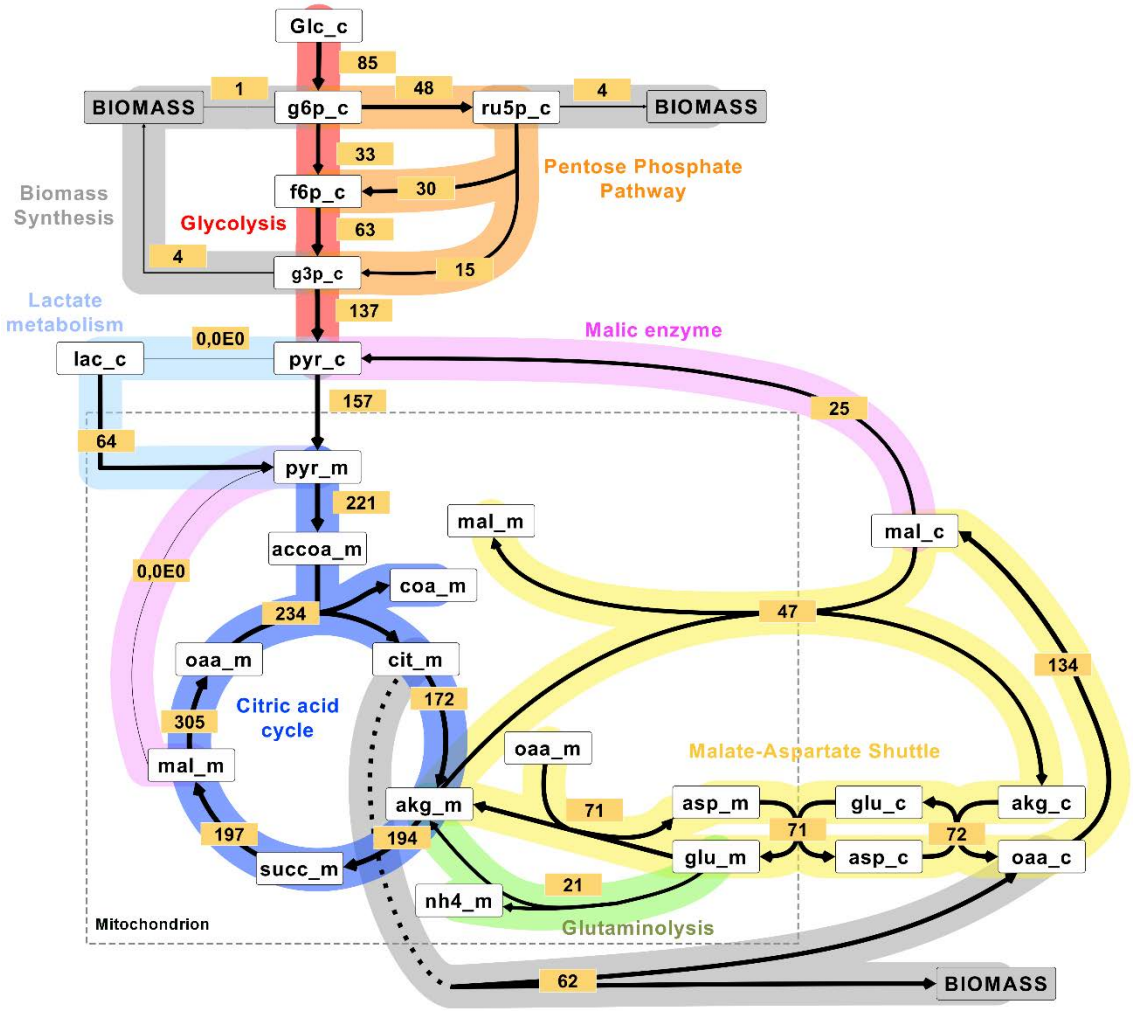

Figure 4.8: Scheme of the main metabolic fluxes calculated for HEK293 in Phase 2 when pH is non-controlled considering m-LDH (glucose and lactate concomitant consumption phase; Phase P2_B2 m-LDH). Arrows indicate the direction of the flux and their width the magnitude of fluxes (the exact value is detailed close to the arrows). The box represents the mitochondrion.

Effect of non pH-controlled conditions on metabolic flux distribution during exponential growth in HEK293 (Phase 1: glucose uptake and lactate production)

As previously described, both HEK293 batch cultures produces a big amount of lactate at the first phase of the culture, regardless of keeping pH controlled or not. Even so, the glucose consumption and lactate production rates, as well as the growth rate, show differences depending whether the process has pH control. This occurs even containing the same levels of cells and carbon sources at the beginning of the culture. These differences resulted in a different uptake/production rate of the other metabolites. The lower growth rate shown by the non-controlled pH experiment is in agreement with a lower glucose uptake and lactate production rates. This could be the result of a lower activity of the glycolytic pathway together with a decreased energy generation (ATP) and biomass synthesis rates.

It could be argued that the extracellular pH decrease resulted in a significant impact in the intracellular biochemical activity. It is well known that mammalian cells maintain their intracellular pH within a narrow margin. It is also known that after a pH change there is a temporal phase where intracellular pH is temporarily off-set, while the usual pH and homeostasis are recovered.

Figures 4.3 and **4.6** show the metabolic flux distribution of the most significant metabolic pathways focused on the central carbon metabolism during the first phase (P1_B1 and P1_B2). When comparing the pH non-controlled culture (**Figure 4.6**) with the reference culture (pH-controlled culture, **Figure 4.3**), it can be seen that the effect of a lower external pH has resulted in a significant decrease of approximately 45% in glucose uptake and in the glycolytic pathway fluxes, while TCA activity it's slightly higher. In respect to lactate generation, in the reference culture approximately 77% of the glycolytic carbon is converted to lactate and secreted to the medium, while this value is lower (near 69%) in the non-controlled pH culture, that is in agreement with the lower glycolytic flux observed. This is a consequence of the reduced total carbon uptake.

Although in many organisms pyruvate obtained from glucose through glycolysis is predominantly converted into acetyl-CoA, in mammalian cell lines pyruvate is mainly converted into lactate, particularly in the exponential growth phase. It has already been reported that in HEK293, hybridoma and CHO cells, this conversion takes place at high rates regardless of the level of oxygen in the culture (Lin and Miller, 1992; Ozturk and Palsson, 1991). It must be mentioned that in the present study, O_2 was not limiting at any phase of the cultures (always kept above 25% D.O. (dissolved oxygen), data not shown).

During Phase 1 of pH-controlled conditions (P1_B1), glucose was rapidly consumed and the flux through glycolysis was 1432 $nmol \cdot mg_{DW}^{-1} \cdot h^{-1}$ (from G3P to PEP) (**Figure 4.3**). Nevertheless, only about 24% of the pyruvate generated via glycolysis was eventually transported into mitochondria via pyruvate, being completely metabolized in the tricarboxylic acid cycle (TCA), hence, obtaining the maximal energy from the carbon source.

Since mitochondria is not permeable to $NADH + H^+$, an indirect transport system named Malate-Aspartate Shuttle is needed for its regeneration (Barron et al., 1998). As it is shown in **Figures 4.3** and **4.6**, the flux of redox equivalents inside the mitochondria via Malate-Aspartate shuttle seems to be limited to around 141 $nmol \cdot mg_{DW}^{-1} \cdot h^{-1}$, meaning that the remaining should be regenerated in the cytoplasm, via lactate dehydrogenase (c-LDH).

It must be pointed out that although the rates of pyruvate that is completely oxidized into the mitochondria were quite similar for both conditions, the glycolytic fluxes were almost reduced by half in the non-controlled pH culture. The activity of the Mal/Asp Shuttle was higher for the reference experiment with controlled pH. In any case, it can be stated that the cell metabolism in Phase 1 of both batch cultures is highly inefficient, as the majority of the carbon source is not used for the generation of energy and biomass but secreted as lactate. Therefore, this metabolism could be understood as "unbalanced" metabolism, as the rate of TCA is unable to

cope with the reduction equivalents generated in glycolysis, resulting in lactate formation and secretion.

In both cases, the calculated TCA fluxes of pyruvate uptake by mitochondria were similar: 347 and 311 $nmol \cdot mg_{DW}^{-1} \cdot h^{-1}$ respectively. If this were an upper limit, it could be the cause behind the limitation of pyruvate entrance to the mitochondria.

Effect of non -controlled pH conditions on metabolic flux distribution during lactate consumption phase (Phase 2).

The striking difference observed in the second phases (in which lactate is consumed) between controlled (Phase 3) and non-controlled pH experiments (Phase 2) resulted in dramatically different metabolic fluxes distribution. When glucose was completely depleted from media (P3_B1), lactate was used as a sole carbon source: about 21% of the lactate influx was directed to gluconeogenesis (PEP to G3P) (**Figure 4.4**, where cytoplasmic LDH was considered for fluxes calculation and **Figure 4.5**, where mitochondrial LDH was considered for fluxes calculation). The total carbon influx into the cell trough lactate was much lower than the carbon influx through glucose and the consequent lactate generation in the previous phase. Also, in Phase 3, the fluxes in Malate-Aspartate Shunt were significantly reduced and as shown in **Figures 4.4 and 4.5**, and the TCA fluxes were 6-7-fold reduced in comparison to Phase 1 (P1_B1). Altogether results in a strong cell growth rate reduction (about 7 times decrease). At this lower growth rate, cells continued growing for additional 60 hours and, thereafter, the culture entered into death phase.

In contrast, in the Phase 2 of non pH-controlled experiments (P2_B2), both glycolysis and lactate pathways contribute to the TCA cycle. This allows for a higher growth rate (3-fold) compared with the Phase 3 of the reference experiment (P3_B1). According to the TCA cycle fluxes obtained, the energy available in non pH-controlled experiment for cells to grow in Phase 2 was smaller to that available in Phase 1 and specific cell growth was reduced (about 37% of reduction). In any case, this resulted in the achievement of higher cell densities in non pH-controlled compared with pH-controlled cell culture.

Alternative LDH pathway in lactate consumption in HEK293

As explained in the Introduction section, during the last years, several authors have reported the consumption of lactate by mammalian cells, but still exists a considerable controversy about how lactate reaches the mitochondrial matrix. While many authors state the conversion of lactate to pyruvate in the cytoplasm (Martínez et al., 2013), others report the conversion of pyruvate to lactate in the mitochondrial matrix (Luo et al., 2012; Passarella et al., 2014). The existence of mitochondrial lactate dehydrogenase (m-LDH) in mammalian cells (Hashimoto et al., 2008; Passarella et al., 2008) as well as the entrance of lactate into mitochondria (Hashimoto et al., 2008; Passarella et al., 2008) has also been demonstrated for several authors. However, the existence of m-LDH is not universally accepted for the scientific community (Gladden, 2007).

Although the capability of lactate metabolization by isolated mitochondria has been demonstrated, the possibility of lactate being converted into pyruvate in the cytosol cannot be

excluded from the discussion. To further explore both alternatives, we have in silico compared an active cytoplasmic LDH (c-LDH) or, alternatively, the mitochondrial LDH (m-LDH). As expected, the results show that most of the TCA cycle operates at similar rate in both cases. However, a significant difference can be mentioned at the level of Mal/Asp Shuttle. This shuttle shows lower rates in case of mitochondrial LDH activity. This appears to be the result of releasing NADH electron carriers directly into mitochondria, thus relieving Mal/Asp Shuttle of this task.

It can be observed that in Phase 2 (**Figure 4.7**, where cytoplasmic LDH was considered for fluxes calculation and **Figure 4.8**, where mitochondrial LDH was considered instead), the TCA influx came from two different sources: the majority of the influx came from glycolysis and the rest from lactate influx, either via conversion to pyruvate in cytoplasm or directly transported into mitochondria. In the end, the pyruvate dehydrogenase flux is the same for both cases (221 $nmol \cdot mg \cdot h^{-1}$). Interestingly, lactate influx was in the same range as in Phase 3, regardless of its use as a sole carbon source (Phase 3) or in combination with glucose (Phase 2). This may indicate that the limit of lactate transport and metabolization was reached in both cases.

However, the most interesting fact of the fluxes obtained in Phase 2 was the drastic reduction on glycolysis fluxes. As shown in **Figures 4.3** and **4.6**, when glucose was the unique carbon influx (phases P1_B1/P1_B2), fluxes through glycolysis pathway (G3P to PEP) were around 1432/798 $nmol \cdot mg \cdot h^{-1}$ respectively whereas when glucose and lactate were concomitantly consumed, the fluxes through glycolysis was only about 137 $nmol \cdot mg \cdot h^{-1}$, which represents approximately about 10% of P1_B1 flux rate.

The difference observed in Malate-Aspartate Shuttle in Phase 2 between both hypothesis analyzed (c-LDH or m-LDH), arises from the fact that when cytoplasmic LDH was considered, the Shuttle operated at higher rates (111 $nmol \cdot mg \cdot h^{-1}$) in Malate-Aspartate transport reaction) than when compared to the case where mitochondrial LDH was considered (47 $nmol \cdot mg \cdot h^{-1}$). In other words, the alternative m-LDH hypothesis results in a 58% of Malate-Aspartate Shuttle reduction. Moreover, fluxes in TCA cycle are identical. Therefore, it can be stated that the energy obtained under such conditions was quite important, even when glucose uptake rate was diminished by 89 % in comparison to the same flux in Phase 1 (P1_B1).

From the results obtained it can be deduced that the sum of the fluxes coming from glycolysis and lactate influx resulted in a similar flux of TCA that the obtained in Phase 1 (P1_B1). In other words, entering to Phase 2 (glucose and lactate co-metabolization) triggered a change from an unbalanced metabolism during Phase 1 (high glycolysis influx rates in comparison to TCA fluxes and lactate production and secretion) to a better-balanced metabolism (glycolysis fluxes in concordance to TCA fluxes and lactate consumption) on Phase 2. This balanced metabolism avoids the typical lactate production and secretion observed in Phase 1 (P1_B1 and P1_B2), what is nowadays one of the major drawbacks of animal cells-based bioprocesses.

4.3.3 Metabolic flux analysis in the different glucose/lactate metabolism in CHO

Once a flux analysis of HEK293 in the different phases was done, similar protocol to study the metabolic fluxes in CHO cell culture was performed. In this case, the metabolic flux analysis was

performed with the results obtained in Bioreactor in Phase 1 when pH was non-controlled (P1_B2) and in phase 2 when concomitant consumption was obtained from the beginning of the culture (P2_B3).

The original idea of this chapter was studying the switch from Phase 1 to Phase 2 performing a Dynamic Flux Balance Analysis (D-FBA) with the data obtained in the Bioreactor when pH is non-controlled. Due to the lack of points in the experiment was very difficult to fix the model, for this reason as previous step to the D-FBA and to compare the results with the HEK293 FBA presented in the previous chapter, it was decided to perform first a Flux Balance Analysis with the data obtained in both phases. In addition, it was thought very interesting to present the fluxes in Phase 2, but in the case when the concomitant glucose/lactate consumption was trigger from the beginning of the culture, with a similar growth rate in comparison to the obtained in the exponential Phase 1. Furthermore, a study of the amount of energy (ATP) generated by cells in both phases, as well as the distribution of ATP consumed and generated in the different pathways of the metabolism is presented at the end of the chapter.

The protocol followed for the flux calculation was the same as for the HEK293 flux analysis presented in the previous section, using the specific metabolic model for CHO presented in Materials and Methods. As for the HEK293, for the phase in which lactate was consumed (P2_B3) the two alternatives for lactate metabolization are presented (c-LDH and m-LDH). Three pFBA for the different glucose/lactate metabolisms are depicted in **Figures 4.9** to **4.11**:

1. **FBA1_CHO**: Phase 1, non pH-controlled (P1_B2): glucose consumption, lactate production (**Figure 4.9** for c-LDH).
2. **FBA2_CHO**: Phase 2, pH controlled to 6.80 adding 15 mM of sodium lactate (P2_B3): glucose and lactate concomitant consumption from the beginning of the culture (**Figure 4.10** for c-LDH and **Figure 4.11** for m-LDH).

Experimental consumption/production rates for the different metabolic phases modelized for CHO are summarized in **Table 3**.

Table 3: Summary of input/output experimental fluxes of the different metabolic phases modelized for CHO. All data in nmol·mg_{DW}^{-1}·h^{-1} except biomass mg·g_{DW}^{-1}·h^{-1}.

	Phase 1 (P1_B2)	Phase 2 (P2_B3)
	Non pH-controlled	pH-controlled to 6.8 + 15 mM of $C_3H_5NaO_3$
Alanine	105.96 ± 5.30	31.29 ± 1.56
Arginine	-25.89 ± 1.29	-15.93 ± 0.80
Asparagine	-10.69 ± 0.53	-9.74 ± 0.49
Aspartate	-24.98 ± 1.25	-4.81 ± 0.24
Biomass	39.30 ± 1.97	35.80 ± 1.79
Cysteine	-8.82 ± 0.44	-5.10 ± 0.26
Glucose	-343.12 ± 17.16	-64.72 ± 3.24
Glutamate	-12.46 ± 0.62	-18.16 ± 0.91
GlutaMax	-93.30 ± 4.67	-34.63 ± 1.73
Glutamine	40.27 ± 2.01	3.63 ± 0.18
Glycine	7.34 ± 0.37	3.78 ± 0.19
Histidine	-6.02 ± 0.30	-5.49 ± 0.27
Isoleucine	-24.04 ± 1.20	-14.12 ± 0.71
Lactate	555.29 ± 27.76	-79.77 ± 3.99
Leucine	-33.61 ± 1.68	-22.09 ± 1.10
Lysine	-27.67 ± 1.38	-20.23 ± 1.01
Methionine	-9.94 ± 0.50	-5.96 ± 0.30
NH_4^+	62.05 ± 3.10	23.58 ± 1.18
Oxygen	-485.61 ± 24.28	-458.47 ± 22.92
Phenylalanine	-12.75 ± 0.64	-5.93 ± 0.30
Proline	-25.80 ± 1.29	-10.49 ± 0.52
Serine	-55.00 ± 2.75	-35.00 ± 1.75
Threonine	-24.39 ± 1.22	-20.52 ± 1.03
Tryptophan	-7.48 ± 0.37	-3.45 ± 0.17
Tyrosine	-8.92 ± 0.45	-4.95 ± 0.25
Valine	-25.73 ± 1.29	-16.12 ± 0.81

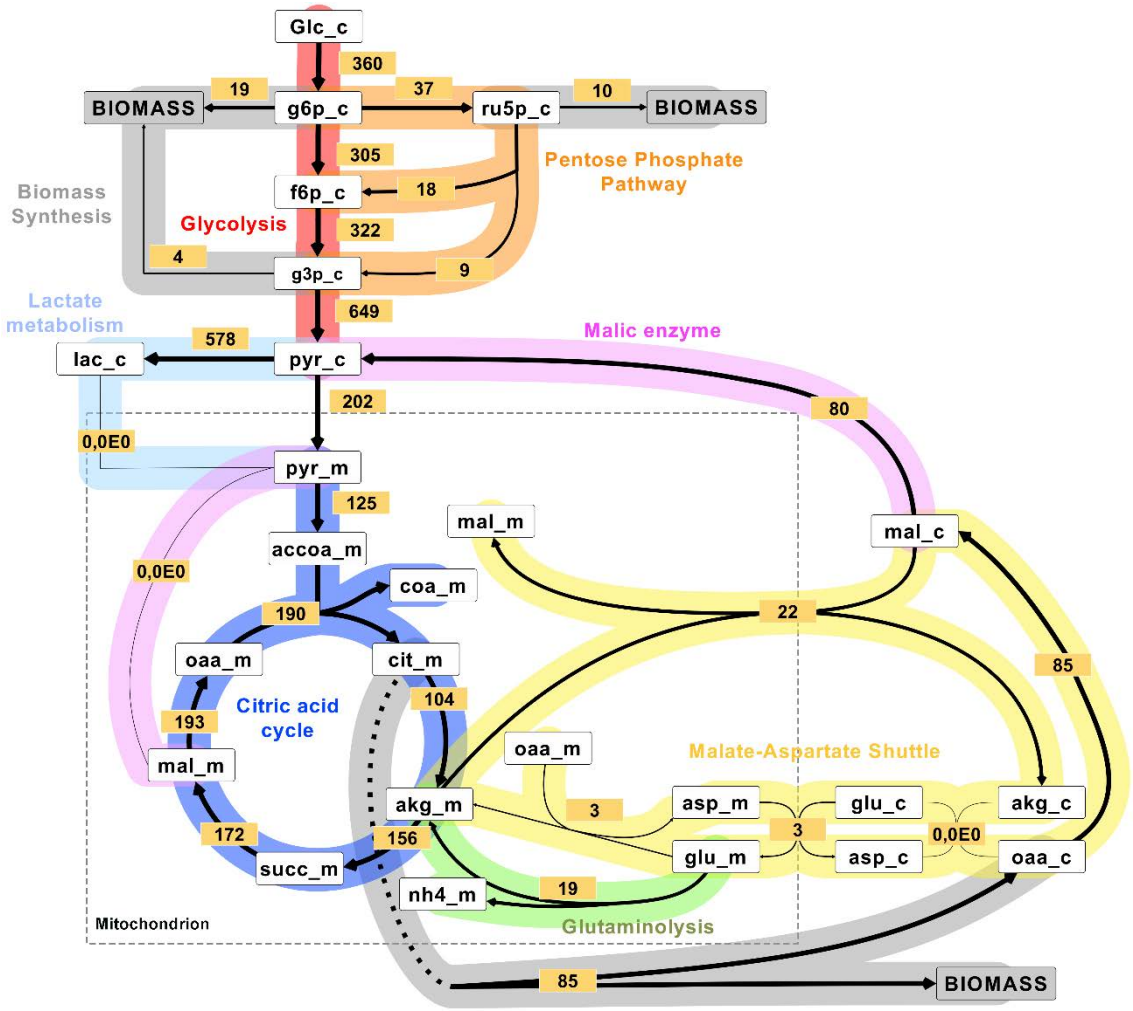

Figure 4.9: Scheme of the main metabolic fluxes calculated for CHO in Phase 1 when pH is non-controlled (glucose consumption and lactate production phase; Phase P1_B2). Arrows indicate the direction of the flux and their width the magnitude of fluxes (the exact value is detailed close to the arrows). The box represents the mitochondrion.

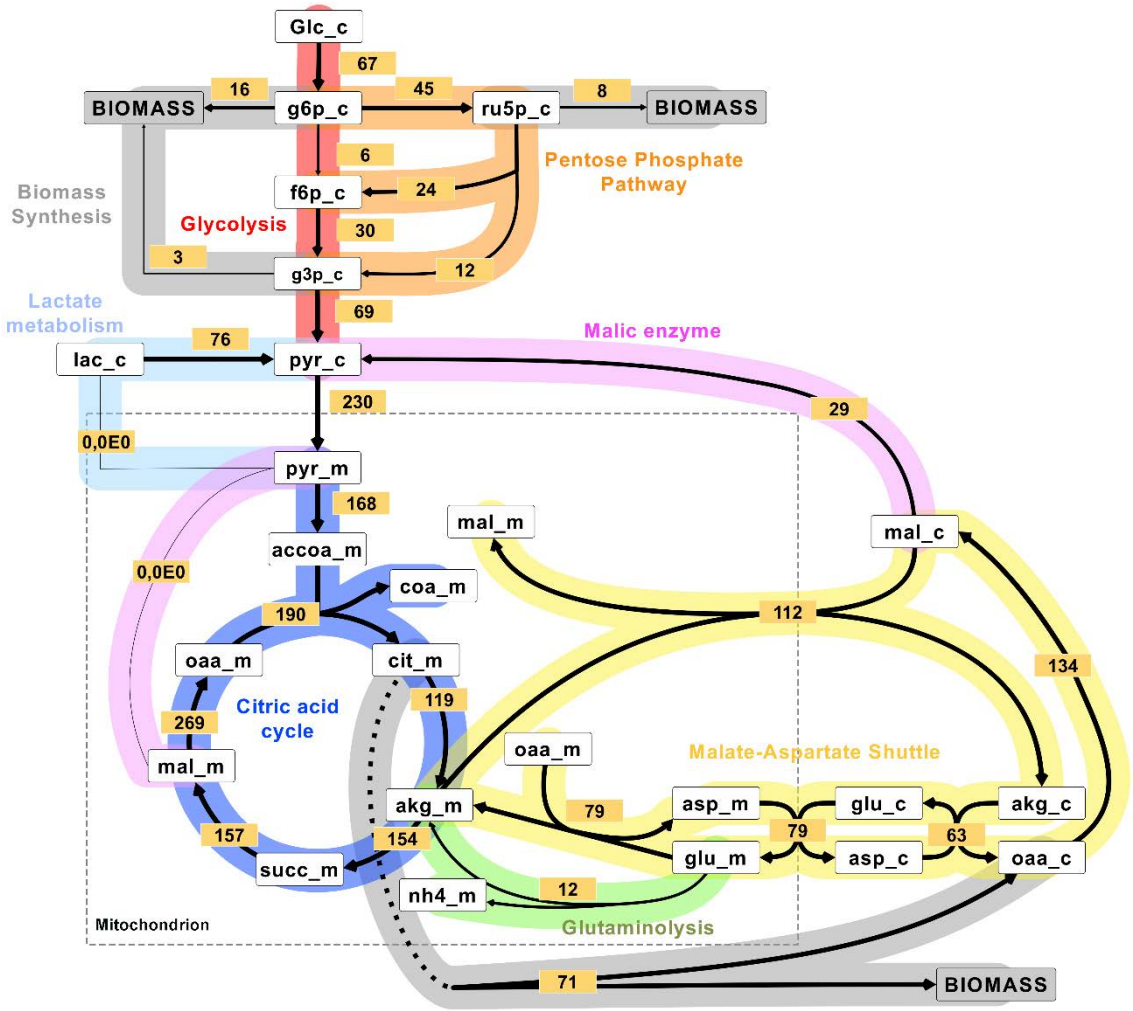

Figure 4.10: Scheme of the main metabolic fluxes calculated for CHO in Phase 2 when pH is controlled to 6.80 adding 15 mM of sodium lactate and considering c-LDH (glucose and lactate concomitant consumption phase; Phase P2_B3 c-LDH). Arrows indicate the direction of the flux and their width the magnitude of fluxes (the exact value is detailed close to the arrows). The box represents the mitochondrion.

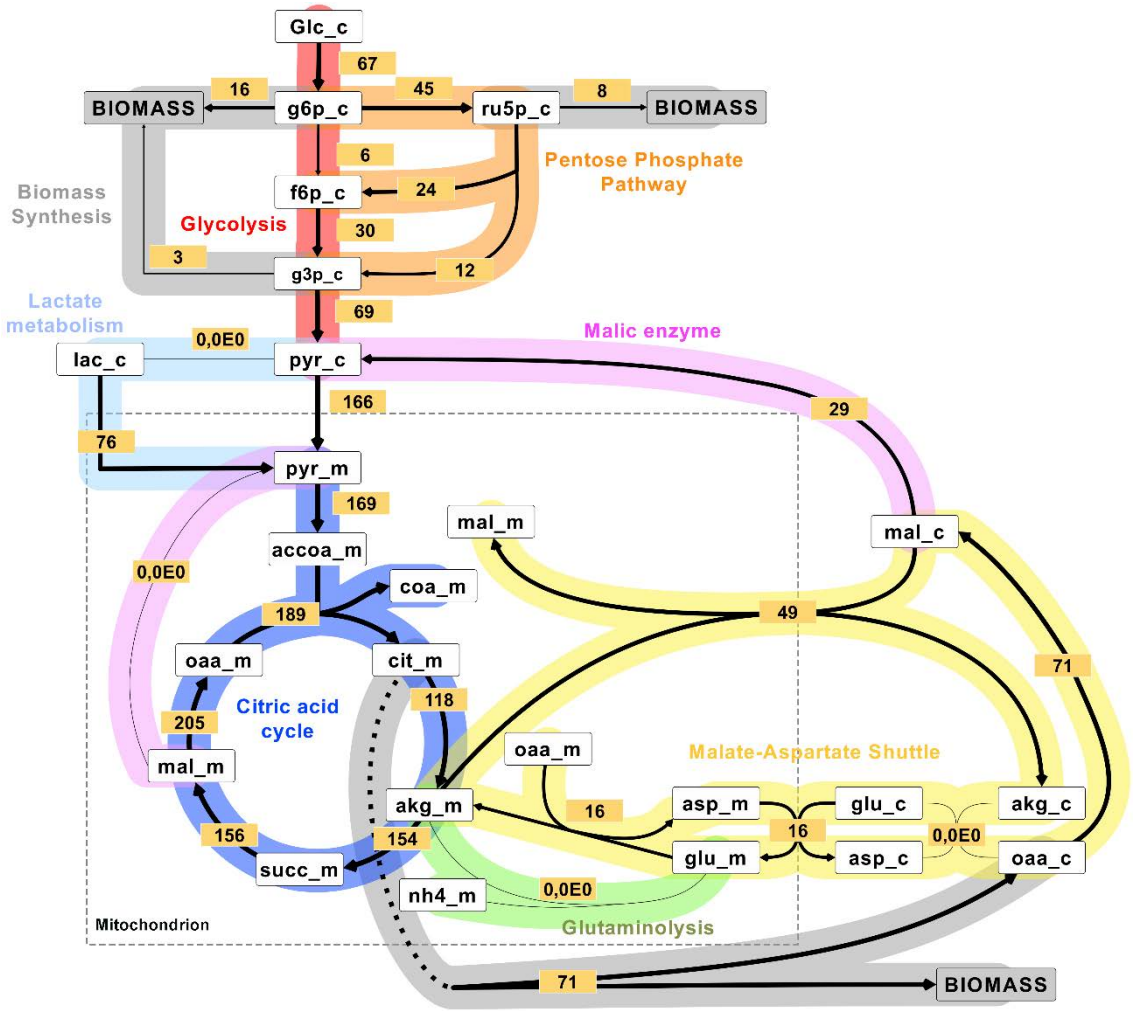

Figure 4.11: Scheme of the main metabolic fluxes calculated for CHO in Phase 2 when pH is controlled to 6.80 adding 15 mM of sodium lactate and considering m-LDH (glucose and lactate concomitant consumption phase; Phase P2_B3 m-LDH). Arrows indicate the direction of the flux and their width the magnitude of fluxes (the exact value is detailed close to the arrows). The box represents the mitochondrion.

Metabolic flux distribution of overflow metabolism in Phase 1 of non pH-controlled conditions and Phase 2 from the beginning of the culture in CHO

The same overflow metabolism characterized by a high glucose uptake rate and the production of high amounts of lactate observed in HEK293 was obtained in Phase 1 of CHO non pH-controlled culture (**Figure 4.9**). Since the majority of glucose consumed was not used for the generation of biomass and energy, it can be considered as a wasteful metabolism. Only 28% of total carbon income (from glucose) was converted into pyruvate and was used for the generation of biomass and energy. The conversion of pyruvate to lactate is the most significant way for completing cytoplasmic NADH regeneration, which has been generated in glycolysis.

On this basis, pyruvate obtained from glucose is primarily converted into lactate, instead of acetyl-CoA, which is further oxidized in the TCA cycle. Besides the lactate production, the

Malate-Aspartate shuttle works as an indirect transport system for NADH from the cytoplasm to the mitochondria (85 nmol·mg·h^{-1}). The malate dehydrogenase catalyzes the reaction from oxaloacetate to malate, regenerating NADH into the cytoplasm. This metabolic behavior is generally accepted as conventional metabolism by the scientific community in mammalian cell cultures (Barron et al., 1998).

In contrast, significant different results were obtained in Phase 2. Glycolysis fluxes were more than 5-fold reduced (67 nmol·mg·h-1 compared to 360 nmol·mg·h^{-1} for the glucose uptake rate) and the carbon income came both from both glucose and lactate. The really interesting fact, comparing both models, is that the TCA fluxes were very similar (around 160 nmol·mg·h^{-1} on the lower part), so similar amounts of energy and thus, similar cell growth rate was obtained. Of the total carbon income in Phase 2 consumed by the cells; the 47% came from glucose and the rest 53% from lactate. As it can be observed in **Table 3**, glucose and lactate co-metabolization resulted in a better-balanced cell metabolism, with reduction of glucose and amino acids uptake rate, without affecting cell growth.

Alternative LDH pathway in lactate consumption in CHO

In order to enrich the discussion of the two hypotheses for lactate consumption presented above (c-LDH and m-LDH), and with the results obtained in simultaneous glucose and lactate consumption, two different models were assessed for Phase 2 obtained from the beginning of the culture, constraining either cytoplasmic or mitochondrial lactate dehydrogenase.

In Phase 1, where high glucose uptake is observed, as with HEK293, the results presented state the necessity of the conversion of pyruvate to lactate by cytoplasmic lactate dehydrogenase (c-LDH) to regenerate the NADH in the cytoplasm. From a biological point of view, there is no reason for carrying out this conversion into the mitochondrial matrix because the NADH regeneration in this compartment could be done by the oxidative phosphorylation pathway. Moreover, an indirect transport system, the malate-aspartate shuttle, is required also for the NADH regeneration in the cytoplasm.

A completely different situation is obtained in Phase 2, because lactate is consumed instead of being produced. In this case, the conversion of lactate to pyruvate leads to a NADH formation, and it is interesting to analyze how the fluxes change in the metabolic network if this reaction occurs in the cytoplasm or into the mitochondria. Comparing both scenarios (**Figure 4.10** for c-LDH and **Figure 4.11** for m-LDH), it can be observed that when c-LDH is considered, the release of NADH in the cytoplasm lead to have a significant higher flux in the malate-aspartate shuttle to regenerate the NADH formed both in glycolysis and in the conversion from lactate to pyruvate in the cytoplasm. In the second approach, when m-LDH is considered, the regeneration of NADH formed in the conversion of lactate to pyruvate is done into the mitochondria, through oxidative phosphorylation pathway. As a consequence, the flux of the malate-aspartate shuttle is considerably reduced, obtaining similar values than in the Phase 1.

This could indicate that the consideration of m-LDH for the lactate metabolization is in some way beneficial for the cell, although the increase of the malate-aspartate shuttle is completely possible from a biological point of view.

4.3.4 Energy study in Phase 1 and Phase 2 obtained in CHO cell cultures

To further explore both possibilities (c-LDH and m-LDH) in Phase 2, a study of the amount of energy (ATP) generated by cells, as well as the distribution of ATP consumed and generated in the different pathways of the metabolism is presented in **Figure 4.12** for Phase 1 (P1_B2) and Phase 2 (P2_B3). In Phase 2 the total ATP generated is slightly lower than in Phase 1 (a bit less biomass generation in Phase 2). It must be said that the total amount of ATP generated that comes from glycolysis was significantly reduced in Phase 2 due to the glucose intake reduction. Anyway, the oxidative phosphorylation pathway was incremented in Phase 2 to compensate the glycolysis reduction. Moreover, comparing both possible scenarios in Phase 2 (c-LDH and m-LDH), the amount of energy produced/consumed is the same, showing that m-LDH is a possible alternative due to this consideration does not involve an energy wasting in the metabolism. In terms of the ATP distribution in the metabolism, the amount of ATP generated and consumed in the different pathways comparing Phases 1 and 2 (both alternatives) is similar. The ATP generated comes principally from the oxidative phosphorylation pathway and in minor ratio from glycolysis. This ATP is mostly used for cells maintenance and biomass formation. These results fit with other studies previously published for mammalian cells (Kilburn et al., 1969).

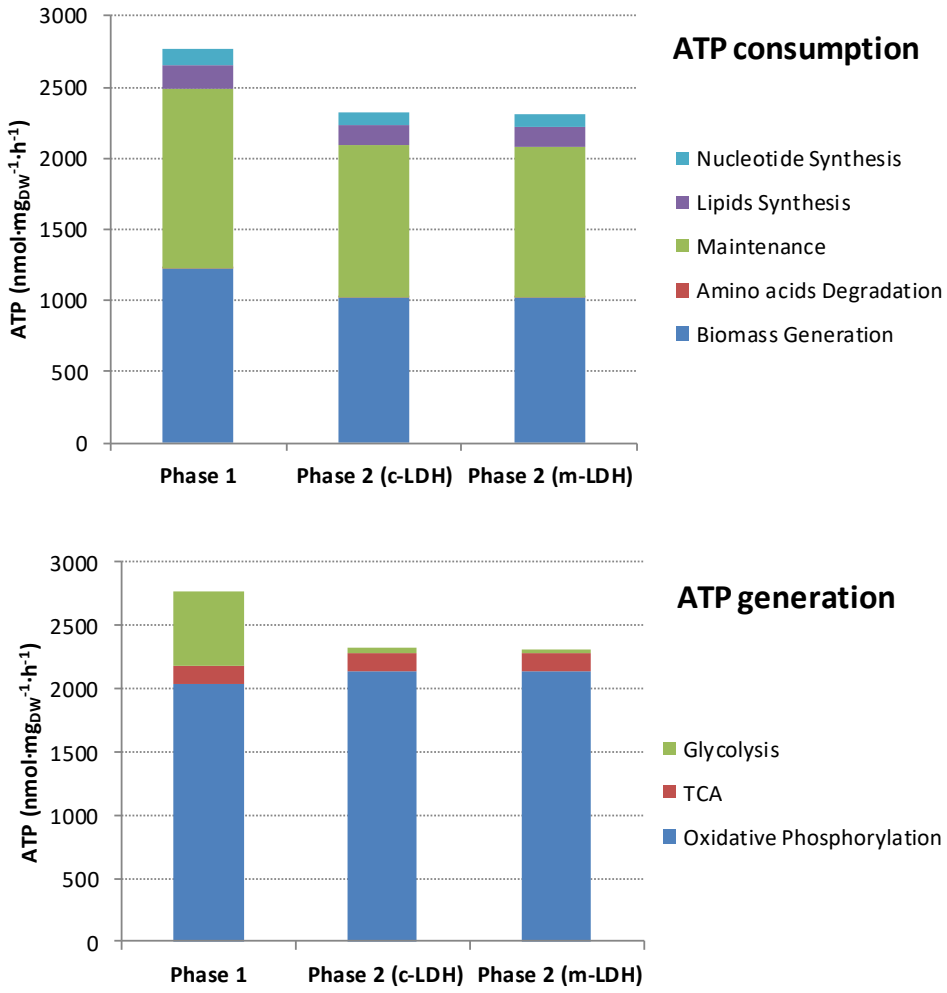

Figure 4.12: Total ATP generated and distribution in ATP consumed and generated in the different pathways of metabolism in phase 1 and 2 (c-LDH and m-LDH).

4.4 Conclusions

An extensive study of the metabolic flux analysis for the three glucose and lactate metabolic behaviors obtained in HEK293 and CHO cell cultures have been presented in this chapter. The most well-known and accepted by the scientific community as standard takes place during the exponential growth phase is the one in which glucose is metabolized while lactate is generated and secreted to the media, either at controlled or not controlled pH, although in controlled pH the glycolytic flux and lactate production are much higher than in non-controlled pH. Such metabolic behavior is considered universal for all mammalian cell lines.

The analysis of the metabolic fluxes allows to the conclusion that this metabolism should be understood under the perspective that animal cells are the symbiosis of two different metabolisms that belong to two different ancestors. One anaerobic, that takes place in the cytoplasm, and the other aerobic, located into mitochondria (Endosymbiotic Theory (Mereschkowsky and C., 1910; Sagan, 1967)). The anaerobic metabolism must be able to uptake and process larger carbon source molecules at high rates. Only 2 ATPs (i.e. low energy amount)

can be obtained from each glucose molecule. On the contrary, the aerobic metabolism can generate larger amounts of energy (34 ATPs) from each glucose molecule. Hence, the flux rates related to the aerobic metabolism are much lower than those from the anaerobic metabolism.

The co-existence of both metabolisms with different flux rates leads to a by-product (lactate) generation and secretion. Both metabolisms are somehow uncoupled in terms of flux rates, affecting the NADH regeneration, that takes place mainly in the cytoplasm instead of mitochondria. In principle, a more efficient metabolism is possible and would be based on coupling the flux rates of both metabolisms by reducing the glycolytic fluxes accordingly to the TCA fluxes.

The second behavior appears when glucose has been completely depleted from the media. In this phase of culture cells consume the lactate produced during the previous phase (exponential growth phase) as a sole carbon and energy source. Analyzing the metabolic fluxes of this behavior, biosynthesis and energy production are much lower when compared with the behavior described above. TCA fluxes were drastically reduced. Consequently, only residual cell growth at very low growth rates was observed.

The third metabolic behavior observed is based on the co-metabolization of glucose and lactate. Such metabolic behavior has not usually been observed in cell cultures and occurs when lactate and protons reach high concentrations outside the cells. In those conditions, cells are able, to co-transport extracellular protons together with lactate into the cytosol. Once in the cytosolic space, lactate could be oxidized to pyruvate which is transported into mitochondria or, alternatively (in this work both hypothesis were taked into account), lactate could be directly transported into mitochondria being then oxidized. Our empirical data obtained by respirometry assays, using isolated mitochondria of HEK293 cells, indicated that both possibilities are feasible. Then, both alternative routes have been considered into the model proposed when performing the metabolic flux balance analysis for HEK293 and CHO cell lines. The metabolic flux balances performed with this model converged in a solution for both hypothesis (c-LDHc and m-LDH), meaning that the alternative route proposed is feasible. The outcome of such model where lactate can be metabolized directly into the mitochondria shows lower fluxes at the Malate/Aspartate shuttle since NADH is directly released into mitochondria, where it is regenerated again as NAD^+ and H^+. As NADH is not generated in the cytosol, there is no need to transport it into the mitochondria reducing the requirement for transporting NADH through the Malate/Aspartate Shuttle, as pointed above.

Interestingly, switching to a glucose and lactate co-metabolization resulted in a better-balanced cell metabolism, as can be seen from the metabolic fluxes calculated. Moreover, the generation and secretion of lactate is totally reverted, so the main drawback of processes based on mammalian cell cultures is also eliminated.

In summary, the modification of extracellular conditions (lower pH and presence of lactate in the medium) triggers the uptake and co-consumption of lactate and glucose in HEK293 and CHO cells. The uptake of lactate is possible due to the concentration differences between extracellular and intracellular spaces, having as a consequence the reorganization of the

metabolic pathways. The main differences were observed in glycolysis, the pathways around the TCA cycle and amino acids consumption rates. The metabolic reorganization could happen as a consequence of up-regulation or down-regulation of different genes coding for the enzymes involved in those pathways.

This novel hypothesis about the lactate metabolism control in HEK293 and CHO cells opens the door to re-directing genetic engineering strategies in order to obtain improved engineered cell lines with more efficient metabolism, and also, to further develop mammalian cell technology applications.

Therefore, further studies and deeper knowledge on cell metabolism and better understanding of the metabolic pathways and fluxes distribution are essential to develop novel engineered cell lines that will be able to overcome the current metabolic drawbacks or limitations of mammalian cell lines.

4.5 References

1. Altamirano C, Illanes A, Casablancas A, Gamez X, Cairo JJ, Godia C. 2001. Analysis of CHO Cells Metabolic Redistribution in a Glutamate-Based Defined Medium in Continuous Culture. *Biotechnol. Prog.* **17**:1032–1041. http://doi.wiley.com/10.1021/bp0100981.
2. Altamirano C, Illanes A, Becerra S, Cairó JJ, Gòdia F. 2006. Considerations on the lactate consumption by CHO cells in the presence of galactose. *J. Biotechnol.* **125**:547–556. https://www.sciencedirect.com/science/article/pii/S0168165606002471.
3. Andersen DC, Goochee CF. 1995. The effect of ammonia on theO-linked glycosylation of granulocyte colony-stimulating factor produced by chinese hamster ovary cells. *Biotechnol. Bioeng.* **47**:96–105. http://doi.wiley.com/10.1002/bit.260470112.
4. De Bari L, Atlante A, Valenti D, Passarella S. 2004. Partial reconstruction of in vitro gluconeogenesis arising from mitochondrial l-lactate uptake/metabolism and oxaloacetate export via novel L-lactate translocators. *Biochem. J.* **380**:231–42. http://www.ncbi.nlm.nih.gov/pubmed/14960150.
5. Barron JT, Gu L, Parrillo JE. 1998. Malate-Aspartate Shuttle, Cytoplasmic NADH Redox Potential, and Energetics in Vascular Smooth Muscle. *J. Mol. Cell. Cardiol.* **30**:1571–1579. https://www.sciencedirect.com/science/article/pii/S0022282898907222.
6. Bonarius HPJ, Hatzimanikatis V, Meesters KPH, de Gooijer CD, Schmid G, Tramper J. 1996. Metabolic flux analysis of hybridoma cells in different culture media using mass balances. *Biotechnol. Bioeng.* **50**:299–318. http://doi.wiley.com/10.1002/%28SICI%291097-0290%2819960505%2950%3A3%3C299%3A%3AAID-BIT9%3E3.0.CO%3B2-B.
7. Bradford MM. 1976. A rapid and sensitive method for the quantitation of microgram quantities of protein utilizing the principle of protein-dye binding. *Anal. Biochem.* **72**:248–254. https://www.sciencedirect.com/science/article/pii/0003269776905273.
8. Brooks GA, Dubouchaud H, Brown M, Sicurello JP, Butz CE. 1999. Role of mitochondrial lactate dehydrogenase and lactate oxidation in the intracellular lactate shuttle. *Proc. Natl. Acad. Sci. U. S. A.* **96**:1129–34. http://www.ncbi.nlm.nih.gov/pubmed/9927705.

9. Brown GC. 1992. Control of respiration and ATP synthesis in mammalian mitochondria and cells. *Biochem. J.* **284 (Pt 1)**:1–13. http://www.ncbi.nlm.nih.gov/pubmed/1599389.

10. Brunner M, Doppler P, Klein T, Herwig C, Fricke J. 2018. Elevated pCO2 affects the lactate metabolic shift in CHO cell culture processes. *Eng. Life Sci.* **18**:204–214. http://doi.wiley.com/10.1002/elsc.201700131.

11. Cruz HJ, Moreira JL, Carrondo MJ. 1999. Metabolic shifts by nutrient manipulation in continuous cultures of BHK cells. *Biotechnol. Bioeng.* **66**:104–13. http://www.ncbi.nlm.nih.gov/pubmed/10567068.

12. Droste P, Miebach S, Niedenführ S, Wiechert W, Nöh K. 2011. Visualizing multi-omics data in metabolic networks with the software Omix—A case study. *Biosystems* **105**:154–161. https://www.sciencedirect.com/science/article/pii/S0303264711000761.

13. Fox JEM, Meredith D, Halestrap AP. 2000. Characterisation of human monocarboxylate transporter 4 substantiates its role in lactic acid efflux from skeletal muscle. *J. Physiol.* **529**:285–293. http://doi.wiley.com/10.1111/j.1469-7793.2000.00285.x.

14. Gladden LB. 2007. Is there an intracellular lactate shuttle in skeletal muscle? *J. Physiol.* **582**:899–899. http://doi.wiley.com/10.1113/jphysiol.2007.138487.

15. Hashimoto T, Hussien R, Brooks GA. 2006. Colocalization of MCT1, CD147, and LDH in mitochondrial inner membrane of L6 muscle cells: evidence of a mitochondrial lactate oxidation complex. *Am. J. Physiol. Metab.* **290**:E1237–E1244. http://www.physiology.org/doi/10.1152/ajpendo.00594.2005.

16. Hashimoto T, Hussien R, Cho H-S, Kaufer D, Brooks GA. 2008. Evidence for the Mitochondrial Lactate Oxidation Complex in Rat Neurons: Demonstration of an Essential Component of Brain Lactate Shuttles. Ed. Mark R. Cookson. *PLoS One* **3**:e2915. http://dx.plos.org/10.1371/journal.pone.0002915.

17. Hefzi H, Ang KS, Hanscho M, Bordbar A, Ruckerbauer D, Lakshmanan M, Orellana CA, Baycin-Hizal D, Huang Y, Ley D, Martinez VS, Kyriakopoulos S, Jiménez NE, Zielinski DC, Quek L-E, Wulff T, Arnsdorf J, Li S, Lee JS, Paglia G, Loira N, Spahn PN, Pedersen LE, Gutierrez JM, King ZA, Lund AM, Nagarajan H, Thomas A, Abdel-Haleem AM, Zanghellini J, Kildegaard HF, Voldborg BG, Gerdtzen ZP, Betenbaugh MJ, Palsson BO, Andersen MR, Nielsen LK, Borth N, Lee D-Y, Lewis NE. 2016. A Consensus Genome-scale Reconstruction of Chinese Hamster Ovary Cell Metabolism. *Cell Syst.* **3**:434–443.e8. https://www.sciencedirect.com/science/article/pii/S2405471216303635.

18. Henry O, Perrier M, Kamen A. 2005. Metabolic flux analysis of HEK-293 cells in perfusion cultures for the production of adenoviral vectors. *Metab. Eng.* **7**:467–476. https://www.sciencedirect.com/science/article/pii/S1096717605000686.

19. Iglesias-González J, Sánchez-Iglesias S, Méndez-Álvarez E, Rose S, Hikima A, Jenner P, Soto-Otero R. 2012. Differential Toxicity of 6-Hydroxydopamine in SH-SY5Y Human Neuroblastoma Cells and Rat Brain Mitochondria: Protective Role of Catalase and Superoxide Dismutase. *Neurochem. Res.* **37**:2150–2160. http://link.springer.com/10.1007/s11064-012-0838-6.

20. Jastroch M, Hirschberg V, Klingenspor M. 2012. Functional characterization of UCP1 in mammalian HEK293 cells excludes mitochondrial uncoupling artefacts and reveals no contribution to basal proton leak. *Biochim. Biophys. Acta - Bioenerg.* **1817**:1660–1670.

https://www.sciencedirect.com/science/article/pii/S0005272812001831.

21. Kennedy KM, Dewhirst MW. 2010. Tumor metabolism of lactate: the influence and therapeutic potential for MCT and CD147 regulation. *Futur. Oncol.* **6**:127–148. http://www.futuremedicine.com/doi/10.2217/fon.09.145.
22. KILBURN DG, LILLY MD, WEBB FC. 1969. The Energetics of Mammalian Cell Growth. *J. Cell Sci.* **4**. http://jcs.biologists.org/content/4/3/645.short.
23. Li C, Donizelli M, Rodriguez N, Dharuri H, Endler L, Chelliah V, Li L, He E, Henry A, Stefan MI, Snoep JL, Hucka M, Le Novère N, Laibe C. 2010. BioModels Database: An enhanced, curated and annotated resource for published quantitative kinetic models. *BMC Syst. Biol.* **4**:92. http://bmcsystbiol.biomedcentral.com/articles/10.1186/1752-0509-4-92.
24. Lin AA, Miller WM. 1992. CHO cell responses to low oxygen: Regulation of oxygen consumption and sensitization to oxidative stress. *Biotechnol. Bioeng.* **40**:505–516. http://doi.wiley.com/10.1002/bit.260400409.
25. Lodish H, Berk A, Darnell JE, Kaiser CA, Krieger M, Scott MP, Bretscher A, Ploegh H, Matsudaira P. 2008. Molecular cell biology. Macmillan.
26. Luo J, Vijayasankaran N, Autsen J, Santuray R, Hudson T, Amanullah A, Li F. 2012. Comparative metabolite analysis to understand lactate metabolism shift in Chinese hamster ovary cell culture process. *Biotechnol. Bioeng.* **109**:146–156. http://doi.wiley.com/10.1002/bit.23291.
27. Martinelle K, Westlund A, H�ggstr�m L. 1996. Ammonium ion transport?a cause of cell death. *Cytotechnology* **22**:251–254. http://link.springer.com/10.1007/BF00353945.
28. Martínez VS, Dietmair S, Quek L-E, Hodson MP, Gray P, Nielsen LK. 2013. Flux balance analysis of CHO cells before and after a metabolic switch from lactate production to consumption. *Biotechnol. Bioeng.* **110**:660–666. http://doi.wiley.com/10.1002/bit.24728.
29. MERESCHKOWSKY, C. 1910. Theorie der zwei Plasmaarten als Grundlage der Symbiogenesis, einer neuen Lehre von der Entstehung der Organismen. *Biol. Cent.* **30**:278-288,289-303,322-374,353–367. https://ci.nii.ac.jp/naid/10020710101/.
30. Mulukutla BC, Gramer M, Hu W-S. 2012. On metabolic shift to lactate consumption in fed-batch culture of mammalian cells. *Metab. Eng.* **14**:138–149. https://www.sciencedirect.com/science/article/pii/S1096717611001285.
31. Oliveira A, Nielsen J, Förster J. 2005. Modeling Lactococcus lactis using a genome-scale flux model. *BMC Microbiol.* **5**:39. http://bmcmicrobiol.biomedcentral.com/articles/10.1186/1471-2180-5-39.
32. Ozturk SS, Palsson BO. 1991. Growth, metabolic, and antibody production kinetics of hybridoma cell culture: 2. Effects of serum concentration, dissolved oxygen concentration, and medium pH in a batch reactor. *Biotechnol. Prog.* **7**:481–494. http://doi.wiley.com/10.1021/bp00012a002.
33. Ozturk SS, Riley MR, Palsson BO. 1992. Effects of ammonia and lactate on hybridoma growth, metabolism, and antibody production. *Biotechnol. Bioeng.* **39**:418–431. http://doi.wiley.com/10.1002/bit.260390408.
34. Paredes C, Sanfeliu A, Cardenas F, Cairó JJ, Gòdia F. 1998. Estimation of the

intracellular fluxes for a hybridoma cell line by material balances. *Enzyme Microb. Technol.* **23**:187–198. https://www.sciencedirect.com/science/article/pii/S0141022998000234.

35. Passarella S, de Bari L, Valenti D, Pizzuto R, Paventi G, Atlante A. 2008. Mitochondria and l -lactate metabolism. *FEBS Lett.* **582**:3569–3576. http://doi.wiley.com/10.1016/j.febslet.2008.09.042.

36. Passarella S, Paventi G, Pizzuto R. 2014. The mitochondrial L-lactate dehydrogenase affair. *Front. Neurosci.* **8**:407. http://journal.frontiersin.org/article/10.3389/fnins.2014.00407/abstract.

37. Quek L-E, Dietmair S, Hanscho M, Martínez VS, Borth N, Nielsen LK. 2014. Reducing Recon 2 for steady-state flux analysis of HEK cell culture. *J. Biotechnol.* **184**:172–178. https://www.sciencedirect.com/science/article/pii/S0168165614002673.

38. Quek L-E, Dietmair S, Krömer JO, Nielsen LK. 2010. Metabolic flux analysis in mammalian cell culture. *Metab. Eng.* **12**:161–171. https://www.sciencedirect.com/science/article/pii/S1096717609000858.

39. Quek L-E, Nielsen LK. 2008. On the reconstruction of the Mus musculus genome-scale metabolic network model. In: . *Genome Informatics 2008 Genome Informatics Ser. Vol. 21*. World Scientific, pp. 89–100.

40. Rocha I, Maia P, Evangelista P, Vilaça P, Soares S, Pinto JP, Nielsen J, Patil KR, Ferreira EC, Rocha M. 2010. OptFlux: an open-source software platform for in silico metabolic engineering. *BMC Syst. Biol.* **4**:45. http://bmcsystbiol.biomedcentral.com/articles/10.1186/1752-0509-4-45.

41. Sagan L. 1967. On the origin of mitosing cells. *J. Theor. Biol.* **14**:225-IN6. https://www.sciencedirect.com/science/article/pii/0022519367900793.

42. Savinell JM, Palsson BO. 1992. Network analysis of intermediary metabolism using linear optimization. I. Development of mathematical formalism. *J. Theor. Biol.* **154**:421–454. https://www.sciencedirect.com/science/article/pii/S0022519305801614.

43. Sellick CA, Croxford AS, Maqsood AR, Stephens G, Westerhoff H V., Goodacre R, Dickson AJ. 2011. Metabolite profiling of recombinant CHO cells: Designing tailored feeding regimes that enhance recombinant antibody production. *Biotechnol. Bioeng.* **108**:3025–3031. http://doi.wiley.com/10.1002/bit.23269.

44. Sheikh K, Förster J, Nielsen LK. 2005. Modeling Hybridoma Cell Metabolism Using a Generic Genome-Scale Metabolic Model of Mus musculus. *Biotechnol. Prog.* **21**:112–121. http://doi.wiley.com/10.1021/bp0498138.

45. Swainston N, Smallbone K, Hefzi H, Dobson PD, Brewer J, Hanscho M, Zielinski DC, Ang KS, Gardiner NJ, Gutierrez JM, Kyriakopoulos S, Lakshmanan M, Li S, Liu JK, Martínez VS, Orellana CA, Quek L-E, Thomas A, Zanghellini J, Borth N, Lee D-Y, Nielsen LK, Kell DB, Lewis NE, Mendes P. 2016. Recon 2.2: from reconstruction to model of human metabolism. *Metabolomics* **12**:109. http://link.springer.com/10.1007/s11306-016-1051-4.

46. Thiele I, Swainston N, Fleming RMT, Hoppe A, Sahoo S, Aurich MK, Haraldsdottir H, Mo ML, Rolfsson O, Stobbe MD, Thorleifsson SG, Agren R, Bölling C, Bordel S, Chavali AK, Dobson P, Dunn WB, Endler L, Hala D, Hucka M, Hull D, Jameson D, Jamshidi N, Jonsson JJ, Juty N, Keating S, Nookaew I, Le Novère N, Malys N, Mazein A, Papin JA,

Price ND, Selkov E, Sigurdsson MI, Simeonidis E, Sonnenschein N, Smallbone K, Sorokin A, van Beek JHGM, Weichart D, Goryanin I, Nielsen J, Westerhoff H V, Kell DB, Mendes P, Palsson BØ. 2013. A community-driven global reconstruction of human metabolism. *Nat. Biotechnol.* **31**:419–425. http://www.nature.com/articles/nbt.2488.

47. Vallino JJ, Stephanopoulos G. 1993. Metabolic flux distributions inCorynebacterium glutamicum during growth and lysine overproduction. *Biotechnol. Bioeng.* **41**:633–646. http://doi.wiley.com/10.1002/bit.260410606.
48. Vriezen N, van Dijken JP. 1998. Fluxes and enzyme activities in central metabolism of myeloma cells grown in chemostat culture. *Biotechnol. Bioeng.* **59**:28–39. http://doi.wiley.com/10.1002/%28SICI%291097-0290%2819980705%2959%3A1%3C28%3A%3AAID-BIT5%3E3.0.CO%3B2-V.
49. Xie L, Wang DIC. 2000. Material balance studies on animal cell metabolism using a stoichiometrically based reaction network. *Biotechnol. Bioeng.* **52**:579–590. http://doi.wiley.com/10.1002/%28SICI%291097-0290%2819961205%2952%3A5%3C579%3A%3AAID-BIT5%3E3.0.CO%3B2-G.
50. Yang M, Butler M. 2000. Effects of ammonia on CHO cell growth, erythropoietin production, and glycosylation. *Biotechnol. Bioeng.* **68**:370–380. http://doi.wiley.com/10.1002/%28SICI%291097-0290%2820000520%2968%3A4%3C370%3A%3AAID-BIT2%3E3.0.CO%3B2-K.
51. Zupke C, Sinskey AJ, Stephanopoulos G. 1995. Intracellular flux analysis applied to the effect of dissolved oxygen on hybridomas. *Appl. Microbiol. Biotechnol.* **44**:27–36. http://link.springer.com/10.1007/BF00164476.

CHAPTER 5. RESULTS (III) A NEW STRATEGY FOR FED-BATCH PROCESS CONTROL OF HEK293 CELL CULTURES BASED ON ALKALI BUFFER ADDITION MONITORING: COMPARISON WITH O.U.R. DYNAMIC METHOD

Abstract

Once the different glucose/lactate metabolism for HEK293/CHO have been studied the next step is to apply this knowledge in bioprocess engineering. The cell metabolism study can be directly applied to develop new monitoring and controlling systems for increasing the productivity of the process. HEK293 producing IFN-γ cell line constructed by our group has been chosen as a model cell line for this work.

In the context of bioprocess engineering, the increasing demand for biopharmaceuticals produced in mammalian cells has driven industry to enhance productivity of bioprocesses through different strategies. Regarding this, fed-batch and perfusion cultures are considered more attractive choices than batch processes. However, the efficient application of these processes requires the availability of reliable on-line measuring systems for cell density and cell metabolic activity estimation.

The present work focuses on the comparison of two different monitoring tools for indirect biomass concentration estimation in a HEK293 cell cultures producing IFN-γ: on one side, the Oxygen Uptake Rate (O.U.R.) determination, by means of application of the dynamic method measurement which is already a widely used tool and, on the other side a new robust on-line monitoring tool based on the alkali buffer addition used to maintain the pH set-point.

Both strategies allow a proper of cell growth and metabolic activity monitoring, with precise identification of the balanced cell growth and the most important action in the process, as is media feeding. The application of these monitoring systems in fed-batch processes allows extending the exponential growth of HEK293 cells, which in turn results in higher cell concentrations compared with batch strategy ($7x10^6$ cells·$mL^{-1)}$, achieving $14x10^6$ cells·mL^{-1} for the O.U.R. strategy and $19x10^6$ cells·mL^{-1} for the alkali addition-based strategy. Product titter is also increased in respect of the batch strategy (3.70 mg·L^{-1}), resulting in 8.27 mg·L^{-1} for O.U.R. and 11.49 mg·L^{-1} for the alkali buffer strategy.

Results prove that fed-batch strategy based on the alkali buffer addition is a robust on-line monitoring method that has shown its great potential to optimize the feeding strategy in 293HEK cells fed-batch cultures.

Nomenclature

$[Product]_{final}$: final product concentration (µg·mL^{-1} for q_P) and (µg·L^{-1} for V_P)
ΔV_{alkali}: alkali buffer addition from time t_0 (L)
q_m: specific consumption/production rate of the metabolite m (nmols·10^{6}cells $^{-1}$·h^{-1})
C_{O_2}: oxygen concentration in the liquid phase (mmols·L^{-1})
$C_{m,0}$: concentration of the metabolite m at time t_0 (mmols·L^{-1})
C_m: concentration of the metabolite m (mmols·L^{-1})
K_{des}: O_2 desorption constant in N_2 (headspace) (h^{-1})
V_0: bioreactor volume at the beginning of each feed cycle (L)
V_P: volumetric productivity of the process (µg·L^{-1}·h^{-1})
V_f: total feed volume needed for each cycle (fed-batch) (mL)
X_0: viable cell concentration at the beginning of each feed cycle (10^{6}cells·mL^{-1})
$X_{v,0}$: viable cell concentration at time t_0 (10^{6}cells·mL^{-1})
X_v: viable cell concentration (10^{6}cells·mL^{-1})
$Y_{\frac{S}{X}}$: glucose-biomass yield (mmol$_{gluc}$·10^{6}cells^{-1})
$Y_{\frac{lac}{X}}$: lactate-biomass yield (mmol$_{lac}$·10^{6}cells^{-1})
$Y_{\frac{lac}{gluc}}$: lactate-glucose yield (nmol$_{lac}$·nmol$_{gluc}$$^{-1}$)
k_b: constant that relates the lactate generated with the alkali buffer addition (mmol$_{lac}$·mmol$_{NaOH}$$^{-1}$)
k_d: glutamine descomposition rate (h^{-1})
qO_2: specific oxygen consumption rate (nmol$_{O2}$·10^{6}cells^{-1}·h^{-1})
q_P: specific productivity of the cells (µg·10^{6}cells^{-1}·h^{-1})
q_{gluc}: specific glucose consumption rate (nmol·10^{6}cells^{-1}·h^{-1})
q_{lac}: specific lactate consumption rate (nmol·10^{6}cells^{-1}·h^{-1})
r_X: growth rate (10^{6}cells·mL^{-1}·h^{-1})
r_m: consumption/production rate of the metabolite m (mmols·L^{-1}·h^{-1})
t_{total}: total process time (h^{-1})
μ_{max}: maximum specific growth rate (h^{-1})
$[S]_{alkali}$: alkali concentration in the buffer solution (mmols·L^{-1})
$[lac]$: lactate concentration (mmols·L^{-1})
Δt: time range of each cycle (fed-batch) (h)
D.O.: relative oxygen concentration in the liquid phase in respect to the air saturation in equilibrium (%)
Fp: feed media pump flow (mL·min^{-1})
O.U.R.: oxygen uptake rate (mmols·L^{-1}·h^{-1})
S: glucose concentration in the bioreactor (fed-batch) (mmols·L^{-1})
S_0: glucose concentration in the feed media (fed-batch) (mmols·L^{-1})
t: time (h)
V: bioreactor volume (L)
Dt: duplication time (h)

$F(t)$: feed flow rate (mL·h^{-1})
ICV: Integral of viable cells (10^{6}cells·mL^{-1}·h^{-1})

5.1 Introduction

Mammalian cells are a well-established system for the production of a wide range of proteins with both diagnostic and therapeutic applications (Dingermann, 2008; De Jesus and Wurm, 2011). In particular, HEK293 cell line has been gaining importance during the last decade, due to its capacity to perform some post-transitional modifications that other commonly used cell lines, as CHO cells, perform inadequately (Durocher and Butler, 2009).

Many of the established processes of cell culture are based on batch systems, which offer the advantage of simplicity and allow to culture cells in suspension in homogeneous bioreactors. In these culture systems cells reach a maximum concentration quite poor and, when this cell concentration is reached, their growth decays in a very sharp pattern (Abu-Absi et al., 2013). There are different reasons for this decay, primarily nutrient exhaustion (mainly glucose and glutamine in batch cultures) or toxic metabolite accumulation, among which lactate and ammonium have received a lot of attention in the past (Cruz et al., 2000).

All these factors, together with the intrinsic low growth rate of mammalian cells, render low productivities in these processes that are compensated, in many cases, by the high added value of the obtained products. The improvement of such a process, directed to maximize the product yield and process efficiency, requires the identification and study of reliable on-line monitoring systems. Specially for cell culture processes, the monitoring method should allow the determination of culture parameters, as cell growth and metabolic activity, through the monitoring of cell density and nutrient concentration (i.e. glucose, glutamine, lactate or oxygen) and their specific consumption or generation rates (Casablancas et al., 2013).

The media commonly used in batch cell cultures contain high concentrations of nutrients needed for cell growth, being glucose the main energy and carbon source and glutamine, also carbon and nitrogen sources. However, this high concentration of glucose causes a metabolic deregulation in the inflows of this substrate. Thus, glucose enters the glycolysis pathway with a higher rate than its incorporation as acetyl coenzyme-A into the Krebs cycle, so there is a bottleneck caused by the excess of glucose that leads to the formation of lactate that can reach almost the same mass quantities (Altamirano et al., 2000; Sanfeliu et al., 1997). The formation of lactate from glucose is a process far less efficient from an energy perspective to its oxidation in the Krebs cycle (Martínez et al., 2013), and moreover, involves the accumulation of high concentrations of lactic acid which is significantly detrimental to the culture (Ozturk et al., 1992). The deregulation in the cellular metabolism involves a rapid consumption of glucose and glutamine and the generation of by-products, resulting in their fast depletion and thus the end of the culture (Altamirano et al., 2000).

CHAPTER 5. RESULTS (III) A NEW STRATEGY FOR FED-BATCH PROCESS CONTROL OF HEK293 CELL CULTURES BASED ON ALKALI BUFFER ADDITION MONITORING: COMPARISON WITH O.U.R. DYNAMIC METHOD

To overcome the disadvantages of batch cultures, other alternative cell culture strategies providing an environment closer to the physiological state of cells *in vivo* systems have already been implemented, such as fed batch (Casablancas et al., 2013; Huang et al., 2010) or perfusion processes (Lecina et al., 2011). In any case, to effectively implement these culture strategies it is necessary to have on line measurements of cell concentration and activity, as well as the concentration of key compounds of media.

Over the recent years, various methods for measuring some of the most important variables in cell culture have been proposed-. substrates concentration such as glucose and glutamine, by-products concentration such as lactate and ammonium using chromatographic techniques (ex. HPLC) or by flow injection analysis (FIA) coupled with biosensors (Casablancas et al., 2013; Kurokawa et al., 1994; Lee et al., 2003; Sauer et al., 2000). In the same way, commercial probes have been proposed for monitoring cell density through turbidimetric principles (Junker et al., 1994) or image analysis (Höpfner et al., 2010). Cell activity can be measured indirectly through different substrates uptake rates, as is the oxygen uptake rate (O.U.R.) (Fontova et al., 2018; Kussow et al., 1995; Ruffieux et al., 1998; Zhou and Hu, 1994).

The work presented examines the application of two cell culture monitoring methods. On one hand an easily measurable parameter, the oxygen uptake rate (O.U.R.), was used as measurement that correlates the physiological state of cells to predict the concentration of viable cells (Kamen et al., 1996; Lecina et al., 2006; Wong et al., 1994). On the other hand, a new monitoring tool based on the alkali buffer addition to neutralize the acid by-product generation in order to maintain the pH in culture is also presented.

The particularities in the development of the monitoring systems and the results obtained when applied to fed-batch cultures of the HEK293 cells are described, allowing the comparison of the two monitoring options studied.

5.2 Materials and Methods

5.2.1 Cell line and cell maintenance

The HEK293SF-3F6 cell line was kindly provided by Dr. A. Kamen (National Research Council of Canada) which was obtained as reported before (Côté et al., 1998). The cell line was transfected to produce an IFN-γ immune-cytokine obtained from human white blood cells. Cell line maintenance was performed in 125 mL shake flasks (Corning Inc.) continuously agitated at 110 rpm on an orbital shaking platform (Stuart SSL110, Bibby Scientific Ltd.), in a 5% CO_2 air mixture and humidified at 37°C (Forma Scientific CO_2 incubator). Cultures were maintained in 15 mL volumes, sampled, and diluted every 2 or 3 days with fresh medium to get an initial seeding density of 0.25 x 10^6 viable cells mL^{-1}.

5.2.2 Cell number and viability

Viable cell concentration and viability were determined by the trypan blue exclusion method using a haemocytometer (Neubauer improved, Brand) and a phase contrast microscope (Nikon eclypse, TS100). After cell counting, the remainder of each sample was centrifuged at 300 rpm for 3 minutes to remove the cells, and the supernatant was 0.22µm filtered and frozen for further analysis.

5.2.3 Culture medium.

The basal medium used in all cultures was SFMtransFx-293 w/o L-glutamine (Hyclone, Thermo Scientific) and it was supplemented with thermally inactivated foetal bovine serum, 5% v/v (Sigma, 043M3397); GlutaMAX, 4 mM (Invitrogen); cell shear protector Kolliphor, 2 $g \cdot L^{-1}$ (Sigma) and Antifoam C emulsion, 50 $mg \cdot L^{-1}$ (Sigma).

5.2.4 Feed medium for fed-batch processes

Feed medium was composed of CellBoost 5, 20 $g \cdot L^{-1}$ (Hyclone); D-glucose, 50 $g \cdot L^{-1}$ (Sigma); Vitamins, 6% v/v (MEM Vitamin 100X, Gibco); Aminoacid Solution, 6% v/v (MEM Aminoacid 50X, Gibco); GlutaMAX, 14 mM (GlutaMAX 200mM, Invitrogen); Cell Shear Protector Kolliphor, 5 $g \cdot L^{-1}$ (Sigma) and Antifoam C Emulsion, 200 $mg \cdot L^{-1}$ (Sigma).

5.2.5 Stirred-tank bioreactor for batch and fed-batch: operational conditions

The stirred-tank bioreactor used in the present study was a commercial bioreactor (Biostat B DCUII Sartorius Stedim Biotech, Germany) with 2L cylindrical vessel, equipped with probes and control systems for pH, D.O. (relative oxygen partial pressure) and temperature, stirred with two marine impellers at 100 rpm. Dissolved oxygen concentration was monitored with an optical probe (VisiFerm DO, Hamilton), and maintained at 30% of saturation by a sparger aeration flow of 0.35 $L \cdot min^{-1}$ and a gas mixing unit. Temperature was maintained at 37ºC. pH was measured with a standard electrode (EasyFerm Plus, Hamilton), and it was maintained at 7.02 initially by CO_2 sparging, and subsequently by addition of NaOH 0.5M (Panreac). A minimum 5% CO_2 set-point in the gas-mixing was fixed and maintained during the culture operation. For the fed-batch cultures, a peristaltic pump was used for nutrients feeding, adding the calculated feed media required every 3 h O.U.R.s cycles. The working volume for the batch cultures was 2L, and for the fed-batch cultures were 1.3L initially.

5.2.6 MFCS/win. Software for Data Acquisition, Monitoring and Control

BioPat® MFCS/win 3.0 (Sartorius Stedim Biotech, Germany) was used for monitoring and controlling the cell culture. Three different control recipes were programmed for performing the three different cell cultures (Batch, Fed-batch based on O.U.R. and Fed-batch based on alkali addition). The control recipes were able to do the actions required automatically. Briefly, depending on the fed-batch operation mode, the recipe performed the O.U.R. or alkali addition measure, the estimation of the number of cells in the bioreactor and turned on the feed pump

adding the required feed media to maintain the glucose concentration in a narrow range. The control recipes performed are detailed in the Results section.

5.2.7 Determination of glucose/lactate concentrations

Glucose and lactate concentrations were measured using an automatic glucose and lactate analyzer (YSI, Yellow Springs Instrument, 2700 Select).

5.2.8 Determination of product concentration (IFN- γ)

IFN- γ concentration was quantitatively determined using an enzyme-linked immunoassay: Human IFN-γ CytosetTM (Invitrogen, ThermoFisher Scientific).

5.2.9 Evaluation of maximum specific growth rate and specific consumption/production rates for glucose and lactate

Cell growth rate can be expressed by **Equation 5.1**. The maximum specific growth rate (μ_{max}) was calculated in the exponential growth phase from **Equation 5.2**.

$$\frac{dX_v}{dt} = r_X = \mu_{max} \cdot X_v \qquad [5.1]$$

$$\ln(X_v) = \ln(X_{v,0}) + \mu_{max} \cdot (t - t_0) \qquad [5.2]$$

Once the maximum specific growth rate was calculated, the doubling time (Dt) could be obtained with the **Equation 5.3**.

$$Dt = \frac{\ln(2)}{\mu_{max}} \qquad [5.3]$$

The consumption/production rate for glucose (q_{glc}) and lactate (q_{lac}) are expressed by **Equation 5.4**. The specific consumption/production rate (q_m) was calculated from the **Equation 5.5** (by integration and rearrangement of **Equations 5.1** and **5.4**).

$$\frac{dC_m}{dt} = r_m = q_m \cdot 10^{-3} \cdot X_v \qquad [5.4]$$

$$C_m = C_{m,0} + \frac{q_m \cdot 10^{-3} \cdot X_{v,0}}{\mu_{max} \cdot e^{\mu_{max} \cdot t_0}} \cdot [e^{\mu_{max} \cdot t} - e^{\mu_{max} \cdot t_0}] \qquad [5.5]$$

5.2.10 Oxygen Uptake Rate (O.U.R.) for biomass estimation

O.U.R. was determined along the bioreactor cultures by means of the dynamic method (Yoon and Konstantinov, 1994; Zhou and Hu, 1994) the specific methodology used in this work is detailed somewhere else (Lecina et al., 2006). Briefly, the sequence starts by increasing D.O. (dissolved oxygen, relative oxygen concentration in the liquid phase in respect to the air

saturation in equilibrium (%)) up to 60% of saturation using an aeration flow-rate of 0.35 L·min^{-1}. When 60% D.O. is reached, the air supply is stopped and a N_2 flow (0.15 L·min^{-1}) is introduced to the bioreactor headspace to avoid any oxygen transport back to the culture medium. O.U.R. was calculated from the decreasing D.O. profile between 56-29% of oxygen saturation. A detailed protocol and results obtained for the K_{des} determination are presented in ***Appendix D***.

The N_2 purging of the headspace causes a certain O_2 desorption from the liquid that has to be considered in the corresponding mass balance equation. The desorption constant for system and conditions used was determined (at least 3 repetitions) before inoculation for each culture. The values obtained were K_{des} = 0.9553 h^{-1} for batch and K_{des} = 1.1042 h^{-1} for fed-batch based on O.U.R.. The O.U.R. value is then obtained from the time profile of dissolved oxygen, as the decrease in oxygen concentration is the result of cell metabolism in the culture. To convert D.O. into absolute oxygen concentration (C_{O2}), the oxygen solubility was considered constant during the culture and equal to 0.194 mmol/L (Higareda et al., 1997; Miller et al., 1988; Ramirez and Mutharasan, 1990). As shown in **Equation 5.6**, the first term of the dissolved oxygen balance corresponds to cells consumption, and the second one to the oxygen desorption forced by N_2 flow in headspace. The O.U.R. measurement frequency was three hours.

$$OUR = \frac{C_{O_2}(t_0) - C_{O_2}(t_f)}{t_f - t_0} + \frac{\int_{t_0}^{t_f}(-K_{des} \cdot C_{O_2}(t))\, dt}{t_f - t_0} \quad [5.6]$$

Once O.U.R. was determined, the biomass calculation was performed using **Equation 5.7**.

$$\frac{dO_2}{dt} = OUR = qO_2 \cdot X_v \cdot 10^{-3} \quad [5.7]$$

The qO_2 constant was experimentally determined during the batch phase and recalculated during the feed-batch, as presented in results section. Every three hours, biomass concentration was estimated through the O.U.R. measurement. Then the amount of feeding media was calculated accordingly to the estimated biomass at the beginning of each 3-hour cycle with the aim of maintaining the glucose concentration constant.

5.2.11 Biomass estimation by Alkali buffer addition method

An alkali buffer solution (NaOH 0.5M (Panreac)) was needed to neutralize the effect of lactic acid accumulation during cell culture, keeping the pH at the desired set-point. By means of the alkali buffer addition measurement, the biomass was estimated at each point of the cell culture, in order to add the exact feed media necessary to maintain a constant glucose concentration.

The mathematical relation between the alkali addition volume and lactate concentration in culture is presented in **Equation 5.8**, were the ratio of alkali buffer solution added vs. lactate generated by the cells is defined as the k_b constant.

$$\frac{[lac]_f.V_f - [lac]_0.V_0}{t_f - t_0} = k_b \cdot \frac{[S]_{alkali}.\Delta V_{alkali}}{t_f - t_0} \quad [5.8]$$

This constant, were $[S]_{alkali}$ corresponds to NaOH concentration, was experimentally determined in the batch phase and recalculated during the feed-batch phase, as presented in results section.

As cell culture produced lactate as a by-product during growth, lactate production could be correlated to cell growth. In this way, the number of cells in the bioreactor were calculated using the **Equation 5.9**.

$$\frac{[lac]_f.V_f - [lac]_0.V_0}{t_f - t_0} = Y_{\frac{lac}{X}} \cdot \frac{X_f.V_f - X_0.V_0}{t_f - t_0} \cdot 10^3 \quad [5.9]$$

In this equation, the lactate-biomass yield $Y_{\frac{lac}{X}}$ is the molar ratio of lactate generated to biomass formed, and it was determined experimentally in the batch and feed-batch phases following the **Equation 5.10**.

$$Y_{\frac{lac}{X}} = \frac{q_{lac}}{\mu_{max}} \cdot 10^{-6} \quad [5.10]$$

Since **Equations 5.8** and **5.9** were applied to fed-batch culture calculations, in which volume was changing due to alkali/acid, feed and antifoam addition as well as to samples taken, culture volume variations in time were considered.

In this way, the lactate concentration as well as the number of cells were estimated on-line during the culture. As the feed addition was performed in three hours cycles, the amount of feed necessary to maintain a constant glucose concentration was recalculated and added at the beginning of each cycle.

5.2.12 Feed volume calculation

Culture feeding was performed in a three hours cycle ($\Delta t = 3hours$), in which the volume of feeding solution necessary to maintain a constant glucose concentration (S) was recalculated. The feeding was conducted at the beginning of each 3-hours cycle since constant feeding was not suitable because of the small feeding volume (flow in continuous addition) required.

Equation 5.9 was used to calculate the flow of the feed addition during the three hours. Then the total feed volume needed (V_f) was calculated using **Equation 5.11**.

$$F(t) = \frac{Y_{\frac{S}{X}} \cdot \mu_{max} \cdot X_0 \cdot V_0 \cdot e^{\mu_{max} \cdot \Delta t}}{S_0 - S} \quad [5.11]$$

$$V_f = F(t) \cdot 3\ hours \quad [5.12]$$

The feeding pump was activated by the control recipe the period of time necessary to add the exact volume calculated above, depending on the flow of the pump used.

5.2.13 Specific and volumetric productivity calculation

The specific productivity (q_p) for the cells in the process was calculated using the integral of viable cells (ICV) and the product concentration between the first and the last point as presented in **Equation 5.13**. ICV was calculated using the trapezoidal rule with the function trapz included in Matlab 2015b (Mathworks).

$$q_P = \frac{[Product]_{final}}{ICV} \quad [5.13]$$

For the volumetric productivity (V_P), the final product concentration and the total process time was used as shown in **Equation 5.14**.

$$V_P = \frac{[Product]_{final}}{t_{total}} \quad [5.14]$$

5.2.14 Statistics

Duplicates for each culture conditions were performed. One of the repetitions is presented for each set of experiments (Batch, Fed-batch based on O.U.R. and Fed-batch based on alkali buffer addition).

5.3 Results

5.3.1 Batch culture of HEK293 IFN-γ cells characterisation. Development of oxygen uptake rate (O.U.R.) and alkali buffer addition (ABA) monitoring system.

Batch cultures were carried out in order to develop and validate the two different on-line monitoring systems for biomass estimation: oxygen uptake rate (O.U.R.) and alkali buffer addition (ABA).

Figure 5.1 shows the time evolution of main variables obtained from a batch culture performed with the HEK293 cells. In **Figure 5.1-A** time profile of viable cells, viability, glucose, lactate and final product (t=143 h) concentration are shown (off-line variables), while in **Figure 5.1-B** pH, total alkali buffer addition and O.U.R. are shown (on-line variables).

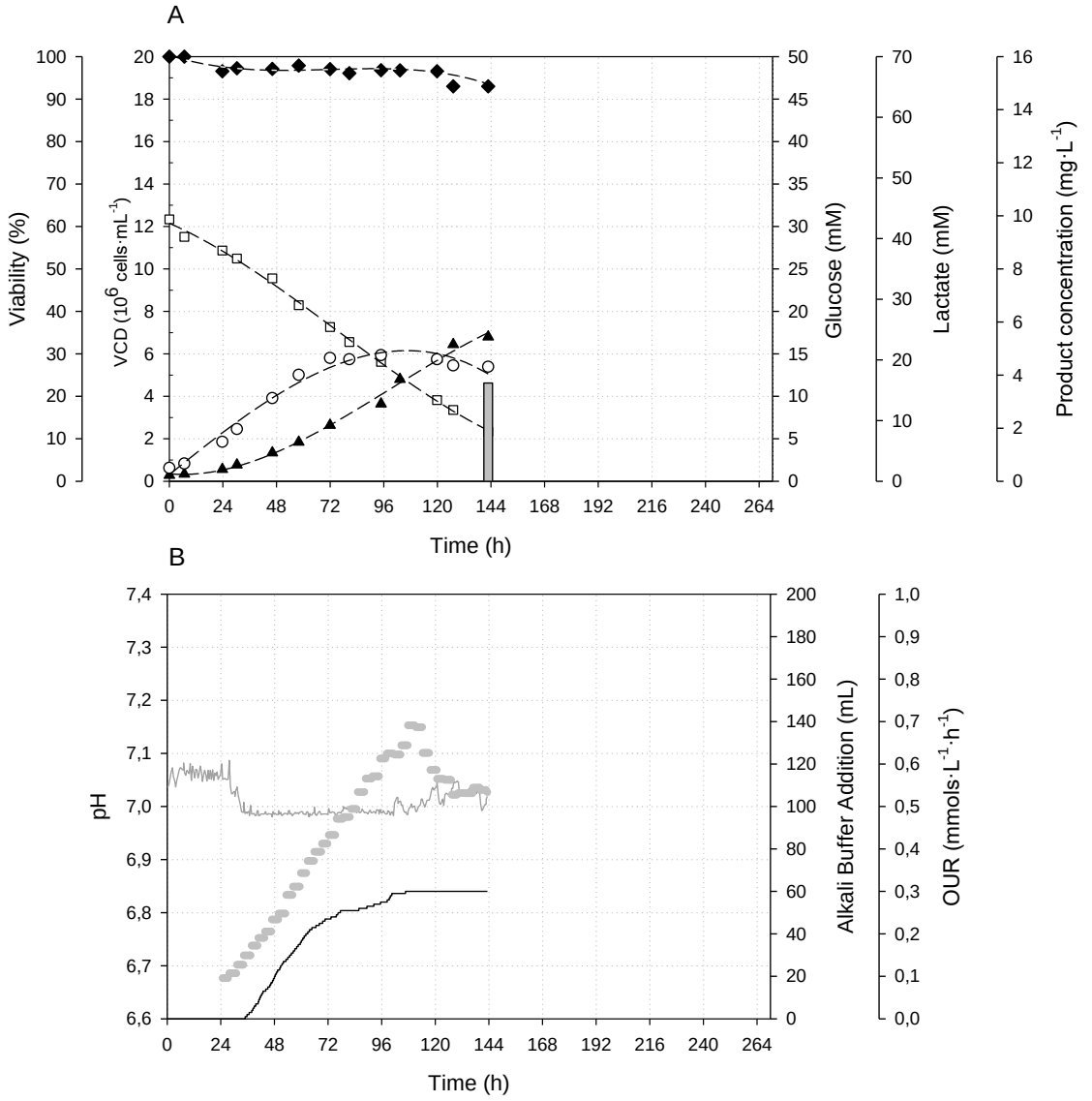

Figure 5.1: Profile of viable cells (▲), viability (◆), glucose (□), lactate concentration (○) and product concentration (bar) (off-line variables) (A); and pH (—), total alkali (—)/acid (- -) buffer addition, and O.U.R. (●) (on-line variables) (B) for batch cell culture.

After inoculation, an exponential growth phase was depicted, where glucose was highly consumed as the main carbon source and lactate was produced as a non-desired by-product. This behaviour presents the typically metabolic deregulation observed on glucose uptake in mammalian cells batch cultures. Lactate secretion is caused by the small amount of pyruvate entering the Tricarboxylic Acid Cycle (TCA), motivated by NADH regeneration that has to be done in the cytoplasm, with the concomitant production of high amounts of lactate which is eventually secreted to the culture broth. It is widely known that proton-linked monocarboxylate transporters (MCTs) are largely the responsible for the lactate secretion/uptake through the cell membrane (Halestrap and Price, 1999; Poole and Halestrap, 1993). Each lactate molecule is co-

transported together with a proton, causing the culture pH rising when lactate is generated (Liste-Calleja et al., 2015).

A maximum viable cell concentration of $6.80 \cdot 10^6$ cells·mL^{-1} was reached at 143 h in batch culture, with a final product concentration of 3.70 mg·L^{-1} which represents a volumetric productivity of 25.87 µg·L^{-1}·h^{-1}. The specific productivity was $8.73 \cdot 10^{-3}$ µg·10^6cells^{-1}·h^{-1}. The maximum specific growth rate obtained was μ_{max}=0.029 h^{-1}, resulting in a duplication time of Dt = 24.13 h. A specific glucose consumption of q_{gluc}=-144.12 nmol$_{gluc}$·10^6cells^{-1}·h^{-1} and a specific lactate generation q_{lac}=335.56 nmol$_{lac}$·10^6cells^{-1}·h^{-1} were observed, obtaining a ratio of lactate production to glucose uptake of $Y_{lac/gluc}$=2.3 nmol$_{lac}$·nmol$_{gluc}^{-1}$. That means that a high proportion of glucose is directed to lactate formation reaching a final lactate concentration around 20 mM of lactate. In addition lactate secretion alters culture pH and, in order to maintain constant pH for having optimal growth conditions, alkali buffer must be added.

O.U.R. and the alkali buffer addition followed the profile of the cell growth in the culture, proving that both variables can be used as an on-line measure to estimate the number of viable cells when the culture is in exponential growth phase, but also can be used in the stationary phase. Moreover, both variables reflect earlier any metabolic limitation, in response to the decrease in oxygen consumption and lactate generation. This property of the studied variables pH or O.U.R. is an advantage that can be translated to the possibility to achieve faster and more accurate actions, mainly starting the feeding strategy. An initial O.U.R. of 0.0955 mmol O_2·L^{-1}·h^{-1} increases exponentially to a maximum of 0.6910 mmol O_2·L^{-1}·h^{-1}. In the case of the alkali buffer addition, a maximum volume of 60 mL of NaOH solution at 0.5M was reached at the end of the culture.

The oxygen specific consumption rate (qO_2) can be obtained through the slope resulting from the direct representation of O.U.R. values versus the concentration of viable cells, as presented in **Figure 5.2**. This ratio confirms the proportional relationship between O.U.R. and cell density during the exponential growth phase, when cells are thriving without any limitation, neither physical nor metabolic. The specific oxygen consumption rate was kept nearly constant along the growth phase at values around 158 nmol$_{O2}$·10^6cells^{-1}·h^{-1}.

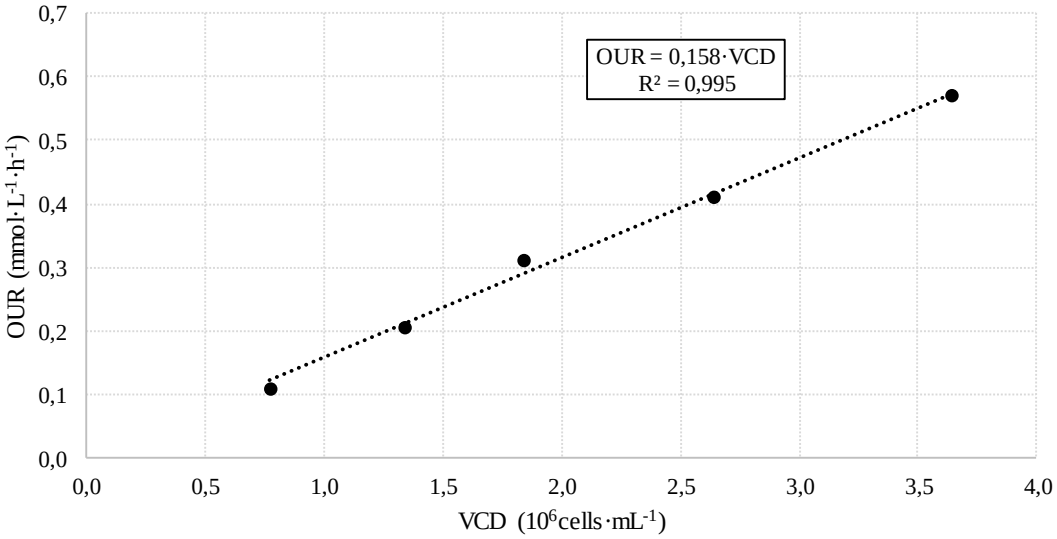

Figure 5.2: Oxygen specific consumption rate (qO_2) calculation from the slope resulting of the direct representation of O.U.R. values versus the concentration of viable cells. Batch cell culture with HEK293.

Similar behaviour was noticed with the alkali addition, as presented in **Figure 5.3**, the kB constant can be obtained representing the variation of alkali buffer added with the lactate accumulated in culture (kB=0.7446 $mmol_{lac}$·$mmols_{NaOH}^{-1}$). For the first 35 hours, alkali buffer was not added instead of cells were producing lactate. This is due to the $\%CO_2$ in the sparger inlet control, that went from 10 to 5% to counter the acidification. After this moment, CO_2 was maintained constant at 5%. According the **Equation 5.7**, the amount of lactate generated during this period was considered in the data to determine the kB constant. This way the plot presented in **Figure 5.4** was forced to go through 0.0.

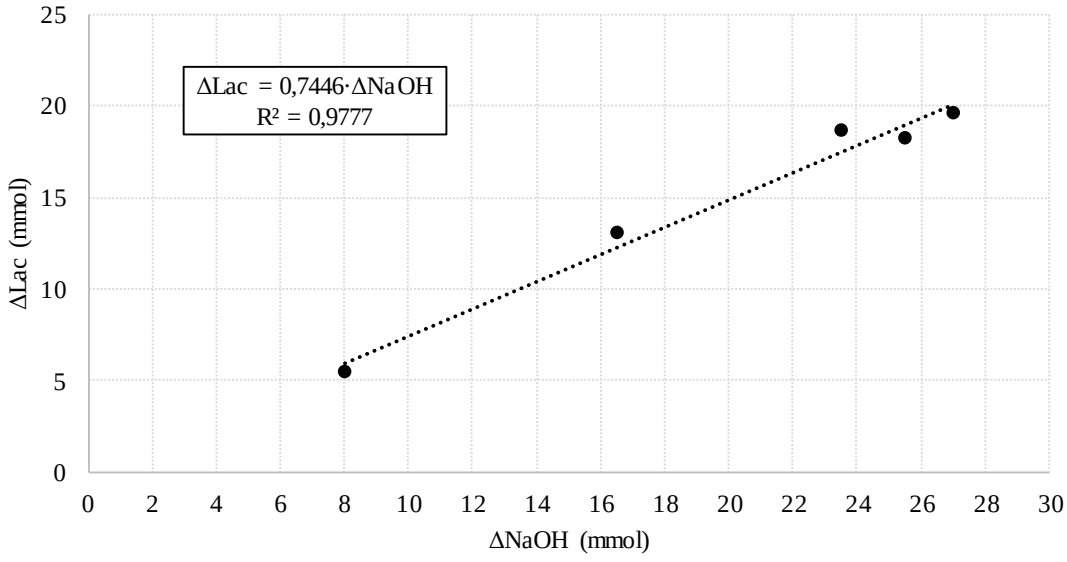

Figure 5.3: Kb constant calculation from the slope resulting of the representation of lactate concentration variation versus the total alkali buffer addition for this period (each point). Batch cell culture with HEK293.

Then $Y_{lac/X}$ can be obtained with the slope of the direct relation between the lactate generated versus the variation of the amount of cells in culture ($Y_{lac/X}$=0.0062 $mmol_{lac} \cdot 10^6 cells^{-1}$), as presented in **Figure 5.4**. Alternatively, $Y_{lac/X}$ can be calculated using **Equation 5.9** once μ_{max} and q_{lac} have been obtained ($Y_{lac/X}$=0.0064 $mmol_{lac} \cdot 10^6 cells^{-1}$) Similar but slightly different values were obtained depending on the method used because the **Equation 5.9** considers a constant μ_{max} calculated as presented in Materials and Methods section.

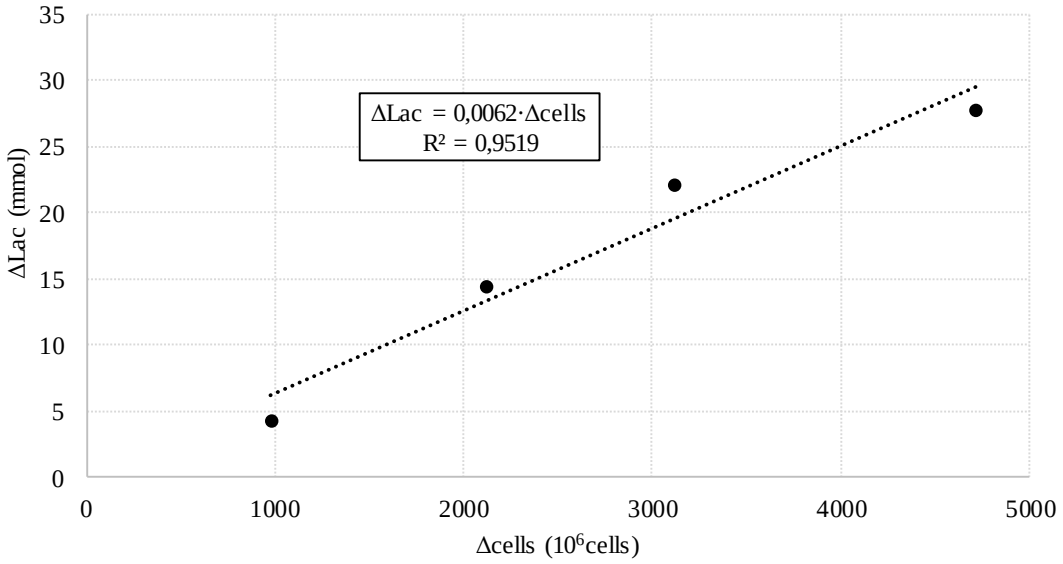

Figure 5.4: Relation of lactate generated and cell concentration variation in batch culture, given by the $Y_{lac/X}$ (slope) according the **Equation 5.8**.

The block diagram implemented for the O.U.R. monitoring is presented in **Figure 5.5**, while alkali buffer addition, as well as main operating variables, is monitored by the DCU system by default, so it is not necessary to program a recipe to perform this function. The recipe for O.U.R. was divided in two blocks: the initial phase, in which variables, controls and set-points were set; and the batch phase, in which O.U.R. measurement was performed every 3 hours, following the protocol presented in Materials and Methods. As the O.U.R. protocol modifies the culture conditions (D.O. and pH), the O.U.R. measurements started after 24 hours of inoculation (manual transition), letting the cells to adapt from shake-flasks to bioreactor operation.

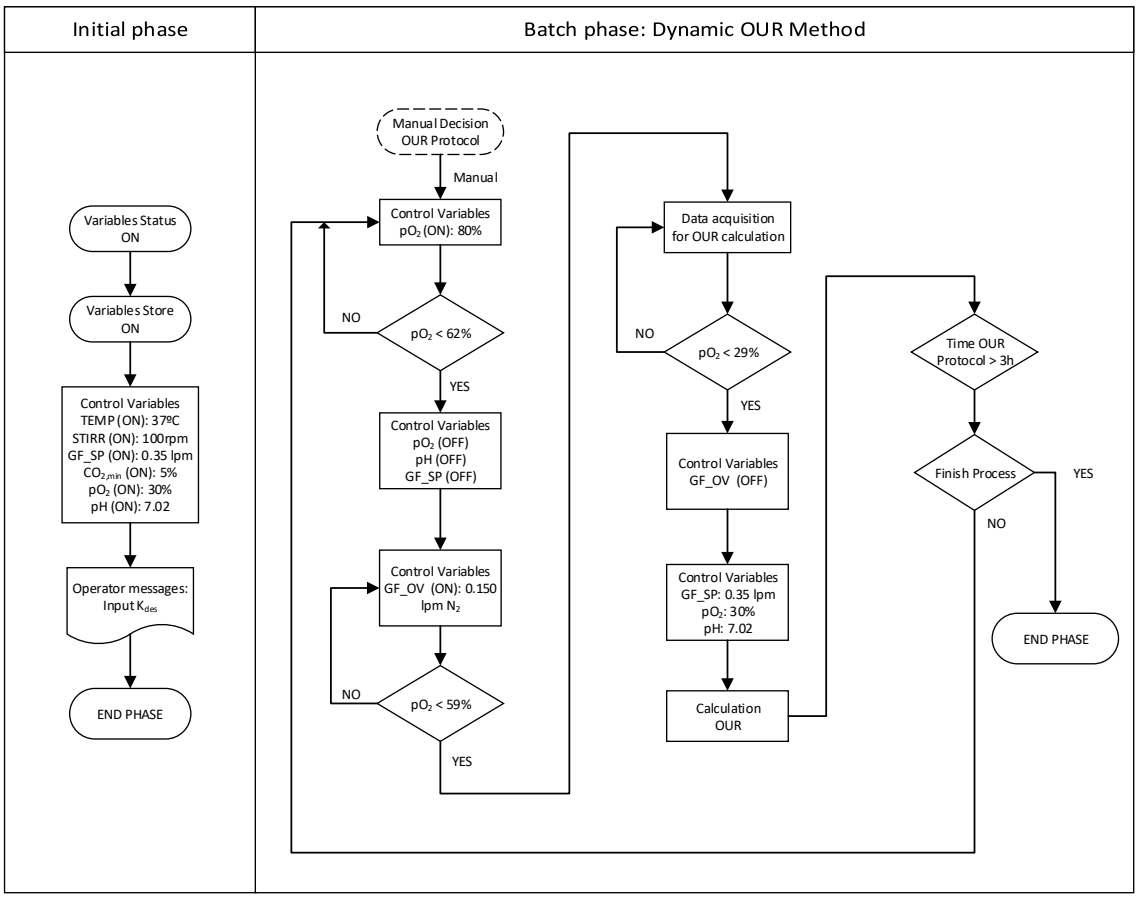

Figure 5.5: Block diagram control for the estimation of O.U.R. using the dynamic method measurement in batch cell culture of HEK293. Recipe implemented in MFCS/win 3.0 in Biostat B DCU II.

Results presented in batch demonstrated that both O.U.R. and alkali addition can be used as on-line measures to estimate the number of viable cells in culture. In this study, the monitoring systems developed were applied to control glucose concentration in fed-batch cultures at such a concentration that will keep HEK293 cells in an efficient metabolic state. Thus, a high concentration of glucose leads to saturation and deregulation of the cell metabolism, while any drop in glucose level could lead to the irreversible process of programmed cell death. Considering these issues, we decided to apply different control strategies for nutrients feeding in order to maintain glucose concentration at 20 mM.

5.3.2 Fed-batch strategy based on online oxygen uptake rate (O.U.R.) for the optimal feeding estimation at constant glucose concentration

Once suitability of on-line O.U.R. measurement as an indicator of cell concentration and physiological activity in bioreactor cultures has been demonstrated, a fed-batch process was performed using O.U.R. as a tool to estimate the feeding rate needed to keep HEK293 cells in exponential growth while maintaining glucose around 20 mM.

The block diagram for the O.U.R. monitoring is presented in **Figure 5.6**. The recipe for fed-batch based on O.U.R. is divided in two blocks: the initial phase, in which variables, controls and set-points are set; and the culture phase that contains batch and fed-batch phases. Feeding was started in the middle of the exponentially growth phase (t=78h) manually by the user. In each cycle (3 hours), first dynamic O.U.R. was used to estimate VCD through the qO_2; then taking into account the values for growth rate, glucose consumption, bioreactor volume and bioreactor glucose concentration, the feed flow rate was calculated as detailed in Materials and Methods. The total volume of nutrient solution required for the next three hours was fed at the beginning of each cycle.

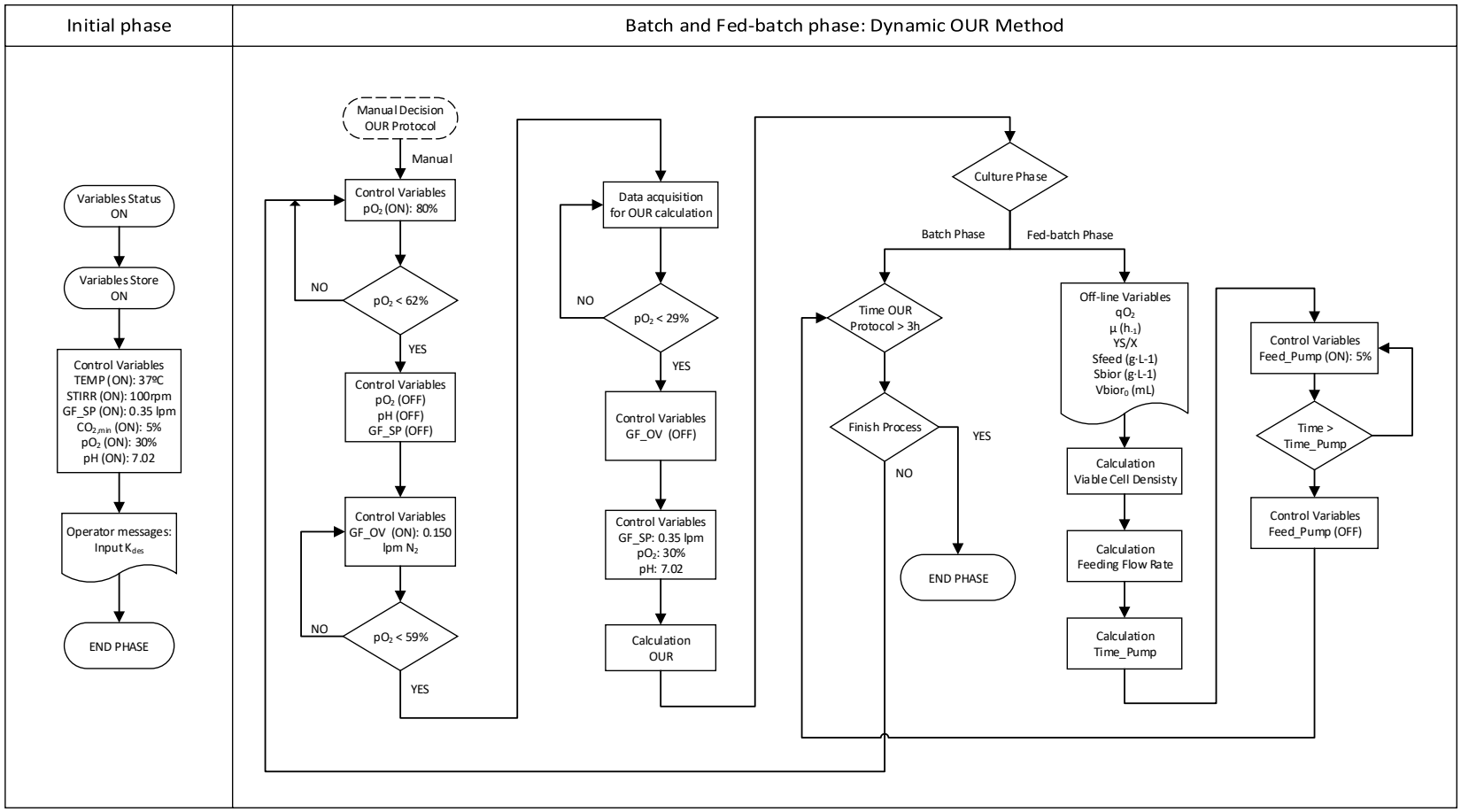

Figure 5.6: Block diagram control for the fed-batch based on O.U.R. dynamic measurement in cell culture of HEK293. Recipe implemented in MFCS/win 3.0 in Biostat B DCU II.

Figure 5.7 shows the monitoring of main variables of the HEK293 fed-batch based on O.U.R. feeding strategy. In **Figure 5.7-A** profile of viable cells, viability, glucose, lactate and final product (t=191h) concentration are presented (off-line variables), while in **Figure 5.7-B** pH, total alkali/acid buffer addition, O.U.R. and total feed volume added are presented (on-line variables).

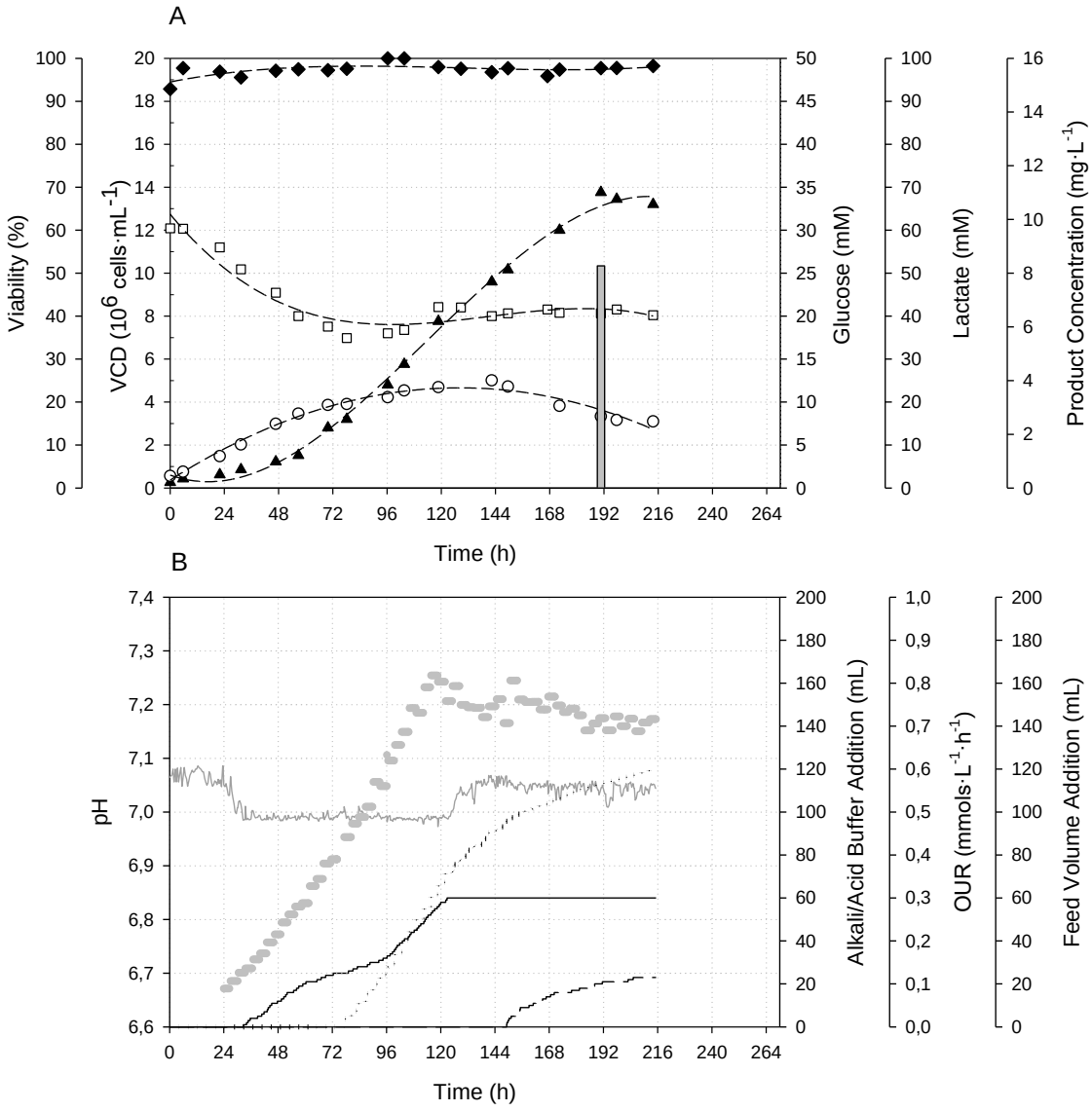

Figure 5.7: Profile of viable cells (▲), viability (◆), glucose (□), lactate concentration (○) and product concentration (bar) (off-line variables) (A); and pH (—), total alkali (—)/acid (— .) buffer addition, O.U.R. (●) and total feed addition (...) (on-line variables) (B) for fed-batch cell culture based on O.U.R..

During the exponential growth along the batch phase, viable cell density was linearly related to O.U.R. indicating a constant value for the specific oxygen consumption rate (q_{O2}). The oxygen specific consumption rate (qO_2) can be obtained through the slope resulting from the direct representation of O.U.R. values versus the concentration of viable cells, as presented in **Figure**

5.8. In this way, the feeding rate of substrate can be predicted from the estimation of cell concentration in the bioreactor through the O.U.R. values, assuming that therein the exponential growing period of the culture the specific oxygen consumption rate is constant. The qO_2 was kept nearly constant along the growth phase at values around 130 $nmol_{O2} \cdot 10^6 cells^{-1} \cdot h^{-1}$.When O.U.R. started to decay, a constant addition was kept, maintaining the culture growing for some time.

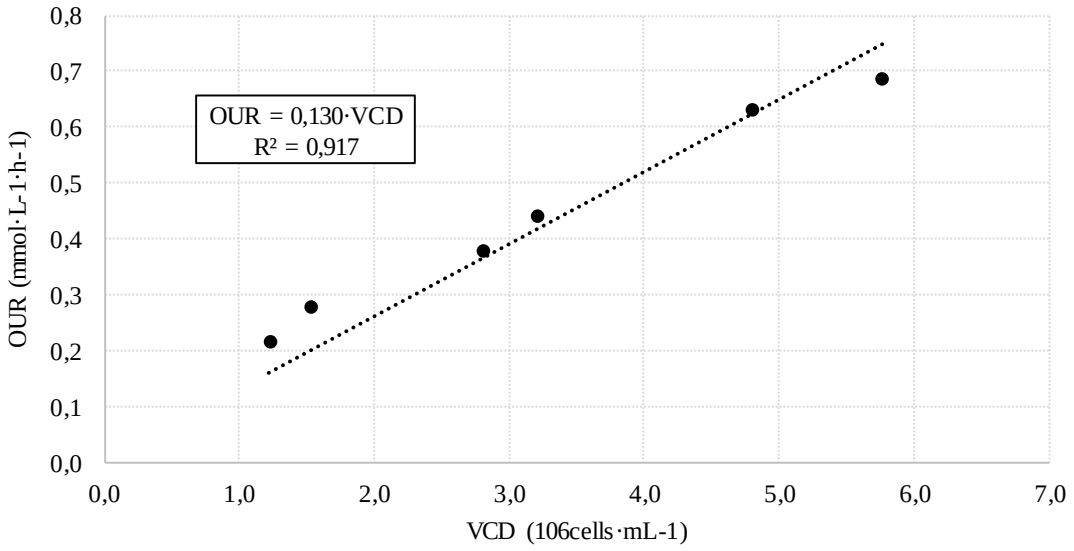

Figure 5.8: Oxygen specific consumption rate (qO_2) calculation from the slope resulting of the direct representation of O.U.R. values versus the concentration of viable cells. Fed-batch cell culture based on O.U.R. with HEK293.

For fed-batch strategy performed, feed addition started at 72 hours when around $3 \cdot 10^6 cells \cdot mL^{-1}$ were reached. Considering the results obtained in batch culture, at this time cells were in the mid-exponentially growth phase. At this moment, a concentration around 18-20 mM of glucose was observed in the bioreactor, which means that while keeping this glucose concentration cells should not be limited by any substrate since in a batch culture starting from 20 mM glucose they are able to grow up to $6 \cdot 10^6$ cells/mL without any limitation.

These results show that fed-batch culture overcame the batch culture limitations in terms of viable cells reached and protein productivity. The maximum viable cell concentration was $13.76 \cdot 10^6$ $cells \cdot mL^{-1}$ at 190 h and the final product concentration reached was 8.27 $mg \cdot L^{-1}$, with a volumetric productivity of 43.53 $\mu g \cdot L^{-1} \cdot h^{-1}$. The specific productivity was $7.67 \cdot 10^{-3}$ $\mu g \cdot 10^6 cells^{-1} \cdot h^{-1}$. To summarize, total viable cell concentration was incremented in 102% compared with the batch strategy. Extension of exponential growth phase and increase in maximum viable cell concentration resulted in a 124% and 68% increment of final product titer concentration and volumetric productivity respectively.

After starting the culture feeding, glucose concentration was maintained in a narrowed-range (18-22 mM), showing that the feeding strategy fitted with cell growth and glucose consumption.

In **Figure 5.9** the VCD prediction performed by the recipe control is compared to the real VCD, showing that the values were very similar and that O.U.R. estimates the viable cells correctly during the exponential growth phase (24-110 h).

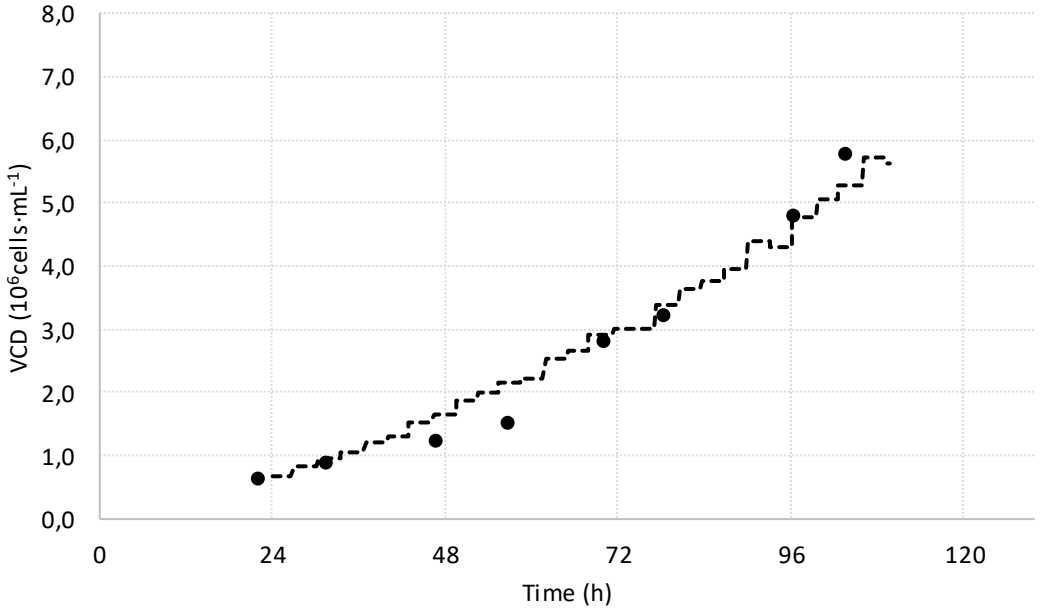

Figure 5.9: Comparison of real VCD (●) with the estimated VCD (▬) calculated through O.U.R. estimation.

5.3.3 Fed-batch strategy based on online alkali buffer addition (ABA) for the optimal feeding estimation

As it has been shown in batch culture, monitoring of the alkali buffer addition added in a culture allows to calculate the cellular concentration evolution along time. Through this monitoring system, it is possible to carry out the controlled addition of nutrients according to their consumption by the cell culture.

The block diagram for the alkali buffer addition method (ABA) is presented in **Figure 5.10**. The recipe for fed-batch based on ABA was divided in two blocks: the initial phase, in which variables, controls, and set-points are set, and the culture phase, that contains batch and fed-batch phases. The feeding was started in the middle of the exponential growth phase (t=77h) operated manually by the user. At the beginning of each cycle (3 hours), lactate concentration was calculated from the total alkali added and VCD was estimated from the Ylac/X; then, according the growth rate, the glucose consumption, the bioreactor volume, and bioreactor glucose concentration the feed flow rate was calculated as described in Materials and Methods. The total volume required for the three hours was fed at the beginning of each cycle.

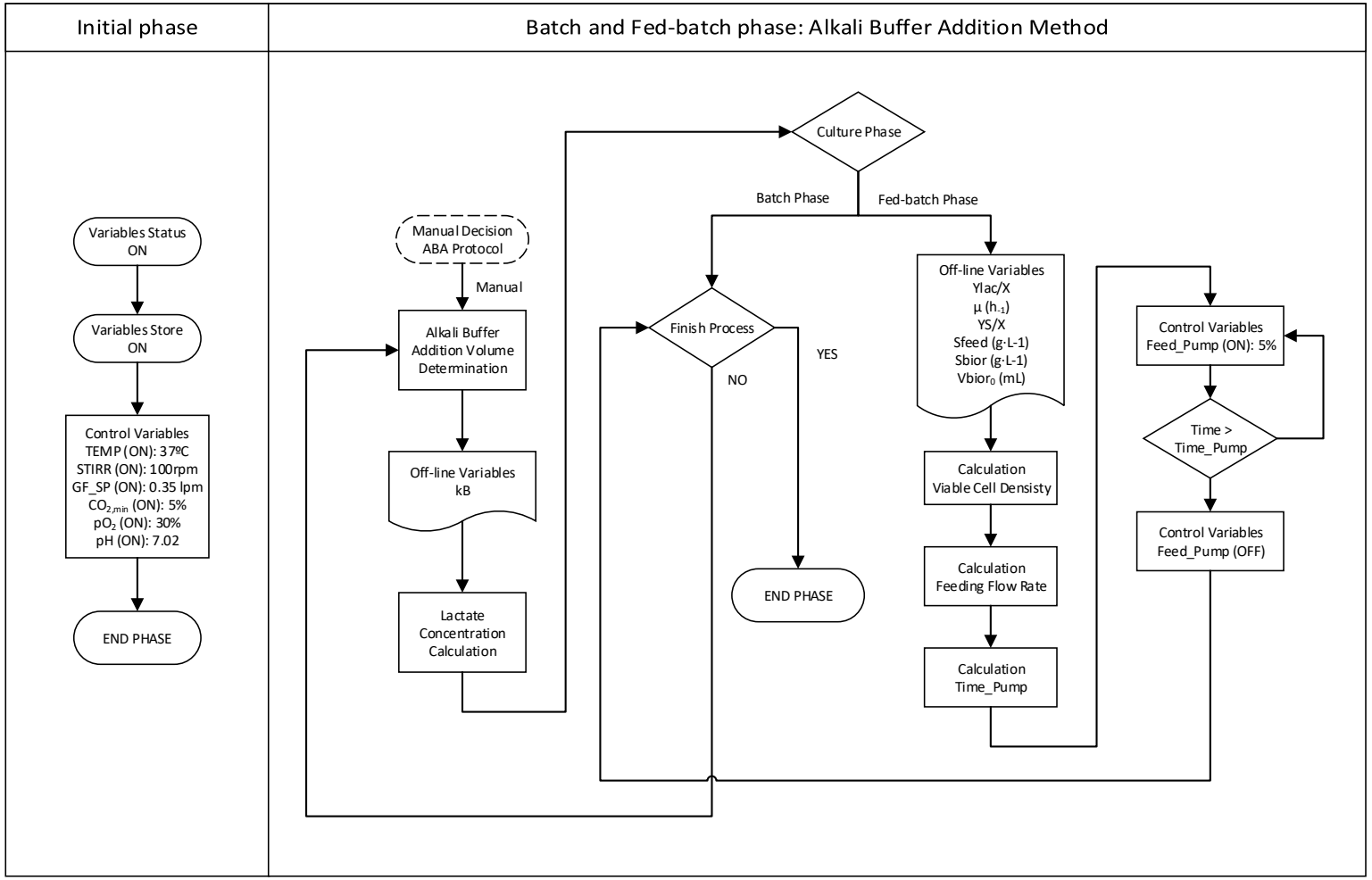

Figure 5.10: Block diagram control for the fed-batch based on alkali buffer addition measurements in cell culture of HEK293. Recipe implemented in MFCS/win 3.0 in Biostat B DCU II.

Figure 5.11 shows the monitoring of main variables of a HEK293 fed-batch based on alkali buffer addition. In **Figure 5.11-A** profile of viable cells, viability, glucose, lactate and final product (t=244h) concentration are presented (off-line variables), while in **Figure 5.11-B** pH, total alkali/acid buffer addition and total feed volume added are depicted (on-line variables).

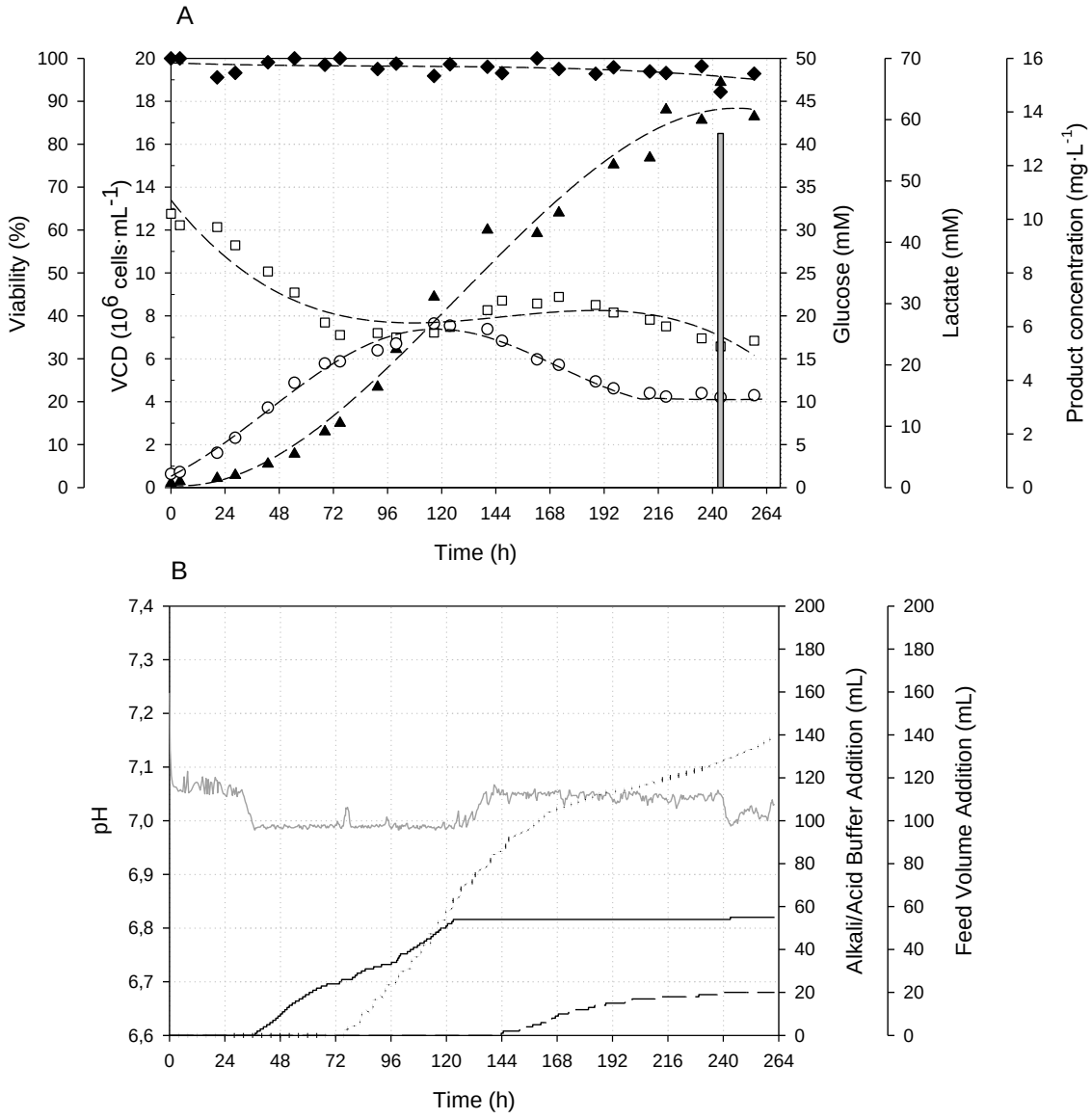

Figure 5.11: Profile of viable cells (▲), viability (◆), glucose (□), lactate concentration (○) and product concentration (bar) (off-line variables) (A); and pH (—), total alkali (—)/acid (– .) buffer addition, O.U.R. (●) and total feed addition (...) (on-line variables) (B) for fed-batch cell culture based on alkali buffer addition.

The results presented show that fed-batch culture overcame both the batch culture and fed-batch culture based on O.U.R., in terms of both final viable cell concentration reached and productivity. The maximum viable cell concentration was $18.88 \cdot 10^6$ cells·mL^{-1}, obtained at 244 h. The final product concentration reached was 13.20 mg·L^{-1}, with a volumetric productivity of

54.10 $\mu g \cdot L^{-1} \cdot h^{-1}$. The specific productivity was $6.30 \cdot 10^{-3}$ $\mu g \cdot 10^{6} cells^{-1} \cdot h^{-1}$. As in O.U.R. based fed-batch, glucose concentration was maintained in a narrow range (18-22 mM), proving that the feeding strategy was optimal according the growth and the glucose consumption rates of the cells.

As presented in **Figure 5.12**, the kB constant from **Equation 5.8** can be obtained representing the variation of alkali buffer added versus the lactate accumulated in culture (kB=0.810 $mmol_{lac} \cdot mmols_{NaOH}^{-1}$) following the same method presented for the batch culture. Then $Y_{lac/X}$ can be obtained by means of the slope of the direct relation between the lactate generated versus the variation of the amount of cells in culture ($Y_{lac/X}$=0.0013 $mmol_{lac} \cdot 10^{6} cells\text{-}^{1}$), as presented in **Figure 5.13**; or using **Equation 5.9** once μ_{max} and q_{lac} have been obtained $Y_{lac/X}$=0.0011 $mmol_{lac} \cdot 10^{6} cells\text{-}^{1}$.

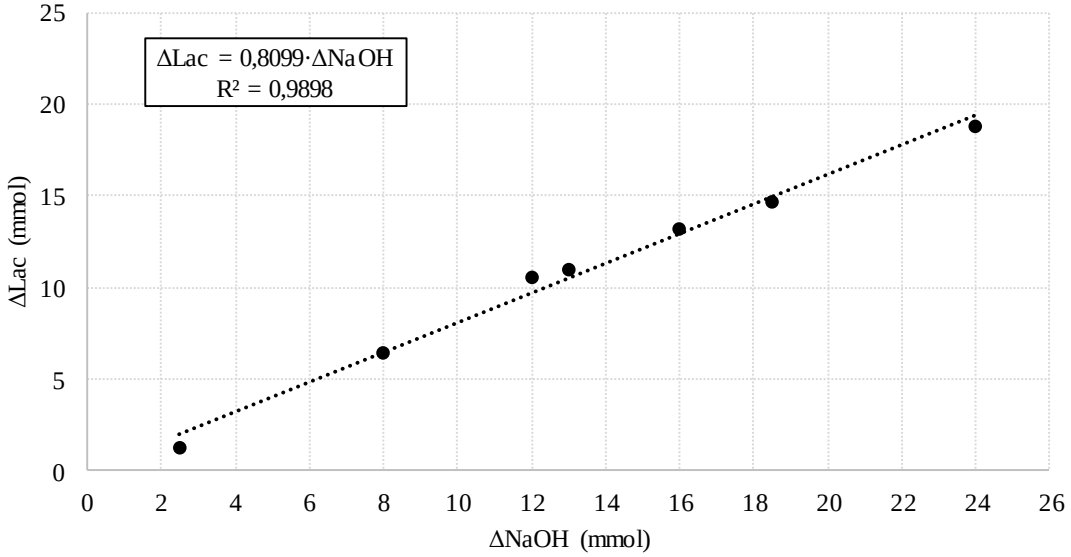

Figure 5.12: Kb constant calculation from the slope resulting of the representation of lactate concentration variation versus the total alkali buffer addition for this period (each point). Fed-batch cell culture base on alkali addition with HEK293.

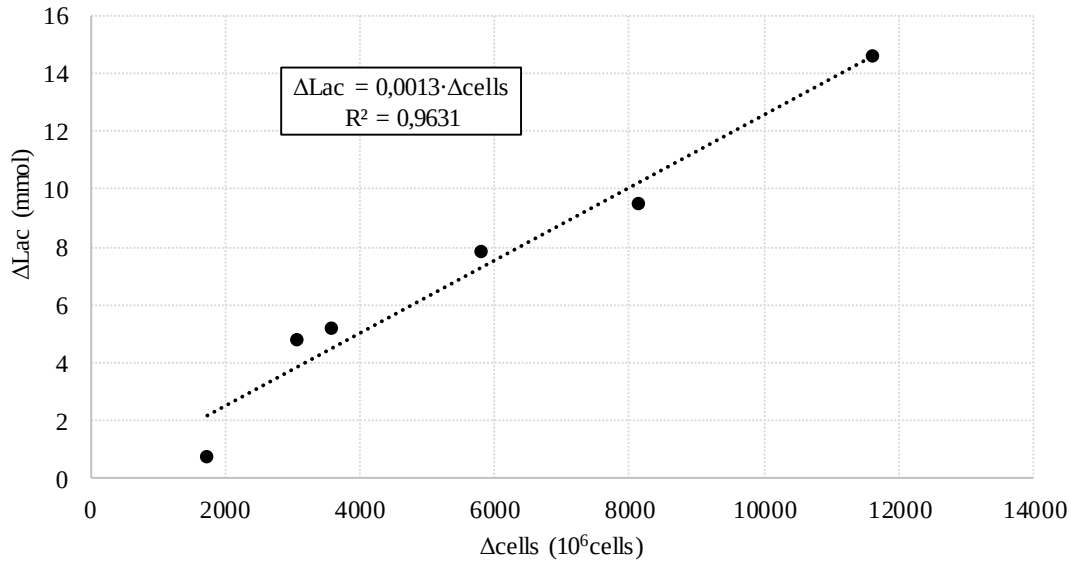

Figure 5.13: Relation of lactate generated with the cell concentration variation in culture, given by the $Y_{lac/X}$ (slope) according the **Equation 5.8**.

During the exponential growth phase lactate concentration was estimated from the alkali buffer addition through kB constant. Then, the viable cell density was calculated through the $Y_{lac/X}$. Thus, using an on-line and simple variable, as is the alkali volume addition, was possible to estimate the concentration of viable cells in the bioreactor along time in order to use this estimation to calculate the optimal feeding.

Figures 5.14 and 5.15 the lactate concentration and VCD off-line measurements and the respective values predicted by the control software, showing that the values were very similar and that alkali addition method estimated correctly lactate concentration and viable cells density along exponential growth phase (37-123 h).

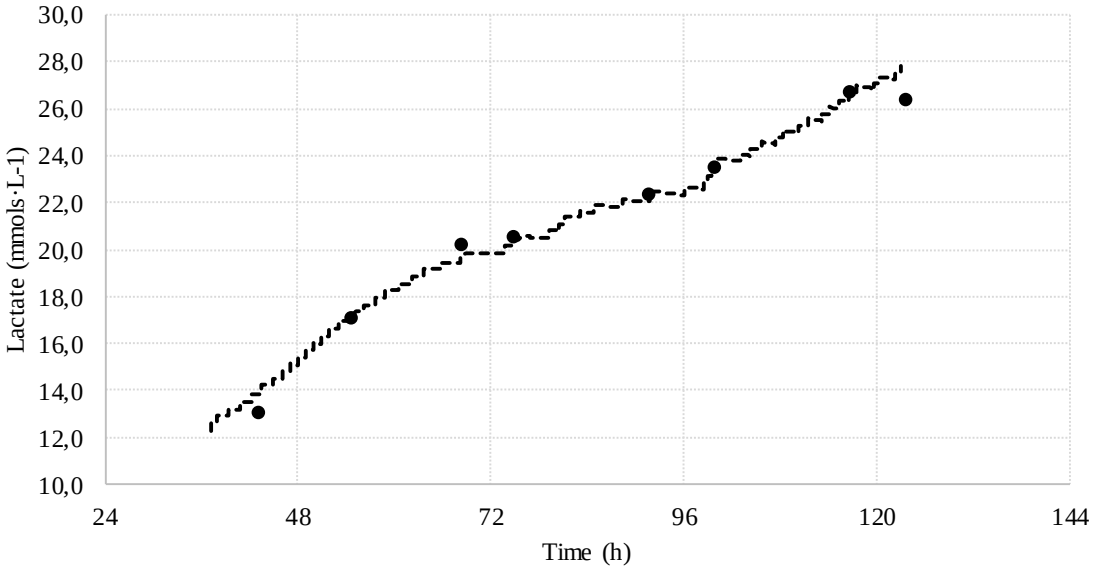

Figure 5.14: Comparison of real lactate concentration (●) with the estimated lactate concentration (▬) calculated through alkali buffer addition.

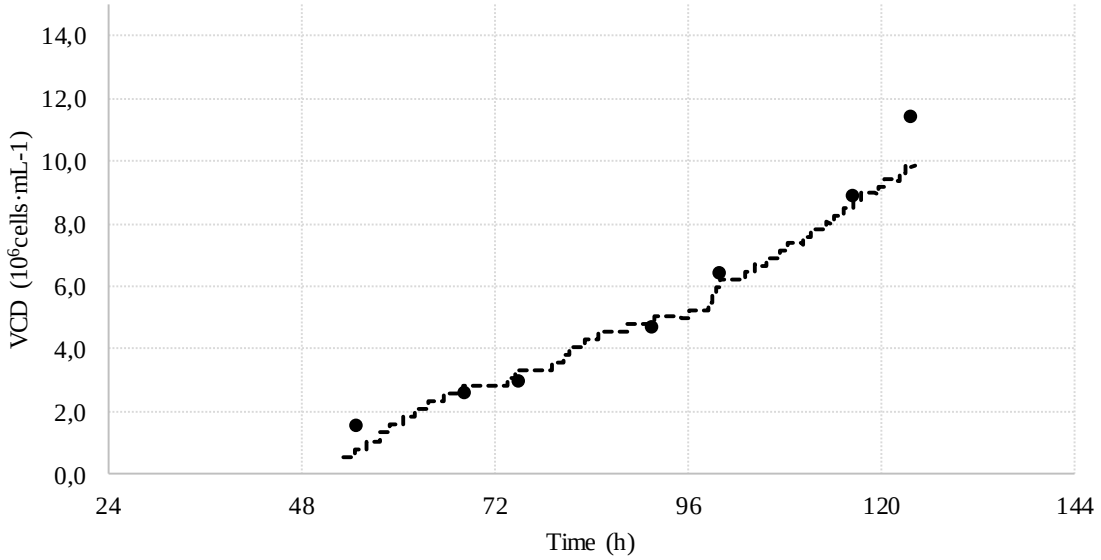

Figure 5.15: Comparison of real VCD (●) with the estimated VCD (▬) calculated through alkali buffer addition.

The addition of alkaline solution presented an exponential tendency, following the same profile as the concentration of viable cells, that is, the tendency of cell growth. The volume profile of nutrient addition adopted an exponential tendency, just as both alkaline solution and concentration of viable cells.

As presented in **Figure 5.11-B**, the ABA method allowed to perform a fed-batch in which glucose concentration was maintained in a narrow range (18-20 mM). The total viable cell concentration was increased by 178% and 37% compared respectively with the batch and the fed-batch based on O.U.R. strategy. Extension of exponential growth phase and increase in maximum viable cell concentration resulted in an increase of the final product concentration of 257% and 60% respect to batch and fed-batch O.U.R. respectively. The volumetric productivity was also increased in 109% and 24% compared to batch and fed-batch O.U.R. respectively. These results show that this type of monitoring of the physiological state was very accurate and suitable for nutrient feeding command. This precision is reflected reflectively from the similar tendencies obtained between the volume of addition of concentrated nutrient solution and the profile of growth of viable cells. The results obtained also demonstrate that the cultivation strategy based on the correct pH action as a monitoring tool is a better cultivation strategy in terms of obtaining a high concentration of viable cells and final product titers.

5.4 Conclusions

The results presented in this study demonstrated the applicability of the two monitoring systems tested: O.U.R. and alkali buffer addition, as reliable tools for feed control in fed-batch processes

of 293HEK cells. Controlled feeding based on maintaining a constant glucose concentration in cell culture has allowed to keep the culture in a more adequate environment that has resulted in a more efficient substrate consumption. Although both control systems have been successful applied for extending exponential growth phase and increasing final viable cell concentration and product titers, there are diverse operational aspects that might be taken into account when a choice has to be done.

Control system based on dynamic O.U.R. determination has been widely applied in fed-batch cultures to predict culture growth. Although it is a simple method that requires only an oxygen probe, the culture constant distortions of the D.O. and pH performed in every O.U.R. measurement cycle has led to obtain less final VCD and product concentration in the culture. Nevertheless, alternatives to the dynamic method to measure O.U.R. has been published, but they require more complex systems to be implemented (Fontova et al., 2018).

The alternative method presented in this work, based on the alkali buffer addition, allows a proper tracking of cell growth rate and cell concentration and a precise determination of the feeding rate in order to control the cell environment by the addition of nutrients. In this way, a greater maximum cell concentration and product titer has been obtained when compared to O.U.R. method. The alkali addition to maintain constant pH in the culture is directly linked to the physiological activity of the cells in culture, which implies that such a methodology should be valid as well for other processes using different cell lines. In addition, this method is also simple and robust. The incorporation of this simple measurement system should be an attractive procedure providing a reliable measurement of the main events to be monitored and controlled by means of the feeding strategy: cellular growth and glucose concentration, resulting in a more efficient substrate consumption.

The two alternatives to conventional batch processes presented for the culture of HEK293 cell line have shown clear advantages in respect to final product titer and, especially, volumetric productivities. The O.U.R. method allowed to increase the total viable cell concentration and product titer by 102% and 124% respectively, compared with the batch strategy. The volumetric productivity was also increased in 68%. Better results have been obtained with the alkali addition strategy, increasing the total viable cell concentration and product titer by 178% and 257% respectively, and obtaining a 109% increment of the process volumetric productivity.

Fed-batch cultivation allows control on the cell environment by the addition of nutrients to maintain the concentrations of glucose at levels that the cell can more efficiently regulate their metabolism, and control the level of by-products. However, in fed-batch strategies, limitations due to toxic metabolites normally cause that these processes end up by a drop in cell viability. Thus, further work should be orientated to the implementation of the developed monitoring and control systems in other culture strategies more adequate to limit accumulation of toxic by-products, like perfusion systems.

5.5 References

1. Abu-Absi S, Xu S, Graham H, Dalal N, Boyer M, Dave K. 2013. Cell Culture Process Operations for Recombinant Protein Production. In: . *Springer*, pp. 35–68. https://link.springer.com/chapter/10.1007/10_2013_252.
2. Altamirano C, Paredes C, Cairo JJ, Godia F. 2000. Improvement of CHO Cell Culture Medium Formulation: Simultaneous Substitution of Glucose and Glutamine. *Biotechnol. Prog.* **16**:69–75. http://doi.wiley.com/10.1021/bp990124j.
3. Casablancas A, Gámez X, Lecina M, Solà C, Cairó JJ, Gòdia F. 2013. Comparison of control strategies for fed-batch culture of hybridoma cells based on on-line monitoring of oxygen uptake rate, optical cell density and glucose concentration. *J. Chem. Technol. Biotechnol.* **88**:1680–1689. http://doi.wiley.com/10.1002/jctb.4019.
4. Côté J, Garnier A, Massie B, Kamen A. 1998. Serum-free production of recombinant proteins and adenoviral vectors by 293SF-3F6 cells. *Biotechnol. Bioeng.* **59**:567–575. http://doi.wiley.com/10.1002/%28SICI%291097-0290%2819980905%2959%3A5%3C567%3A%3AAID-BIT6%3E3.0.CO%3B2-8.
5. Cruz HJ, Freitas CM, Alves PM, Moreira JL, Carrondo MJT. 2000. Effects of ammonia and lactate on growth, metabolism, and productivity of BHK cells. *Enzyme Microb. Technol.* **27**:43–52. https://www.sciencedirect.com/science/article/pii/S0141022900001514.
6. Dingermann T. 2008. Recombinant therapeutic proteins: Production platforms and challenges. *Biotechnol. J.* **3**:90–97. http://doi.wiley.com/10.1002/biot.200700214.
7. Durocher Y, Butler M. 2009. Expression systems for therapeutic glycoprotein production. *Curr. Opin. Biotechnol.* https://www.sciencedirect.com/science/article/pii/S0958166909001360.
8. Fontova A, Lecina M, López-Repullo J, Martínez-Monge I, Comas P, Bragós R, Cairó JJ. 2018. A simplified implementation of the stationary liquid mass balance method for on-line OUR monitoring in animal cell cultures. *J. Chem. Technol. Biotechnol.* **93**:1757–1766. http://doi.wiley.com/10.1002/jctb.5551.
9. Halestrap A, Price N. 1999. The proton-linked monocarboxylate transporter (MCT) family: structure, function and regulation. *Biochem. J.* **343 Pt 2**:281–299. http://www.biochemj.org/content/343/2/281.abstract.
10. Higareda AE, Possani LD, Ramírez OT. 1997. The use of culture redox potential and oxygen uptake rate for assessing glucose and glutamine depletion in hybridoma cultures. *Biotechnol. Bioeng.* **56**:555–563. http://doi.wiley.com/10.1002/%28SICI%291097-0290%2819971205%2956%3A5%3C555%3A%3AAID-BIT9%3E3.0.CO%3B2-H.
11. Höpfner T, Bluma A, Rudolph G, Lindner P, Scheper T. 2010. A review of non-invasive optical-based image analysis systems for continuous bioprocess monitoring. *Bioprocess Biosyst. Eng.* **33**:247–256. http://link.springer.com/10.1007/s00449-009-0319-8.
12. Huang Y-M, Hu W, Rustandi E, Chang K, Yusuf-Makagiansar H, Ryll T. 2010. Maximizing productivity of CHO cell-based fed-batch culture using chemically defined media conditions and typical manufacturing equipment. *Biotechnol. Prog.* **26**:1400–1410.

http://doi.wiley.com/10.1002/btpr.436.

13. De Jesus M, Wurm FM. 2011. Manufacturing recombinant proteins in kg-ton quantities using animal cells in bioreactors. *Eur. J. Pharm. Biopharm.* **78**:184–188. https://www.sciencedirect.com/science/article/pii/S0939641111000129.
14. Junker BH, Reddy J, Gbewonyo K, Greasham R. 1994. On-line and in-situ monitoring technology for cell density measurement in microbial and animal cell cultures. *Bioprocess Eng.* **10**:195–207. http://link.springer.com/10.1007/BF00369530.
15. Kamen AA, Bédard C, Tom R, Perret S, Jardin B. 1996. On-line monitoring of respiration in recombinant-baculovirus infected and uninfected insect cell bioreactor cultures. *Biotechnol. Bioeng.* **50**:36–48. http://doi.wiley.com/10.1002/%28SICI%291097-0290%2819960405%2950%3A1%3C36%3A%3AAID-BIT5%3E3.0.CO%3B2-2.
16. Kurokawa H, Park YS, Iijima S, Kobayashi T. 1994. Growth characteristics in fed-batch culture of hybridoma cells with control of glucose and glutamine concentrations. *Biotechnol. Bioeng.* **44**:95–103. http://doi.wiley.com/10.1002/bit.260440114.
17. Kussow CM, Zhou W, Gryte DM, Hu W-S. 1995. Monitoring of mammalian cell growth and virus production process using on-line oxygen uptake rate measurement. *Enzyme Microb. Technol.* **17**:779–783. https://www.sciencedirect.com/science/article/pii/014102299400035P.
18. Lecina M, Soley A, Gràcia J, Espunya E, Lázaro B, Cairó JJ, Gòdia F. 2006. Application of on-line OUR measurements to detect actions points to improve baculovirus-insect cell cultures in bioreactors. *J. Biotechnol.* **125**:385–394. https://www.sciencedirect.com/science/article/pii/S0168165606002112.
19. Lecina M, Tintó A, Gálvez J, Gòdia F, Cairó JJ. 2011. Continuous perfusion culture of encapsulated hybridoma cells. *J. Chem. Technol. Biotechnol.* **86**:1555–1564. http://doi.wiley.com/10.1002/jctb.2680.
20. Lee YY, Yap MGS, Hu W-S, Wong KTK. 2003. Low-Glutamine Fed-Batch Cultures of 293-HEK Serum-Free Suspension Cells for Adenovirus Production. *Biotechnol. Prog.* **19**:501–509. http://doi.wiley.com/10.1021/bp025638o.
21. Liste-Calleja L, Lecina M, Lopez-Repullo J, Albiol J, Solà C, Cairó JJ. 2015. Lactate and glucose concomitant consumption as a self-regulated pH detoxification mechanism in HEK293 cell cultures. *Appl. Microbiol. Biotechnol.* **99**:9951–9960. http://link.springer.com/10.1007/s00253-015-6855-z.
22. Martínez VS, Dietmair S, Quek L-E, Hodson MP, Gray P, Nielsen LK. 2013. Flux balance analysis of CHO cells before and after a metabolic switch from lactate production to consumption. *Biotechnol. Bioeng.* **110**:660–666. http://doi.wiley.com/10.1002/bit.24728.
23. Miller WM, Blanch HW, Wilke CR. 1988. A kinetic analysis of hybridoma growth and metabolism in batch and continuous suspension culture: Effect of nutrient concentration, dilution rate, and pH. *Biotechnol. Bioeng.* **32**:947–965. http://doi.wiley.com/10.1002/bit.260320803.
24. Ozturk SS, Riley MR, Palsson BO. 1992. Effects of ammonia and lactate on hybridoma growth, metabolism, and antibody production. *Biotechnol. Bioeng.* **39**:418–431. http://doi.wiley.com/10.1002/bit.260390408.

25. Poole RC, Halestrap AP. 1993. Transport of lactate and other monocarboxylates across mammalian plasma membranes. *Am. J. Physiol. Physiol.* **264**:C761–C782. http://www.physiology.org/doi/10.1152/ajpcell.1993.264.4.C761.

26. Ramirez OT, Mutharasan R. 1990. Cell cycle- and growth phase-dependent variations in size distribution, antibody productivity, and oxygen demand in hybridoma cultures. *Biotechnol. Bioeng.* **36**:839–848. http://doi.wiley.com/10.1002/bit.260360814.

27. Ruffieux P-A, Von Stockar U, Marison IW. 1998. Measurement of volumetric (OUR) and determination of specific (q O 2) oxygen uptake rates in animal cell cultures. *J. Biotechnol.* **63**:85–95. https://www.sciencedirect.com/science/article/pii/S0168165698000467.

28. Sanfeliu A, Paredes C, Cairó JJ, Gódia F. 1997. Identification of key patterns in the metabolism of hybridoma cells in culture. *Enzyme Microb. Technol.* **21**:421–428. https://www.sciencedirect.com/science/article/pii/S014102299700015X.

29. Sauer PW, Burky JE, Wesson MC, Sternard HD, Qu L. 2000. A high-yielding, generic fed-batch cell culture process for production of recombinant antibodies. *Biotechnol. Bioeng.* **67**:585–597. http://doi.wiley.com/10.1002/%28SICI%291097-0290%2820000305%2967%3A5%3C585%3A%3AAID-BIT9%3E3.0.CO%3B2-H.

30. Wong TKK, Nielsen LK, Greenfield PF, Reid S. 1994. Relationship between oxygen uptake rate and time of infection of Sf9 insect cells infected with a recombinant baculovirus. *Cytotechnology* **15**:157–167. http://link.springer.com/10.1007/BF00762390.

31. Yoon S, Konstantinov KB. 1994. Continuous, real-time monitoring of the oxygen uptake rate (OUR) in animal cell bioreactors. *Biotechnol. Bioeng.* **44**:983–990. http://doi.wiley.com/10.1002/bit.260440815.

32. Zhou W, Hu W-S. 1994. On-line characterization of a hybridoma cell culture process. *Biotechnol. Bioeng.* **44**:170–177. http://doi.wiley.com/10.1002/bit.260440205.

CHAPTER 6. RESULTS (IV) A SIMPLIFIED IMPLEMENTATION OF THE STATIONARY LIQUID MASS BALANCE METHOD FOR ON-LINE O.U.R MONITORING IN ANIMAL CELL CULTURES

Abstract

As presented in the chapter 5, classical O.U.R dynamic method determination is an invasive method that may provoke cell stress in the culture due to the D.O. (dissolved oxygen)/pH variation every time O.U.R. determination was performed. In this chapter, different non-invasive methods for O.U.R. determination were presented and compared: dynamic method (reference), global mass balance and the stationary liquid mass balance.

The methods developed were empirically tested in 2L bioreactor HEK293 batch cultures. Compared to other methods, the stationary liquid mass balance method for O.U.R. determination offers advantages in terms of estimation accuracy and reduction of stress due. However, the need for sophisticated instrumentation, like mass flow controllers and gas analyzers, has historically limited a wider implementation of such method.

In this chapter, a new simplified method based on inexpensive valves for the continuous estimation of O.U.R. in animal cell cultures is evaluated. The determination of O.U.R. values is based on the accurate operation of the D.O. control loop and monitoring of its internal variables.

The results show how O.U.R. profile obtained with the proposed method better follows the off-line cell density determination. The frequency of O.U.R. estimation was also increased, increasing the method capabilities and applications., The method's theoretical rationale was extended to the sensitivity analysis which was analytically and numerically approached.

The results demonstrated to be not only a cheap method, but also a reliable alternative to monitor the metabolic activity in bioreactors in many biotechnological processes, being a useful tool for high cell density culture strategies implementation based on O.U.R. monitoring.

Nomenclature

O.U.R.: Oxygen Uptake Rate [mol·L^{-1}·h^{-1}]
k_La: Volumetric mass transfer coefficient [h^{-1}]
H: Henry's constant [L·atm·mol^{-1}]
K: Oxygen's dissolution constant for a given culture medium and reference temperature [°K]
T_o: Oxygen's dissolution constant reference temperature [°K]
T: Culture temperature [°K]
P: Bioreactor's gas phase absolute pressure [atm]
P_{atm}: Atmospheric pressure [atm]
P_{S1}, P_{S2}: Relative pressure for Air/O_2 and the N_2 supplies respectively. Where will typically be the same. $P_{S1} = P_{S2} = P_S$ [atm]
R_{Inlet}, R_{Outlet}: Equivalent pneumatic resistance shown by the gas filters of the bioreactor's gas lines (inlet and outlet respectively). Same type of filters gives $R_{Inlet} = R_{Outlet}$ [atm·lpm^{-1}]
χ_{O_2} : Gas phase oxygen composition [%]
pO_2: Bioreactor's gas phase oxygen partial pressure [atm]
D.O.: Relative dissolved oxygen typically referred with respect to the concentration in equilibrium with the gas phase [%]
C_L: Absolute dissolved oxygen concentration [mol·L^{-1}]
C_L^*: Absolute dissolved oxygen concentration in equilibrium with the gas phase [mol·L^{-1}]
$\overline{C_L^*}$: Average absolute dissolved oxygen concentration in equilibrium with the gas phase [mol·L^{-1}]
C_L^{SP}: Absolute dissolved oxygen set-point [mol·L^{-1}]
ctn: Arbitrary constant value [mol·L^{-1}]
C_o: Initial dissolved oxygen concentration [mol·L^{-1}]
e : Error signal [mol·L^{-1}]
qO_2: Specific oxygen consumption rate [mol·$cell^{-1}$·h^{-1}]
x_o: Cell seeding density [cell·mL^{-1}]
t_d: Cell duplication time [h]
: Valves control signal. Duty cycle ∈ (0…100) [%]
K_p: Proportional gain [L·mol^{-1}]
K_i: Integration gain [L·mol^{-1}·h^{-1}]
K_d: Differential gain [L·h mol^{-1}]
O.P.C.: Open Platform Communications
O.L.E.: Object Linking and Embedding (for process control)
Slpm: Standard liters per minute

CHAPTER 6. RESULTS (IV) A SIMPLIFIED IMPLEMENTATION OF THE STATIONARY LIQUID MASS BALANCE METHOD FOR ON-LINE O.U.R MONITORING IN ANIMAL CELL CULTURES

6.1 Introduction

Big efforts have been invested in the development of high cell density culture strategies for animal cell culture processes (Casablancas et al., 2013). Implementation of such strategies in bioreactors requires the use of suitable monitoring systems for automated control and process optimization. Therefore, approaches based on simple measurements of primary variables using cheap technologies easy to implement are of great interest.

Oxygen is a key substrate in animal cell metabolism (Doran, 2013; Ratledge, 2001) and the monitoring of its consumption known as oxygen uptake rate (O.U.R.) is a straightforward way to estimate viable cell density (Gálvez et al., 2012; Garcia-Ochoa et al., 2010; Garcia-Ochoa and Gomez, 2009). In addition, O.U.R. correlates well with the physiological state of cells (Lecina et al., 2006b).

Three different methods for the determination of O.U.R. in animal cell cultivation have been developed (Ruffieux et al., 1998): The dynamic technique based on the periodic measurement of the D.O. extinction profile in the liquid phase, this technique can be considered as a golden standard due to its simplicity and constitutes the operation fundamentals of some respiratory monitoring system like RAMOS (Anderlei et al., 2004; Hansen et al., 2012; Scheidle et al., 2007); the global mass balance which consists on analyzing the differential oxygen concentration (X_{O2}) between the bioreactor's gas inlet and outlet whilst the D.O. concentration is kept constant; and thirdly, the stationary liquid mass balance which is based on measuring the X_{O2} in the bioreactor's gas phase whilst the D.O. concentration is kept constant by controlling the oxygen supply according to the cell's consumption needs.

Due to its simplicity of implementation, the dynamic technique is by far the most commonly used method. Nevertheless, when coming to animal cell culture, it shows two considerable disadvantages: The necessary variation on the D.O. concentration increases the shear stress caused by bioreactor aeration system, which may affect negatively the cell growth and viability (Baez and Shiloach, 2014; Cooper et al., 1958; Halliwell, 2003). Moreover, the dynamic technique may not be compatible with the current trends in biopharmaceutical G.M.P. (Good Manufacturing Processes) (Kunkel et al., 1998; Li et al., 2010), since the cyclic changes on dissolved oxygen concentration (from > 60% to < 25%) and aeration rates needed for the dynamic technique implementation can have significant effects on product quality and potency, especially with respect to glycosylation, post-transcriptional modifications and impurity profiles. In addition, the time resolution provided by the dynamic technique is very poor, typically not higher than 1 sample per 1-2 hours, depending on the cell concentration. Alternatively, gas phase global mass balancing has several advantages: is a fully non-invasive method, there is no need for knowing the k_La value and yields a higher time resolution, increasing the density of accurate data obtained. In any case, global mass balancing has not been widely used in mammalian cell culture due to the need for complex and expensive instrumentation like mass spectrometers and extremely accurate D.O. control systems.

The recent introduction into the market of zirconium dioxide-based oxygen analyzers (Aehle et al., 2011), which are less expensive but still offer a good measurement accuracy, is propitiating

a wider use of such method for bioprocesses monitoring. However, at low cell densities the analytical error of such oxygen analyzers is too close to the range of measurements, being the determination of O.U.R. not accurate enough during the initial stages of cultures. The stationary liquid mass balance method offers minimum cell stress and good estimation accuracy, but still has need of significant investment in mass flow controllers, as well as additional instrumentation to measure the oxygen concentration in the bioreactor's gas phase (Ducommun et al., 2000).

The novelty of the hereby presented work relies on a simplified embodiment of a stationary liquid mass balance method for continuous O.U.R. on-line estimation. The outstanding advantages of the new approach described in this work are its simplicity and the low cost associated to the equipment needed. The O.U.R. estimation is based on inexpensive proportional valves and the observation of the control loop signals. In this way, there is no need for additional X_{O2} measurement on the bioreactor's gas phase.

6.2 Materials and Methods

6.2.1 Description of the test setup

A Biostat B-plus bioreactor (Sartorius-Stedim, Germany) was used as the basis for the test setup (**Figure 6.1**), where the native D.O. control system, based on ON-OFF valves, was bypassed by means of two external simple P.W.M. (Pulse Width Modulated) proportional valves (VSO-Low Flow from Parker, U.S.) to regulate the inlet flow of the supply gasses (Air/O_2, N_2). The gas mixing and conditioning was performed in a humidification bottle and the valves were actuated by means of a custom driver connected to a Microsoft Windows based computer through a RS-232 interface. The computer was in charge of reading the D.O. data acquired by the Biostat B-plus using an O.P.C. client (OLE for Process Control), running the D.O. control loop and solving the O.U.R. estimation algorithm. To that end, customized external control software used was developed using LabView (National Instruments, U.S.). An additional gas line for CO_2 was directly applied to the humidification bottle in order to compensate the high initial pH of the medium and was kept constant along the fermentation at a flow rate of 0.05 slpm. The total flow of the

gas mixture in the inlet was 0.4 slpm and was also kept constant during the experiments.

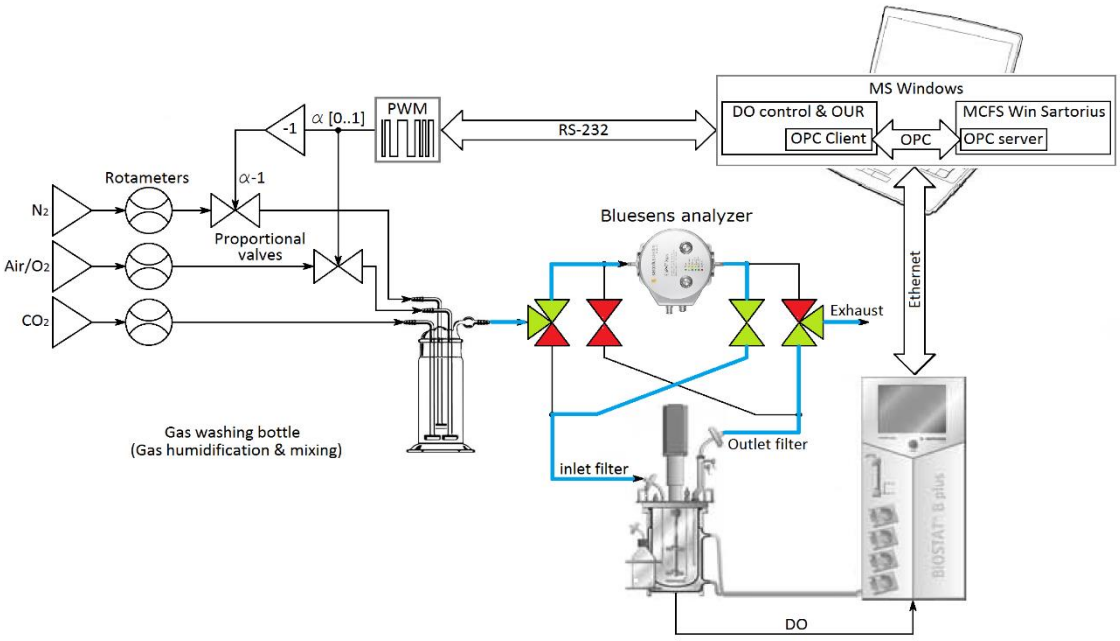

Figure 6.1: Block diagram of the test setup used for D.O. control and O.U.R. on-line monitoring. In blue is also depicted the setup for counter measurement of O.U.R. using a gas analyzer (Global mass balance method).

The Sartorius Biostat B-plus is commanded by a D.C.U. (Digital Control Unit), and consists in a polyvalent bioreactor system intended to be used with a 2-liter stirred tank. The unit is an embedded solution including all the basic probes and actuators to carry out main cultivation strategies (Batch and Fed-Batch). The D.C.U. can be operated by means of the control software (MFCS/win) through a remote computer connected to the D.C.U. via Ethernet.

On-line data exchange is provided by means of an O.P.C. Server, a software module intended to allow communication between different applications. So D.O. data is transferred to the custom controller (D.O. Control & O.U.R.) which generates the control signal to command the Pulse Width Modulator to drive the proportional valves. The need for a constant gas flow through the bioreactor imposes that the addition of the duty cycles, independently applied to both valves, has to be constant too. The key factor for an adequate O.U.R estimation relies on proper characterization of the valves used, as well as the ability to correct their non-linearity.

Finally, a BlueSens analyzer connected between the bioreactor's gas inlet and outlet was used for pseudo-continuous monitoring of the differential XO_2 across the bioreactor. An additional set of switching valves was necessary to sequentially measure the inlet and the outlet flows. The acquisition of the BlueSens data, as well as the valves actuation and the Global mass balance calculation, were carried out by the D.C.U.

For the implementation of the dynamic method the same setup was used, but the proportional valves were actuated as ON-OFF valves for periodically flushing the bioreactor's gas phase with N_2 to generate a D.O. extinction profile as explained by Lecina et al., 2006.

6.2.2 Bioreactor setup. Bioreactor aeration control & Mass transfer

A 2-liter bioreactor vessel equipped with 2 pitch blade stirrers (Biostat B-plus Sartorius-Stedim, Germany) was used for all the different set up for O.U.R. monitoring. For all cases bioreactor's setting were as follows: stirring rate of 100 rpm, a temperature of 37 ºC, a pH of 7.1 and an aeration rate of 0.35 slpm, with the exception of the gas mixing method (described in **Figure 6.1**) used for D.O. control, which was involved in the estimation of O.U.R. values. Bioreactors were seeded at 0.2-0.3·10^6 cells·mL^{-1}. A CO_2 inlet gas, 1 M of HCl buffer (Sigma, USA) and 1 M of NaOH (Sigma, USA) buffer were used for pH control.

Moreover, in order to maintain the integrity of cell's membrane and to reduce the effects of shear stress, non-ionic surfactant Pluronic F-68 (Sigma, USA) was added to the culture medium at 0.2% (w/v). The k_La value was determined by means of the Van Riet's gassing out method and it was found to be 6.53 h^{-1} for PBS at 37 °C and 100 rpm.

It is important to emphasize the fact that the k_La value is susceptible of drifting along the experiment period, thus leading to an error on the O.U.R. estimation. Hence, it becomes of significant importance to previously measure the k_La value under realistic and representative conditions of those of the later experiment.

6.2.3 Method description and modelization

Although, D.O. (dissolved oxygen) is the most common variable used in Bioreactors to reflect the oxygen concentration in the liquid phase, it must be said that D.O. corresponds to the relative oxygen concentration in the liquid phase in respect to the air saturation in equilibrium (%). To convert D.O. into absolute oxygen concentration (C_L), the oxygen solubility could be used as presented in the previous chapters to perform dynamic O.U.R..
The proposed method was inspired by the O.U.R. estimation strategies applied in the monitoring of activated sludge reactors for environmental purposes. Where fast switching On-Off valves are P.W.M. commanded for pseudo-continuous O.U.R. estimation (Catunda et al., 1999; Lira et al., 2003; Lira et al., 2004). In O.U.R. case, the gas phase oxygen molar fraction is regulated by means of two independent gas supplies (Oxygen and Nitrogen). Such regulation is performed by two P.W.M. driven valves allowing an accurate control of the D.O. concentration. Additionally, unlike for the dynamic method, O.U.R. will be estimated without generating a glimpse of cellular distress by simply observing the control loop internal signals.
Figure 6.2 shows the gas mixing station scheme, where the dissolved oxygen concentration in equilibrium with the gas phase is given by the Henry's law and the Air/O_2 flow through the corresponding valve is considered proportional with respect to the control signal's duty cycle α. Then, the averaged $\overline{C_L^*}$ concentration in equilibrium with the gas phase can be written as shown by **Equation 6.1**, where *H*: Henry's constant [L·atm·mol^{-1}], P_{atm}: Atmospheric pressure [atm], P_{S1}, P_{S2}: Relative pressure for Air/O_2 and the N_2 supplies respectively [atm], R_{Inlet}, R_{Outlet}: Equivalent pneumatic resistance shown by the gas filters of the bioreactor's gas lines [atm·lpm^{-1}], χ_{O_2} : Gas phase oxygen composition[%], pO_2: Bioreactor's gas phase oxygen partial pressure [atm], $\overline{C_L^*}$:

Average absolute dissolved oxygen concentration in equilibrium with the gas phase [mol·L^{-1}], α: Valves control signal. Duty cycle ∈ (0…100) [%].

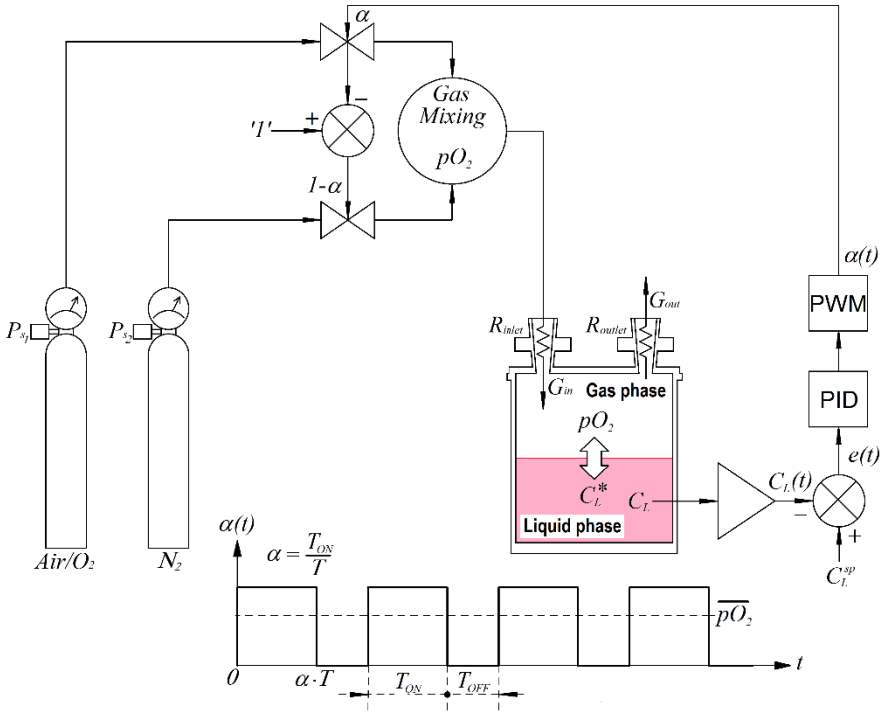

Figure 6.2: PID D.O. control loop implementation based on the PWM action of complementary proportional valves.

$$\overline{C_L^*} = \frac{pO_2}{H}\bigg|_{\substack{P_{S1}=P_{S2}=P_S \\ R_{Inlet}=R_{Outlet}}} = \frac{\left(\alpha \cdot \frac{P_S}{2} + P_{atm}\right) \cdot \chi_{O_2}/100}{H} \qquad [6.1]$$

As for any of the previously reported methods, O.U.R. estimation will also be derived from the mass balance, in this case over the liquid phase. If appropriate operating conditions are applied, the shown above control topology will behave as a causal linear and time invariant system, meaning that the mass balance equation allows to be written as a function of the duty cycle applied to the proportional valves, see **Equation 6.2** with O.U.R.: Oxygen Uptake Rate [mol·L^{-1}·h^{-1}], k_La: Volumetric mass transfer coefficient [h^{-1}], C_L: Absolute dissolved oxygen concentration [mol·L^{-1}], C_L^*: Absolute dissolved oxygen concentration in equilibrium with the gas phase [mol·L^{-1}], α: Valves control signal. Duty cycle ∈ (0…100) [%].

$$\frac{dC_L(t)}{dt} = k_L a \cdot \left(\alpha \cdot C_L^* - C_L(t)\right) - O.U.R. \qquad [6.2]$$

Equation 6.2 matches the form of a first order linear differential equation that can be easily solved. In this case, O.U.R. was replaced by a simple exponential growing model like the one shown by **Equation 6.3**. qO_2: Specific oxygen consumption rate [mol·cell^{-1}·h^{-1}], x_o: Cell seeding density [cell·mL^{-1}], t_d: Cell duplication time [h].

$$O.U.R. = qO_2 \cdot x_0 \cdot e^{\frac{\ln(2)}{t_d} \cdot t} \quad [6.3]$$

The solution to the linear differential **Equation 6.2** is given by **Equation 6.4**. C_o: Initial dissolved oxygen concentration [mol·L^{-1}]

$$C_L(t) = \alpha \cdot C_L^* \left(1 - e^{-k_l a \cdot t}\right) + C_o \cdot e^{-k_l a \cdot t} + \frac{qO_2 \cdot x_o}{\frac{ln2}{t_d} + k_l \cdot a}\left(e^{-k_l a \cdot t} - e^{\frac{ln2}{t_d} t}\right) \quad [6.4]$$

Hence, the corresponding transfer function can be expressed and solved by means of the Laplace transformation:

$$C_L(s) = L\{C_L(t)\} = \frac{\alpha \cdot C_L^*}{s(s + k_l a)} + \frac{C_o}{s + k_l a} - \frac{qO_2 \cdot x_o}{(s + k_l a) \cdot \left(s - \frac{ln2}{t_d}\right)} \quad [6.5]$$

Equations 6.4 and **6.5** clearly show that the open loop transfer function is only dependent on the bioreactor's mass transfer capability; "disturbances" are also introduced by the evolution of the metabolic activity and the D.O. initial conditions. The control theory approach offers a useful way to write the mass balance equations taking into consideration the control loop external components. Therefore, if a constant value of the set point is considered, it can be easily demonstrated that the control loop's differential error equals the dissolved oxygen accumulation term. This is shown by **Equation 6.6**. Thus, if the accumulation term in **Equation 6.2** is also replaced by the differential error, a new expression of the O.U.R. described in function of the control loop variables α and e is obtained (**Equation 6.7**).

$$\frac{de}{dt} = \frac{dC_L^{sp}}{dt} - \frac{dC_L}{dt}\bigg|_{C_L^{sp}=ctn} \Rightarrow \frac{de}{dt} = -\frac{dC_L}{dt} \quad [6.6]$$

$$O.U.R. = k_L a \cdot \left(\alpha \cdot C_L^* - C_L\right) + \frac{de}{dt} \quad [6.7]$$

Since the aim of the current approach is not just to estimate the oxygen consumption, but to keep a constant level of D.O., it will be necessary to match a good compromise between the control loop performance and the sensitivity of the control signal α with respect to the biological "disturbance". In other words, the control loop parameters need to be chosen according to a given transient response and stationary error. To that end, several simulations based on classical P-PI-PID control strategies were carried out. The control parameters were chosen in order to emphasize the effect of the oxygen consumption on the performance of each control strategy for an arbitrary cell line (data not shown). On one hand, it was found that the three control methods provided a good enough long-term estimation of the O.U.R. On the other hand, pretty different stationary errors were observed. At a first glance, the logical control strategy selection was always PID. However, the presence of real unpredictable phenomena, such as variable

inertia or unknown dead times, could easily produce unexpected behaviors, due to the action of the differential term, something highly undesirable due to the cells sensitivity to D.O. changes. Therefore, PI controller was found as the control strategy offering the best trade-off.

Under the stationary regime, when the control loop's error signal dwindles around zero, the different error sources can then be considered as independent, and the O.U.R. estimation error can be analytically approached by a Taylor's first order development, which its relative form follows the expression:

$$\frac{\Delta \mathrm{O.U.R.}}{\mathrm{O.U.R.}} = \sum_{i=0}^{n} \frac{\partial(\ln(\mathrm{O.U.R.}))}{\partial x_i} \cdot \partial x_i = \sum_{i=0}^{n} \frac{\partial(\mathrm{O.U.R.})}{\partial x_i} \cdot \partial x_i \quad [6.8]$$

As the control signal α is the outcome of a PID and the dissolved oxygen concentration in equilibrium with the gas phase is dependent on the Henry's law, the O.U.R. expression shown in **Equation 6.7** needs to be expanded considering the tuning parameters as well as the physical variables affecting the oxygen's diffusion through the medium:

$$O.U.R. = k_L a \cdot \left[\frac{P \cdot \chi_{O_2}}{H_0 \cdot e^{-K\left(1/T - 1/T_0\right)}} \cdot \left(K_P + K_i \cdot \int_0^t e \cdot d\tau + K_d \cdot \frac{de}{dt} \right) - C_L \right] + \frac{de}{dt} \quad [6.9]$$

The sensitivity analysis was carried out considering only the most relevant sources of error K_La and C_L. Remaining variables were assumed to be constant or of an insignificant contribution. Subsequently, the overall uncertainty is given by the Taylor's first order development:

$$\frac{\Delta \mathrm{O.U.R.}}{\mathrm{O.U.R.}} = \frac{\partial \mathrm{O.U.R.}}{\partial k_L a} \cdot \partial k_L + \frac{\partial \mathrm{O.U.R.}}{\partial C_L} \cdot \partial C_L \quad [6.10]$$

The first partial derivative is trivial and can easily be solved. However, $\partial O.U.R./\partial C_L$ which is the most interesting provided that offers the sensitivity with respect to the error related to the dissolved oxygen measurement, can only be solved by considering C_L time independent and applying the Schwarz theorem. The corresponding solutions are expressed as follows:

$$\frac{\partial \mathrm{O.U.R.}}{\partial k_L a} = \frac{P \cdot \chi_{O_2}}{H_0 \cdot e^{-K\left(1/T - 1/T_0\right)}} \cdot \left[K_P \cdot \left(C_L^{sp} - C_L \right) + K_i \cdot \left(C_L^{sp} \cdot t - \int_0^t C_L \cdot d\tau \right) - K_d \cdot \frac{dC_L}{dt} \right] - C_L \quad [6.11]$$

$$\frac{\partial \mathrm{O.U.R.}}{\partial C_L} = -k_L a \cdot \left[\frac{P \cdot \chi_{O_2}}{H_0 \cdot e^{-K\left(1/T - 1/T_0\right)}} \left(K_P + K_I \cdot t \right) + 1 \right] \quad [6.12]$$

A straightforward interpretation of the equations above is not advisable due to the assumptions taken, especially for $\partial O.U.R./\partial C_L$, where their dependency with respect to the control loop action and the cell culture dynamics itself are not considered. Therefore, a local/derivative based

sensitivity analysis was carried out applying the one-factor-at-a-time method. In order to avoid unrealistic results on the contribution of each error source, some previous considerations about the nature of the errors were taken into account. First, a major difference between k_La and C_L shall be noticed. Volumetric mass transfer can slowly evolve along the culture time due to the interaction of the cell concentration with the culture medium. C_L however, should show a faster fluctuation around a given set point adhering to some statistical distribution in addition to a bias error directly given by the instrument's accuracy. Consequently, to feed the analysis, an exponential evolution of up to -10 % was assumed for k_La and a ±1 % constant measurement off-set was modeled for C_L. Since the numerical analysis was just focused on the assessment of the mean values no probability distribution function was considered for C_L.

The simulation was carried out for arbitrary but realistic animal cell line species, featured by a specific oxygen consumption of 0.5 $pmol \cdot cell^{-1} \cdot h^{-1}$, 24h of duplication time and initial cell concentration of $0.35 \cdot 10^6$ $cell \cdot mL^{-1}$. The bioreactor was assumed to offer a nominal volumetric mass transfer of 40 h^{-1} under 21 % oxygen molar fraction aeration, at 1.1 atm of absolute pressure and 30 % D.O. set point. Finally, medium's D.O. saturation was calculated for an aqueous solution at 37°C assuming water equivalent oxygen solubility.

Figure 6.3 shows the 3-D profile for O.U.R. estimation uncertainties along the culture time and depending on both k_La. and C_L errors. It can be seen how the O.U.R. uncertainty approximately equals k_La uncertainty as cell density increases. Interestingly, O.U.R. estimation error tends to become less and less significant as the oxygen demands increases. Nevertheless, there is a clear limit related to the D.O. control settling time: a much higher uncertainties estimation than 10 % could be expected if O.U.R. is attempted to be estimated during the transient period. In other words, as far the control loop reaches the steady state and the D.O. concentration approaches the set-point, the O.U.R. estimation uncertainty approximately equals the relative drift experienced by the k_La along the culture time.

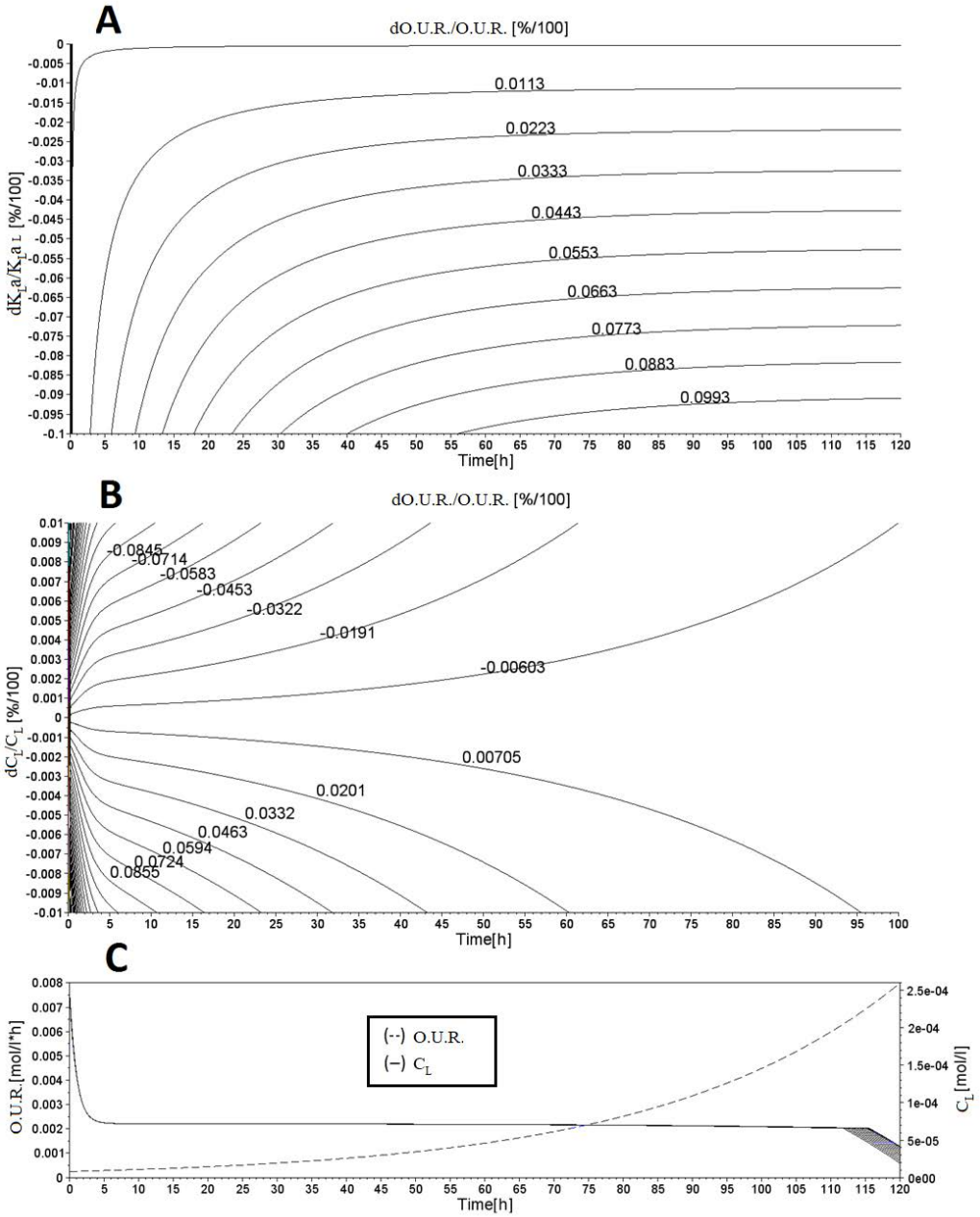

Figure 6.3: Analysis of O.U.R estimation uncertainty with respect k_La (A) and C_L (B) errors along the culture time. (C) O.U.R. reference profile & D.O. control performance

6.2.4 Cell line and culturing medium

The HEK293SF-3F6 cell line was kindly provided by Dr. A. Kamen (National Research Council of Canada). Cells were passaged at $2 \cdot 10^5$ cell·mL^{-1} three times a week as previously reported (Liste-Calleja et al., 2014). Cell maintenance was performed in 125mL polycarbonate shake flasks (Corning Inc.) with 20mL of culture, and maintained at 37°C in a humidified atmosphere within a 5% CO_2 incubator (Steri-cult 2000 Incubator, Forma Scientific). Flasks were continuously agitated at 110 rpm on an orbital shaking platform (Stuart SSL110). Culture medium consisted in SFMTransFx-293 (HyClone, Thermo Scientific) supplemented with 4mM GlutaMAX (Gibco,

Invitrogen), 5% FBS (v/v) (Sigma Aldrich) and 10% of Cell Boost 5 (80 g/L) (HyClone, Thermo Scientific).

6.2.5 Cell growth assessment and metabolite analysis

Cell number was determined by manual counting using a Neubauer hemocytometer and a phase contrast microscope (Nikon eclypse, TS100). Viability was assessed using the Trypan blue dye exclusion method. Glucose and lactate concentrations were measured using an automatic glucose and lactate analyzer (YSI, Yellow Springs Instrument, 2700 Select).

6.3 Results

Three different methods for the on-line determination of O.U.R. in HEK293 cultures were implemented in the 2-liter bioreactor in order to compare the performance of such methods and how their implementation may affect other culturing parameters, as detailed in the Materials and Methods section.

In general terms, the different techniques for the determination of O.U.R. had no influence on cell culture development in batch culture (**Figure 6.4**). In all cases, cell density reached values about 13-15·10^6 cells·mL^{-1} after 192-216 hours of culture. Those little differences may be related to little differences on inoculum cell densities and are normally observed in cell cultures. Also, no significant differences in glucose and lactate concentration profiles were observed. Glucose was only exhausted after the exponential growth phase when the stationary liquid mass balance method was applied (**Figure 6.4-C**) while was even not depleted at all when the dynamic technique and gas analyzers were used for O.U.R. determination (**Figure 6.4-A** and **6.4-B**). Those differences were not reflected on the cell density profiles, but in the lactate generation and accumulation. Differences in the maximum lactate concentration about 2-fold increase are consistent with the observation of different glucose consumption profiles while cell density reached was similar. It is relevant to state that the lactate concentration reached is not detrimental for cell growth in any case (other cultures reached concentration over 25mM without affecting cell growth, data not shown). This observation denotes that the aeration strategies used when implementing the different O.U.R. determination method has an effect on cell physiology and metabolism. The culturing conditions (D.O. and pH) were kept nicely constant when the simplified method was used, but D.O. and pH were affected when the dynamic technique was applied (depicted in **Figure 6.5**). Dynamic Technique generates a D.O. fluctuation from 60% to 25% for each measurement, and during the analysis pH control is switched off. Since HEK293 metabolism are sensitive to lactate concentration and pH (and probably to other parameters such as D.O. and shear stress), a change on metabolism (Liste-Calleja et al., 2015) (from glucose consumption to co-consumption of glucose and lactate) was observed when culturing conditions were affected by the O.U.R. determination technique. In O.U.R. hands we have recently observed differences in metabolism and in the total cell density reached (about 20%) when fed-batch cultures were performed using different monitoring systems. Again, when the dynamic technique was implemented the fed-batch culture performance was negatively affected (metabolism altered) even the glucose set point control

was kept therein the range set. Differently, when fed-batch nutrient feeding was commanded by the alkali buffer addition, those limitations were not observed (unpublished data).

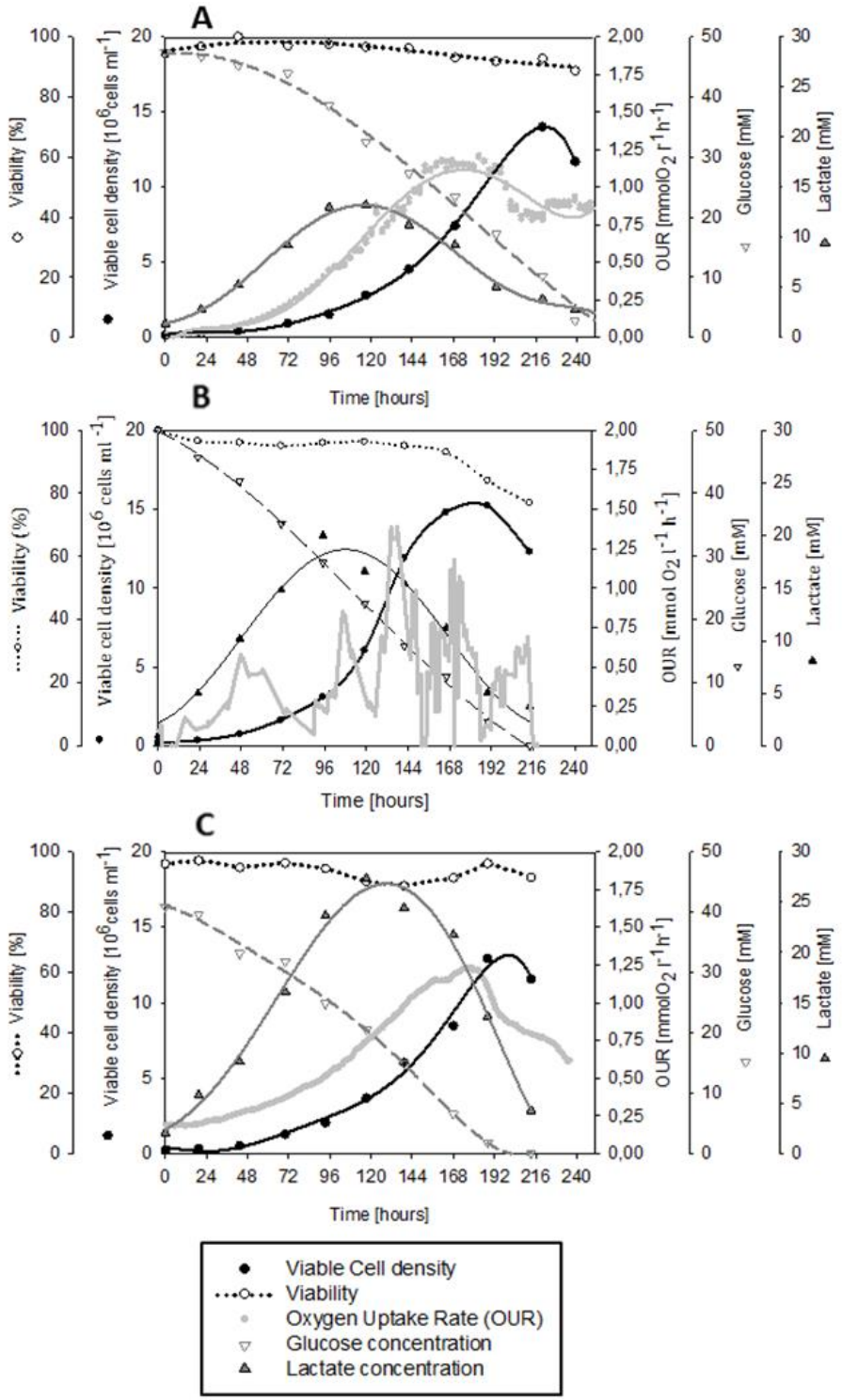

Figure 6.4: Comparison of the different O.U.R. estimation methods implemented in 2-liter bioreactor: A) Dynamic method, B) Global Mass Balance by means of gas analyzers and C) Simplified stationary Liquid Mass Balance.

Regarding O.U.R. measurements, again similar profiles were obtained, except for O.U.R. calculated using the global mass balance by means of the Bluesens gas analyzer, that shows and erratic and a high dispersion in the measurements. As can be seen in the **Figure 6.4** for the O.U.R. calculated from the dynamic method and the stationary liquid mass balance using the valves controllers, only small differences where observed on the time in which the maximum was reached, what was in good concordance with the differences observed on cell density profiles as well. In those cases, in which the maximum cell density was reached 24 hours earlier, the maximum of O.U.R. profile was also accordingly anticipated. As it can be seen in **Figure 6.4**, cell density measurements and O.U.R. estimation showed parallel profiles for the dynamic and the stationary liquid mass balance methods. In two of three cases, a very short lag phase (which corresponds to an adaptation time for cells to growth) was detected in both O.U.R. and cell density profiles during the first 24 hours post-inoculation. Afterwards cell density and O.U.R. profiles showed exponential curves, which corresponds to the exponential growth phase of cultures.

Interestingly, the end of the exponential growth phase was clearly detected by O.U.R. measurements, corresponding to the maximum of the O.U.R. profile, although the maximal cell density was reached about 48 hours later. Therefore, O.U.R. monitoring allowed detecting on-line the middle of the exponential cell growth reflected in the inflexion point in the O.U.R. curve. It is assumed that the inflexion point of the exponential growth phase corresponds to a suitable time to start feeding strategies in order to achieve high cell density cultures (Lecina et al., 2006a).

In the two cases where O.U.R. profile follow the cell growth, the maximum O.U.R. values were comprised therein the range about 1-1.25·10^{-3} mol·L^{-1}·h^{-1}. When comparing O.U.R. profiles obtained by means of the different methods, the global mass balance using gas analyzers shows an erratic and a high dispersion in the measurements. The dynamic method, as has been mentioned before, showed an important measurement dispersion, whereas the O.U.R. determination by means of the stationary liquid mass balance using the valves control signals was more accurate.

The simplified implementation of O.U.R. estimation by stationary liquid mass balance using D.O. control loop signals showed an additional advantage in comparison to the dynamic method in terms of D.O. and pH control. Intrinsically to the dynamic method, the D.O. has to be risen up over 60% of saturation, and then the gas mixture inlet is discontinued including the CO_2 used for pH control. Under these conditions, D.O. and pH profiles showed higher oscillations as it can be seen in **Figure 6.5**. Values from 25 to 80% for D.O. and from 7 to 7.2 on the pH were observed (grey lines) when the dynamic method was implemented, whereas such parameters were almost constant for the stationary liquid mass balance method (black lines). The D.O. control for the latter strategy needed about 10 hours in order to reach the desired set point (50% of air saturation), which could be considered as the control stabilization time, but once the set point was reached it was kept constant along the fermentation (only 1-2 % of stationary error was observed). The peak of D.O. observed at 96 hours of culture corresponds to the replacement of the air flow for pure oxygen, so that the control needed a few hours to adapt the response to the gas composition change, and D.O, was stabilized again after few hours. Altogether made the

D.O. and pH controls used for stationary mass liquid balance more suitable for those processes in which D.O. and pH disturbances should be avoided.

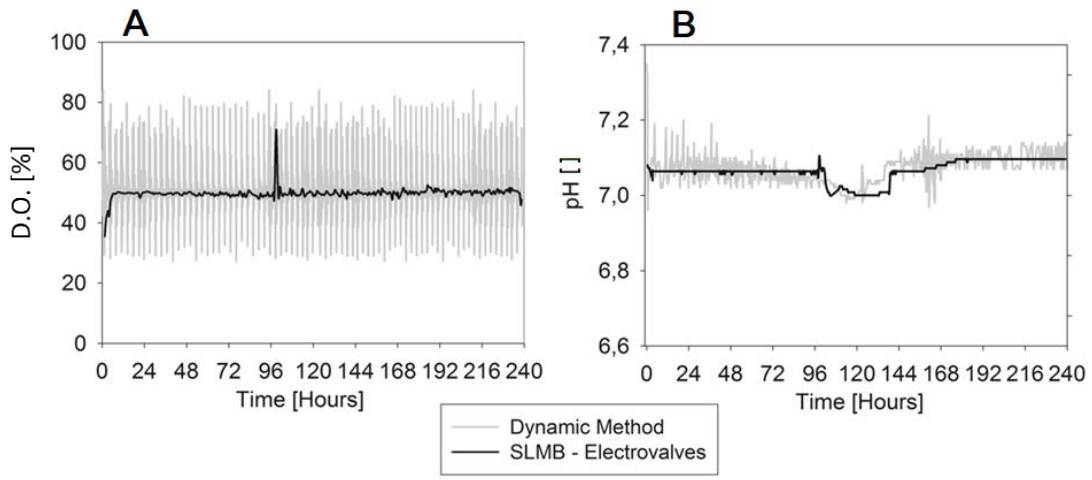

Figure 6.5: Effect of the method for O.U.R. estimation implemented on the main culture parameters. Comparison of (A) D.O. and (B) pH profiles obtained from batch cultures in which Dynamic method (grey line) and Simplified Liquid mass balance (black line) were implemented.

Eventually, O.U.R. values determined by means of the two successful methodologies were represented *versus* viable cell density obtained from the profile fitted to the experimental values (Figure 6.6). As it can be seen, both profiles were quite similar, meaning that any of both methods can be used for the determination of O.U.R.. However, the profiles obtained using the dynamic method showed higher point dispersion due to the intrinsic estimation error of the method. On the contrary, the profile obtained with the stationary liquid mass balance was smoother and showed fewer transients, and therefore it would be a more suitable method to be used in future culture strategies based on O.U.R. estimation.

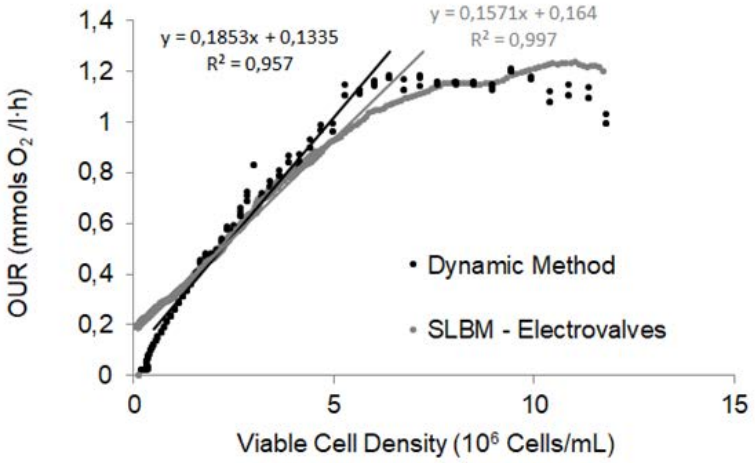

Monitoring System	qO_2 (mmols /10^9 cells ·h)	R^2
Dynamic Method	0,1853	0,957
SLMB - Electrovalves	0,1571	0,997

Figure 6.6: Comparison of the calculated specific oxygen consumption rate by correlating Viable Cell Density and O.U.R. profiles obtained by the different estimation methods

Additionally, the specific oxygen consumption rates (qO_2) for HEK293 cells were evaluated from the linear part of the profiles, as the slope of the linear regressions. The estimated qO_2 values are compiled in the table endorsed to **Figure 6.6**. For the two different methods used for the evaluation of O.U.R. values, the estimated qO_2were of the same range to previously published values for HEK293 cells (Aehle et al., 2011; Li et al., 2010) indicating that all methods were suitable for the determination of O.U.R. Again, the coefficient of determination (R^2) obtained from the linear regression analysis for each data set, shows that the lowest variance between the experimental data and the linear adjustment for the data obtained with the stationary liquid mass balance method with a R^2 about 0.997 in comparison to the dynamic method (0.957).

6.4 Conclusions

A simplified stationary liquid mass balance method for the O.U.R. estimation has been proposed, implemented and tested, based on the knowledge of the D.O. control loop variables and the volumetric mass transfer coefficient. The feasibility of the method was demonstrated for animal cells in a bench-scale bioreactor. Regarding the method's accuracy, any standard procedure to mimic a known profile of oxygen consumption has not been reported yet, unfortunately. Therefore, it was not possible to provide a measured value on the estimation error. Nevertheless, the method was empirically and successfully compared with the dynamic and the global mass balance methods, obtaining analogous results using the dynamic method, but clearly much less dispersed. Additionally, the sensitivity and uncertainty analysis were analytically and numerically approached. Ending conclusion is that as far the D.O. measurement error can be kept below reasonable limits (<5 %) and despite that during the D.O. settling time the O.U.R. estimation cannot be considered valid, once the set point is reached, the overall

uncertainty trends to be mostly related just to the k_La drift as it happens for the dynamic method and the stationary liquid mass balance (Zhang et al., 1997). Interestingly, the simplified stationary liquid mass balance method offers outstanding advantages: 1) is the cheapest method tested in this work, 2) higher measurements frequency can be performed compared to others methods, 3) D.O. can stably been kept therein a narrow range and 4) eradicates the cell stress produced by gas flow pulses variations.

With the aid of this method it was possible to find a correlation between the O.U.R., the cell concentration (Kamen et al., 1996) and the glucose consumption during the first phase of the culture. In a second phase, in which HEK293 were able to metabolize lactate as other human cell lines (Khoo and Al-Rubeai, 2009), a change in the O.U.R. profile, characterized by a decrease in the specific oxygen consumption rate was detected. Additionally, the off-line data available permitted a crucial observation, the fact that the turning point in the O.U.R. graphs allowed anticipating the time of maximum viable cell concentration (≈48 hours before). The ability of HEK293 cells to consume endogenous lactate and glucose (Liste-Calleja et al., 2015) opens up the possibility of defining different culture strategies (i.e. diauxic strategies). More interesting was that the metabolic change, from a phase in which glucose was consumed as a single carbon source to another phase in which glucose and lactate were simultaneously consumed, was also reflected in the O.U.R. values obtained by the monitoring methods.

The feasibility of a new method based on inexpensive valves for the continuous estimation of O.U.R. in animal cell cultures has been demonstrated. The performance of said method (Simplified implementation of the stationary liquid mass balance) has been compared with respect to the Global mass balance and Dynamic methods. The proposed method showed obvious advantages in terms of time resolution, D.O. stability (lack of cell stress) and cost. Additionally, the results obtained could be applied to the optimization of high cell density culture strategies like fed-batch or continuous perfused cultivation in which the proposed method can be applied.

6.5 References

1. Aehle M, Kuprijanov A, Schaepe S, Simutis R, Lübbert A. 2011. Simplified off-gas analyses in animal cell cultures for process monitoring and control purposes. *Biotechnol. Lett.* **33**:2103–2110. http://link.springer.com/10.1007/s10529-011-0686-5.
2. Anderlei T, Zang W, Papaspyrou M, Büchs J. 2004. Online respiration activity measurement (OTR, CTR, RQ) in shake flasks. *Biochem. Eng. J.* **17**:187–194. https://www.sciencedirect.com/science/article/pii/S1369703X03001815.
3. Baez A, Shiloach J. 2014. Effect of elevated oxygen concentration on bacteria, yeasts, and cells propagated for production of biological compounds. *Microb. Cell Fact.* **13**:181. http://microbialcellfactories.biomedcentral.com/articles/10.1186/s12934-014-0181-5.
4. Casablancas A, Gámez X, Lecina M, Solà C, Cairó JJ, Gòdia F. 2013. Comparison of control strategies for fed-batch culture of hybridoma cells based on on-line monitoring of oxygen uptake rate, optical cell density and glucose concentration. *J. Chem. Technol. Biotechnol.* **88**:1680–1689. http://doi.wiley.com/10.1002/jctb.4019.

5. Catunda SYC, Deep GS, van Haandel AC, Freire RCS. 1999. Feedback control method for estimating the oxygen uptake rate in activated sludge systems. *IEEE Trans. Instrum. Meas.* **48**:864–869. http://ieeexplore.ieee.org/document/779191/.
6. COOPER PD, BURT AM, WILSON JN. 1958. Critical Effect of Oxygen Tension on Rate of Growth of Animal Cells in Continuous Suspended Culture. *Nature* **182**:1508–1509. http://www.nature.com/doifinder/10.1038/1821508b0.
7. Doran PM. 2013. Bioprocess engineering principles. Elsevier/Academic Press 919 p.
8. Ducommun P, Ruffieux P, Furter M, Marison I, von Stockar U. 2000. A new method for on-line measurement of the volumetric oxygen uptake rate in membrane aerated animal cell cultures. *J. Biotechnol.* **78**:139–47. http://www.ncbi.nlm.nih.gov/pubmed/10725537.
9. Gálvez J, Lecina M, Solà C, Cairó JJ, Gòdia F. 2012. Optimization of HEK-293S cell cultures for the production of adenoviral vectors in bioreactors using on-line OUR measurements. *J. Biotechnol.* **157**:214–222. https://www.sciencedirect.com/science/article/pii/S0168165611006419.
10. Garcia-Ochoa F, Gomez E. 2009. Bioreactor scale-up and oxygen transfer rate in microbial processes: An overview. *Biotechnol. Adv.* **27**:153–176. https://www.sciencedirect.com/science/article/pii/S0734975008001079.
11. Garcia-Ochoa F, Gomez E, Santos VE, Merchuk JC. 2010. Oxygen uptake rate in microbial processes: An overview. *Biochem. Eng. J.* **49**:289–307. https://www.sciencedirect.com/science/article/pii/S1369703X10000380.
12. Halliwell B. 2003. Oxidative stress in cell culture: an under-appreciated problem? *FEBS Lett.* **540**:3–6. http://www.ncbi.nlm.nih.gov/pubmed/12681474.
13. Hansen S, Hariskos I, Luchterhand B, Büchs J. 2012. Development of a modified Respiration Activity Monitoring System for accurate and highly resolved measurement of respiration activity in shake flask fermentations. *J. Biol. Eng.* **6**:11. http://jbioleng.biomedcentral.com/articles/10.1186/1754-1611-6-11.
14. Kamen AA, Bédard C, Tom R, Perret S, Jardin B. 1996. On-line monitoring of respiration in recombinant-baculovirus infected and uninfected insect cell bioreactor cultures. *Biotechnol. Bioeng.* **50**:36–48. http://doi.wiley.com/10.1002/%28SICI%291097-0290%2819960405%2950%3A1%3C36%3A%3AAID-BIT5%3E3.0.CO%3B2-2.
15. Khoo SHG, Al-Rubeai M. 2009. Metabolic characterization of a hyper-productive state in an antibody producing NS0 myeloma cell line. *Metab. Eng.* **11**:199–211. https://www.sciencedirect.com/science/article/pii/S1096717609000135.
16. Kunkel JP, Jan DC., Jamieson JC, Butler M. 1998. Dissolved oxygen concentration in serum-free continuous culture affects N-linked glycosylation of a monoclonal antibody. *J. Biotechnol.* **62**:55–71. https://www.sciencedirect.com/science/article/pii/S0168165698000443.
17. Lecina M, Soley A, Gràcia J, Espunya E, Lázaro B, Cairó JJ, Gòdia F. 2006a. Application of on-line OUR measurements to detect actions points to improve baculovirus-insect cell cultures in bioreactors. *J. Biotechnol.* **125**:385–394. https://www.sciencedirect.com/science/article/pii/S0168165606002112.
18. Lecina M, Soley A, Gràcia J, Espunya E, Lázaro B, Cairó JJ, Gòdia F. 2006b. Application of on-line OUR measurements to detect actions points to improve baculovirus-insect cell

cultures in bioreactors. *J. Biotechnol.* **125**:385–394. https://www.sciencedirect.com/science/article/pii/S0168165606002112.

19. Li F, Vijayasankaran N, Shen A (Yijuan), Kiss R, Amanullah A. 2010. Cell culture processes for monoclonal antibody production. *MAbs* **2**:466–479. http://www.tandfonline.com/doi/abs/10.4161/mabs.2.5.12720.
20. Lira VV, Barros PR, da Rocha Neto JS, van Haandel AC. 2004. Estimation of dissolved oxygen dynamics for sequencing batch aerobic reactors. In: . *Proc. 21st IEEE Instrum. Meas. Technol. Conf. (IEEE Cat. No.04CH37510)*. IEEE, pp. 14–19. http://ieeexplore.ieee.org/document/1350984/.
21. Lira VV, da Rocha Neto JS, Barros PR, van Haandel AC. 2003. Automation of an anaerobic~aerobic wastewater treatment process. *IEEE Trans. Instrum. Meas.* **52**:909–915. http://ieeexplore.ieee.org/document/1213681/.
22. Liste-Calleja L, Lecina M, Cairó JJ. 2014. HEK293 cell culture media study towards bioprocess optimization: Animal derived component free and animal derived component containing platforms. *J. Biosci. Bioeng.* **117**:471–477. https://www.sciencedirect.com/science/article/pii/S1389172313003551.
23. Liste-Calleja L, Lecina M, Lopez-Repullo J, Albiol J, Solà C, Cairó JJ. 2015. Lactate and glucose concomitant consumption as a self-regulated pH detoxification mechanism in HEK293 cell cultures. *Appl. Microbiol. Biotechnol.* **99**:9951–9960. http://link.springer.com/10.1007/s00253-015-6855-z.
24. Ratledge C. 2001. Biochemistry and physiology of growth and metabolism. *Basic Biotechnol. C Ratledge, B Kristiansen, Ed.*
25. Ruffieux P-A, Von Stockar U, Marison IW. 1998. Measurement of volumetric (OUR) and determination of specific (q O 2) oxygen uptake rates in animal cell cultures. *J. Biotechnol.* **63**:85–95. https://www.sciencedirect.com/science/article/pii/S0168165698000467.
26. Scheidle M, Klinger J, Büchs J. 2007. Combination of On-line pH and Oxygen Transfer Rate Measurement in Shake Flasks by Fiber Optical Technique and Respiration Activity MOnitoring System (RAMOS). *Sensors* **7**:3472–3480. http://www.mdpi.com/1424-8220/7/12/3472.
27. Zhang Y-H, Wang H-Q, Liu S, Yu J-T, Zhong J-J. 1997. Regulation of apparent viscosity and O transfer coefficient by osmotic pressure in cell suspensions of Panax notoginseng. *Biotechnol. Lett.* **19**:943–945. http://link.springer.com/10.1023/A:1018370511494.

CHAPTER 7. CONCLUDING REMARKS

The work presented in the thesis has been conducted with the aim of improving the bioprocess productivity using mammalian cell cultures in Bioreactor. With this goal, substantial contributions have been made in Bioprocess Engineering and Systems Biology fields. The metabolism of both HEK293 and CHO cell lines have been characterized using genome scale metabolic models. These models have been adapted by the author to simplify and obtain the key results to understand the core metabolism of both cell lines in culture. All the knowledge gained in the metabolic study has been applied to develop a new robust monitoring and controlling tool to increase the productivity using a fed-batch strategy. The new tool, based on the alkali buffer addition made by the control system to maintain the pH in culture, has been compared with a widely used monitoring tool as O.U.R. (dynamic method), showing better results in terms of cell density and productivity. To close the work, a different non-invasive method for O.U.R. determination based on the stationary liquid mass balance was presented and tested successfully in batch culture.

From the work developed and the obtained results it can be conducted that:

- Three different glucose and lactate metabolisms have been obtained in the different experiments performed with HEK293 and CHO cells in Shake-Flasks and Bioreactor, captured in the three phases mentioned above (Phase 1: glucose consumption and lactate production (exponentially growth), Phase 2: glucose and lactate simultaneous consumption (exponentially growth), and Phase 3: lactate consumption as a sole carbon source (no cell growth)).
- The different metabolic phases obtained mainly depend on two cell culture conditions: the pH and the lactate concentration in the culture media. When pH was controlled in the Bioreactor, Phase 1 appeared at the beginning of the culture, but when glucose was depleted Phase 3 was obtained. In contrast, when pH was leaved free both in Shake-Flasks and Bioreactor, Phase 1 was obtained but when pH dropped below 6.80, due to lactic acid secretion, the Phase 2 appeared, both in exponentially growth phase.
- Phase 2 can be triggered at will in CHO cell cultures by adding lactate to the initial media and keeping pH below 6.80. As far as we know, any experiment in which glucose and lactate simultaneous consumption is obtained from the beginning of the culture has been reported for mammalian cells in the literature.
- The co-existence of two metabolisms with different flux rates for glycolysis and TCA cycle leads cells to generate a non-desired by-product as lactate. Both metabolisms are somehow uncoupled in terms of flux rates, affecting the NADH regeneration, that takes place mainly in the cytoplasm instead of mitochondria. Our hypothesis lies in that this metabolism should be understood under the perspective that animal cells are the symbiosis of two different metabolisms that belong to two different ancestors. One anaerobic, that takes place in the cytoplasm, and the other aerobic, located into mitochondria (Endosymbiotic Theory (Mereschkowsky and C., 1910; Sagan, 1967)). Hence, the flux rates related to the aerobic metabolism are much lower than those from the anaerobic metabolism.

- The co-metabolization of glucose and lactate has not usually been observed in cell cultures and occurs when lactate and protons reach high concentrations outside the cells. In those conditions, cells are able to co-transport extracellular protons together with lactate into the cytosol. Once in the cytosolic space, lactate could be oxidized to pyruvate which is transported into mitochondria or, alternatively (in this work both hypothesis were taken into account), lactate could be directly transported into mitochondria, being then oxidized. This has been demonstrated with empirical data obtained by respirometry assays, using isolated mitochondria of HEK293 cells, indicated that both possibilities are feasible.
- The metabolic flux balances performed with the metabolic models converged in a solution for both hypothesis (c-LDHc and m-LDH), meaning that the alternative route proposed is feasible. The outcome of such model where lactate can be metabolized directly into the mitochondria shows lower fluxes at the Malate/Aspartate shuttle since NADH is directly released into mitochondria, where it is regenerated again as NAD^+ and H^+. As NADH is not generated in the cytosol, there is no need to transport it into the mitochondria, reducing the requirement for transporting NADH through the Malate/Aspartate Shuttle, as pointed above. This fact demonstrate that switching to a glucose and lactate co-metabolization resulted in a better-balanced cell metabolism, as can be seen from the metabolic fluxes calculated. Moreover, the generation and secretion of lactate is totally reverted, so the main drawback of processes based on mammalian cell cultures is also eliminated.
- Another glucose and lactate metabolism is obtained when glucose has been completely depleted from the media. In this phase of culture, cells consume the lactate produced during the previous phase as a sole carbon and energy source. Analyzing the metabolic fluxes of this behavior, biosynthesis and energy production are much lower when compared with the behavior described above. TCA fluxes were drastically reduced. Consequently, only residual cell growth at very low growth rates was observed.
- The results presented demonstrated the applicability of O.U.R. and alkali buffer addition as reliable tools for feed control in fed-batch processes of HEK293 cells. Controlled feeding based on maintaining a constant glucose concentration in cell culture has allowed to keept the culture in a more adequate environment that has resulted in a more efficient substrate consumption.
- Although dynamic O.U.R. it is a simple and widely applied method that requires only an oxygen probe, the culture constant distortions of the D.O. and pH performed in every O.U.R. measurement cycle has led to obtain less final VCD and product concentration in the culture.
- The new method presented based on the alkali buffer addition, allows a proper tracking of cell growth rate and cell concentration and a precise determination of the feeding rate in order to control the cell environment by the addition of nutrients. In this way, a greater maximum cell concentration and product titer has been obtained when compared to O.U.R. method. This method is also simple and robust.
- The O.U.R. method allowed to increase the total viable cell concentration and product titer by 102% and 124% respectively, compared with the batch strategy. The volumetric productivity was also increased in 68%. Better results have been obtained with the alkali

addition strategy, increasing the total viable cell concentration and product titer by 178% and 257% respectively, and obtaining a 109% increment of the process volumetric productivity.

- To overcome the problem of the culture constant distortions when dynamic O.U.R. method is applied, a simplified stationary liquid mass balance method for the O.U.R. estimation has been implemented and tested. The feasibility of the method was demonstrated for HEK293 cell cultures in bioreactor.
- The results clearly show that O.U.R. calculated using the global mass balance by means of the Bluesens gas analyzer cannot be used for mammalian cell cultures due to the low oxygen consumption of the cells. Erratic and high dispersion O.U.R. measurements have been obtained.
- The simplified stationary liquid mass balance method offers outstanding advantages in respect of the dynamic method: 1) is cheaper, 2) higher measurements frequency can be performed compared to others methods, 3) D.O. can stably been kept therein a narrow range and 4) eradicates the cell stress produced by gas flow pulses variations.

APPENDIX A

The HEK293 metabolic model used for p-FBA presented in the Chapter 4 was derived from the last reconstruction published for the *Homo sapiens* RECON2.2 (Swainston et al., 2016). The metabolic model was reduced following the protocol performed by Quek (Quek et al., 2014) for adaptation of the RECON2.0 (Thiele et al., 2013) model for HEK293 cells. The resulting model, that contains 354 reactions and 335 metabolites, used for the metabolic flux calculation is detailed in **Table A.1**.

Table A.1: List of reactions included in the HEK293 reduced model developed and used in the Chapter 4.

R_biomass_reaction	Generic human biomass reaction	0.054*M_biomass_other_c + 0.058*M_biomass_RNA_c + 0.706*M_biomass_protein_c + 0.097*M_biomass_lipid_c + 0.071*M_biomass_carbohydrate_c + 0.014*M_biomass_DNA_c	----->	M_biomass_c
R_FAS120COA	fatty-acyl-CoA synthase (n-C12:0CoA)	3.0*M_h_c + 2.0*M_nadph_c + M_malcoa_c + M_dcacoa_c	----->	M_co2_c + 2.0*M_nadp_c + M_h2o_c + M_ddcacoa_c + M_coa_c
R_IMPC	IMP cyclohydrolase	M_h2o_c + M_imp_c	<---->	M_fprica_c
R_IMPD	IMP dehydrogenase	M_h2o_c + M_imp_c + M_nad_c	----->	M_h_c + M_nadh_c + M_xmp_c
R_r0127	L-Asparagine amidohydrolase Alanine and aspartate metabolism / Cyanoamino acid metabolism / Nitrogen metabolism EC:3.5.1.1 EC:3.5.1.38	M_h2o_c + M_asn_L_c	----->	M_nh4_c + M_asp_L_c
R_LSTO1r	Lathosterol oxidase	M_h_r + M_nadph_r + M_o2_r + M_chlstol_r	----->	M_nadp_r + M_ddsmsterol_r + 2.0*M_h2o_r
R_ORNTArm	ornithine transaminase reversible (m)	M_orn_m + M_akg_m	<---->	M_glu5sa_m + M_glu_L_m
R_PHEtec	L-phenylalanine transport via diffusion (extracellular to cytosol)	M_phe_L_e	<---->	M_phe_L_c
R_DTMPK	dTMP kinase	M_atp_c + M_dtmp_c	----->	M_adp_c + M_dtdp_c
R_TYRt	L-tyrosine transport	M_tyr_L_e	<---->	M_tyr_L_c
R_r1144	Major Facilitator(MFS) TCDB:2.A.18.6.3	M_glu_L_e + M_na1_e	----->	M_na1_c + M_glu_L_c
R_VALTAm	valine transaminase, mitochondiral	M_akg_m + M_val_L_m	<---->	M_glu_L_m + M_3mob_m

R_r1143	Major Facilitator(MFS) TCDB:2.A.18.6.3	M_na1_e + M_asp_L_e	----->	M_asp_L_c + M_na1_c
R_r1146	Biosynthesis of steroids Enzyme catalyzed	M_h_r + M_HC02110_r + M_ahcys_r	<---->	M_zymst_r + M_amet_r
R_DSREDUCr	Desmosterol reductase	M_h_r + M_nadph_r + M_dsmsterol_r	----->	M_nadp_r + M_chsterol_r
R_H2CO3D	carboxylic acid dissociation	M_co2_c + M_h2o_c	<---->	M_h_c + M_hco3_c
R_GNDc	phosphogluconate dehydrogenase	M_nadp_c + M_6pgc_c	----->	M_co2_c + M_nadph_c + M_ru5p_D_c
R_OIVD3m	2-oxoisovalerate dehydrogenase (acylating; 3-methyl-2-oxopentanoate), mitochondrial	M_3mop_m + M_coa_m + M_nad_m	----->	M_2mbcoa_m + M_nadh_m + M_co2_m
R_DGTPtn	dGTP diffusion in nucleus	M_dgtp_c	<---->	M_dgtp_n
R_HMGCOASi	Hydroxymethylglutaryl CoA synthase (ir)	M_h2o_c + M_aacoa_c + M_accoa_c	----->	M_coa_c + M_h_c + M_hmgcoa_c
R_O2tm	O2 transport (diffusion)	M_o2_c	<---->	M_o2_m
R_ASPTA	aspartate transaminase	M_asp_L_c + M_akg_c	<---->	M_glu_L_c + M_oaa_c
R_L_LACt2r	L-lactate reversible transport via proton symport	M_h_e + M_lac_L_e	<---->	M_h_c + M_lac_L_c
R_r0666	2-(Formamido)-N1-(5-phosphoribosyl)acetamidine cyclo-ligase (ADP-forming) Purine metabolism EC:6.3.3.1	M_atp_c + M_fpram_c	<---->	2.0*M_h_c + M_adp_c + M_air_c + M_pi_c
R_NaKt	Na+/K+ exchanging ATPase	M_h2o_c + M_atp_c + M_na1_c + M_k_e	----->	M_h_c + M_adp_c + M_na1_e + M_pi_c + M_k_c
R_PMEVKc	phosphomevalonate kinase, cytosol	M_atp_c + M_5pmev_c	----->	M_adp_c + M_5dpmev_c
R_GLUDxm	glutamate dehydrogenase (NAD) (mitochondrial)	M_glu_L_m + M_nad_m + M_h2o_m	<---->	M_akg_m + M_nadh_m + M_nh4_m + M_h_m
R_HACD9m	3-hydroxyacyl-CoA dehydrogenase (2-	M_nad_m + M_3hmbcoa_m	<---->	M_nadh_m + M_h_m + M_2maacoa_m

	Methylacetoacetyl-CoA), mitochondrial			
R_PSFLIPm	phosphatidylserine flippase	M_h2o_c + M_atp_c + M_ps_hs_c	----->	M_h_c + M_adp_c + M_pi_c + M_ps_hs_m
R_PGI	glucose-6-phosphate isomerase	M_g6p_c	<---->	M_f6p_c
R_AKGDm	2-oxoglutarate dehydrogenase	M_akg_m + M_coa_m + M_nad_m	----->	M_nadh_m + M_co2_m + M_succoa_m
R_FAS140COA	fatty-acyl-CoA synthase (n-C14:0CoA)	M_ddcacoa_c + 3.0*M_h_c + 2.0*M_nadph_c + M_malcoa_c	----->	M_co2_c + 2.0*M_nadp_c + M_h2o_c + M_coa_c + M_tdcoa_c
R_ORNtiDF	ornithine transport via diffusion (extracellular to cytosol)	M_orn_e	----->	M_orn_c
R_OIVD2m	2-oxoisovalerate dehydrogenase (acylating; 3-methyl-2-oxobutanoate), mitochondrial	M_3mob_m + M_coa_m + M_nad_m	----->	M_nadh_m + M_co2_m + M_ibcoa_m
R_PGK	phosphoglycerate kinase	M_atp_c + M_3pg_c	<---->	M_adp_c + M_13dpg_c
R_H2CO3Dm	carboxylic acid dissociation	M_co2_m + M_h2o_m	<---->	M_h_m + M_hco3_m
R_ARTPLM3	R group to palmitate conversion	M_Rtotalcoa_c	<---->	4.0*M_h_c + M_pmtcoa_c
R_PGM	phosphoglycerate mutase	M_2pg_c	<---->	M_3pg_c
R_KYN3OX	kynurenine 3-monooxygenase	M_h_c + M_nadph_c + M_o2_c + M_Lkynr_c	----->	M_nadp_c + M_h2o_c + M_hLkynr_c
R_PGL	6-phosphogluconolactonase	M_h2o_c + M_6pgl_c	----->	M_h_c + M_6pgc_c
R_TRDR	thioredoxin reductase (NADPH)	M_h_c + M_nadph_c + M_trdox_c	----->	M_nadp_c + M_trdrd_c
R_HKYNH	3-Hydroxy-L-kynurenine hydrolase	M_h2o_c + M_hLkynr_c	----->	M_ala_L_c + M_3hanthrn_c
R_MTHFC	methenyltetrahydrofolate cyclohydrolase	M_h2o_c + M_methf_c	<---->	M_h_c + M_10fthf_c

R_TRPO2	L-Tryptophan:oxygen 2,3-oxidoreductase (decyclizing)	M_o2_c + M_trp_L_c	----->	M_Lfmkynr_c
R_PCFLOPm	phosphatidylcholine flippase	M_h2o_c + M_atp_c + M_pchol_hs_m	----->	M_h_c + M_adp_c + M_pi_c + M_pchol_hs_c
R_MTHFD	methylenetetrahydrofolate dehydrogenase (NADP)	M_nadp_c + M_mlthf_c	<---->	M_nadph_c + M_methf_c
R_FAS100COA	fatty acyl-CoA synthase (n-C10:0CoA)	3.0*M_h_c + 2.0*M_nadph_c + M_malcoa_c + M_occoa_c	----->	M_co2_c + 2.0*M_nadp_c + M_h2o_c + M_coa_c + M_dcacoa_c
R_r1135	hydroxysteroid (17-beta) dehydrogenase 7 Biosynthesis of steroids EC:1.1.1.270	M_h_r + M_nadph_r + M_4mzym_int2_r	<---->	M_nadp_r + M_HC02110_r
R_GLUVESSEC	L-glutamate secretion via secretory vesicle (ATP driven)	M_h2o_c + M_atp_c + M_glu_L_c	----->	M_h_c + M_adp_c + M_glu_L_e + M_pi_c
R_r0525	N6-(L-1,3-Dicarboxypropyl)-L-lysine:NAD+ oxidoreductase; N6-(L-1,3-Dicarboxypropyl)-L-lysine:NAD+ oxidoreductase (L-glutamate-forming) Lysine degradation EC:1.5.1.9	M_nad_m + M_h2o_m + M_saccrp_L_m	<---->	M_glu_L_m + M_nadh_m + M_h_m + M_L2aadp6sa_m
R_CLS_hs	cardiolipin synthase (homo sapiens)	M_h_c + M_pglyc_hs_c + M_cdpdag_hs_c	----->	M_cmp_c + M_clpn_hs_c
R_LNSTLSr	lanosterol synthase	M_Ssq23epx_r	----->	M_lanost_r
R_VALt5m	Valine reversible mitochondrial transport	M_val_L_c	<---->	M_val_L_m
R_PEPCK	Phosphoenolpyruvate carboxykinase (GTP)	M_oaa_c + M_gtp_c	----->	M_co2_c + M_pep_c + M_gdp_c
R_COAtm	CoA transporter	M_coa_c	<---->	M_coa_m
R_HMGCOARc	Hydroxymethylglutaryl CoA reductase (ir) in cytosol	2.0*M_h_c + 2.0*M_nadph_c + M_hmgcoa_c	----->	2.0*M_nadp_c + M_coa_c + M_mev_R_c

R_PROtm	L-proline transport, mitochondrial	M_pro_L_c	<---->	M_pro_L_m
R_DCTPtn	dCTP diffusion in nucleus	M_dctp_c	<---->	M_dctp_n
R_3HCO3_NAt	3HCO3_NAt	M_na1_e + 3.0*M_hco3_e	<---->	M_na1_c + 3.0*M_hco3_c
R_ASPCTr	aspartate carbamoyltransferase (reversible)	M_asp_L_c + M_cbp_c	<---->	M_h_c + M_pi_c + M_cbasp_c
R_CHSTEROLtrc	transport of cholesterol into the cytosol	M_chsterol_r	<---->	M_chsterol_c
R_2AMACHYD	2-Aminoacrylate hydrolysis	M_h2o_c + M_2amac_c	----->	M_nh4_c + M_pyr_c
R_CYTK1	cytidylate kinase (CMP)	M_atp_c + M_cmp_c	<---->	M_adp_c + M_cdp_c
R_GLUDym	glutamate dehydrogenase (NADP), mitochondrial	M_glu_L_m + M_h2o_m + M_nadp_m	<---->	M_akg_m + M_nh4_m + M_h_m + M_nadph_m
R_METAT	methionine adenosyltransferase	M_h2o_c + M_atp_c + M_met_L_c	----->	M_pi_c + M_ppi_c + M_amet_c
R_SUCOASm	Succinate--CoA ligase (ADP-forming)	M_coa_m + M_atp_m + M_succ_m	<---->	M_succoa_m + M_pi_m + M_adp_m
R_PFK	phosphofructokinase	M_atp_c + M_f6p_c	----->	M_h_c + M_adp_c + M_fdp_c
R_FKYNH	N-Formyl-L-kynurenine amidohydrolase	M_h2o_c + M_Lfmkynr_c	----->	M_h_c + M_Lkynr_c + M_for_c
R_PPAP	phosphatidic acid phosphatase	M_h2o_c + M_pa_hs_c	----->	M_pi_c + M_dag_hs_c
R_CO2tm	CO2 transport (diffusion), mitochondrial	M_co2_c	<---->	M_co2_m
R_PE_HSter	phosphatidylethanolamine scramblase	M_pe_hs_c	<---->	M_pe_hs_r
R_2OXOADPTm	2-oxoadipate shuttle (cytosol/mitochondria)	M_akg_m + M_2oxoadp_c	<---->	M_akg_c + M_2oxoadp_m
R_HMGCOAtm	Hydroxymethylglutaryl-CoA reversible mitochondrial transport	M_hmgcoa_c	<---->	M_hmgcoa_m

R_GluForTx	Glutamate formimidoyltransferase	M_h_c + M_forglu_c + M_thf_c	----->	M_glu_L_c + M_5forthf_c
R_ENO	enolase	M_2pg_c	<---->	M_h2o_c + M_pep_c
R_PRFGS	phosphoribosylformylglycinamidine synthase	M_h2o_c + M_atp_c + M_gln_L_c + M_fgam_c	----->	M_h_c + M_adp_c + M_glu_L_c + M_pi_c + M_fpram_c
R_r0781	Lanosterol,NADPH:oxygen oxidoreductase (14-methyl cleaving) Biosynthesis of steroids EC:1.14.13.70	2.0*M_h_r + 3.0*M_nadph_r + 3.0*M_o2_r + M_lanost_r	<---->	3.0*M_nadp_r + 4.0*M_h2o_r + M_44mctr_r + M_for_r
R_GHMT2r	glycine hydroxymethyltransferase, reversible	M_thf_c + M_ser_L_c	<---->	M_h2o_c + M_mlthf_c + M_gly_c
R_GUAPRT	guanine phosphoribosyltransferase	M_gua_c + M_prpp_c	----->	M_ppi_c + M_gmp_c
R_biomass_lipid	lipid component of biomass	0.0600927835051546*M_ps_hs_c + 1.59237113402062*M_pchol_hs_c + 0.120185567010309*M_clpn_hs_c + 0.0300412371134021*M_pglyc_hs_c + 0.210319587628866*M_chsterol_c + 0.570865979381443*M_pe_hs_c + 0.180268041237113*M_sphmyln_hs_c + 0.240360824742268*M_pail_hs_c	----->	M_biomass_lipid_c
R_O2ter	O2 transport, endoplasmic reticulum	M_o2_c	<---->	M_o2_r
R_FTCD	formimidoyltransferase cyclodeaminase	2.0*M_h_c + M_5forthf_c	----->	M_nh4_c + M_methf_c
R_MGCHrm	methylglutaconyl-CoA hydratase (reversible), mitochondrial	M_h2o_m + M_3mgcoa_m	<---->	M_hmgcoa_m
R_GARFT	phosphoribosylglycinamide formyltransferase	M_10fthf_c + M_gar_c	<---->	M_h_c + M_thf_c + M_fgam_c
R_RPI	ribose-5-phosphate isomerase	M_r5p_c	<---->	M_ru5p_D_c
R_DSAT	dihydrosphingosine N-acyltransferase	M_Rtotalcoa_c + M_sphgn_c	----->	M_coa_c + 5.0*M_h_c + M_dhcrm_hs_c

R_2OXOADOXm	2-Oxoadipate:lipoamde 2-oxidoreductase(decarboxylating and acceptor-succinylating) (mitochondria)	M_coa_m + M_nad_m + M_2oxoadp_m	----->	M_nadh_m + M_co2_m + M_glutcoa_m
R_ORPT	orotate phosphoribosyltransferase	M_ppi_c + M_orot5p_c	<---->	M_prpp_c + M_orot_c
R_PIter	phosphate transport, endoplasmic reticulum	M_pi_r	<---->	M_pi_c
R_PYK	pyruvate kinase	M_h_c + M_adp_c + M_pep_c	----->	M_atp_c + M_pyr_c
R_TALA	transaldolase	M_g3p_c + M_s7p_c	<---->	M_f6p_c + M_e4p_c
R_ACACT10m	acetyl-CoA C-acetyltransferase, mitochondrial	M_coa_m + M_2maacoa_m	<---->	M_ppcoa_m + M_accoa_m
R_RPE	ribulose 5-phosphate 3-epimerase	M_ru5p_D_c	<---->	M_xu5p_D_c
R_r0295	glycine synthase Nitrogen metabolism EC:2.1.2.10	M_nadh_m + M_co2_m + M_nh4_m + M_mlthf_m	----->	M_nad_m + M_gly_m + M_thf_m
R_HISD	histidase	M_his_L_c	----->	M_nh4_c + M_urcan_c
R_r0165	UTP:pyruvate O2-phosphotransferase EC:2.7.1.40	M_h_c + M_pep_c + M_udp_c	----->	M_pyr_c + M_utp_c
R_FDH	formate dehydrogenase	M_nad_c + M_for_c	----->	M_co2_c + M_nadh_c
R_ADK1	adenylate kinase	M_atp_c + M_amp_c	<---->	2.0*M_adp_c
R_LEUTAm	leucine transaminase, mitochondrial	M_akg_m + M_leu_L_m	<---->	M_glu_L_m + M_4mop_m
R_ADNK1	adenosine kinase	M_atp_c + M_adn_c	----->	M_h_c + M_adp_c + M_amp_c
R_PGPP_hs	Phosphatidylglycerol phosphate phosphatase (homo sapiens)	M_h2o_c + M_pgp_hs_c	----->	3.0*M_h_c + M_pi_c + M_pglyc_hs_c
R_PCm	pyruvate carboxylase	M_hco3_m + M_atp_m + M_pyr_m	----->	M_h_m + M_pi_m + M_adp_m + M_oaa_m

R_ILEtec	L-isoleucine transport via diffusion (extracellular to cytosol)	M_ile_L_e	<---->	M_ile_L_c
R_r1418	Carbonic acid hydro-lyase Nitrogen metabolism EC:4.2.1.1	M_h_e + M_hco3_e	<---->	M_co2_e + M_h2o_e
R_DPMVDc	diphosphomevalonate decarboxylase, cytosol	M_atp_c + M_5dpmev_c	----->	M_co2_c + M_adp_c + M_pi_c + M_ipdp_c
R_C14STRr	C-14 sterol reductase	M_h_r + M_nadph_r + M_44mctr_r	----->	M_nadp_r + M_44mzym_r
R_LYStiDF	L-lysine transport via diffusion (extracellular to cytosol)	M_lys_L_e	----->	M_lys_L_c
R_H2Oter	H2O endoplasmic reticulum transport	M_h2o_c	<---->	M_h2o_r
R_MMSAD1m	methylmalonate-semialdehyde dehydrogenase	M_coa_m + M_nad_m + M_2mop_m	----->	M_nadh_m + M_co2_m + M_ppcoa_m
R_UREAt5	urea, water cotransport	M_h2o_e + M_urea_e	<---->	M_h2o_c + M_urea_c
R_P5CDm	1-pyrroline-5-carboxylate dehydrogenase, mitochondrial	M_nad_m + 2.0*M_h2o_m + M_1pyr5c_m	----->	M_glu_L_m + M_nadh_m + M_h_m
R_DAGK_hs	Diacylglycerol phosphate kinase (homo sapiens)	M_atp_c + M_dag_hs_c	<---->	M_h_c + M_adp_c + M_pa_hs_c
R_H2Ot	H2O transport via diffusion	M_h2o_e	<---->	M_h2o_c
R_ECOAH9m	2-Methylprop-2-enoyl-CoA (2-Methylbut-2-enoyl-CoA), mitochondrial	M_h2o_m + M_2mb2coa_m	<---->	M_3hmbcoa_m
R_H2Otm	H2O transport, mitochondrial	M_h2o_c	<---->	M_h2o_m
R_PPCOACm	Propionyl-CoA carboxylase, mitochondrial	M_hco3_m + M_atp_m + M_ppcoa_m	----->	M_h_m + M_pi_m + M_adp_m + M_mmcoa_S_m

R_CSm	citrate synthase	M_h2o_m + M_accoa_m + M_oaa_m	----->	M_coa_m + M_h_m + M_cit_m
R_CTPS2	CTP synthase (glutamine)	M_h2o_c + M_atp_c + M_gln_L_c + M_utp_c	----->	2.0*M_h_c + M_adp_c + M_glu_L_c + M_pi_c + M_ctp_c
R_MCCCrm	methylcrotonoyl-CoA carboxylase, mitochondrial	M_hco3_m + M_atp_m + M_3mb2coa_m	<---->	M_h_m + M_pi_m + M_adp_m + M_3mgcoa_m
R_GLUPRT	glutamine phosphoribosyldiphosphate amidotransferase	M_h2o_c + M_gln_L_c + M_prpp_c	----->	M_glu_L_c + M_ppi_c + M_pram_c
R_G5SADrm	L-glutamate 5-semialdehyde dehydratase, reversible, mitochondrial	M_glu5sa_m	----->	M_h_m + M_h2o_m + M_1pyr5c_m
R_FAS160COA	fatty-acyl-CoA synthase (n-C16:0CoA)	3.0*M_h_c + 2.0*M_nadph_c + M_malcoa_c + M_tdcoa_c	----->	M_co2_c + 2.0*M_nadp_c + M_h2o_c + M_coa_c + M_pmtcoa_c
R_AMETtd	diffusion of S-Adenosyl-L-methionine	M_amet_c	<---->	M_amet_m
R_RE3301C	RE3301	M_h2o_c + M_ps_hs_c	<---->	M_h_c + M_pa_hs_c + M_ser_L_c
R_GAPD	glyceraldehyde-3-phosphate dehydrogenase	M_nad_c + M_pi_c + M_g3p_c	<---->	M_h_c + M_nadh_c + M_13dpg_c
R_G6PDH2r	glucose 6-phosphate dehydrogenase	M_nadp_c + M_g6p_c	<---->	M_h_c + M_nadph_c + M_6pgl_c
R_ADSL2	adenylosuccinate lyase	M_25aics_c	----->	M_aicar_c + M_fum_c
R_O2t	o2 transport (diffusion)	M_o2_e	<---->	M_o2_c
R_ADSL1	adenylosuccinate lyase	M_dcamp_c	----->	M_amp_c + M_fum_c
R_biomass_DNA	DNA component of biomass	0.707*M_dgtp_n + 0.674428571428572*M_dctp_n + 0.935071428571429*M_dttp_n + 0.941642857142857*M_datp_n	----->	M_biomass_DNA_c
R_FBA	fructose-bisphosphate aldolase	M_fdp_c	<---->	M_g3p_c + M_dhap_c

R_DMATT	dimethylallyltranstransferase	M_ipdp_c + M_dmpp_c	----->	M_ppi_c + M_grdp_c
R_NDPK8	Nucleoside-diphosphate kinase (ATP:dADP)	M_atp_c + M_dadp_c	<---->	M_adp_c + M_datp_c
R_NDPK7	nucleoside-diphosphate kinase (ATP:dCDP)	M_atp_c + M_dcdp_c	<---->	M_adp_c + M_dctp_c
R_NDPK5	Nucleoside-diphosphate kinase (ATP:dGDP)	M_atp_c + M_dgdp_c	<---->	M_adp_c + M_dgtp_c
R_NDPK4	nucleoside-diphosphate kinase (ATP:dTDP)	M_dtdp_c + M_atp_c	<---->	M_adp_c + M_dttp_c
R_NDPK3	nucleoside-diphosphate kinase (ATP:CDP)	M_atp_c + M_cdp_c	<---->	M_adp_c + M_ctp_c
R_NDPK1	nucleoside-diphosphate kinase (ATP:GDP)	M_atp_c + M_gdp_c	<---->	M_adp_c + M_gtp_c
R_LEUtec	L-leucine transport via diffusion (extracellular to cytosol)	M_leu_L_e	<---->	M_leu_L_c
R_PDHm	pyruvate dehydrogenase	M_coa_m + M_nad_m + M_pyr_m	----->	M_nadh_m + M_co2_m + M_accoa_m
R_P5CRm	pyrroline-5-carboxylate reductase (m)	2.0*M_h_m + M_nadph_m + M_1pyr5c_m	----->	M_pro_L_m + M_nadp_m
R_IPDDI	isopentenyl-diphosphate D-isomerase	M_ipdp_c	<---->	M_dmpp_c
R_DATPtn	dATP diffusion in nucleus	M_datp_c	<---->	M_datp_n
R_AGPAT1	1-acylglycerol-3-phosphate O-acyltransferase 1	M_Rtotalcoa_c + M_alpa_hs_c	----->	M_coa_c + 6.0*M_h_c + M_pa_hs_c
R_PSDm_hs	Phosphatidylserine decarboxylase	M_h_m + M_ps_hs_m	----->	M_co2_m + M_pe_hs_m
R_THFtm	5,6,7,8-Tetrahydrofolate transport, diffusion, mitochondrial	M_thf_c	<---->	M_thf_m
R_TKT1	transketolase	M_r5p_c + M_xu5p_D_c	<---->	M_g3p_c + M_s7p_c
R_TKT2	transketolase	M_e4p_c + M_xu5p_D_c	<---->	M_f6p_c + M_g3p_c

R_r0450	L-2-Aminoadipate:2-oxoglutarate aminotransferase Lysine biosynthesis / Lysine degradation EC:2.6.1.39	M_akg_m + M_L2aadp_m	<---->	M_glu_L_m + M_2oxoadp_m
R_GLNS	glutamine synthetase	M_nh4_c + M_atp_c + M_glu_L_c	----->	M_h_c + M_adp_c + M_pi_c + M_gln_L_c
R_GLYtm	glycine passive transport to mitochondria	M_gly_c	<---->	M_gly_m
R_SERPT	serine C-palmitoyltransferase	M_h_c + M_pmtcoa_c + M_ser_L_c	----->	M_co2_c + M_coa_c + M_3dsphgn_c
R_HIBDm	3-hydroxyisobutyrate dehydrogenase, mitochondrial	M_nad_m + M_3hmp_m	<---->	M_nadh_m + M_h_m + M_2mop_m
R_r0645	2-Aminomuconate semialdehyde:NAD+ 6-oxidoreductase Tryptophan metabolism EC:1.2.1.32	M_h2o_c + M_nad_c + M_am6sa_c	<---->	2.0*M_h_c + M_nadh_c + M_amuco_c
R_CBPS	carbamoyl-phosphate synthase (glutamine-hydrolysing)	M_h2o_c + 2.0*M_atp_c + M_hco3_c + M_gln_L_c	----->	2.0*M_h_c + 2.0*M_adp_c + M_glu_L_c + M_pi_c + M_cbp_c
R_MMEm	methylmalonyl-CoA epimerase/racemase	M_mmcoa_R_m	<---->	M_mmcoa_S_m
R_r1400	Active transport	M_crn_m + M_ppcoa_c	----->	M_ppcoa_m + M_crn_c
R_GPAM_hs	glycerol-3-phosphate acyltransferase	M_Rtotalcoa_c + M_glyc3p_c	----->	M_coa_c + 2.0*M_h_c + M_alpa_hs_c
R_r1401	Facilitated diffusion	M_crn_c + M_btcoa_m	----->	M_crn_m + M_btcoa_c
R_biomass_protein	protein component of biomass	29.2504249291785*M_h2o_c + 0.499447592067989*M_asp_L_c + 0.395779036827196*M_asn_L_c + 0.367521246458923*M_phe_L_c + 29.2504249291785*M_atp_c + 0.226161473087819*M_tyr_L_c + 0.546558073654391*M_glu_L_c + 0.716189801699717*M_ala_L_c + 0.0188470254957507*M_trp_L_c + 0.499447592067989*M_val_L_c +	----->	M_biomass_protein_c + 29.2504249291785*M_h_c + 29.2504249291785*M_adp_c +

		0.584249291784703*M_pro_L_c + 0.216742209631728*M_met_L_c + 0.461756373937677*M_gln_L_c + 0.763300283286119*M_gly_c + 0.555991501416431*M_ser_L_c + 0.179050991501416*M_his_L_c + 0.405212464589235*M_ile_L_c + 0.838682719546742*M_lys_L_c + 0.77271954674221*M_leu_L_c + 0.508866855524079*M_arg_L_c + 0.0659645892351275*M_cys_L_c + 0.442903682719547*M_thr_L_c		29.2504249291785*M_pi_c
R_LDH_L	L-lactate dehydrogenase	M_nad_c + M_lac_L_c	<---->	M_h_c + M_nadh_c + M_pyr_c
R_CYOR_u10m	ubiquinol-6 cytochrome c reductase, Complex III	2.0*M_h_m + 2.0*M_ficytC_m + M_q10h2_m	----->	M_q10_m + 2.0*M_focytC_m + 4.0*M_h_i
R_CDS	phosphatidate cytidylyltransferase	M_h_c + M_pa_hs_c + M_ctp_c	----->	M_cdpdag_hs_c + M_ppi_c
R_ASPte	diffusion of aspartate into blood	M_asp_L_c	----->	M_asp_L_e
R_MDHm	malate dehydrogenase, mitochondrial	M_nad_m + M_mal_L_m	<---->	M_nadh_m + M_h_m + M_oaa_m
R_ATPtm	ADP/ATP transporter, mitochondrial	M_adp_c + M_atp_m	----->	M_atp_c + M_adp_m
R_FBP	fructose-bisphosphatase	M_h2o_c + M_fdp_c	----->	M_pi_c + M_f6p_c
R_PETOHMr_hs	phosphatidylethanolamine N-methyltransferase	3.0*M_amet_r + M_pe_hs_r	----->	3.0*M_h_r + 3.0*M_ahcys_r + M_pchol_hs_r
R_PUNP3	purine-nucleoside phosphorylase (Guanosine)	M_pi_c + M_gsn_c	<---->	M_gua_c + M_r1p_c
R_PPAer	inorganic diphosphatase, endoplasmic reticulum	M_h2o_r + M_ppi_r	----->	M_h_r + 2.0*M_pi_r
R_L_LACtm	L-lactate transport, mitochondrial	M_h_c + M_lac_L_c	<---->	M_h_m + M_lac_L_m
R_SERHL	L-Serine hydro-lyase	M_ser_L_c	----->	M_h2o_c + M_2amac_c
R_ASPGLUm	aspartate-glutamate mitochondrial shuttle	M_glu_L_c + M_h_i + M_asp_L_m	----->	M_asp_L_c + M_glu_L_m + M_h_m
R_RE2954C	RE2954	M_h_c + M_dtdp_c + M_pep_c	<---->	M_pyr_c + M_dttp_c

R_r0074	L-Glutamate 5-semialdehyde:NAD+ oxidoreductase Arginine and proline metabolism EC:1.5.1.12	M_glu5sa_m + M_nad_m + M_h2o_m	<---->	M_glu_L_m + M_nadh_m + 2.0*M_h_m
R_3HAO	3-hydroxyanthranilate 3,4-dioxygenase	M_o2_c + M_3hanthrn_c	----->	M_h_c + M_cmusa_c
R_METS	methionine synthase	M_5mthf_c + M_hcys_L_c	----->	M_h_c + M_met_L_c + M_thf_c
R_NH4t3r	ammonia transport via proton antiport	M_nh4_c + M_h_e	<---->	M_h_c + M_nh4_e
R_UMPK	UMP kinase	M_atp_c + M_ump_c	<---->	M_adp_c + M_udp_c
R_PYRt2m	pyruvate mitochondrial transport via proton symport	M_h_c + M_pyr_c	----->	M_h_m + M_pyr_m
R_TPI	triose-phosphate isomerase	M_dhap_c	<---->	M_g3p_c
R_AICART	phosphoribosylaminoimidazolecarboxamide formyltransferase	M_10fthf_c + M_aicar_c	<---->	M_fprica_c + M_thf_c
R_RNDR4	ribonucleoside-diphosphate reductase (UDP)	M_trdrd_c + M_udp_c	----->	M_h2o_c + M_trdox_c + M_dudp_c
R_RNDR3	ribonucleoside-diphosphate reductase (CDP)	M_trdrd_c + M_cdp_c	----->	M_h2o_c + M_trdox_c + M_dcdp_c
R_OBDHc	2-Oxobutanoate dehydrogenase, cytosolic	M_coa_c + M_nad_c + M_2obut_c	----->	M_co2_c + M_nadh_c + M_ppcoa_c
R_C3STDH1Pr	C-3 sterol dehydrogenase (4-methylzymosterol)	M_nadp_r + M_4mzym_int1_r	----->	M_h_r + M_nadph_r + M_4mzym_int2_r + M_co2_r
R_RNDR2	ribonucleoside-diphosphate reductase (GDP)	M_trdrd_c + M_gdp_c	----->	M_h2o_c + M_trdox_c + M_dgdp_c
R_RNDR1	ribonucleoside-diphosphate reductase (ADP)	M_adp_c + M_trdrd_c	----->	M_h2o_c + M_trdox_c + M_dadp_c

R_ARGtiDF	L-arginine transport via diffusion (extracellular to cytosol)	M_arg_L_e	----->	M_arg_L_c
R_C4CRNCPT2	transport of butyryl carnitine in the mitochondrial matrix for final hydrolysis	M_coa_m + M_c4crn_m	<---->	M_crn_m + M_btcoa_m
R_PROPAT4te	transport of proline via PAT4	M_pro_L_e	<---->	M_pro_L_c
R_biomass_RNA	RNA component of biomass	0.925862068965503*M_atp_c + 0.622706896551724*M_gtp_c + 0.92148275862069*M_utp_c + 0.673034482758621*M_ctp_c	----->	M_biomass_RNA_c
R_TMDS	thymidylate synthase	M_mlthf_c + M_dump_c	----->	M_dtmp_c + M_dhf_c
R_biomass_carbohydrate	carbohydrate component of biomass	3.87591549295775*M_g6p_c	----->	M_biomass_carbohydrate_c
R_ACITL	ATP-Citrate lyase	M_coa_c + M_atp_c + M_cit_c	----->	M_adp_c + M_accoa_c + M_oaa_c + M_pi_c
R_OMPDC	orotidine-5-phosphate decarboxylase	M_h_c + M_orot5p_c	----->	M_co2_c + M_ump_c
R_NADH2_u10m	NADH dehydrogenase, mitochondrial	M_nadh_m + 5.0*M_h_m + M_q10_m	----->	M_nad_m + 4.0*M_h_i + M_q10h2_m
R_ILETAm	isoleucine transaminase, mitochondrial	M_akg_m + M_ile_L_m	<---->	M_glu_L_m + M_3mop_m
R_NADPHtru	NADPH transporter, endoplasmic reticulum	M_nadph_c	----->	M_nadph_r
R_METtec	L-methionine transport via diffusion (extracellular to cytosol)	M_met_L_e	<---->	M_met_L_c
R_AKGMALtm	alpha-ketoglutarate/malate transporter	M_akg_m + M_mal_L_c	<---->	M_akg_c + M_mal_L_m
R_Htr	H transporter, endoplasmic reticulum	M_h_c	<---->	M_h_r
R_AHCYStd	diffusion of S-Adenosyl-L-homocysteine	M_ahcys_m	<---->	M_ahcys_c
R_FORtr	FOR transporter, endoplasmic reticulum	M_for_c	<---->	M_for_r

R_PPA	inorganic diphosphatase	M_h2o_c + M_ppi_c	----->	M_h_c + 2.0*M_pi_c
R_ETF	electron transfer flavoprotein	M_etfox_m + M_fadh2_m	----->	M_etfrd_m + M_fad_m
R_GLUNm	glutaminase (mitochondrial)	M_h2o_m + M_gln_L_m	----->	M_glu_L_m + M_nh4_m
R_CITRtm	citrulline mitochondrial transport via proton antiport	M_citr_L_m	<---->	M_citr_L_c
R_DM_atp_c_	DM atp(c)	M_h2o_c + M_atp_c	----->	M_h_c + M_adp_c + M_pi_c
R_GRTT	geranyltranstransferase	M_ipdp_c + M_grdp_c	----->	M_ppi_c + M_frdp_c
R_SACCD3m	saccharopine dehydrogenase (NADP, L-lysine forming), mitochondrial	M_akg_m + M_h_m + M_nadph_m + M_lys_L_m	----->	M_h2o_m + M_saccrp_L_m + M_nadp_m
R_DHCR71r	7-dehydrocholesterol reductase	M_ddsmsterol_r + M_h_r + M_nadph_r	----->	M_nadp_r + M_dsmsterol_r
R_ETFQO	Electron transfer flavoprotein-ubiquinone oxidoreductase	M_q10_m + M_etfrd_m	----->	M_q10h2_m + M_etfox_m
R_PRPPS	phosphoribosylpyrophosphate synthetase	M_atp_c + M_r5p_c	----->	M_h_c + M_prpp_c + M_amp_c
R_MTHFCm	methenyltetrahydrifikate cyclohydrolase, mitochondrial	M_h2o_m + M_methf_m	<---->	M_h_m + M_10fthf_m
R_ATPS4m	ATP synthase (four protons for one ATP)	M_pi_m + M_adp_m + 4.0*M_h_i	----->	3.0*M_h_m + M_h2o_m + M_atp_m
R_GLUTCOADHm	glutaryl-CoA dehydrogenase (mitochondria)	M_h_m + M_glutcoa_m + M_fad_m	----->	M_co2_m + M_fadh2_m + M_b2coa_m
R_LYStm	Lysine mitochondrial transport via ornithine carrier	M_h_m + M_lys_L_c	<---->	M_h_c + M_lys_L_m
R_r0193	L-Cysteine L-homocysteine-lyase (deaminating) Cysteine metabolism EC:4.4.1.1	M_h2o_c + M_cys_L_c	<---->	M_h_c + M_nh4_c + M_pyr_c + M_HC00250_c

R_CYSTGL	cystathionine g-lyase	M_h2o_c + M_cyst_L_c	----->	M_nh4_c + M_cys_L_c + M_2obut_c
R_AHC	adenosylhomocysteinase	M_h2o_c + M_ahcys_c	<---->	M_adn_c + M_hcys_L_c
R_3HBCOAHLm	3-hydroxyisobutyryl-CoA hydrolase, mitochondrial	M_h2o_m + M_3hibutcoa_m	----->	M_coa_m + M_h_m + M_3hmp_m
R_PCHOL_HSter	phosphatidylcholine scramblase	M_pchol_hs_c	<---->	M_pchol_hs_r
R_LEUt5m	leucine mitochondrial transport	M_leu_L_c	<---->	M_leu_L_m
R_PETOHMm_hs	phosphatidylethanolamine N-methyltransferase	3.0*M_amet_m + M_pe_hs_m	----->	3.0*M_h_m + M_pchol_hs_m + 3.0*M_ahcys_m
R_r0838	Free diffusion	M_nh4_c	<---->	M_nh4_m
R_ME2	malic enzyme (NADP)	M_nadp_c + M_mal_L_c	----->	M_co2_c + M_nadph_c + M_pyr_c
R_r0940	Free diffusion	M_HC00250_c	<---->	M_HC00250_e
R_r0941	Free diffusion	M_hco3_c	<---->	M_hco3_m
R_MDH	malate dehydrogenase	M_nad_c + M_mal_L_c	<---->	M_h_c + M_nadh_c + M_oaa_c
R_ICDHxm	Isocitrate dehydrogenase (NAD+)	M_nad_m + M_icit_m	----->	M_akg_m + M_nadh_m + M_co2_m
R_r0947	Mitochondrial Carrier (MC) TCDB:2.A.29.19.1	M_orn_m + M_citr_L_c	<---->	M_orn_c + M_citr_L_m
R_PE_HStm	phosphatidylethanolamine scramblase	M_pe_hs_c	<---->	M_pe_hs_m
R_CYStec	L-cysteine transport via diffusion (extracellular to cytosol)	M_cys_L_e	<---->	M_cys_L_c
R_ADSS	adenylosuccinate synthase	M_imp_c + M_asp_L_c + M_gtp_c	----->	2.0*M_h_c + M_pi_c + M_gdp_c + M_dcamp_c
R_TRPt	L-tryptophan transport	M_trp_L_e	<---->	M_trp_L_c
R_ASPTAm	aspartate transaminase	M_akg_m + M_asp_L_m	<---->	M_glu_L_m + M_oaa_m

R_DTTPtn	dTTP diffusion in nucleus	M_dttp_c	<---->	M_dttp_n
R_ACACT1r	acetyl-CoA C-acetyltransferase	2.0*M_accoa_c	<---->	M_coa_c + M_aacoa_c
R_NDP8	nucleoside-diphosphatase (dUDP)	M_h2o_c + M_dudp_c	----->	M_h_c + M_pi_c + M_dump_c
R_PPM	phosphopentomutase	M_r1p_c	<---->	M_r5p_c
R_SUCD1m	succinate dehydrogenase	M_succ_m + M_fad_m	<---->	M_fadh2_m + M_fum_m
R_EX_GLTX_hydrolysis	Glutamax hydrolysis	M_GLTX_e	----->	M_gln_L_e + M_ala_L_e
R_ACONTm	Aconitate hydratase	M_cit_m	<---->	M_icit_m
R_GLCt4	glucose transport via sodium symport	M_na1_e + M_glc_D_e	<---->	M_na1_c + M_glc_D_c
R_3DSPHR	3-Dehydrosphinganine reductase	M_h_c + M_nadph_c + M_3dsphgn_c	----->	M_nadp_c + M_sphgn_c
R_r2534	Major Facilitator(MFS) TCDB:2.A.1.44.1	M_thr_L_e	<---->	M_thr_L_c
R_ILEt5m	Isoleucine mitochondrial transport	M_ile_L_c	<---->	M_ile_L_m
R_HEX1	hexokinase (D-glucose:ATP)	M_atp_c + M_glc_D_c	----->	M_h_c + M_adp_c + M_g6p_c
R_r2438	Mitochondrial Carrier (MC) TCDB:2.A.29.8.3	M_crn_m + M_c4crn_c	----->	M_crn_c + M_c4crn_m
R_CYSTS	cystathionine beta-synthase	M_ser_L_c + M_hcys_L_c	----->	M_h2o_c + M_cyst_L_c
R_r2532	Major Facilitator(MFS) TCDB:2.A.1.44.1	M_asn_L_e	<---->	M_asn_L_c
R_PCLAD	picolinic acid decarboxylase	M_h_c + M_cmusa_c	----->	M_co2_c + M_am6sa_c
R_NADPtru	NADP transporter, endoplasmic reticulum	M_nadp_r	----->	M_nadp_c
R_r1554	Amino Acid-Polyamine-Organocation (APC) TCDB:2.A.3.8.1	M_val_L_c + M_gly_e	<---->	M_gly_c + M_val_L_e

R_MTHFR3	5,10-methylenetetrahydrofolatereductase (NADPH)	2.0*M_h_c + M_nadph_c + M_mlthf_c	----->	M_nadp_c + M_5mthf_c
R_DHFR	dihydrofolate reductase	M_h_c + M_nadph_c + M_dhf_c	<---->	M_nadp_c + M_thf_c
R_ACOAD10m	acyl-CoA dehydrogenase (2-methylbutanoyl-CoA), mitochondrial	M_2mbcoa_m + M_fad_m	----->	M_2mb2coa_m + M_fadh2_m
R_r2136	Major Facilitator(MFS) TCDB:2.A.1.14.6	M_na1_e + M_pi_e	----->	M_na1_c + M_pi_c
R_CDIPTr	phosphatidylinositol synthase (Homo sapiens)	M_cdpdag_hs_c + M_inost_c	<---->	M_h_c + M_cmp_c + M_pail_hs_c
R_MTHFD2m	methylenetetrahydrofolate dehydrogenase (NAD), mitochondrial	M_nad_m + M_mlthf_m	<---->	M_nadh_m + M_methf_m
R_r2525	Major Facilitator(MFS) TCDB:2.A.1.44.1	M_gln_L_e	<---->	M_gln_L_c
R_VALtec	L-valine transport via diffusion (extracellular to cytosol)	M_val_L_e	<---->	M_val_L_c
R_r2526	Major Facilitator(MFS) TCDB:2.A.1.44.1	M_ser_L_e	<---->	M_ser_L_c
R_AASAD3m	L-aminoadipate-semialdehyde dehydrogenase (NADH), mitochondrial	M_nad_m + M_h2o_m + M_L2aadp6sa_m	----->	M_nadh_m + 2.0*M_h_m + M_L2aadp_m
R_SQLSr	Squalene synthase	M_h_r + M_nadph_r + 2.0*M_frdp_r	----->	M_nadp_r + 2.0*M_ppi_r + M_sql_r
R_ALATA_L	L-alanine transaminase	M_akg_c + M_ala_L_c	<---->	M_glu_L_c + M_pyr_c
R_CITtam	citrate transport, mitochondrial	M_mal_L_m + M_cit_c	<---->	M_cit_m + M_mal_L_c
R_HACD1m	3-hydroxyacyl-CoA dehydrogenase (acetoacetyl-CoA) (mitochondria)	M_nadh_m + M_h_m + M_aacoa_m	<---->	M_nad_m + M_3hbcoa_m

R_ARGN	arginase	M_h2o_c + M_arg_L_c	----->	M_orn_c + M_urea_c
R_10FTHFtm	10-Formyltetrahydrofolate mitochondrial transport via diffusion	M_10fthf_c	<---->	M_10fthf_m
R_r1566	Amino Acid-Polyamine-Organocation (APC) TCDB:2.A.3.8.1	M_pro_L_c + M_ala_L_e	<---->	M_ala_L_c + M_pro_L_e
R_C4STMO1r	C-4 sterol methyl oxidase (4,4-dimethylzymosterol)	3.0*M_h_r + 3.0*M_nadph_r + 3.0*M_o2_r + M_44mzym_r	----->	3.0*M_nadp_r + 4.0*M_h2o_r + M_4mzym_int1_r
R_G3PD1	glycerol-3-phosphate dehydrogenase (NAD)	M_nad_c + M_glyc3p_c	<---->	M_h_c + M_nadh_c + M_dhap_c
R_ACCOAC	acetyl-CoA carboxylase	M_atp_c + M_hco3_c + M_accoa_c	----->	M_h_c + M_malcoa_c + M_adp_c + M_pi_c
R_ECOAH12m	3-hydroxyacyl-CoA dehydratase (3-hydroxyisobutyryl-CoA) (mitochondria)	M_h2o_m + M_2mp2coa_m	<---->	M_3hibutcoa_m
R_CO2t	CO2 transporter via diffusion	M_co2_e	<---->	M_co2_c
R_AMCOXO	2-aminomuconate reductase	M_h2o_c + M_h_c + M_nadph_c + M_amuco_c	----->	M_nadp_c + M_nh4_c + M_2oxoadp_c
R_KHte	KHte	M_h_c + M_k_e	<---->	M_h_e + M_k_c
R_PGPPT	phosphatidyl-CMP: glycerophosphate phosphatidyltransferase	2.0*M_h_c + M_cdpdag_hs_c + M_glyc3p_c	----->	M_cmp_c + M_pgp_hs_c
R_PRAGSr	phosphoribosylglycinamide synthase	M_atp_c + M_gly_c + M_pram_c	<---->	M_h_c + M_adp_c + M_pi_c + M_gar_c
R_IZPN	Imidazolonepropionase	M_h2o_c + M_4izp_c	----->	M_h_c + M_forglu_c
R_DHORD9	dihydoorotic acid dehydrogenase (quinone10)	M_q10_m + M_dhor_S_c	----->	M_orot_c + M_q10h2_m
R_ACOAD8m	acyl-CoA dehydrogenase (isovaleryl-CoA), mitochondrial	M_fad_m + M_ivcoa_m	----->	M_3mb2coa_m + M_fadh2_m

R_ME2m	malic enzyme (NADP), mitochondrial	M_nadp_m + M_mal_L_m	----->	M_co2_m + M_nadph_m + M_pyr_m
R_SQLEr	Squalene epoxidase, endoplasmic reticular (NADP)	M_h_r + M_nadph_r + M_o2_r + M_sql_r	----->	M_nadp_r + M_h2o_r + M_Ssq23epx_r
R_r0911	Facilitated diffusion	M_glu_L_m + M_pro_L_c	<---->	M_glu_L_c + M_pro_L_m
R_ECOAH1m	3-hydroxyacyl-CoA dehydratase (3-hydroxybutanoyl-CoA) (mitochondria)	M_3hbcoa_m	<---->	M_h2o_m + M_b2coa_m
R_AIRCr_PRASCS	phosphoribosylaminoimidazole carboxylase / phosphoribosylaminoimidazolesuccinocarboxamide synthase	M_co2_c + M_asp_L_c + M_atp_c + M_air_c	<---->	2.0*M_h_c + M_adp_c + M_pi_c + M_25aics_c
R_MEVK1c	mevalonate kinase (atp) cytosol	M_atp_c + M_mev_R_c	----->	M_h_c + M_adp_c + M_5pmev_c
R_r2419	Mitochondrial Carrier (MC) TCDB:2.A.29.2.7	M_akg_c + M_pi_m	----->	M_akg_m + M_pi_c
R_ACACT1rm	acetyl-CoA C-acetyltransferase, mitochondrial	2.0*M_accoa_m	----->	M_coa_m + M_aacoa_m
R_EBP1r	3-beta-hydroxysteroid-delta(8),delta(7)-isomerase	M_zymst_r	----->	M_chlstol_r
R_LDH_Lm	L-lactate dehydrogenase	M_nad_m + M_lac_L_m	<---->	M_nadh_m + M_h_m + M_pyr_m
R_SMS	Sphingomyelin synthase (homo sapiens)	M_h_c + M_pchol_hs_c + M_crm_hs_c	----->	M_dag_hs_c + M_sphmyln_hs_c
R_FRDPtcr	transport of Farnesyl diphosphate into the endoplasmic reticulum	M_frdp_c	<---->	M_frdp_r
R_URCN	URCN	M_h2o_c + M_urcan_c	----->	M_4izp_c
R_C40CPT1	production of butyrylcarnitine	M_crn_c + M_btcoa_c	<---->	M_coa_c + M_c4crn_c

R_PIt2m	phosphate transporter, mitochondrial	M_h_c + M_pi_c	----->	M_h_m + M_pi_m
R_OIVD1m	2-oxoisovalerate dehydrogenase (acylating; 4-methyl-2-oxopentaoate), mitochondrial	M_coa_m + M_nad_m + M_4mop_m	----->	M_nadh_m + M_co2_m + M_ivcoa_m
R_GK1	guanylate kinase (GMP:ATP)	M_atp_c + M_gmp_c	<---->	M_adp_c + M_gdp_c
R_PROt2r	L-proline reversible transport via proton symport	M_h_e + M_pro_L_e	<---->	M_h_c + M_pro_L_c
R_CO2ter	CO2 endoplasmic reticular transport via diffusion	M_co2_c	<---->	M_co2_r
R_HMGCOASim	Hydroxymethylglutaryl CoA synthase (ir)	M_h2o_m + M_accoa_m + M_aacoa_m	----->	M_coa_m + M_h_m + M_hmgcoa_m
R_r1384	Guanosine aminohydrolase EC:3.5.4.15	M_h2o_c + M_h_c + M_gsn_c	<---->	M_nh4_c + M_xtsn_c
R_ME1m	malic enzyme (NAD), mitochondrial	M_nad_m + M_mal_L_m	----->	M_nadh_m + M_co2_m + M_pyr_m
R_MMMm	methylmalonyl-CoA mutase	M_mmcoa_R_m	<---->	M_succoa_m
R_ACOAD9m	acyl-CoA dehydrogenase (isobutyryl-CoA), mitochondrial	M_ibcoa_m + M_fad_m	----->	M_fadh2_m + M_2mp2coa_m
R_GLNtm	L-glutamine transport via electroneutral transporter	M_gln_L_c	----->	M_gln_L_m
R_NTD10	5-nucleotidase (XMP)	M_h2o_c + M_xmp_c	----->	M_pi_c + M_xtsn_c
R_DHCRD1	dihydroceramide desaturase	M_nadp_c + M_dhcrm_hs_c	----->	M_h_c + M_nadph_c + M_crm_hs_c
R_MI1PP	myo-inositol 1-phosphatase	M_h2o_c + M_mi1p_D_c	----->	M_pi_c + M_inost_c
R_FUMtm	fumarate transport, mitochondrial	M_pi_m + M_fum_c	<---->	M_pi_c + M_fum_m
R_MI1PS	myo-Inositol-1-phosphate synthase	M_g6p_c	----->	M_mi1p_D_c

R_HIStiDF	L-histidine transport via diffusion (extracellular to cytosol)	M_his_L_e	----->	M_his_L_c
R_DHORTS	dihydroorotase	M_h2o_c + M_dhor_S_c	<---->	M_h_c + M_cbasp_c
R_FUMm	fumarase, mitochondrial	M_h2o_m + M_fum_m	<---->	M_mal_L_m
R_CYOOm3	cytochrome c oxidase, mitochondrial Complex IV	M_o2_m + 8.0*M_h_m + 4.0*M_focytC_m	----->	2.0*M_h2o_m + 4.0*M_h_i + 4.0*M_ficytC_m
R_FAS80COA_L	fatty acyl-CoA synthase (n-C8:0CoA), lumped reaction	9.0*M_h_c + 6.0*M_nadph_c + 3.0*M_malcoa_c + M_accoa_c	----->	3.0*M_co2_c + 6.0*M_nadp_c + 3.0*M_h2o_c + 3.0*M_coa_c + M_occoa_c
R_EX_leu_L_LPAREN_e_RPAREN_	L-Leucine exchange	M_leu_L_e	<---->	
R_EX_h_LPAREN_e_RPAREN_	exchange reaction for proton	M_h_e	<---->	
R_biomass_other	other component of biomass	M_biomass_other_c	<-----	
R_EX_lac_L_LPAREN_e_RPAREN_	L-Lactate exchange	M_lac_L_e	<---->	
R_EX_pro_L_LPAREN_e_RPAREN_	L-Proline exchange	M_pro_L_e	<---->	
R_EX_nh4_LPAREN_e_RPAREN_	Ammonia exchange	M_nh4_e	<---->	
R_EX_ile_L_LPAREN_e_RPAREN_	L-Isoleucine exchange	M_ile_L_e	<---->	
R_EX_lys_L_LPAREN_e_RPAREN_	L-Lysine exchange	M_lys_L_e	<---->	
R_EX_thr_L_LPAREN_e_RPAREN_	L-Threonine exchange	M_thr_L_e	<---->	
R_EX_trp_L_LPAREN_e_RPAREN_	L-Tryptophan exchange	M_trp_L_e	<---->	

R_EX_cys_L_LPAREN_e_RPAREN_	exchange reaction for L-cysteine	M_cys_L_e	<---->	
R_EX_gln_L_LPAREN_e_RPAREN_	exchange reaction for L-glutamine	M_gln_L_e	<---->	
R_EX_phe_L_LPAREN_e_RPAREN_	exchange reaction for L-phenylalanine	M_phe_L_e	<---->	
R_EX_tyr_L_LPAREN_e_RPAREN_	L-Tyrosine exchange	M_tyr_L_e	<---->	
R_EX_pi_LPAREN_e_RPAREN_	Phosphate exchange	M_pi_e	<---->	
R_EX_ser_L_LPAREN_e_RPAREN_	exchange reaction for L-serine	M_ser_L_e	<---->	
R_EX_urea_LPAREN_e_RPAREN_	Urea exchange	M_urea_e	<---->	
R_EX_orn_LPAREN_e_RPAREN_	Ornithine exchange	M_orn_e	<---->	
R_EX_o2_LPAREN_e_RPAREN_	exchange reaction for oxugen	M_o2_e	<---->	
R_EX_co2_LPAREN_e_RPAREN_	CO2 exchange	M_co2_e	<---->	
R_Ex_Biomass	Ex_Biomass	M_biomass_c	----->	
R_EX_his_L_LPAREN_e_RPAREN_	exchange reaction for L-histidine	M_his_L_e	<---->	
R_EX_asp_L_LPAREN_e_RPAREN_	L-Aspartate exchange	M_asp_L_e	<---->	
R_EX_asn_L_LPAREN_e_RPAREN_	exchange reaction for L-asparagine	M_asn_L_e	<---->	
R_EX_glu_L_LPAREN_e_RPAREN_	L-Glutamate exchange	M_glu_L_e	<---->	
R_EX_hco3_LPAREN_e_RPAREN_	Bicarbonate exchange	M_hco3_e	<---->	
R_EX_gly_LPAREN_e_RPAREN_	exchange reaction for Glycine	M_gly_e	<---->	

R_EX_glc_LPAREN_e_RPAREN_	D-Glucose exchange	M_glc_D_e	<---->	
R_EX_h2o_LPAREN_e_RPAREN_	H2O exchange	M_h2o_e	<---->	
R_EX_val_L_LPAREN_e_RPAREN_	L-Valine exchange	M_val_L_e	<---->	
R_EX_met_L_LPAREN_e_RPAREN_	L-Methionine exchange	M_met_L_e	<---->	
R_EX_HC00250_LPAREN_e_RPAREN_	Exchange of hydrosulfide	M_HC00250_e	<---->	
R_EX_GLTX	Glutamax transport	M_GLTX_e	<---->	
R_EX_arg_L_LPAREN_e_RPAREN_	L-Arginine exchange	M_arg_L_e	<---->	
R_EX_ala_L_LPAREN_e_RPAREN_	exchange reaction for L-alanine	M_ala_L_e	<---->	

APPENDIX B

The CHO model available does not contain the biomass equation because the authors maximized the ATP yield as objective function (Martínez et al., 2013). Therefore, a biomass equation was developed based on the literature, as presented in detail in the **Tables B.1 to B.8**.

Table B.1
General Composition

Altamirano, C., Illanes, A., Casablancas, A., Gamez, X., Cairo, J. J., & Godia, C. (2001). Analysis of CHO Cells Metabolic Redistribution in a Glutamate-Based Defined Medium in Continuous Culture. *Biotechnology Progress*, *17*(6), 1032-1041.
Vriezen, N., & van Dijken, J. P. (1998). Fluxes and enzyme activities in central metabolism of myeloma cells grown in chemostat culture. *Biotechnology and bioengineering*, *59*(1), 28-39.
Bonarius, H. P., Hatzimanikatis, V., Meesters, K. P., de Gooijer, C. D., Schmid, G., & Tramper, J. (1996). Metabolic flux analysis of hybridoma cells in different culture media using mass balances. *Biotechnology and bioengineering*, *50*(3), 299-318.
Xie, L., & Wang, D. I. (1996). Material balance studies on animal cell metabolism using a stoichiometrically based reaction network. *Biotechnology and bioengineering*, *52*(5), 579-590.

Compost	w/w	Adj 100%	MW compost (g comp/mol comp)	mmol x/g DW	Total
Protein	70.6	75.91	109.983	6.902	0.759
DNA	1.9	2.04	332.319	0.061	0.020
RNA	5.8	6.24	331.08	0.188	0.062
Carbohydrates	7	7.53	162.00	0.465	0.075
Lipids	7.7	8.28	726.27	0.114	0.083
	93	100			**1**

Table B.2
Amino Acid Composition

Altamirano, C., Illanes, A., Casablancas, A., Gamez, X., Cairo, J. J., & Godia, C. (2001). Analysis of CHO Cells Metabolic Redistribution in a Glutamate-Based Defined Medium in Continuous Culture. *Biotechnology Progress*, *17*(6), 1032-1041.
Vriezen, N., & van Dijken, J. P. (1998). Fluxes and enzyme activities in central metabolism of myeloma cells grown in chemostat culture. *Biotechnology and bioengineering*, *59*(1), 28-39.
Bonarius, H. P., Hatzimanikatis, V., Meesters, K. P., de Gooijer, C. D., Schmid, G., & Tramper, J. (1996). Metabolic flux analysis of hybridoma cells in different culture media using mass balances. *Biotechnology and bioengineering*, *50*(3), 299-318.
Xie, L., & Wang, D. I. (1996). Material balance studies on animal cell metabolism using a stoichiometrically based reaction network. *Biotechnology and bioengineering*, *52*(5), 579-590.

Amino acid	Aa content in bprot **mol Aa/mol bprot**	Aa content in bprot **mol Aa/mol bprot 100**	MW **g Aa/mol Aa**	**g Aa/ mol bprot**	**g Aa/ g bprot**	**mmol Aa/g DW**
Ala	0.095	0.0960	71.08	6.821	0.06202	0.6623
Arg	0.063	0.0636	156.19	9.939	0.09037	0.4392
Asp	0.048	0.0485	114.1	5.532	0.05030	0.3347
Asn	0.039	0.0394	115.09	4.534	0.04122	0.2719
Cys	0.028	0.0283	103.14	2.917	0.02652	0.1952
Gln	0.052	0.0525	128.13	6.730	0.06119	0.3625
Glu	0.064	0.0646	129.12	8.347	0.07590	0.4462
Gly	0.078	0.0788	57.05	4.495	0.04087	0.5438
His	0.022	0.0222	137.14	3.048	0.02771	0.1534
Ile	0.052	0.0525	113.16	5.944	0.05404	0.3625
Leu	0.088	0.0889	113.16	10.059	0.09146	0.6135
Lys	0.089	0.0899	128.17	11.522	0.10477	0.6205
Met	0.020	0.0202	131.19	2.650	0.02410	0.1394
Phe	0.021	0.0212	147.18	3.122	0.02839	0.1464
Pro	0.028	0.0283	97.12	2.747	0.02498	0.1952
Ser	0.057	0.0576	87.08	5.014	0.04559	0.3974
Thr	0.061	0.0616	101.1	6.229	0.05664	0.4253
Trp	0.006	0.0061	186.21	1.129	0.01026	0.0418
Tyr	0.020	0.0202	163.18	3.297	0.02997	0.1394
Val	0.059	0.0596	99.13	5.908	0.05372	0.4114
	0.99	1	**g prot /mol bprot**	109.983		

Table B.3
Deoxyribonucleotide Composition

Sheikh, K., Förster, J., & Nielsen, L. K. (2005). Modeling hybridoma cell metabolism using a generic genome-scale metabolic model of Mus musculus. *Biotechnology progress*, *21*(1), 112-121.
Altamirano, C., Illanes, A., Casablancas, A., Gamez, X., Cairo, J. J., & Godia, C. (2001). Analysis of CHO Cells Metabolic Redistribution in a Glutamate-Based Defined Medium in Continuous Culture. *Biotechnology Progress*, *17*(6), 1032-1041.
Vriezen, N., & van Dijken, J. P. (1998). Fluxes and enzyme activities in central metabolism of myeloma cells grown in chemostat culture. *Biotechnology and bioengineering*, *59*(1), 28-39.
Bonarius, H. P., Hatzimanikatis, V., Meesters, K. P., de Gooijer, C. D., Schmid, G., & Tramper, J. (1996). Metabolic flux analysis of hybridoma cells in different culture media using mass balances. *Biotechnology and bioengineering*, *50*(3), 299-318.
Xie, L., & Wang, D. I. (1996). Material balance studies on animal cell metabolism using a stoichiometrically based reaction network. *Biotechnology and bioengineering*, *52*(5), 579-590.
Savinell, J. M., & Palsson, B. O. (1992). Network analysis of intermediary metabolism using linear optimization: II. Interpretation of hybridoma cell metabolism. *Journal of theoretical biology*, *154*(4), 455-473.
Darnell, J.; Lodish, H.; Baltimore, D. Molecular Cell Biology, 2nd ed.; Scientific American Books: New York, 1990.

Component	**mol dxMP/mol DNA**	MW **g dxMP/mol dxMP**	**g dxMP/ mol DNA**	**g dxMP/ g DNA**	**mmol dxMP/g DW**
dAMP	0.3	349.24	104.77	0.3153	0.0184
dCMP	0.2	307.2	61.44	0.1849	0.0123
dGMP	0.2	347.22	69.44	0.2090	0.0123
dTMP	0.3	322.21	96.66	0.2909	0.0184
	1	**g DNA /mol DNA**	332.32		

Table B.4
Ribonucleotide Composition

Sheikh, K., Förster, J., & Nielsen, L. K. (2005). Modeling hybridoma cell metabolism using a generic genome-scale metabolic model of Mus musculus. *Biotechnology progress*, *21*(1), 112-121.
Altamirano, C., Illanes, A., Casablancas, A., Gamez, X., Cairo, J. J., & Godia, C. (2001). Analysis of CHO Cells Metabolic Redistribution in a Glutamate-Based Defined Medium in Continuous Culture. *Biotechnology Progress*, *17*(6), 1032-1041.
Vriezen, N., & van Dijken, J. P. (1998). Fluxes and enzyme activities in central metabolism of myeloma cells grown in chemostat culture. *Biotechnology and bioengineering*, *59*(1), 28-39.
Bonarius, H. P., Hatzimanikatis, V., Meesters, K. P., de Gooijer, C. D., Schmid, G., & Tramper, J. (1996). Metabolic flux analysis of hybridoma cells in different culture media using mass balances. *Biotechnology and bioengineering*, *50*(3), 299-318.
Xie, L., & Wang, D. I. (1996). Material balance studies on animal cell metabolism using a stoichiometrically based reaction network. *Biotechnology and bioengineering*, *52*(5), 579-590.
Savinell, J. M., & Palsson, B. O. (1992). Network analysis of intermediary metabolism using linear optimization: II. Interpretation of hybridoma cell metabolism. *Journal of theoretical biology*, *154*(4), 455-473.
Darnell, J.; Lodish, H.; Baltimore, D. Molecular Cell Biology, 2nd ed.; Scientific American Books: New York, 1990.

Component	**mol xMP/mol RNA**	MW **g xMP/mol xMP**	**g xMP/ mol RNA**	**g xMP/ g RNA**	**mmol xMP/g DW**
AMP	0.1800	349.24	62.86	0.1899	0.0339
CMP	0.3000	307.20	92.16	0.2784	0.0565
GMP	0.3400	347.22	118.05	0.3566	0.0640
UMP	0.1800	322.21	58.00	0.1752	0.0339
	1.0000	**g RNA /mol RNA**	331.08		

Table B.5 Lipid Composition

Sheikh, K., Förster, J., & Nielsen, L. K. (2005). Modeling hybridoma cell metabolism using a generic genome-scale metabolic model of Mus musculus. *Biotechnology progress*, *21*(1), 112-121.

Altamirano, C., Illanes, A., Casablancas, A., Gamez, X., Cairo, J. J., & Godia, C. (2001). Analysis of CHO Cells Metabolic Redistribution in a Glutamate-Based Defined Medium in Continuous Culture. *Biotechnology Progress*, *17*(6), 1032-1041.

Vriezen, N., & van Dijken, J. P. (1998). Fluxes and enzyme activities in central metabolism of myeloma cells grown in chemostat culture. *Biotechnology and bioengineering*, *59*(1), 28-39.

Bonarius, H. P., Hatzimanikatis, V., Meesters, K. P., de Gooijer, C. D., Schmid, G., & Tramper, J. (1996). Metabolic flux analysis of hybridoma cells in different culture media using mass balances. *Biotechnology and bioengineering*, *50*(3), 299-318.

Xie, L., & Wang, D. I. (1996). Material balance studies on animal cell metabolism using a stoichiometrically based reaction network. *Biotechnology and bioengineering*, *52*(5), 579-590.

Savinell, J. M., & Palsson, B. O. (1992). Network analysis of intermediary metabolism using linear optimization: II. Interpretation of hybridoma cell metabolism. *Journal of theoretical biology*, *154*(4), 455-473.

Darnell, J.; Lodish, H.; Baltimore, D. Molecular Cell Biology, 2nd ed.; Scientific American Books: New York, 1990.

Component	**g xL/g LIP**	MW **g xL/mol xL**	**mmol xL/g L**	**mol xL/mol L**	**mmol xL/g DW**
Cholesterol	0.07	386.70	0.1810	0.1315	0.0150
Phosphatidyl choline	0.53	769.00	0.6892	0.5006	0.0571
Phosphatidyl ethanolamine	0.19	727.00	0.2613	0.1898	0.0216
Phosphatidyl inositol	0.08	845.00	0.0947	0.0688	0.0078
Phosphatidyl serine	0.02	770.00	0.0260	0.0189	0.0022
Phosphatidyl glycerol	0.01	757.00	0.0132	0.0096	0.0011
Cardiolipin	0.04	1422.10	0.0281	0.0204	0.0023
Sphingomyelin	0.06	720.00	0.0833	0.0605	0.0069
	1	**mmol L/g L**	1.3769	1.0000	
		g L/mol L	726.273		

Table B.6
Carbohydrate Composition

Sheikh, K., Förster, J., & Nielsen, L. K. (2005). Modeling hybridoma cell metabolism using a generic genome-scale metabolic model of Mus musculus. *Biotechnology progress*, *21*(1), 112-121.
Altamirano, C., Illanes, A., Casablancas, A., Gamez, X., Cairo, J. J., & Godia, C. (2001). Analysis of CHO Cells Metabolic Redistribution in a Glutamate-Based Defined Medium in Continuous Culture. *Biotechnology Progress*, *17*(6), 1032-1041.
Vriezen, N., & van Dijken, J. P. (1998). Fluxes and enzyme activities in central metabolism of myeloma cells grown in chemostat culture. *Biotechnology and bioengineering*, *59*(1), 28-39.
Bonarius, H. P., Hatzimanikatis, V., Meesters, K. P., de Gooijer, C. D., Schmid, G., & Tramper, J. (1996). Metabolic flux analysis of hybridoma cells in different culture media using mass balances. *Biotechnology and bioengineering*, *50*(3), 299-318.
Xie, L., & Wang, D. I. (1996). Material balance studies on animal cell metabolism using a stoichiometrically based reaction network. *Biotechnology and bioengineering*, *52*(5), 579-590.
Savinell, J. M., & Palsson, B. O. (1992). Network analysis of intermediary metabolism using linear optimization: II. Interpretation of hybridoma cell metabolism. *Journal of theoretical biology*, *154*(4), 455-473.
Darnell, J.; Lodish, H.; Baltimore, D. Molecular Cell Biology, 2nd ed.; Scientific American Books: New York, 1990.

Component	**mmol glyc/g DW**	**mmol glyc /g CARB**	**mol glyc /mol CARB**
Glycogen (monomer)	0.28	3.7200	1
	mmol CARB/g CARB	3.7200	
	g CARB/mol CARB	**268.82**	
	g CARB/mol CARB Considered	162	

Table B.7 Energy Requirements for Polymerization of Macromolecules

Sheikh, K., Förster, J., & Nielsen, L. K. (2005). Modeling hybridoma cell metabolism using a generic genome-scale metabolic model of Mus musculus. *Biotechnology progress*, *21*(1), 112-121.
Neidhardt, F. C.; Ingraham, J. L.; Low, K. B.; Magasanik, B.; Schaechter, M. et al. Escherichia coli and Salmonella typhimurium: Cellular and Molecular Biology; American Society for Microbiology: Washington, DC, 1987.

Process	Energy Required (mol ATP /mol x)
Protein synthesis and processing	4.306
RNA sythesis and processing	0.400
DNA synthesis and processing	1.372

Table B.8 Total equations

Oliveira, A. P., Nielsen, J., & Förster, J. (2005). Modeling Lactococcus lactis using a genome-scale flux model. *BMC microbiology*, *5*(1), 1.

BIOM_PROT	**0.0960 LAlanine +0.0636 LArginine + 0.0485 LAspartate + 0.0394 LAsparagine + 0.0283 LCysteine + 0.0525 LGlutamine + 0.0646 LGlutamate + 0.0788 Glycine + 0.0222 LHistidine + 0.0525 LIsoleucine + 0.0889 LLeucine + 0.0899 LLysine + 0.0202 LMethionine + 0.0212 LPhenylalanine + 0.0283 LProline + 0.0576 LSerine + 0.0616 LThreonine + 0.0061 LTryptophan + 0.0202 LTyrosine + 0.0596 LValine + 4.306 ATP + 4.306 H2O -> PROT + 4.306 ADP + 4.306 Orthophosphate + 1 H2O**
BIOM_DNA	**0.3 dAMP + 0.2 dCMP + 0.2 dGMP + 0.3 dTMP + 1.372 ATP + 1.372 H2O -> DNA + 1.372 ADP + 1.372 Orthophosphate**
BIOM_RNA	**0.18 AMP + 0.30 CMP + 0.34 GMP + 0.18 UMP + 0.4 ATP + 0.4 H2O -> RNA + 0.4 ADP + 0.4 Orthophosphate**
BIOM_LIP	**0.1315 Cholesterol + 0.5006 Phosphatidylcholine + 0.1898 Phosphatidylethanolamine + 0.0688 1PhosphatidylDmyoinositol + 0.0189 Phosphatidylserine + 0.0096 Phosphatidylglycerol + 0.0204 Cardiolipin + 0.0605 Sphingomyelin -> LIP**
BIOM_CARB	**Amylose -> CAR**
BIOM_T	**6.902 PROT + 0.061 DNA + 0.188 RNA + 0.114 LIP + 0.465 CAR -> BIOMASS**

APPENDIX C

The CHO metabolic model used for p-FBA presented in the Chapter 4 was derived from the reduced model obtained from a generic *Mus musculus* genome-scale metabolic model (Quek and Nielsen, 2008). The resulting model, that contains 397 reactions and 395 metabolites, used for the metabolic flux calculation is detailed in **Table C.1**.

Table C.1: List of reactions included in the CHO reduced model developed and used in the Chapter 4.

R01786_added	ATP + alphaDGlucose -> ADP + alphaDGlucose6phosphate	ATP_cytosol + alphaDGlucose_cytosol	----->	ADP_cytosol + alphaDGlucose6phosphate_cytosol
R02740	alphaDGlucose6phosphate <-> betaDFructose6phosphate	alphaDGlucose6phosphate_cytosol	<---->	betaDFructose6phosphate_cytosol
R04779_added	ATP + betaDFructose6phosphate -> ADP + betaDFructose16bisphosphate	ATP_cytosol + betaDFructose6phosphate_cytosol	----->	ADP_cytosol + betaDFructose16bisphosphate_cytosol
R01070	betaDFructose16bisphosphate <-> 2R2Hydroxy3phosphonooxypropanal + Glyceronephosphate	betaDFructose16bisphosphate_cytosol	<---->	Glyceronephosphate_cytosol + 2R2Hydroxy3phosphonooxypropanal_cytosol
R01015	2R2Hydroxy3phosphonooxypropanal <-> Glyceronephosphate	2R2Hydroxy3phosphonooxypropanal_cytosol	<---->	Glyceronephosphate_cytosol
R01061	Orthophosphate + NAD + 2R2Hydroxy3phosphonooxypropanal <-> H + NADH + 3PhosphoDglyceroylphosphate	2R2Hydroxy3phosphonooxypropanal_cytosol + NAD_cytosol + Orthophosphate_cytosol	<---->	3PhosphoDglyceroylphosphate_cytosol + NADH_cytosol + H_cytosol
R01512	ATP + 3PhosphoDglycerate <-> ADP + 3PhosphoDglyceroylphosphate	ATP_cytosol + 3PhosphoDglycerate_cytosol	<---->	ADP_cytosol + 3PhosphoDglyceroylphosphate_cytosol
R01518	2PhosphoDglycerate <-> 3PhosphoDglycerate	2PhosphoDglycerate_cytosol	<---->	3PhosphoDglycerate_cytosol
R00658	2PhosphoDglycerate <-> H2O + Phosphoenolpyruvate	2PhosphoDglycerate_cytosol	<---->	H2O_cytosol + Phosphoenolpyruvate_cytosol
R00200	ADP + Phosphoenolpyruvate -> Pyruvate + ATP	ADP_cytosol + Phosphoenolpyruvate_cytosol	----->	ATP_cytosol + Pyruvate_cytosol
R04780	H2O + betaDFructose16bisphosphate -> Orthophosphate + betaDFructose6phosphate	betaDFructose16bisphosphate_cytosol + H2O_cytosol	----->	betaDFructose6phosphate_cytosol + Orthophosphate_cytosol
R01830	betaDFructose6phosphate + 2R2Hydroxy3phosphonooxypropanal <-> DXylulose5phosphate + DErythrose4phosphate	betaDFructose6phosphate_cytosol + 2R2Hydroxy3phosphonooxypropanal_cytosol	<---->	DErythrose4phosphate_cytosol + DXylulose5phosphate_cytosol
R02739	alphaDGlucose6phosphate <-> betaDGlucose6phosphate	alphaDGlucose6phosphate_cytosol	<---->	betaDGlucose6phosphate_cytosol

R02736	NADP + betaDGlucose6phosphate -> H + NADPH + DGlucono15lactone6phosphate	betaDGlucose6phosphate_cytosol + NADP_cytosol	----->	H_cytosol + DGlucono15lactone6phosphate_cytosol + NADPH_cytosol
R02035	H2O + DGlucono15lactone6phosphate -> 6PhosphoDgluconate	H2O_cytosol + DGlucono15lactone6phosphate_cytosol	----->	6PhosphoDgluconate_cytosol
R01528	NADP + 6PhosphoDgluconate <-> H + NADPH + CO2 + DRibulose5phosphate	NADP_cytosol + 6PhosphoDgluconate_cytosol	<---->	H_cytosol + NADPH_cytosol + CO2_cytosol + DRibulose5phosphate_cytosol
R01056	DRibose5phosphate <-> DRibulose5phosphate	DRibose5phosphate_cytosol	<---->	DRibulose5phosphate_cytosol
R01529	DRibulose5phosphate <-> DXylulose5phosphate	DRibulose5phosphate_cytosol	<---->	DXylulose5phosphate_cytosol
R01641	2R2Hydroxy3phosphonooxypropanal + DSedoheptulose7phosphate <-> DRibose5phosphate + DXylulose5phosphate	2R2Hydroxy3phosphonooxypropanal_cytosol + DSedoheptulose7phosphate_cytosol	<---->	DXylulose5phosphate_cytosol + DRibose5phosphate_cytosol
R01827	2R2Hydroxy3phosphonooxypropanal + DSedoheptulose7phosphate <-> betaDFructose6phosphate + DErythrose4phosphate	2R2Hydroxy3phosphonooxypropanal_cytosol + DSedoheptulose7phosphate_cytosol	<---->	betaDFructose6phosphate_cytosol + DErythrose4phosphate_cytosol
R00703	NAD + SLactate <-> H + Pyruvate + NADH	NAD_cytosol + SLactate_cytosol	<---->	NADH_cytosol + H_cytosol + Pyruvate_cytosol
R00703_added_2.1	NAD [mitoc] + SLactate [mitoc] <-> H [mitoc] + Pyruvate [mitoc] + NADH [mitoc]	SLactate_mitoc + NAD_mitoc	<---->	H_mitoc + Pyruvate_mitoc + NADH_mitoc
TF00703_added_2.1	SLactate -> SLactate [mitoc]	SLactate_cytosol	----->	SLactate_mitoc
R01513_added	NAD + 3PhosphoDglycerate <-> H + 3Phosphonooxypyruvate + NADH	NAD_cytosol + 3PhosphoDglycerate_cytosol	<---->	NADH_cytosol + H_cytosol + 3Phosphonooxypyruvate_cytosol
R04173_added	2Oxoglutarate + OPhosphoLserine <-> LGlutamate + 3Phosphonooxypyruvate	OPhosphoLserine_cytosol + 2Oxoglutarate_cytosol	<---->	3Phosphonooxypyruvate_cytosol + LGlutamate_cytosol
R00582_added	H2O + OPhosphoLserine -> Orthophosphate + LSerine	H2O_cytosol + OPhosphoLserine_cytosol	----->	Orthophosphate_cytosol + LSerine_cytosol
R00945	H2O + 510Methylenetetrahydrofolate + Glycine <-> LSerine + Tetrahydrofolate	H2O_cytosol + Glycine_cytosol + 510Methylenetetrahydrofolate_cytosol	<---->	LSerine_cytosol + Tetrahydrofolate_cytosol

R01221	Tetrahydrofolate + Glycine + NAD <-> H + NH3 + CO2 + 510Methylenetetrahydrofolate + NADH	NAD_cytosol + Tetrahydrofolate_cytosol + Glycine_cytosol	<---->	NADH_cytosol + H_cytosol + CO2_cytosol + 510Methylenetetrahydrofolate_cytosol + NH3_cytosol
R01220	NADP + 510Methylenetetrahydrofolate <-> H + NADPH + 510Methenyltetrahydrofolate	NADP_cytosol + 510Methylenetetrahydrofolate_cytosol	<---->	H_cytosol + NADPH_cytosol + 510Methenyltetrahydrofolate_cytosol
R01655	H2O + 510Methenyltetrahydrofolate <-> H + 10Formyltetrahydrofolate	H2O_cytosol + 510Methenyltetrahydrofolate_cytosol	<---->	H_cytosol + 10Formyltetrahydrofolate_cytosol
R00939	H + NADPH + Dihydrofolate -> NADP + Tetrahydrofolate	H_cytosol + NADPH_cytosol + Dihydrofolate_cytosol	----->	NADP_cytosol + Tetrahydrofolate_cytosol
R00209 [mitoc]	NAD [mitoc] + CoA [mitoc] + Pyruvate [mitoc] -> NADH [mitoc] + H [mitoc] + CO2 [mitoc] + AcetylCoA [mitoc]	Pyruvate_mitoc + NAD_mitoc + CoA_mitoc	----->	H_mitoc + NADH_mitoc + CO2_mitoc + AcetylCoA_mitoc
R00351 [mitoc]	Oxaloacetate [mitoc] + H2O [mitoc] + AcetylCoA [mitoc] -> Citrate [mitoc] + CoA [mitoc]	AcetylCoA_mitoc + H2O_mitoc + Oxaloacetate_mitoc	----->	CoA_mitoc + Citrate_mitoc
R01324 [mitoc]	Citrate [mitoc] <-> Isocitrate [mitoc]	Citrate_mitoc	<---->	Isocitrate_mitoc
R00709 [mitoc]	NAD [mitoc] + Isocitrate [mitoc] -> NADH [mitoc] + H [mitoc] + CO2 [mitoc] + 2Oxoglutarate [mitoc]	NAD_mitoc + Isocitrate_mitoc	----->	H_mitoc + NADH_mitoc + CO2_mitoc + 2Oxoglutarate_mitoc
R00621 [mitoc]	NAD [mitoc] + CoA [mitoc] + 2Oxoglutarate [mitoc] -> NADH [mitoc] + CO2 [mitoc] + SuccinylCoA [mitoc]	NAD_mitoc + CoA_mitoc + 2Oxoglutarate_mitoc	----->	NADH_mitoc + CO2_mitoc + SuccinylCoA_mitoc
R00405 [mitoc]	CoA [mitoc] + ATP [mitoc] + Succinate [mitoc] <-> SuccinylCoA [mitoc] + ADP [mitoc] + Orthophosphate [mitoc]	CoA_mitoc + Succinate_mitoc + ATP_mitoc	<---->	SuccinylCoA_mitoc + ADP_mitoc + Orthophosphate_mitoc
R00412 [mitoc]	FAD [mitoc] + Succinate [mitoc] <-> FADH2 [mitoc] + Fumarate [mitoc]	Succinate_mitoc + FAD_mitoc	<---->	Fumarate_mitoc + FADH2_mitoc
R01082 [mitoc]	SMalate [mitoc] <-> H2O [mitoc] + Fumarate [mitoc]	SMalate_mitoc	<---->	H2O_mitoc + Fumarate_mitoc
R00342 [mitoc]	NAD [mitoc] + SMalate [mitoc] <-> Oxaloacetate [mitoc] + NADH [mitoc] + H [mitoc]	NAD_mitoc + SMalate_mitoc	<---->	H_mitoc + NADH_mitoc + Oxaloacetate_mitoc

K00007 [mitoc]	FADH2 [mitoc] + 0.5 Oxygen [mitoc] + 1.5 ADP [mitoc] + 1.5 Orthophosphate [mitoc] -> FAD [mitoc] + 2.5 H2O [mitoc] + 1.5 ATP [mitoc]	1.5*ADP_mitoc + 1.5*Orthophosphate_mitoc + FADH2_mitoc + 0.5*Oxygen_mitoc	----->	2.5*H2O_mitoc + 1.5*ATP_mitoc + FAD_mitoc
K00006 [mitoc]	NADH [mitoc] + H [mitoc] + 0.5 Oxygen [mitoc] + 2.5 ADP [mitoc] + 2.5 Orthophosphate [mitoc] -> NAD [mitoc] + 3.5 H2O [mitoc] + 2.5 ATP [mitoc]	H_mitoc + NADH_mitoc + 2.5*ADP_mitoc + 2.5*Orthophosphate_mitoc + 0.5*Oxygen_mitoc	----->	NAD_mitoc + 3.5*H2O_mitoc + 2.5*ATP_mitoc
R00216 [mitoc]	SMalate [mitoc] + NADP [mitoc] -> CO2 [mitoc] + NADPH [mitoc] + Pyruvate [mitoc]	SMalate_mitoc + NADP_mitoc	----->	Pyruvate_mitoc + CO2_mitoc + NADPH_mitoc
R00214 [mitoc]	NAD [mitoc] + SMalate [mitoc] -> NADH [mitoc] + CO2 [mitoc] + Pyruvate [mitoc]	NAD_mitoc + SMalate_mitoc	----->	Pyruvate_mitoc + NADH_mitoc + CO2_mitoc
R00258 [mitoc]	2Oxoglutarate [mitoc] + LAlanine [mitoc] <-> LGlutamate [mitoc] + Pyruvate [mitoc]	2Oxoglutarate_mitoc + LAlanine_mitoc	<---->	Pyruvate_mitoc + LGlutamate_mitoc
R00355 [mitoc]	2Oxoglutarate [mitoc] + LAspartate [mitoc] <-> Oxaloacetate [mitoc] + LGlutamate [mitoc]	2Oxoglutarate_mitoc + LAspartate_mitoc	<---->	Oxaloacetate_mitoc + LGlutamate_mitoc
R00256 [mitoc]	H2O [mitoc] + LGlutamine [mitoc] -> LGlutamate [mitoc] + NH3 [mitoc]	H2O_mitoc + LGlutamine_mitoc	----->	LGlutamate_mitoc + NH3_mitoc
TF0020	LProline <-> LProline [mitoc]	LProline_cytosol	<---->	LProline_mitoc
R01253 [mitoc]	LProline [mitoc] + Acceptor [mitoc] -> Reducedacceptor [mitoc] + S1Pyrroline5carboxylate [mitoc]	LProline_mitoc + Acceptor_mitoc	----->	Reducedacceptor_mitoc + S1Pyrroline5carboxylate_mitoc
gCat06 [mitoc]	LGlutamate5semialdehyde [mitoc] <-> S1Pyrroline5carboxylate [mitoc]	LGlutamate5semialdehyde_mitoc	<---->	S1Pyrroline5carboxylate_mitoc
R00707 [mitoc]	NAD [mitoc] + H2O [mitoc] + LGlutamate5semialdehyde [mitoc] -> NADH [mitoc] + H [mitoc] + LGlutamate [mitoc]	NAD_mitoc + H2O_mitoc + LGlutamate5semialdehyde_mitoc	----->	H_mitoc + NADH_mitoc + LGlutamate_mitoc
R00243 [mitoc]	NAD [mitoc] + H2O [mitoc] + LGlutamate [mitoc] <-> NADH [mitoc] + H [mitoc] + 2Oxoglutarate [mitoc] + NH3 [mitoc]	NAD_mitoc + H2O_mitoc + LGlutamate_mitoc	<---->	H_mitoc + NADH_mitoc + 2Oxoglutarate_mitoc + NH3_mitoc

R00216	NADP + SMalate -> NADPH + Pyruvate + CO2	NADP_cytosol + SMalate_cytosol	----->	Pyruvate_cytosol + NADPH_cytosol + CO2_cytosol
R00342	SMalate + NAD <-> H + NADH + Oxaloacetate	NAD_cytosol + SMalate_cytosol	<---->	NADH_cytosol + H_cytosol + Oxaloacetate_cytosol
R00352	ATP + CoA + Citrate -> ADP + Orthophosphate + AcetylCoA + Oxaloacetate	ATP_cytosol + Citrate_cytosol + CoA_cytosol	----->	ADP_cytosol + Orthophosphate_cytosol + Oxaloacetate_cytosol + AcetylCoA_cytosol
R01082	SMalate <-> H2O + Fumarate	SMalate_cytosol	<---->	H2O_cytosol + Fumarate_cytosol
R00959	alphaDGlucose1phosphate <-> alphaDGlucose6phosphate	alphaDGlucose1phosphate_cytosol	<---->	alphaDGlucose6phosphate_cytosol
R00289	UTP + alphaDGlucose1phosphate -> Pyrophosphate + UDPglucose	alphaDGlucose1phosphate_cytosol + UTP_cytosol	----->	Pyrophosphate_cytosol + UDPglucose_cytosol
R00292	UDPglucose -> Amylose + UDP	UDPglucose_cytosol	----->	Amylose_cytosol + UDP_cytosol
R00258	2Oxoglutarate + LAlanine <-> Pyruvate + LGlutamate	2Oxoglutarate_cytosol + LAlanine_cytosol	<---->	Pyruvate_cytosol + LGlutamate_cytosol
R00355	LAspartate + 2Oxoglutarate <-> LGlutamate + Oxaloacetate	2Oxoglutarate_cytosol + LAspartate_cytosol	<---->	LGlutamate_cytosol + Oxaloacetate_cytosol
R00485	H2O + LAsparagine <-> NH3 + LAspartate	H2O_cytosol + LAsparagine_cytosol	<---->	NH3_cytosol + LAspartate_cytosol
R00239_added	LGlutamate + ATP -> ADP + LGlutamyl5phosphate	ATP_cytosol + LGlutamate_cytosol	----->	ADP_cytosol + LGlutamyl5phosphate_cytosol
R03313_added	H + NADPH + LGlutamyl5phosphate -> NADP + Orthophosphate + LGlutamate5semialdehyde	H_cytosol + NADPH_cytosol + LGlutamyl5phosphate_cytosol	----->	Orthophosphate_cytosol + NADP_cytosol + LGlutamate5semialdehyde_cytosol
gCat06_added	LGlutamate5semialdehyde <-> S1Pyrroline5carboxylate	LGlutamate5semialdehyde_cytosol	<---->	S1Pyrroline5carboxylate_cytosol
R01251_added	H + NADPH + S1Pyrroline5carboxylate -> NADP + LProline	H_cytosol + NADPH_cytosol + S1Pyrroline5carboxylate_cytosol	----->	NADP_cytosol + LProline_cytosol
R00848	snGlycerol3phosphate + FAD <-> Glyceronephosphate + FADH2	snGlycerol3phosphate_cytosol + FAD_cytosol	<---->	Glyceronephosphate_cytosol + FADH2_cytosol
R00842	NAD + snGlycerol3phosphate <-> H + NADH + Glyceronephosphate	NAD_cytosol + snGlycerol3phosphate_cytosol	<---->	Glyceronephosphate_cytosol + NADH_cytosol + H_cytosol
R00851	AcylCoA + snGlycerol3phosphate -> CoA + 1Acylsnglycerol3phosphate	snGlycerol3phosphate_cytosol + AcylCoA_cytosol	----->	CoA_cytosol + 1Acylsnglycerol3phosphate_cytosol

R02241	1Acylsnglycerol3phosphate + AcylCoA -> CoA + Phosphatidate	1Acylsnglycerol3phosphate_cytosol + AcylCoA_cytosol	----->	CoA_cytosol + Phosphatidate_cytosol
R01799	CTP + Phosphatidate -> Pyrophosphate + CDPdiacylglycerol	Phosphatidate_cytosol + CTP_cytosol	----->	Pyrophosphate_cytosol + CDPdiacylglycerol_cytosol
R02030	CDPdiacylglycerol + Phosphatidylglycerol -> CMP + Cardiolipin	CDPdiacylglycerol_cytosol + Phosphatidylglycerol_cytosol	----->	Cardiolipin_cytosol + CMP_cytosol
R01802	myoInositol + CDPdiacylglycerol -> CMP + 1PhosphatidylDmyoinositol	CDPdiacylglycerol_cytosol + myoInositol_cytosol	----->	CMP_cytosol + 1PhosphatidylDmyoinositol_cytosol
R01801	CDPdiacylglycerol + snGlycerol3phosphate -> CMP + Phosphatidylglycerophosphate	snGlycerol3phosphate_cytosol + CDPdiacylglycerol_cytosol	----->	CMP_cytosol + Phosphatidylglycerophosphate_cytosol
R02239	H2O + Phosphatidate -> Orthophosphate + 12Diacylsnglycerol	H2O_cytosol + Phosphatidate_cytosol	----->	Orthophosphate_cytosol + 12Diacylsnglycerol_cytosol
R02057	12Diacylsnglycerol + CDPethanolamine -> CMP + Phosphatidylethanolamine	12Diacylsnglycerol_cytosol + CDPethanolamine_cytosol	----->	CMP_cytosol + Phosphatidylethanolamine_cytosol
R01890	CTP + Cholinephosphate -> Pyrophosphate + CDPcholine	CTP_cytosol + Cholinephosphate_cytosol	----->	Pyrophosphate_cytosol + CDPcholine_cytosol
R01021	ATP + Choline <-> ADP + Cholinephosphate	ATP_cytosol + Choline_cytosol	<---->	ADP_cytosol + Cholinephosphate_cytosol
R01321	CDPcholine + 12Diacylsnglycerol -> Phosphatidylcholine + CMP	12Diacylsnglycerol_cytosol + CDPcholine_cytosol	----->	CMP_cytosol + Phosphatidylcholine_cytosol
R02038	CTP + Ethanolaminephosphate -> Pyrophosphate + CDPethanolamine	CTP_cytosol + Ethanolaminephosphate_cytosol	----->	Pyrophosphate_cytosol + CDPethanolamine_cytosol
R01468	ATP + Ethanolamine -> ADP + Ethanolaminephosphate	ATP_cytosol + Ethanolamine_cytosol	----->	ADP_cytosol + Ethanolaminephosphate_cytosol
R07377	LSerine + Phosphatidylcholine -> Phosphatidylserine + Choline	LSerine_cytosol + Phosphatidylcholine_cytosol	----->	Choline_cytosol + Phosphatidylserine_cytosol
R02029	H2O + Phosphatidylglycerophosphate -> Orthophosphate + Phosphatidylglycerol	H2O_cytosol + Phosphatidylglycerophosphate_cytosol	----->	Orthophosphate_cytosol + Phosphatidylglycerol_cytosol
R01978	H2O + AcetylCoA + AcetoacetylCoA -> CoA + S3Hydroxy3methylglutarylCoA	H2O_cytosol + AcetylCoA_cytosol + AcetoacetylCoA_cytosol	----->	CoA_cytosol + S3Hydroxy3methylglutarylCoA_cytosol
R02082	2.0 H + 2.0 NADPH + S3Hydroxy3methylglutarylCoA -> 2.0 NADP + CoA + RMevalonate	2.0*H_cytosol + 2.0*NADPH_cytosol + S3Hydroxy3methylglutarylCoA_cytosol	----->	2.0*NADP_cytosol + CoA_cytosol + RMevalonate_cytosol
R02245	ATP + RMevalonate -> ADP + R5Phosphomevalonate	ATP_cytosol + RMevalonate_cytosol	----->	ADP_cytosol + R5Phosphomevalonate_cytosol

R03245	ATP + R5Phosphomevalonate -> ADP + R5Diphosphomevalonate	ATP_cytosol + R5Phosphomevalonate_cytosol	----->	ADP_cytosol + R5Diphosphomevalonate_cytosol
R01121	ATP + R5Diphosphomevalonate -> ADP + Orthophosphate + CO2 + Isopentenyldiphosphate	ATP_cytosol + R5Diphosphomevalonate_cytosol	----->	ADP_cytosol + Orthophosphate_cytosol + CO2_cytosol + Isopentenyldiphosphate_cytosol
R01658	Isopentenyldiphosphate + Dimethylallyldiphosphate -> Pyrophosphate + Geranyldiphosphate	Isopentenyldiphosphate_cytosol + Dimethylallyldiphosphate_cytosol	----->	Pyrophosphate_cytosol + Geranyldiphosphate_cytosol
R01123	Isopentenyldiphosphate <-> Dimethylallyldiphosphate	Isopentenyldiphosphate_cytosol	<---->	Dimethylallyldiphosphate_cytosol
R02003	Geranyldiphosphate + Isopentenyldiphosphate -> Pyrophosphate + transtransFarnesyldiphosphate	Isopentenyldiphosphate_cytosol + Geranyldiphosphate_cytosol	----->	Pyrophosphate_cytosol + transtransFarnesyldiphosphate_cytosol
R00702	2.0 transtransFarnesyldiphosphate -> H + Pyrophosphate + Presqualenediphosphate	2.0*transtransFarnesyldiphosphate_cytosol	----->	H_cytosol + Pyrophosphate_cytosol + Presqualenediphosphate_cytosol
R02872	H + NADPH + Presqualenediphosphate -> NADP + Squalene + Pyrophosphate	H_cytosol + NADPH_cytosol + Presqualenediphosphate_cytosol	----->	NADP_cytosol + Pyrophosphate_cytosol + Squalene_cytosol
R01456	H + NADPH + Cholesta57dien3betaol -> NADP + Cholesterol	H_cytosol + NADPH_cytosol + Cholesta57dien3betaol_cytosol	----->	NADP_cytosol + Cholesterol_cytosol
R03310	H + Oxygen + NADH + 5alphaCholest7en3betaol -> 2.0 H2O + NAD + Cholesta57dien3betaol	NADH_cytosol + H_cytosol + Oxygen_cytosol + 5alphaCholest7en3betaol_cytosol	----->	NAD_cytosol + 2.0*H2O_cytosol + Cholesta57dien3betaol_cytosol
R05703	H + NADPH + 5alphaCholesta724dien3betaol -> NADP + 5alphaCholest7en3betaol	H_cytosol + NADPH_cytosol + 5alphaCholesta724dien3betaol_cytosol	----->	NADP_cytosol + 5alphaCholest7en3betaol_cytosol
R04804	Zymosterol -> 5alphaCholesta724dien3betaol	Zymosterol_cytosol	----->	5alphaCholesta724dien3betaol_cytosol
R07496	4alphaMethylzymosterol -> Zymosterol	4alphaMethylzymosterol_cytosol	----->	Zymosterol_cytosol
R07495	NADP + 3Keto4methylzymosterol -> H + NADPH + 4alphaMethylzymosterol	NADP_cytosol + 3Keto4methylzymosterol_cytosol	----->	H_cytosol + NADPH_cytosol + 4alphaMethylzymosterol_cytosol
R07494	NADP + 4alphaMethylzymosterol4carboxylate -> H + NADPH + CO2 + 3Keto4methylzymosterol	NADP_cytosol + 4alphaMethylzymosterol4carboxylate_cytosol	----->	H_cytosol + NADPH_cytosol + CO2_cytosol + 3Keto4methylzymosterol_cytosol

R07509	H + NADPH + CO2 + 14Demethyllanosterol -> H2O + NADP + 4alphaMethylzymosterol4carboxylate	H_cytosol + NADPH_cytosol + CO2_cytosol + 14Demethyllanosterol_cytosol	----->	H2O_cytosol + NADP_cytosol + 4alphaMethylzymosterol4carboxylate_cytosol
R05639	NADP + 14Demethyllanosterol <-> 44Dimethyl5alphacholesta81424trien3betaol + H + NADPH	NADP_cytosol + 14Demethyllanosterol_cytosol	<---->	H_cytosol + NADPH_cytosol + 44Dimethyl5alphacholesta81424trien3betaol_cytosol
R05640	3.0 H + 3.0 NADPH + Lanosterol + 3.0 Oxygen -> Formate + 44Dimethyl5alphacholesta81424trien3betaol + 4.0 H2O + 3.0 NADP	3.0*H_cytosol + 3.0*NADPH_cytosol + 3.0*Oxygen_cytosol + Lanosterol_cytosol	----->	4.0*H2O_cytosol + 3.0*NADP_cytosol + 44Dimethyl5alphacholesta81424trien3betaol_cytosol + Formate_cytosol
R03199	S23Epoxysqualene -> Lanosterol	S23Epoxysqualene_cytosol	----->	Lanosterol_cytosol
R02874	H + NADPH + Oxygen + Squalene -> H2O + NADP + S23Epoxysqualene	H_cytosol + NADPH_cytosol + Squalene_cytosol + Oxygen_cytosol	----->	H2O_cytosol + NADP_cytosol + S23Epoxysqualene_cytosol
R02978	H + NADPH + 3Dehydrosphinganine -> NADP + Sphinganine	H_cytosol + NADPH_cytosol + 3Dehydrosphinganine_cytosol	----->	NADP_cytosol + Sphinganine_cytosol
R06517	AcylCoA + Sphinganine -> CoA + Dihydroceramide	AcylCoA_cytosol + Sphinganine_cytosol	----->	CoA_cytosol + Dihydroceramide_cytosol
R06519	Oxygen + Reducedacceptor + Dihydroceramide -> 2.0 H2O + Acceptor + NAcylsphingosine	Oxygen_cytosol + Dihydroceramide_cytosol + Reducedacceptor_cytosol	----->	2.0*H2O_cytosol + NAcylsphingosine_cytosol + Acceptor_cytosol
R01891	CDPcholine + NAcylsphingosine -> Sphingomyelin + CMP	CDPcholine_cytosol + NAcylsphingosine_cytosol	----->	CMP_cytosol + Sphingomyelin_cytosol
R01281	LSerine + PalmitoylCoA -> CO2 + CoA + 3Dehydrosphinganine	LSerine_cytosol + PalmitoylCoA_cytosol	----->	CO2_cytosol + CoA_cytosol + 3Dehydrosphinganine_cytosol
R01706	H2O + Hexadecanoylacp -> Acylcarrierprotein + Hexadecanoicacid	H2O_cytosol + Hexadecanoylacp_cytosol	----->	Hexadecanoicacid_cytosol + Acylcarrierprotein_cytosol
R01280	ATP + CoA + Hexadecanoicacid -> Pyrophosphate + AMP + PalmitoylCoA	ATP_cytosol + CoA_cytosol + Hexadecanoicacid_cytosol	----->	Pyrophosphate_cytosol + PalmitoylCoA_cytosol + AMP_cytosol
K00010	Acceptor + FADH2 <-> Reducedacceptor + FAD	FADH2_cytosol + Acceptor_cytosol	<---->	FAD_cytosol + Reducedacceptor_cytosol
K00010 [mitoc]	FADH2 [mitoc] + Acceptor [mitoc] <-> FAD [mitoc] + Reducedacceptor [mitoc]	FADH2_mitoc + Acceptor_mitoc	<---->	FAD_mitoc + Reducedacceptor_mitoc
R00742	ATP + AcetylCoA + HCO3 -> ADP + Orthophosphate + MalonylCoA	ATP_cytosol + AcetylCoA_cytosol + HCO3_cytosol	----->	ADP_cytosol + Orthophosphate_cytosol + MalonylCoA_cytosol

R01626	MalonylCoA + Acylcarrierprotein <-> Malonylacylcarrierprotein + CoA	Acylcarrierprotein_cytosol + MalonylCoA_cytosol	<---->	CoA_cytosol + Malonylacylcarrierprotein_cytosol
R04726	Malonylacylcarrierprotein + Dodecanoylacylcarrierprotein -> 3Oxotetradecanoylacp + CO2 + Acylcarrierprotein	Malonylacylcarrierprotein_cytosol + Dodecanoylacylcarrierprotein_cytosol	----->	CO2_cytosol + Acylcarrierprotein_cytosol + 3Oxotetradecanoylacp_cytosol
R04566	NADPH + 3Oxotetradecanoylacp -> NADP + 3R3Hydroxytetradecanoylacylcarrierprotein	NADPH_cytosol + 3Oxotetradecanoylacp_cytosol	----->	NADP_cytosol + 3R3Hydroxytetradecanoylacylcarrierprotein_cytosol
R04568	3R3Hydroxytetradecanoylacylcarrierprotein <-> H2O + transTetradec2enoylacp	3R3Hydroxytetradecanoylacylcarrierprotein_cytosol	<---->	H2O_cytosol + transTetradec2enoylacp_cytosol
R04967	NADPH + transTetradec2enoylacp -> NADP + Tetradecanoylacp	NADPH_cytosol + transTetradec2enoylacp_cytosol	----->	NADP_cytosol + Tetradecanoylacp_cytosol
R04968	Malonylacylcarrierprotein + Tetradecanoylacp -> CO2 + Acylcarrierprotein + 3Oxohexadecanoylacp	Malonylacylcarrierprotein_cytosol + Tetradecanoylacp_cytosol	----->	CO2_cytosol + Acylcarrierprotein_cytosol + 3Oxohexadecanoylacp_cytosol
R04543	H + NADPH + 3Oxohexadecanoylacp -> NADP + 3R3Hydroxypalmitoylacylcarrierprotein	H_cytosol + NADPH_cytosol + 3Oxohexadecanoylacp_cytosol	----->	NADP_cytosol + 3R3Hydroxypalmitoylacylcarrierprotein_cytosol
R04544	3R3Hydroxypalmitoylacylcarrierprotein <-> H2O + transHexadec2enoylacp	3R3Hydroxypalmitoylacylcarrierprotein_cytosol	<---->	H2O_cytosol + transHexadec2enoylacp_cytosol
R04970	NADPH + transHexadec2enoylacp -> NADP + Hexadecanoylacp	NADPH_cytosol + transHexadec2enoylacp_cytosol	----->	NADP_cytosol + Hexadecanoylacp_cytosol
R00238	2.0 AcetylCoA <-> CoA + AcetoacetylCoA	2.0*AcetylCoA_cytosol	<---->	CoA_cytosol + AcetoacetylCoA_cytosol
R01624	Acylcarrierprotein + AcetylCoA -> CoA + Acetylacylcarrierprotein	AcetylCoA_cytosol + Acylcarrierprotein_cytosol	----->	CoA_cytosol + Acetylacylcarrierprotein_cytosol
R04355	Malonylacylcarrierprotein + Acetylacylcarrierprotein -> CO2 + Acylcarrierprotein + Acetoacetylacp	Malonylacylcarrierprotein_cytosol + Acetylacylcarrierprotein_cytosol	----->	CO2_cytosol + Acylcarrierprotein_cytosol + Acetoacetylacp_cytosol
R04533	H + NADPH + Acetoacetylacp -> NADP + 3R3Hydroxybutanoylacylcarrierprotein	H_cytosol + NADPH_cytosol + Acetoacetylacp_cytosol	----->	NADP_cytosol + 3R3Hydroxybutanoylacylcarrierprotein_cytosol
R04428	3R3Hydroxybutanoylacylcarrierprotein <-> H2O + But2enoylacylcarrierprotein	3R3Hydroxybutanoylacylcarrierprotein_cytosol	<---->	H2O_cytosol + But2enoylacylcarrierprotein_cytosol

R04430	H + NADPH + But2enoylacylcarrierprotein -> NADP + Butyrylacp	H_cytosol + NADPH_cytosol + But2enoylacylcarrierprotein_cytosol	----->	NADP_cytosol + Butyrylacp_cytosol
R04952	Malonylacylcarrierprotein + Butyrylacp -> CO2 + Acylcarrierprotein + 3Oxohexanoylacp	Malonylacylcarrierprotein_cytosol + Butyrylacp_cytosol	----->	CO2_cytosol + Acylcarrierprotein_cytosol + 3Oxohexanoylacp_cytosol
R04953	NADPH + 3Oxohexanoylacp -> NADP + R3Hydroxyhexanoylacp	NADPH_cytosol + 3Oxohexanoylacp_cytosol	----->	NADP_cytosol + R3Hydroxyhexanoylacp_cytosol
R04954	R3Hydroxyhexanoylacp <-> H2O + transHex2enoylacp	R3Hydroxyhexanoylacp_cytosol	<---->	H2O_cytosol + transHex2enoylacp_cytosol
R04956	NADPH + transHex2enoylacp -> NADP + Hexanoylacp	NADPH_cytosol + transHex2enoylacp_cytosol	----->	NADP_cytosol + Hexanoylacp_cytosol
R04957	Malonylacylcarrierprotein + Hexanoylacp -> CO2 + Acylcarrierprotein + 3Oxooctanoylacp	Malonylacylcarrierprotein_cytosol + Hexanoylacp_cytosol	----->	CO2_cytosol + Acylcarrierprotein_cytosol + 3Oxooctanoylacp_cytosol
R04536	H + NADPH + 3Oxooctanoylacp -> NADP + 3R3Hydroxyoctanoylacylcarrierprotein	H_cytosol + NADPH_cytosol + 3Oxooctanoylacp_cytosol	----->	NADP_cytosol + 3R3Hydroxyoctanoylacylcarrierprotein_cytosol
R04537	3R3Hydroxyoctanoylacylcarrierprotein <-> H2O + transOct2enoylacp	3R3Hydroxyoctanoylacylcarrierprotein_cytosol	<---->	H2O_cytosol + transOct2enoylacp_cytosol
R04959	NADPH + transOct2enoylacp -> NADP + Octanoylacp	NADPH_cytosol + transOct2enoylacp_cytosol	----->	NADP_cytosol + Octanoylacp_cytosol
R04960	Malonylacylcarrierprotein + Octanoylacp -> CO2 + Acylcarrierprotein + 3Oxodecanoylacp	Malonylacylcarrierprotein_cytosol + Octanoylacp_cytosol	----->	CO2_cytosol + Acylcarrierprotein_cytosol + 3Oxodecanoylacp_cytosol
R04534	NADPH + 3Oxodecanoylacp -> NADP + 3R3Hydroxydecanoylacylcarrierprotein	NADPH_cytosol + 3Oxodecanoylacp_cytosol	----->	NADP_cytosol + 3R3Hydroxydecanoylacylcarrierprotein_cytosol
R04535	3R3Hydroxydecanoylacylcarrierprotein <-> H2O + transDec2enoylacp	3R3Hydroxydecanoylacylcarrierprotein_cytosol	<---->	H2O_cytosol + transDec2enoylacp_cytosol
R04962	NADPH + transDec2enoylacp -> NADP + Decanoylacp	NADPH_cytosol + transDec2enoylacp_cytosol	----->	NADP_cytosol + Decanoylacp_cytosol
R04725	H + NADPH + transDodec2enoylacp -> NADP + Dodecanoylacylcarrierprotein	H_cytosol + NADPH_cytosol + transDodec2enoylacp_cytosol	----->	NADP_cytosol + Dodecanoylacylcarrierprotein_cytosol
R04965	R3Hydroxydodecanoylacp <-> H2O + transDodec2enoylacp	R3Hydroxydodecanoylacp_cytosol	<---->	H2O_cytosol + transDodec2enoylacp_cytosol

R04964	NADPH + 3Oxododecanoylacp -> NADP + R3Hydroxydodecanoylacp	NADPH_cytosol + 3Oxododecanoylacp_cytosol	----->	NADP_cytosol + R3Hydroxydodecanoylacp_cytosol
R04963	Malonylacylcarrierprotein + Decanoylacp -> CO2 + Acylcarrierprotein + 3Oxododecanoylacp	Malonylacylcarrierprotein_cytosol + Decanoylacp_cytosol	----->	CO2_cytosol + Acylcarrierprotein_cytosol + 3Oxododecanoylacp_cytosol
K00011	2.0 NADPH + Malonylacylcarrierprotein + Hexadecanoylacp -> H2O + 2.0 NADP + CO2 + Acylcarrierprotein + Octadecanoylacylcarrierprotein	2.0*NADPH_cytosol + Hexadecanoylacp_cytosol + Malonylacylcarrierprotein_cytosol	----->	H2O_cytosol + 2.0*NADP_cytosol + CO2_cytosol + Acylcarrierprotein_cytosol + Octadecanoylacylcarrierprotein_cytosol
R03370	Oxygen + Octadecanoylacylcarrierprotein + Reducedacceptor -> 2.0 H2O + Acceptor + Oleoylacylcarrierprotein	Oxygen_cytosol + Reducedacceptor_cytosol + Octadecanoylacylcarrierprotein_cytosol	----->	2.0*H2O_cytosol + Acceptor_cytosol + Oleoylacylcarrierprotein_cytosol
R02814	H2O + Oleoylacylcarrierprotein -> Acylcarrierprotein + 9ZOctadecenoicacid	H2O_cytosol + Oleoylacylcarrierprotein_cytosol	----->	Acylcarrierprotein_cytosol + 9ZOctadecenoicacid_cytosol
K00008	9ZOctadecenoicacid <-> Fattyacid	9ZOctadecenoicacid_cytosol	<---->	Fattyacid_cytosol
K00009	ATP + CoA + Fattyacid -> Pyrophosphate + AMP + AcylCoA	ATP_cytosol + CoA_cytosol + Fattyacid_cytosol	----->	Pyrophosphate_cytosol + AcylCoA_cytosol + AMP_cytosol
R01049	ATP + DRibose5phosphate -> AMP + 5PhosphoalphaDribose1diphosphate	ATP_cytosol + DRibose5phosphate_cytosol	----->	AMP_cytosol + 5PhosphoalphaDribose1diphosphate_cytosol
R01072	H2O + LGlutamine + 5PhosphoalphaDribose1diphosphate -> LGlutamate + Pyrophosphate + 5Phosphoribosylamine	H2O_cytosol + 5PhosphoalphaDribose1diphosphate_cytosol + LGlutamine_cytosol	----->	LGlutamate_cytosol + Pyrophosphate_cytosol + 5Phosphoribosylamine_cytosol
R04144	ATP + Glycine + 5Phosphoribosylamine -> ADP + Orthophosphate + 5Phosphoribosylglycinamide	ATP_cytosol + Glycine_cytosol + 5Phosphoribosylamine_cytosol	----->	ADP_cytosol + Orthophosphate_cytosol + 5Phosphoribosylglycinamide_cytosol
R04325	10Formyltetrahydrofolate + 5Phosphoribosylglycinamide -> 5PhosphoribosylNformylglycinamide + Tetrahydrofolate	10Formyltetrahydrofolate_cytosol + 5Phosphoribosylglycinamide_cytosol	----->	Tetrahydrofolate_cytosol + 5PhosphoribosylNformylglycinamide_cytosol
R04463	H2O + LGlutamine + ATP + 5PhosphoribosylNformylglycinamide -> LGlutamate +	ATP_cytosol + H2O_cytosol + LGlutamine_cytosol + 5PhosphoribosylNformylglycinamide_cytosol	----->	ADP_cytosol + Orthophosphate_cytosol + LGlutamate_cytosol + 2FormamidoN15phosphoribosylacetamidine_cytosol

	2FormamidoN15phosphoribosylacetamidine + ADP + Orthophosphate			
R04208	2FormamidoN15phosphoribosylacetamidine + ATP -> ADP + Orthophosphate + Aminoimidazoleribotide	ATP_cytosol + 2FormamidoN15phosphoribosylacetamidine_cytosol	----->	ADP_cytosol + Orthophosphate_cytosol + Aminoimidazoleribotide_cytosol
R04209	15PhosphoDribosyl5amino4imidazolecarboxylate <-> CO2 + Aminoimidazoleribotide	15PhosphoDribosyl5amino4imidazolecarboxylate_cytosol	<---->	CO2_cytosol + Aminoimidazoleribotide_cytosol
R04591	ATP + LAspartate + 15PhosphoDribosyl5amino4imidazolecarboxylate <-> ADP + Orthophosphate + 15Phosphoribosyl5amino4Nsuccinocarboxamideimidazole	ATP_cytosol + LAspartate_cytosol + 15PhosphoDribosyl5amino4imidazolecarboxylate_cytosol	<---->	ADP_cytosol + Orthophosphate_cytosol + 15Phosphoribosyl5amino4Nsuccinocarboxamideimidazole_cytosol
R04559	15Phosphoribosyl5amino4Nsuccinocarboxamideimidazole <-> 15Phosphoribosyl5amino4imidazolecarboxamide + Fumarate	15Phosphoribosyl5amino4Nsuccinocarboxamideimidazole_cytosol	<---->	Fumarate_cytosol + 15Phosphoribosyl5amino4imidazolecarboxamide_cytosol
R04560	15Phosphoribosyl5amino4imidazolecarboxamide + 10Formyltetrahydrofolate <-> Tetrahydrofolate + 15Phosphoribosyl5formamido4imidazolecarboxamide	10Formyltetrahydrofolate_cytosol + 15Phosphoribosyl5amino4imidazolecarboxamide_cytosol	<---->	Tetrahydrofolate_cytosol + 15Phosphoribosyl5formamido4imidazolecarboxamide_cytosol
R01127	H2O + IMP <-> 15Phosphoribosyl5formamido4imidazolecarboxamide	H2O_cytosol + IMP_cytosol	<---->	15Phosphoribosyl5formamido4imidazolecarboxamide_cytosol
R01135	LAspartate + GTP + IMP <-> Orthophosphate + N612DicarboxyethylAMP + GDP	LAspartate_cytosol + IMP_cytosol + GTP_cytosol	<---->	Orthophosphate_cytosol + GDP_cytosol + N612DicarboxyethylAMP_cytosol
R01083	N612DicarboxyethylAMP <-> Fumarate + AMP	N612DicarboxyethylAMP_cytosol	<---->	Fumarate_cytosol + AMP_cytosol
R01130	H2O + NAD + IMP -> H + NADH + Xanthosine5phosphate	NAD_cytosol + H2O_cytosol + IMP_cytosol	----->	NADH_cytosol + H_cytosol + Xanthosine5phosphate_cytosol
R01231	H2O + LGlutamine + ATP + Xanthosine5phosphate -> LGlutamate + GMP + Pyrophosphate + AMP	ATP_cytosol + H2O_cytosol + LGlutamine_cytosol + Xanthosine5phosphate_cytosol	----->	LGlutamate_cytosol + Pyrophosphate_cytosol + AMP_cytosol + GMP_cytosol

R00127	ATP + AMP -> 2.0 ADP	ATP_cytosol + AMP_cytosol	----->	2.0*ADP_cytosol
R01857	ATP + dGDP <-> ADP + dGTP	ATP_cytosol + dGDP_cytosol	<---->	ADP_cytosol + dGTP_cytosol
R01137	ATP + dADP <-> ADP + dATP	ATP_cytosol + dADP_cytosol	<---->	ADP_cytosol + dATP_cytosol
EF0002	H2O + ATP <-> ADP + Orthophosphate	ATP_cytosol + H2O_cytosol	<---->	ADP_cytosol + Orthophosphate_cytosol
R00332	ATP + GMP -> ADP + GDP	ATP_cytosol + GMP_cytosol	----->	ADP_cytosol + GDP_cytosol
R00330	ATP + GDP <-> ADP + GTP	ATP_cytosol + GDP_cytosol	<---->	ADP_cytosol + GTP_cytosol
R01870	5PhosphoalphaDribose1diphosphate + Orotate -> Pyrophosphate + Orotidine5phosphate	5PhosphoalphaDribose1diphosphate_cytosol + Orotate_cytosol	----->	Pyrophosphate_cytosol + Orotidine5phosphate_cytosol
R00965	Orotidine5phosphate -> CO2 + UMP	Orotidine5phosphate_cytosol	----->	CO2_cytosol + UMP_cytosol
R00158	ATP + UMP <-> ADP + UDP	ATP_cytosol + UMP_cytosol	<---->	ADP_cytosol + UDP_cytosol
R00156	ATP + UDP <-> ADP + UTP	ATP_cytosol + UDP_cytosol	<---->	ADP_cytosol + UTP_cytosol
R00573	H2O + LGlutamine + ATP + UTP -> LGlutamate + ADP + Orthophosphate + CTP	ATP_cytosol + H2O_cytosol + UTP_cytosol + LGlutamine_cytosol	----->	ADP_cytosol + Orthophosphate_cytosol + LGlutamate_cytosol + CTP_cytosol
R00570	ATP + CDP <-> ADP + CTP	ATP_cytosol + CDP_cytosol	<---->	ADP_cytosol + CTP_cytosol
R00512	ATP + CMP <-> ADP + CDP	ATP_cytosol + CMP_cytosol	<---->	ADP_cytosol + CDP_cytosol
R02024	CDP + Thioredoxin -> H2O + dCDP + Oxidizedthioredoxin	CDP_cytosol + Thioredoxin_cytosol	----->	H2O_cytosol + Oxidizedthioredoxin_cytosol + dCDP_cytosol
R02326	ATP + dCDP <-> ADP + dCTP	ATP_cytosol + dCDP_cytosol	<---->	ADP_cytosol + dCTP_cytosol
R02018	UDP + Thioredoxin -> H2O + Oxidizedthioredoxin + dUDP	UDP_cytosol + Thioredoxin_cytosol	----->	H2O_cytosol + Oxidizedthioredoxin_cytosol + dUDP_cytosol
R02098	ATP + dUMP <-> ADP + dUDP	ATP_cytosol + dUMP_cytosol	<---->	ADP_cytosol + dUDP_cytosol
R02101	510Methylenetetrahydrofolate + dUMP <-> Dihydrofolate + dTMP	510Methylenetetrahydrofolate_cytosol + dUMP_cytosol	<---->	Dihydrofolate_cytosol + dTMP_cytosol
R02094	ATP + dTMP <-> ADP + dTDP	ATP_cytosol + dTMP_cytosol	<---->	ADP_cytosol + dTDP_cytosol
R02093	ATP + dTDP <-> ADP + dTTP	ATP_cytosol + dTDP_cytosol	<---->	ADP_cytosol + dTTP_cytosol
R01867	Oxygen + SDihydroorotate <-> Orotate + H2O2	Oxygen_cytosol + SDihydroorotate_cytosol	<---->	Orotate_cytosol + H2O2_cytosol
R01993	H2O + SDihydroorotate <-> NCarbamoylLaspartate	H2O_cytosol + SDihydroorotate_cytosol	<---->	NCarbamoylLaspartate_cytosol
R01397	LAspartate + Carbamoylphosphate -> Orthophosphate + NCarbamoylLaspartate	LAspartate_cytosol + Carbamoylphosphate_cytosol	----->	Orthophosphate_cytosol + NCarbamoylLaspartate_cytosol

R00575	H2O + LGlutamine + 2.0 ATP + HCO3 -> LGlutamate + 2.0 ADP + Orthophosphate + Carbamoylphosphate	2.0*ATP_cytosol + H2O_cytosol + HCO3_cytosol + LGlutamine_cytosol	----->	2.0*ADP_cytosol + Orthophosphate_cytosol + LGlutamate_cytosol + Carbamoylphosphate_cytosol
R02019	Thioredoxin + GDP -> H2O + dGDP + Oxidizedthioredoxin	GDP_cytosol + Thioredoxin_cytosol	----->	H2O_cytosol + dGDP_cytosol + Oxidizedthioredoxin_cytosol
R02016	H + NADPH + Oxidizedthioredoxin -> NADP + Thioredoxin	H_cytosol + NADPH_cytosol + Oxidizedthioredoxin_cytosol	----->	NADP_cytosol + Thioredoxin_cytosol
R02017	ADP + Thioredoxin -> H2O + Oxidizedthioredoxin + dADP	ADP_cytosol + Thioredoxin_cytosol	----->	H2O_cytosol + dADP_cytosol + Oxidizedthioredoxin_cytosol
gCat07	H2O + CO2 <-> H + HCO3	H2O_cytosol + CO2_cytosol	<---->	H_cytosol + HCO3_cytosol
gCat07 [mitoc]	CO2 [mitoc] + H2O [mitoc] <-> H [mitoc] + HCO3 [mitoc]	CO2_mitoc + H2O_mitoc	<---->	H_mitoc + HCO3_mitoc
R00004	H2O + Pyrophosphate -> 2.0 Orthophosphate	H2O_cytosol + Pyrophosphate_cytosol	----->	2.0*Orthophosphate_cytosol
R00431	Oxaloacetate + GTP -> CO2 + Phosphoenolpyruvate + GDP	Oxaloacetate_cytosol + GTP_cytosol	----->	Phosphoenolpyruvate_cytosol + CO2_cytosol + GDP_cytosol
R00009	2.0 H2O2 -> 2.0 H2O + Oxygen	2.0*H2O2_cytosol	----->	2.0*H2O_cytosol + Oxygen_cytosol
MEMB0034	myoInositol [ext] -> myoInositol	myoInositol_ext	----->	myoInositol_cytosol
MEMB0035	Ethanolamine [ext] -> Ethanolamine	Ethanolamine_ext	----->	Ethanolamine_cytosol
MEMB0033	Choline [ext] -> Choline	Choline_ext	----->	Choline_cytosol
MEMB0030	Formate [ext] <-> Formate	Formate_ext	<---->	Formate_cytosol
MEMB0026	LTyrosine [ext] -> LTyrosine	LTyrosine_ext	----->	LTyrosine_cytosol
MEMB0025	LPhenylalanine [ext] -> LPhenylalanine	LPhenylalanine_ext	----->	LPhenylalanine_cytosol
MEMB0028	LHistidine [ext] -> LHistidine	LHistidine_ext	----->	LHistidine_cytosol
MEMB0027	LTryptophan [ext] -> LTryptophan	LTryptophan_ext	----->	LTryptophan_cytosol
MEMB0022	LLysine [ext] -> LLysine	LLysine_ext	----->	LLysine_cytosol
MEMB0021	LThreonine [ext] -> LThreonine	LThreonine_ext	----->	LThreonine_cytosol
MEMB0024	LMethionine [ext] -> LMethionine	LMethionine_ext	----->	LMethionine_cytosol
MEMB0023	LCysteine [ext] -> LCysteine	LCysteine_ext	----->	LCysteine_cytosol
MEMB0019	LLeucine [ext] -> LLeucine	LLeucine_ext	----->	LLeucine_cytosol
MEMB0018	LIsoleucine [ext] -> LIsoleucine	LIsoleucine_ext	----->	LIsoleucine_cytosol
MEMB0017	LValine [ext] -> LValine	LValine_ext	----->	LValine_cytosol
MEMB0016	LProline [ext] -> LProline	LProline_ext	----->	LProline_cytosol

MEMB0011	LSerine [ext] -> LSerine	LSerine_ext	----->	LSerine_cytosol
MEMB0010	LGlutamate [ext] -> LGlutamate	LGlutamate_ext	----->	LGlutamate_cytosol
MEMB0008	LAsparagine <-> LAsparagine [ext]	LAsparagine_cytosol	<---->	LAsparagine_ext
MEMB0007	LAspartate [ext] -> LAspartate	LAspartate_ext	----->	LAspartate_cytosol
MEMB0009	LGlutamine [ext] <-> LGlutamine	LGlutamine_ext	<---->	LGlutamine_cytosol
MEMB0013	Glycine <-> Glycine [ext]	Glycine_cytosol	<---->	Glycine_ext
MEMB0006	LAlanine -> LAlanine [ext]	LAlanine_cytosol	----->	LAlanine_ext
MEMB0020	LArginine [ext] -> LArginine	LArginine_ext	----->	LArginine_cytosol
MEMB0014	H [ext] <-> H	H_ext	<---->	H_cytosol
MEMB0012	NH3 [ext] <-> NH3	NH3_ext	<---->	NH3_cytosol
MEMB0004	SLactate [ext] <-> SLactate	SLactate_ext	<---->	SLactate_cytosol
MEMB0003	CO2 [ext] <-> CO2	CO2_ext	<---->	CO2_cytosol
MEMB0001	alphaDGlucose [ext] <-> alphaDGlucose	alphaDGlucose_ext	<---->	alphaDGlucose_cytosol
MEMB0005	Oxygen [ext] <-> Oxygen	Oxygen_ext	<---->	Oxygen_cytosol
MEMB0039	Orthophosphate [ext] <-> Orthophosphate	Orthophosphate_ext	<---->	Orthophosphate_cytosol
MEMBBIO	BIOMASS -> BIOMASS [ext]	BIOMASS_cytosol	----->	BIOMASS_ext
MEMBH2O	H2O [ext] <-> H2O	H2O_ext	<---->	H2O_cytosol
TF0001	Pyruvate <-> Pyruvate [mitoc]	Pyruvate_cytosol	<---->	Pyruvate_mitoc
TF0003	LGlutamate <-> LGlutamate [mitoc]	LGlutamate_cytosol	<---->	LGlutamate_mitoc
TF0009	CO2 <-> CO2 [mitoc]	CO2_cytosol	<---->	CO2_mitoc
TF0008	Oxygen <-> Oxygen [mitoc]	Oxygen_cytosol	<---->	Oxygen_mitoc
TF0013	H2O <-> H2O [mitoc]	H2O_cytosol	<---->	H2O_mitoc
TF0014	NH3 <-> NH3 [mitoc]	NH3_cytosol	<---->	NH3_mitoc
TF0012	H <-> H [mitoc]	H_cytosol	<---->	H_mitoc
TF0010	ATP + ADP [mitoc] <-> ADP + ATP [mitoc]	ATP_cytosol + ADP_mitoc	<---->	ADP_cytosol + ATP_mitoc
TF0005	LAlanine <-> LAlanine [mitoc]	LAlanine_cytosol	<---->	LAlanine_mitoc
TF0004	LGlutamine <-> LGlutamine [mitoc]	LGlutamine_cytosol	<---->	LGlutamine_mitoc
TF0006	SMalate + 2Oxoglutarate [mitoc] <-> SMalate [mitoc] + 2Oxoglutarate	2Oxoglutarate_mitoc + SMalate_cytosol	<---->	2Oxoglutarate_cytosol + SMalate_mitoc
TF0002	Citrate <-> Citrate [mitoc]	Citrate_cytosol	<---->	Citrate_mitoc
TF0032	Orthophosphate <-> Orthophosphate [mitoc]	Orthophosphate_cytosol	<---->	Orthophosphate_mitoc

TF0007	LGlutamate + LAspartate [mitoc] <-> LAspartate + LGlutamate [mitoc]	LGlutamate_cytosol + LAspartate_mitoc	<---->	LGlutamate_mitoc + LAspartate_cytosol
TF0023	Glycine <-> Glycine [mitoc]	Glycine_cytosol	<---->	Glycine_mitoc
TF0026	L2Aminoadipate6semialdehyde <-> L2Aminoadipate6semialdehyde [mitoc]	L2Aminoadipate6semialdehyde_cytosol	<---->	L2Aminoadipate6semialdehyde_mitoc
TF0027	2Oxoadipate <-> 2Oxoadipate [mitoc]	2Oxoadipate_cytosol	<---->	2Oxoadipate_mitoc
TF0028	Acetoacetate <-> Acetoacetate [mitoc]	Acetoacetate_cytosol	<---->	Acetoacetate_mitoc
BIOM_AA	0.0960 LAlanine +0.0636 LArginine + 0.0485 LAspartate + 0.0394 LAsparagine + 0.0283 LCysteine + 0.0525 LGlutamine + 0.0646 LGlutamate + 0.0788 Glycine + 0.0222 LHistidine + 0.0525 LIsoleucine + 0.0889 LLeucine + 0.0899 LLysine + 0.0202 LMethionine + 0.0212 LPhenylalanine + 0.0283 LProline + 0.0576 LSerine + 0.0616 LThreonine + 0.0061 LTryptophan + 0.0202 LTyrosine + 0.0596 LValine + 4.306 ATP + 3.306 H2O -> PROT + 4.306 ADP + 4.306 Orthophosphate	4.306*ATP_cytosol + 3.306*H2O_cytosol + 0.0646*LGlutamate_cytosol + 0.0576*LSerine_cytosol + 0.0788*Glycine_cytosol + 0.0283*LProline_cytosol + 0.096*LAlanine_cytosol + 0.0485*LAspartate_cytosol + 0.0394*LAsparagine_cytosol + 0.0525*LGlutamine_cytosol + 0.0202*LTyrosine_cytosol + 0.0212*LPhenylalanine_cytosol + 0.0222*LHistidine_cytosol + 0.0061*LTryptophan_cytosol + 0.0899*LLysine_cytosol + 0.0616*LThreonine_cytosol + 0.0202*LMethionine_cytosol + 0.0283*LCysteine_cytosol + 0.0889*LLeucine_cytosol + 0.0525*LIsoleucine_cytosol + 0.0596*LValine_cytosol + 0.0636*LArginine_cytosol	----->	4.306*ADP_cytosol + 4.306*Orthophosphate_cytosol + PROT_cytosol
BIOM_dAMP	dATP + 2 H2O -> dAMP + 2 Orthophosphate	2.0*H2O_cytosol + dATP_cytosol	----->	2.0*Orthophosphate_cytosol + dAMP_cytosol
BIOM_dCMP	dCTP + 2 H2O -> dCMP + 2 Orthophosphate	2.0*H2O_cytosol + dCTP_cytosol	----->	2.0*Orthophosphate_cytosol + dCMP_cytosol

BIOM_dGMP	dGTP + 2 H2O -> dGMP + 2 Orthophosphate	2.0*H2O_cytosol + dGTP_cytosol	----->	2.0*Orthophosphate_cytosol + dGMP_cytosol
BIOM_dTMP	dTTP + 2 H2O -> dTMP + 2 Orthophosphate	2.0*H2O_cytosol + dTTP_cytosol	----->	2.0*Orthophosphate_cytosol + dTMP_cytosol
BIOM_AMP	ATP + 2 H2O -> AMP + 2 Orthophosphate	ATP_cytosol + 2.0*H2O_cytosol	----->	2.0*Orthophosphate_cytosol + AMP_cytosol
BIOM_CMP	CTP+ 2 H2O -> CMP + 2 Orthophosphate	2.0*H2O_cytosol + CTP_cytosol	----->	2.0*Orthophosphate_cytosol + CMP_cytosol
BIOM_GMP	GTP +2 H2O -> GMP + 2 Orthophosphate	2.0*H2O_cytosol + GTP_cytosol	----->	2.0*Orthophosphate_cytosol + GMP_cytosol
BIOM_UMP	UTP + 2 H2O -> UMP + 2 Orthophosphate	2.0*H2O_cytosol + UTP_cytosol	----->	2.0*Orthophosphate_cytosol + UMP_cytosol
BIOM_DNA	0.3 dAMP + 0.2 dCMP + 0.2 dGMP + 0.3 dTMP + 1.372 ATP + 1.372 H2O -> DNA + 1.372 ADP + 1.372 Orthophosphate	1.372*ATP_cytosol + 1.372*H2O_cytosol + 0.3*dTMP_cytosol + 0.3*dAMP_cytosol + 0.2*dCMP_cytosol + 0.2*dGMP_cytosol	----->	1.372*ADP_cytosol + 1.372*Orthophosphate_cytosol + DNA_cytosol
BIOM_RNA	0.18 AMP + 0.30 CMP + 0.34 GMP + 0.18 UMP + 0.4 ATP + 0.4 H2O -> RNA + 0.4 ADP + 0.4 Orthophosphate	0.4*ATP_cytosol + 0.4*H2O_cytosol + 0.3*CMP_cytosol + 0.18*AMP_cytosol + 0.34*GMP_cytosol + 0.18*UMP_cytosol	----->	0.4*ADP_cytosol + 0.4*Orthophosphate_cytosol + RNA_cytosol
BIOM_LIP	0.1315 Cholesterol + 0.5006 Phosphatidylcholine + 0.1898 Phosphatidylethanolamine + 0.0688 1PhosphatidylDmyoinositol + 0.0189 Phosphatidylserine + 0.0096 Phosphatidylglycerol + 0.0204 Cardiolipin + 0.0605 Sphingomyelin -> LIP	0.0204*Cardiolipin_cytosol + 0.0096*Phosphatidylglycerol_cytosol + 0.0688*1PhosphatidylDmyoinositol_cytosol + 0.1898*Phosphatidylethanolamine_cytosol + 0.5006*Phosphatidylcholine_cytosol + 0.0189*Phosphatidylserine_cytosol + 0.1315*Cholesterol_cytosol + 0.0605*Sphingomyelin_cytosol	----->	LIP_cytosol
BIOM_CARBO	Amylose -> CAR	Amylose_cytosol	----->	CAR_cytosol
BIOM_T	6.902 PROT + 0.061 DNA + 0.188 RNA + 0.114 LIP + 0.465 CAR -> BIOMASS	6.902*PROT_cytosol + 0.061*DNA_cytosol + 0.188*RNA_cytosol + 0.114*LIP_cytosol + 0.465*CAR_cytosol	----->	BIOMASS_cytosol
R02918	3.3 ATP + tRNATyr + LTyrosine -> 2.3 ADP + 2.3 Orthophosphate + Pyrophosphate + AMP + LTyrosyltRNATyr	3.3*ATP_cytosol + LTyrosine_cytosol + tRNATyr_cytosol	----->	2.3*ADP_cytosol + 2.3*Orthophosphate_cytosol + Pyrophosphate_cytosol + AMP_cytosol + LTyrosyltRNATyr_cytosol

R03038	3.3 ATP + LAlanine + tRNAAla -> 2.3 ADP + 2.3 Orthophosphate + Pyrophosphate + AMP + LAlanyltRNA	3.3*ATP_cytosol + LAlanine_cytosol + tRNAAla_cytosol	----->	2.3*ADP_cytosol + 2.3*Orthophosphate_cytosol + Pyrophosphate_cytosol + AMP_cytosol + LAlanyltRNA_cytosol
R03665	3.3 ATP + LValine + tRNAVal -> 2.3 ADP + 2.3 Orthophosphate + Pyrophosphate + AMP + LValyltRNAVal	3.3*ATP_cytosol + LValine_cytosol + tRNAVal_cytosol	----->	2.3*ADP_cytosol + 2.3*Orthophosphate_cytosol + Pyrophosphate_cytosol + AMP_cytosol + LValyltRNAVal_cytosol
R03661	3.3 ATP + LProline + tRNAPro -> 2.3 ADP + 2.3 Orthophosphate + Pyrophosphate + AMP + LProlyltRNAPro	3.3*ATP_cytosol + LProline_cytosol + tRNAPro_cytosol	----->	2.3*ADP_cytosol + 2.3*Orthophosphate_cytosol + Pyrophosphate_cytosol + AMP_cytosol + LProlyltRNAPro_cytosol
R03662	LSerine + 3.3 ATP + tRNASer -> 2.3 ADP + 2.3 Orthophosphate + Pyrophosphate + AMP + LSeryltRNASer	3.3*ATP_cytosol + LSerine_cytosol + tRNASer_cytosol	----->	2.3*ADP_cytosol + 2.3*Orthophosphate_cytosol + Pyrophosphate_cytosol + AMP_cytosol + LSeryltRNASer_cytosol
R03663	3.3 ATP + LThreonine + tRNAThr -> 2.3 ADP + 2.3 Orthophosphate + Pyrophosphate + AMP + LThreonyltRNAThr	3.3*ATP_cytosol + LThreonine_cytosol + tRNAThr_cytosol	----->	2.3*ADP_cytosol + 2.3*Orthophosphate_cytosol + Pyrophosphate_cytosol + AMP_cytosol + LThreonyltRNAThr_cytosol
R03664	3.3 ATP + LTryptophan + tRNATrp -> 2.3 ADP + 2.3 Orthophosphate + Pyrophosphate + AMP + LTryptophanyltRNATrp	3.3*ATP_cytosol + LTryptophan_cytosol + tRNATrp_cytosol	----->	2.3*ADP_cytosol + 2.3*Orthophosphate_cytosol + Pyrophosphate_cytosol + AMP_cytosol + LTryptophanyltRNATrp_cytosol
R03660	3.3 ATP + LPhenylalanine + tRNAPhe -> 2.3 ADP + 2.3 Orthophosphate + Pyrophosphate + AMP + LPhenylalanyltRNAPhe	3.3*ATP_cytosol + LPhenylalanine_cytosol + tRNAPhe_cytosol	----->	2.3*ADP_cytosol + 2.3*Orthophosphate_cytosol + Pyrophosphate_cytosol + AMP_cytosol + LPhenylalanyltRNAPhe_cytosol
R03659	3.3 ATP + LMethionine + tRNAMet -> 2.3 ADP + 2.3 Orthophosphate + Pyrophosphate + AMP + LMethionyltRNA	3.3*ATP_cytosol + LMethionine_cytosol + tRNAMet_cytosol	----->	2.3*ADP_cytosol + 2.3*Orthophosphate_cytosol + Pyrophosphate_cytosol + AMP_cytosol + LMethionyltRNA_cytosol
R03658	3.3 ATP + LLysine + tRNALys -> 2.3 ADP + 2.3 Orthophosphate + Pyrophosphate + AMP + LLysyltRNA	3.3*ATP_cytosol + LLysine_cytosol + tRNALys_cytosol	----->	2.3*ADP_cytosol + 2.3*Orthophosphate_cytosol + Pyrophosphate_cytosol + AMP_cytosol + LLysyltRNA_cytosol
R03655	3.3 ATP + LHistidine + tRNAHis -> 2.3 ADP + 2.3 Orthophosphate + Pyrophosphate + AMP + LHistidyltRNAHis	3.3*ATP_cytosol + LHistidine_cytosol + tRNAHis_cytosol	----->	2.3*ADP_cytosol + 2.3*Orthophosphate_cytosol + Pyrophosphate_cytosol + AMP_cytosol + LHistidyltRNAHis_cytosol

R03654	3.3 ATP + Glycine + tRNAGl -> 2.3 ADP + 2.3 Orthophosphate + Pyrophosphate + AMP + GlycyltRNAGly	3.3*ATP_cytosol + Glycine_cytosol + tRNAGl_cytosol	----->	2.3*ADP_cytosol + 2.3*Orthophosphate_cytosol + Pyrophosphate_cytosol + AMP_cytosol + GlycyltRNAGly_cytosol
R03657	3.3 ATP + LLeucine + tRNALeu -> 2.3 ADP + 2.3 Orthophosphate + Pyrophosphate + AMP + LLeucyltRNA	3.3*ATP_cytosol + LLeucine_cytosol + tRNALeu_cytosol	----->	2.3*ADP_cytosol + 2.3*Orthophosphate_cytosol + Pyrophosphate_cytosol + AMP_cytosol + LLeucyltRNA_cytosol
R03656	3.3 ATP + LIsoleucine + tRNAIle -> 2.3 ADP + 2.3 Orthophosphate + Pyrophosphate + AMP + LIsoleucyltRNAIle	3.3*ATP_cytosol + LIsoleucine_cytosol + tRNAIle_cytosol	----->	2.3*ADP_cytosol + 2.3*Orthophosphate_cytosol + Pyrophosphate_cytosol + AMP_cytosol + LIsoleucyltRNAIle_cytosol
R03650	3.3 ATP + LCysteine + tRNACys -> 2.3 ADP + 2.3 Orthophosphate + Pyrophosphate + AMP + LCysteinyltRNACys	3.3*ATP_cytosol + LCysteine_cytosol + tRNACys_cytosol	----->	2.3*ADP_cytosol + 2.3*Orthophosphate_cytosol + Pyrophosphate_cytosol + AMP_cytosol + LCysteinyltRNACys_cytosol
R03648	3.3 ATP + LAsparagine + tRNAAsn -> 2.3 ADP + 2.3 Orthophosphate + Pyrophosphate + AMP + LAsparaginyltRNAAsn	3.3*ATP_cytosol + LAsparagine_cytosol + tRNAAsn_cytosol	----->	2.3*ADP_cytosol + 2.3*Orthophosphate_cytosol + Pyrophosphate_cytosol + AMP_cytosol + LAsparaginyltRNAAsn_cytosol
R03647	3.3 ATP + LAspartate + tRNAAsn -> 2.3 ADP + 2.3 Orthophosphate + Pyrophosphate + AMP + LAspartyltRNAAsn	3.3*ATP_cytosol + LAspartate_cytosol + tRNAAsn_cytosol	----->	2.3*ADP_cytosol + 2.3*Orthophosphate_cytosol + Pyrophosphate_cytosol + AMP_cytosol + LAspartyltRNAAsn_cytosol
R03646	3.3 ATP + LArginine + tRNAArg -> 2.3 ADP + 2.3 Orthophosphate + Pyrophosphate + AMP + LArginyltRNAArg	3.3*ATP_cytosol + LArginine_cytosol + tRNAArg_cytosol	----->	2.3*ADP_cytosol + 2.3*Orthophosphate_cytosol + Pyrophosphate_cytosol + AMP_cytosol + LArginyltRNAArg_cytosol
R03651	LGlutamate + 3.3 ATP + tRNAGln -> 2.3 ADP + 2.3 Orthophosphate + Pyrophosphate + AMP + LGlutamyltRNAGln	3.3*ATP_cytosol + LGlutamate_cytosol + tRNAGln_cytosol	----->	2.3*ADP_cytosol + 2.3*Orthophosphate_cytosol + Pyrophosphate_cytosol + AMP_cytosol + LGlutamyltRNAGln_cytosol
R03652	LGlutamine + 3.3 ATP + tRNAGln -> 2.3 ADP + 2.3 Orthophosphate + Pyrophosphate + AMP + GlutaminyltRNA	3.3*ATP_cytosol + LGlutamine_cytosol + tRNAGln_cytosol	----->	2.3*ADP_cytosol + 2.3*Orthophosphate_cytosol + Pyrophosphate_cytosol + AMP_cytosol + GlutaminyltRNA_cytosol
R01168	LHistidine <-> NH3 + Urocanate	LHistidine_cytosol	<---->	NH3_cytosol + Urocanate_cytosol
R02914	H2O + Urocanate -> 4Imidazolone5propanoate	H2O_cytosol + Urocanate_cytosol	----->	4Imidazolone5propanoate_cytosol
R00069	Oxygen + 2.0 4Imidazolone5propanoate -> 2.0 Hydantoin5propionate	Oxygen_cytosol + 2.0*4Imidazolone5propanoate_cytosol	----->	2.0*Hydantoin5propionate_cytosol

gCat03	Oxygen + Hydantoin5propionate -> NCarbamylLglutamate	Oxygen_cytosol + Hydantoin5propionate_cytosol	----->	NCarbamylLglutamate_cytosol
gCat04	NCarbamylLglutamate -> NH3 + LGlutamate + CO2	NCarbamylLglutamate_cytosol	----->	CO2_cytosol + LGlutamate_cytosol + NH3_cytosol
R00551	H2O + LArginine -> Urea + LOrnithine	H2O_cytosol + LArginine_cytosol	----->	LOrnithine_cytosol + Urea_cytosol
DEGARG_added	LOrnithine + H [mitoc] -> LOrnithine [mitoc]	H_mitoc + LOrnithine_cytosol	----->	LOrnithine_mitoc
R00667 [mitoc]	2Oxoglutarate [mitoc] + LOrnithine [mitoc] <-> LGlutamate [mitoc] + LGlutamate5semialdehyde [mitoc]	2Oxoglutarate_mitoc + LOrnithine_mitoc	<---->	LGlutamate_mitoc + LGlutamate5semialdehyde_mitoc
MEMBUREA	Urea [ext] <-> Urea	Urea_ext	<---->	Urea_cytosol
DEGCYS1_added	LCysteine + Oxygen -> 3SulfinoLAlanine	Oxygen_cytosol + LCysteine_cytosol	----->	3SulfinoLAlanine_cytosol
DEGCYS2_added	3SulfinoLAlanine + 2Oxoglutarate -> 3Sulfinylpyruvate + LGlutamate	2Oxoglutarate_cytosol + 3SulfinoLAlanine_cytosol	----->	LGlutamate_cytosol + 3Sulfinylpyruvate_cytosol
DEGCYS3_added	3Sulfinylpyruvate -> Pyruvate + SO2	3Sulfinylpyruvate_cytosol	----->	Pyruvate_cytosol + SO2_cytosol
DEGCYS4_added	SO2 -> SO2 [ext]	SO2_cytosol	----->	SO2_ext
R00734	2Oxoglutarate + LTyrosine <-> LGlutamate + 34Hydroxyphenylpyruvate	2Oxoglutarate_cytosol + LTyrosine_cytosol	<---->	LGlutamate_cytosol + 34Hydroxyphenylpyruvate_cytosol
R02521	Oxygen + 34Hydroxyphenylpyruvate -> CO2 + Homogentisate	Oxygen_cytosol + 34Hydroxyphenylpyruvate_cytosol	----->	CO2_cytosol + Homogentisate_cytosol
R02519	Oxygen + Homogentisate -> 4Maleylacetoacetate	Oxygen_cytosol + Homogentisate_cytosol	----->	4Maleylacetoacetate_cytosol
R03181	4Maleylacetoacetate -> 4Fumarylacetoacetate	4Maleylacetoacetate_cytosol	----->	4Fumarylacetoacetate_cytosol
R01364	H2O + 4Fumarylacetoacetate -> Fumarate + Acetoacetate	H2O_cytosol + 4Fumarylacetoacetate_cytosol	----->	Fumarate_cytosol + Acetoacetate_cytosol
TF0017	LValine <-> LValine [mitoc]	LValine_cytosol	<---->	LValine_mitoc
R01214 [mitoc]	2Oxoglutarate [mitoc] + LValine [mitoc] <-> LGlutamate [mitoc] + 3Methyl2oxobutanoicacid [mitoc]	2Oxoglutarate_mitoc + LValine_mitoc	<---->	LGlutamate_mitoc + 3Methyl2oxobutanoicacid_mitoc

R02661 [mitoc]	FAD [mitoc] + 2MethylpropanoylCoA [mitoc] -> FADH2 [mitoc] + 2Methylprop2enoylCoA [mitoc]	FAD_mitoc + 2MethylpropanoylCoA_mitoc	----->	FADH2_mitoc + 2Methylprop2enoylCoA_mitoc
R04224 [mitoc]	H2O [mitoc] + 2Methylprop2enoylCoA [mitoc] -> S3HydroxyisobutyrylCoA [mitoc]	H2O_mitoc + 2Methylprop2enoylCoA_mitoc	----->	S3HydroxyisobutyrylCoA_mitoc
R04203 [mitoc]	NAD [mitoc] + 2S3S3Hydroxy2methylbutanoylCoA [mitoc] <-> NADH [mitoc] + H [mitoc] + 2MethylacetoacetylCoA [mitoc]	NAD_mitoc + 2S3S3Hydroxy2methylbutanoylCoA_mitoc	<---->	H_mitoc + NADH_mitoc + 2MethylacetoacetylCoA_mitoc
R00927 [mitoc]	CoA [mitoc] + 2MethylacetoacetylCoA [mitoc] -> AcetylCoA [mitoc] + PropanoylCoA [mitoc]	CoA_mitoc + 2MethylacetoacetylCoA_mitoc	----->	AcetylCoA_mitoc + PropanoylCoA_mitoc
R01859 [mitoc]	HCO3 [mitoc] + ATP [mitoc] + PropanoylCoA [mitoc] -> ADP [mitoc] + Orthophosphate [mitoc] + S2Methyl3oxopropanoylCoA [mitoc]	ATP_mitoc + HCO3_mitoc + PropanoylCoA_mitoc	----->	ADP_mitoc + Orthophosphate_mitoc + S2Methyl3oxopropanoylCoA_mitoc
R00833 [mitoc]	R2Methyl3oxopropanoylCoA [mitoc] <-> SuccinylCoA [mitoc]	R2Methyl3oxopropanoylCoA_mitoc	<---->	SuccinylCoA_mitoc
R02765 [mitoc]	R2Methyl3oxopropanoylCoA [mitoc] <-> S2Methyl3oxopropanoylCoA [mitoc]	R2Methyl3oxopropanoylCoA_mitoc	<---->	S2Methyl3oxopropanoylCoA_mitoc
R00935 [mitoc]	NAD [mitoc] + CoA [mitoc] + SMethylmalonatesemialdehyde [mitoc] -> NADH [mitoc] + H [mitoc] + CO2 [mitoc] + PropanoylCoA [mitoc]	NAD_mitoc + CoA_mitoc + SMethylmalonatesemialdehyde_mitoc	----->	H_mitoc + NADH_mitoc + CO2_mitoc + PropanoylCoA_mitoc
TF0019	LIsoleucine <-> LIsoleucine [mitoc]	LIsoleucine_cytosol	<---->	LIsoleucine_mitoc
R02198 [mitoc]	2Oxoglutarate [mitoc] + LIsoleucine [mitoc] -> LGlutamate [mitoc] + 3Methyl2oxopentanoate [mitoc]	2Oxoglutarate_mitoc + LIsoleucine_mitoc	----->	LGlutamate_mitoc + 3Methyl2oxopentanoate_mitoc
R02662 [mitoc]	NAD [mitoc] + CoA [mitoc] + 3Methyl2oxobutanoicacid [mitoc] -> NADH [mitoc] + H [mitoc] + CO2 [mitoc] + 2MethylpropanoylCoA [mitoc]	NAD_mitoc + CoA_mitoc + 3Methyl2oxobutanoicacid_mitoc	----->	H_mitoc + NADH_mitoc + CO2_mitoc + 2MethylpropanoylCoA_mitoc

R04204 [mitoc]	H2O [mitoc] + 2Methylbut2enoylCoA [mitoc] -> 2S3S3Hydroxy2methylbutanoylCoA [mitoc]	H2O_mitoc + 2Methylbut2enoylCoA_mitoc	----->	2S3S3Hydroxy2methylbutanoylCoA_mitoc
TF0018	LLeucine <-> LLeucine [mitoc]	LLeucine_cytosol	<---->	LLeucine_mitoc
R01090 [mitoc]	2Oxoglutarate [mitoc] + LLeucine [mitoc] <-> 4Methyl2oxopentanoate [mitoc] + LGlutamate [mitoc]	2Oxoglutarate_mitoc + LLeucine_mitoc	<---->	LGlutamate_mitoc + 4Methyl2oxopentanoate_mitoc
R04097 [mitoc]	NAD [mitoc] + CoA [mitoc] + 4Methyl2oxopentanoate [mitoc] -> NADH [mitoc] + H [mitoc] + CO2 [mitoc] + 3MethylbutanoylCoA [mitoc]	NAD_mitoc + CoA_mitoc + 4Methyl2oxopentanoate_mitoc	----->	H_mitoc + NADH_mitoc + CO2_mitoc + 3MethylbutanoylCoA_mitoc
R04138 [mitoc]	HCO3 [mitoc] + ATP [mitoc] + 3MethylcrotonylCoA [mitoc] -> ADP [mitoc] + Orthophosphate [mitoc] + 3MethylglutaconylCoA [mitoc]	ATP_mitoc + HCO3_mitoc + 3MethylcrotonylCoA_mitoc	----->	ADP_mitoc + Orthophosphate_mitoc + 3MethylglutaconylCoA_mitoc
R01360 [mitoc]	S3Hydroxy3methylCO2 [mitoc] -> AcetylCoA [mitoc] + Acetoacetate [mitoc]	S3Hydroxy3methylCO2_mitoc	----->	AcetylCoA_mitoc + Acetoacetate_mitoc
R00410 [mitoc]	SuccinylCoA [mitoc] + Acetoacetate [mitoc] <-> Succinate [mitoc] + AcetoacetylCoA [mitoc]	SuccinylCoA_mitoc + Acetoacetate_mitoc	<---->	Succinate_mitoc + AcetoacetylCoA_mitoc
R03174 [mitoc]	NAD [mitoc] + CoA [mitoc] + 3Methyl2oxopentanoate [mitoc] -> NADH [mitoc] + H [mitoc] + CO2 [mitoc] + S2MethylbutanoylCoA [mitoc]	NAD_mitoc + CoA_mitoc + 3Methyl2oxopentanoate_mitoc	----->	H_mitoc + NADH_mitoc + CO2_mitoc + S2MethylbutanoylCoA_mitoc
R03172 [mitoc]	FAD [mitoc] + S2MethylbutanoylCoA [mitoc] -> FADH2 [mitoc] + 2Methylbut2enoylCoA [mitoc]	FAD_mitoc + S2MethylbutanoylCoA_mitoc	----->	FADH2_mitoc + 2Methylbut2enoylCoA_mitoc
R04095 [mitoc]	FAD [mitoc] + 3MethylbutanoylCoA [mitoc] -> FADH2 [mitoc] + 3MethylcrotonylCoA [mitoc]	FAD_mitoc + 3MethylbutanoylCoA_mitoc	----->	FADH2_mitoc + 3MethylcrotonylCoA_mitoc
R02085 [mitoc]	S3Hydroxy3methylCO2 [mitoc] <-> H2O [mitoc] + 3MethylglutaconylCoA [mitoc]	S3Hydroxy3methylCO2_mitoc	<---->	H2O_mitoc + 3MethylglutaconylCoA_mitoc
R01794	H + NADPH + Dihydrobiopterin -> NADP + Tetrahydrobiopterin	H_cytosol + NADPH_cytosol + Dihydrobiopterin_cytosol	----->	NADP_cytosol + Tetrahydrobiopterin_cytosol

R01795	Oxygen + LPhenylalanine + Tetrahydrobiopterin -> H2O + LTyrosine + Dihydrobiopterin	Oxygen_cytosol + LPhenylalanine_cytosol + Tetrahydrobiopterin_cytosol	----->	H2O_cytosol + LTyrosine_cytosol + Dihydrobiopterin_cytosol
R00678	Oxygen + LTryptophan -> LFormylkynurenine	Oxygen_cytosol + LTryptophan_cytosol	----->	LFormylkynurenine_cytosol
R01959	H2O + LFormylkynurenine -> Formate + LKynurenine	H2O_cytosol + LFormylkynurenine_cytosol	----->	Formate_cytosol + LKynurenine_cytosol
R01960	H + NADPH + Oxygen + LKynurenine -> H2O + NADP + 3HydroxyLkynurenine	H_cytosol + NADPH_cytosol + Oxygen_cytosol + LKynurenine_cytosol	----->	H2O_cytosol + NADP_cytosol + 3HydroxyLkynurenine_cytosol
R02668	H2O + 3HydroxyLkynurenine -> LAlanine + 3Hydroxyanthranilate	H2O_cytosol + 3HydroxyLkynurenine_cytosol	----->	LAlanine_cytosol + 3Hydroxyanthranilate_cytosol
R02665	Oxygen + 3Hydroxyanthranilate -> 2Amino3carboxymuconatesemialdehyde	Oxygen_cytosol + 3Hydroxyanthranilate_cytosol	----->	2Amino3carboxymuconatesemialdehyde_cytosol
R04323	2Amino3carboxymuconatesemialdehyde -> CO2 + 2Aminomuconatesemialdehyde	2Amino3carboxymuconatesemialdehyde_cytosol	----->	CO2_cytosol + 2Aminomuconatesemialdehyde_cytosol
R03889	H2O + NAD + 2Aminomuconatesemialdehyde -> H + NADH + 2Aminomuconate	NAD_cytosol + H2O_cytosol + 2Aminomuconatesemialdehyde_cytosol	----->	NADH_cytosol + H_cytosol + 2Aminomuconate_cytosol
R01938	H2O + H + NADPH + 2Aminomuconate -> NADP + NH3 + 2Oxoadipate	H_cytosol + H2O_cytosol + NADPH_cytosol + 2Aminomuconate_cytosol	----->	NADP_cytosol + NH3_cytosol + 2Oxoadipate_cytosol
R01933 [mitoc]	NAD [mitoc] + CoA [mitoc] + 2Oxoadipate [mitoc] -> NADH [mitoc] + H [mitoc] + CO2 [mitoc] + GlutarylCoA [mitoc]	NAD_mitoc + CoA_mitoc + 2Oxoadipate_mitoc	----->	H_mitoc + NADH_mitoc + CO2_mitoc + GlutarylCoA_mitoc
TF0024	LThreonine <-> LThreonine [mitoc]	LThreonine_cytosol	<---->	LThreonine_mitoc
R01465 [mitoc]	NAD [mitoc] + LThreonine [mitoc] -> NADH [mitoc] + H [mitoc] + L2Amino3oxobutanoicacid [mitoc]	NAD_mitoc + LThreonine_mitoc	----->	H_mitoc + NADH_mitoc + L2Amino3oxobutanoicacid_mitoc
R00371 [mitoc]	CoA [mitoc] + L2Amino3oxobutanoicacid [mitoc] -> AcetylCoA [mitoc] + Glycine [mitoc]	CoA_mitoc + L2Amino3oxobutanoicacid_mitoc	----->	AcetylCoA_mitoc + Glycine_mitoc
DEGMET1_added	LMethionine + ATP -> Pyrophosphate + Orthophosphate + SAdenosylLMethionine	ATP_cytosol + LMethionine_cytosol	----->	Orthophosphate_cytosol + Pyrophosphate_cytosol + SAdenosylLMethionine_cytosol

DEGMET2_added	SAdenosylLMethionine + Tetrahydrofolate -> SAdenosylLhomocysteine + 5Methyltetrahydrofolate	Tetrahydrofolate_cytosol + SAdenosylLMethionine_cytosol	----->	SAdenosylLhomocysteine_cytosol + 5Methyltetrahydrofolate_cytosol
DEGMET3_added	5Methyltetrahydrofolate + NAD <-> 510Methylenetetrahydrofolate + NADH + H	NAD_cytosol + 5Methyltetrahydrofolate_cytosol	<---->	NADH_cytosol + H_cytosol + 510Methylenetetrahydrofolate_cytosol
DEGMET4_added	SAdenosylLhomocysteine <-> Homocysteine + Adenosine	SAdenosylLhomocysteine_cytosol	<---->	Homocysteine_cytosol + Adenosine_cytosol
DEGMET5_added	LSerine + Homocysteine -> Lcystathionine	LSerine_cytosol + Homocysteine_cytosol	----->	Lcystathionine_cytosol
DEGMET6_added	Lcystathionine -> LCysteine + NH3 + 2Oxobutanoate	Lcystathionine_cytosol	----->	NH3_cytosol + LCysteine_cytosol + 2Oxobutanoate_cytosol
DEGMET7_added	Adenosine + ATP -> AMP + ADP	ATP_cytosol + Adenosine_cytosol	----->	ADP_cytosol + AMP_cytosol
DEGMET8_added	2Oxobutanoate + CoA [mitoc] + NAD [mitoc] -> PropanoylCoA [mitoc] + NADH [mitoc]	NAD_mitoc + CoA_mitoc + 2Oxobutanoate_cytosol	----->	NADH_mitoc + PropanoylCoA_mitoc
TF0025	LLysine <-> LLysine [mitoc]	LLysine_cytosol	<---->	LLysine_mitoc
R00716 [mitoc]	H [mitoc] + 2Oxoglutarate [mitoc] + NADPH [mitoc] + LLysine [mitoc] -> H2O [mitoc] + NADP [mitoc] + N6L13DicarboxypropylLlysine [mitoc]	H_mitoc + 2Oxoglutarate_mitoc + NADPH_mitoc + LLysine_mitoc	----->	H2O_mitoc + NADP_mitoc + N6L13DicarboxypropylLlysine_mitoc
R02313 [mitoc]	NAD [mitoc] + H2O [mitoc] + N6L13DicarboxypropylLlysine [mitoc] <-> NADH [mitoc] + H [mitoc] + LGlutamate [mitoc] + L2Aminoadipate6semialdehyde [mitoc]	NAD_mitoc + H2O_mitoc + N6L13DicarboxypropylLlysine_mitoc	<---->	H_mitoc + NADH_mitoc + LGlutamate_mitoc + L2Aminoadipate6semialdehyde_mitoc
R03103	H2O + NADP + L2Aminoadipate6semialdehyde -> H + NADPH + L2Aminoadipate	H2O_cytosol + NADP_cytosol + L2Aminoadipate6semialdehyde_cytosol	----->	H_cytosol + NADPH_cytosol + L2Aminoadipate_cytosol
R01939	2Oxoglutarate + L2Aminoadipate <-> LGlutamate + 2Oxoadipate	2Oxoglutarate_cytosol + L2Aminoadipate_cytosol	<---->	LGlutamate_cytosol + 2Oxoadipate_cytosol

R02487 [mitoc]	GlutarylCoA [mitoc] + FAD [mitoc] -> CrotonoylCoA [mitoc] + FADH2 [mitoc] + CO2 [mitoc]	FAD_mitoc + GlutarylCoA_mitoc	----->	CO2_mitoc + FADH2_mitoc + CrotonoylCoA_mitoc
R03026 [mitoc]	S3HydroxybutanoylCoA [mitoc] <-> CrotonoylCoA [mitoc] + H2O [mitoc]	S3HydroxybutanoylCoA_mitoc	<---->	H2O_mitoc + CrotonoylCoA_mitoc
R01975 [mitoc]	NAD [mitoc] + S3HydroxybutanoylCoA [mitoc] <-> NADH [mitoc] + H [mitoc] + AcetoacetylCoA [mitoc]	NAD_mitoc + S3HydroxybutanoylCoA_mitoc	<---->	H_mitoc + NADH_mitoc + AcetoacetylCoA_mitoc
R00238 [mitoc]	2.0 AcetylCoA [mitoc] <-> CoA [mitoc] + AcetoacetylCoA [mitoc]	2.0*AcetylCoA_mitoc	<---->	CoA_mitoc + AcetoacetylCoA_mitoc
R05064 [mitoc]	S3HydroxyisobutyrylCoA [mitoc] + H2O [mitoc] -> CoA [mitoc] + S3Hydroxyisobutyrate [mitoc]	H2O_mitoc + S3HydroxyisobutyrylCoA_mitoc	----->	CoA_mitoc + S3Hydroxyisobutyrate_mitoc
R05066 [mitoc]	NAD [mitoc] + S3Hydroxyisobutyrate [mitoc] <-> NADH [mitoc] + H [mitoc] + SMethylmalonatesemialdehyde [mitoc]	NAD_mitoc + S3Hydroxyisobutyrate_mitoc	<---->	H_mitoc + NADH_mitoc + SMethylmalonatesemialdehyde_mitoc
R00220	LSerine -> NH3 + Pyruvate	LSerine_cytosol	----->	Pyruvate_cytosol + NH3_cytosol
RGTXM	Glutamax [ext] -> Glutamax	Glutamax_ext	----->	Glutamax_cytosol
RGTXDE	Glutamax -> LAlanine + LGlutamine	Glutamax_cytosol	----->	LAlanine_cytosol + LGlutamine_cytosol
DEGCYS5_added	SO2 [ext] ->	SO2_ext	----->	
R_EX_BIOMASS [ext]	BIOMASS [ext] ->	BIOMASS_ext	----->	
R_EX_C00001 [ext]	H2O [ext] ->	H2O_ext	----->	
R_EX_C00007 [ext]	Oxygen [ext] ->	Oxygen_ext	----->	
R_EX_C00009 [ext]	Orthophosphate [ext] ->	Orthophosphate_ext	----->	
R_EX_C00011 [ext]	CO2 [ext] ->	CO2_ext	----->	
R_EX_C00014 [ext]	NH3 [ext] ->	NH3_ext	----->	

R_EX_C00025 [ext]	LGlutamate [ext] ->	LGlutamate_ext	----->	
R_EX_C00037 [ext]	Glycine [ext] ->	Glycine_ext	----->	
R_EX_C00041 [ext]	LAlanine [ext] ->	LAlanine_ext	----->	
R_EX_C00047 [ext]	LLysine [ext] ->	LLysine_ext	----->	
R_EX_C00049 [ext]	LAspartate [ext] ->	LAspartate_ext	----->	
R_EX_C00058 [ext]	Formate [ext] ->	Formate_ext	----->	
R_EX_C00062 [ext]	LArginine [ext] ->	LArginine_ext	----->	
R_EX_C00064 [ext]	LGlutamine [ext] ->	LGlutamine_ext	----->	
R_EX_C00065 [ext]	LSerine [ext] ->	LSerine_ext	----->	
R_EX_C00073 [ext]	LMethionine [ext] ->	LMethionine_ext	----->	
R_EX_C00078 [ext]	LTryptophan [ext] ->	LTryptophan_ext	----->	
R_EX_C00079 [ext]	LPhenylalanine [ext] ->	LPhenylalanine_ext	----->	
R_EX_C00080 [ext]	H [ext] ->	H_ext	----->	
R_EX_C00082 [ext]	LTyrosine [ext] ->	LTyrosine_ext	----->	
R_EX_C00097 [ext]	LCysteine [ext] ->	LCysteine_ext	----->	
R_EX_C00114 [ext]	Choline [ext] ->	Choline_ext	----->	
R_EX_C00123 [ext]	LLeucine [ext] ->	LLeucine_ext	----->	

R_EX_C00135 [ext]	LHistidine [ext] ->	LHistidine_ext	----->	
R_EX_C00137 [ext]	myoInositol [ext] ->	myoInositol_ext	----->	
R_EX_C00148 [ext]	LProline [ext] ->	LProline_ext	----->	
R_EX_C00152 [ext]	LAsparagine [ext] ->	LAsparagine_ext	----->	
R_EX_C00183 [ext]	LValine [ext] ->	LValine_ext	----->	
R_EX_C00186 [ext]	SLactate [ext] ->	SLactate_ext	----->	
R_EX_C00188 [ext]	LThreonine [ext] ->	LThreonine_ext	----->	
R_EX_C00189 [ext]	Ethanolamine [ext] ->	Ethanolamine_ext	----->	
R_EX_C00267 [ext]	alphaDGlucose [ext] ->	alphaDGlucose_ext	----->	
R_EX_C00407 [ext]	LIsoleucine [ext] ->	LIsoleucine_ext	----->	
R_EX_UREA_ext	Urea [ext] ->	Urea_ext	----->	
RGTXD [ext]	Glutamax [ext] ->	Glutamax_ext	----->	

APPENDIX D

A detailed protocol (**Figure D.1**) and results obtained for the K_{des} determination (**Figure D.2**) in the Chapter 5 for the O.U.R. determination is presented below.

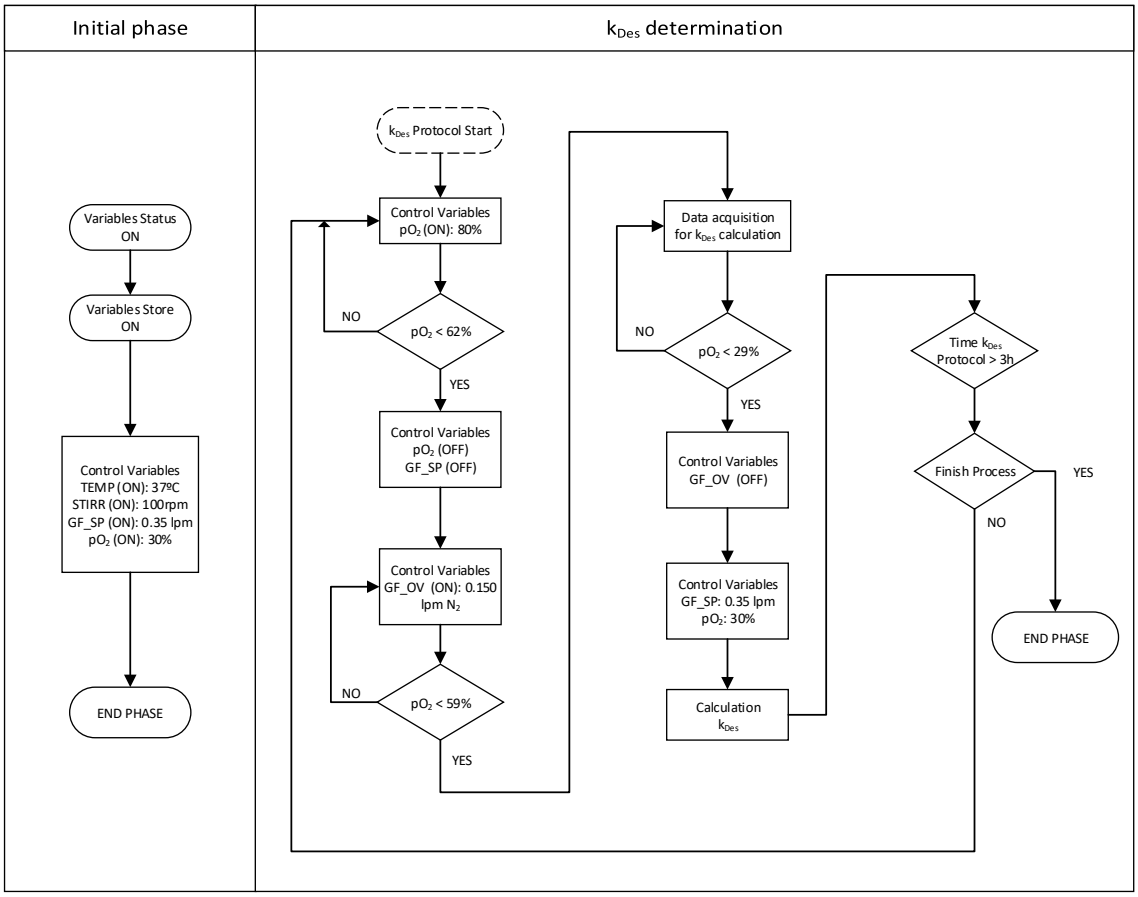

Figure D.1: Block diagram control for the k_{des} determination method before inoculation. Recipe implemented in MFCS/win 3.0 in Biostat B DCU II.

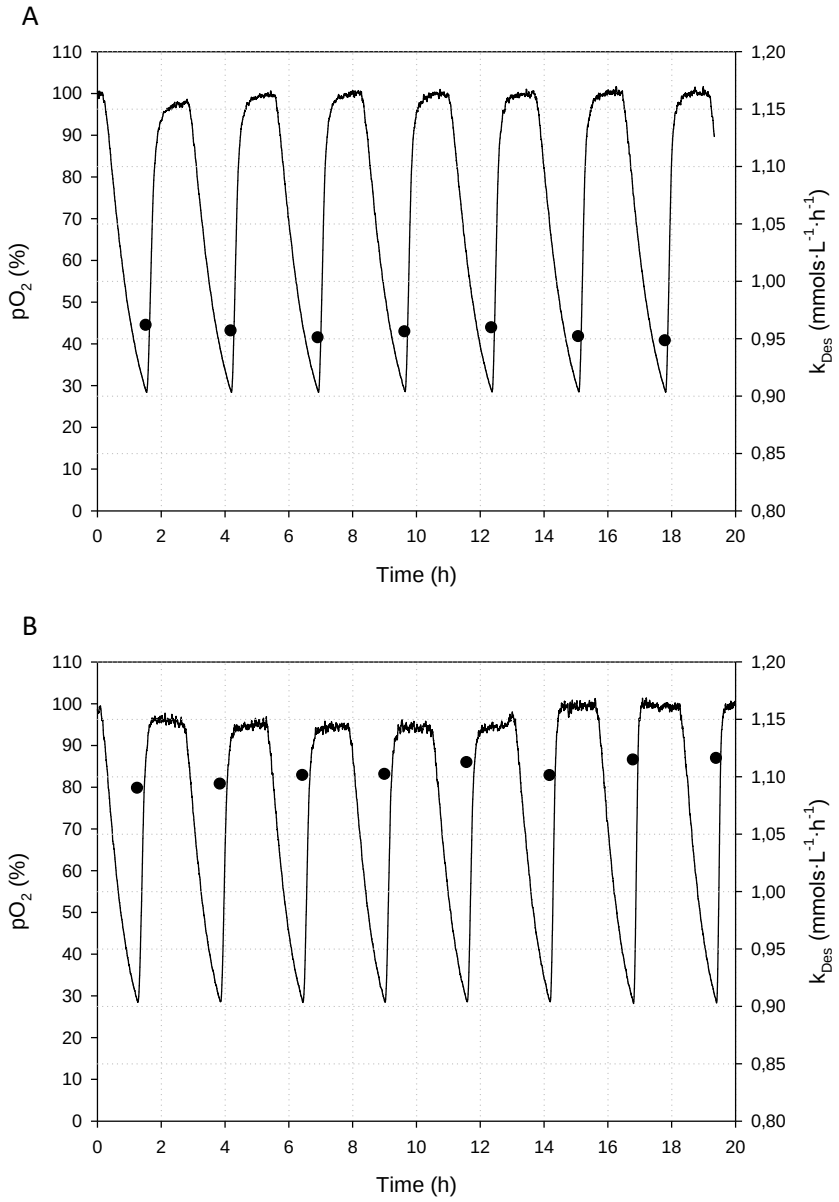

Figure D.2: K_{des} determination in Batch (A) and Fed-batch based on OUR (B) cell culture. pO_2 (line) and K_{des} (points) are depicted.